Ontogeny
in
Dysalotosaurus lettowvorbecki

Dissertation der Fakultät für Geowissenschaften

der Ludwig-Maximilians-Universität München

von Diplom-Geologe

Tom Hübner

Antrag auf Zulassung zur Promotion: 11.08.2010

1. Gutachter: Dr. O.W.M. Rauhut

Bayerische Staatssammlung für Paläontologie und Geobiologie

München

2. Gutachter: Prof. Dr. P.M. Sander

Steinmann-Institut für Geologie, Mineralogie und Paläontologie

der Universität Bonn

Tag der Disputation: 12.01.2011

„Jemand hat mir mal gesagt, die Zeit würde uns wie ein Raubtier ein Leben lang verfolgen. Ich möchte viel lieber glauben, dass die Zeit unser Gefährte ist, der uns auf unserer Reise begleitet und uns daran erinnert, jeden Moment zu genießen, denn er wird nicht wiederkommen. Was wir hinterlassen ist nicht so wichtig wie die Art, wie wir gelebt haben. Denn letztlich [...] sind wir alle nur sterblich."

Jean Luc Picard

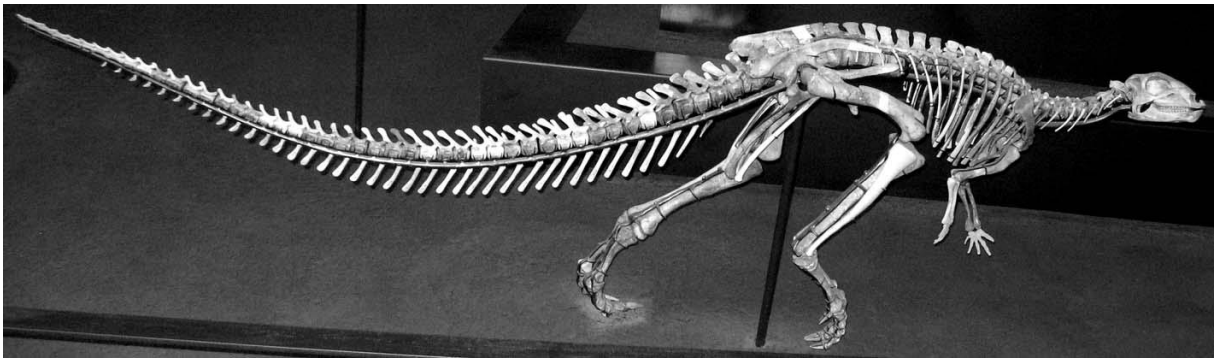

The new mount of a skeleton of *Dysalotosaurus lettowvorbecki* (individual "dy I"), on display in the Museum für Naturkunde, Berlin.

„Mein alter Glitschball-Trainer pflegte immer zu sagen:
Finde raus, was Du nicht gut kannst,
und dann lass es bleiben!"

Gordon Shumway

Summary

This study was inspired by many recent scientific projects, which gave new insight into the ontogeny of an increasing number of extinct species in more detail. The knowledge of the ontogeny and its development is very important for understanding the taphonomy and paleobiology, the taxonomic value of phylogenetic characters, and the evolutionary relationship of an extinct species. Several qualitative and quantitative methods were used in these studies including the observation of suture closure, bone surface texture, bivariate and multivariate statistics, morphometrics, and bone histology. However, most of the published studies dealt only with one or two of these topics and further concentrated only on one or two methods. The importance of the combination of methods to get a more complete picture on the life history and phylogenetic relationships of extinct animals is recognized, however, and more recent studies combine the discovery of a new species with statements on its ontogenetic stage or the description of monodominant bonebeds with the reconstruction of growth patterns and life history for instance. This scientific frame is the starting point for the present study, in which almost all of the mentioned methods were combined for the first time resulting in the most comprehensive ontogenetic study on a single dinosaur species up to date.

The small Upper Jurassic ornithopod dinosaur *Dysalotosaurus lettowvorbecki* was the subject in this study. It was found during the famous German Tendaguru Expedition (1909-1913), which is named after the type locality of the respective Formation, the Tendaguru Hill. This hill is located approximately 60 kilometers west of the seaport of Lindi in the Southeast of Tanzania, East-Africa. In contrast to the gigantic sauropod dinosaurs and the stegosaur *Kentrosaurus*, *Dysalotosaurus* is known from only a single locality 2.5 kilometers northwest of Tendaguru Hill, but the numbers of preserved bones within the two bonebeds were extraordinarily high (more than 14000 catalogue numbers). Additionally, several ontogenetic stages were preserved for the majority of skeletal elements. The bones were mostly isolated, but often well preserved. Plenty of material is housed in

collections in Berlin, Göttingen, London, Munich, Stuttgart, and Tübingen, making this dinosaur one of the best known ornithopods of the world and the ideal object for an ontogenetic study.

The methods used here contain qualitative observations of the timing and degree of suture closure, of the bone surface texture, and of morphological changes in single elements during growth. Furthermore, quantitative calculations were carried out by using the values of the measured bones mainly for bivariate allometric statistics. Ratios between long bones, multivariate statistics, and morphometrics were abandoned due to the lack of articulated material and due to the rather high amount of missing values. The study of the bone histology was also extensive, because each of the chosen skeletal elements was numerously represented in several ontogenetic stages. Thus, variation of bone microstructure of *Dysalotosaurus* could be evaluated and its life history could be reconstructed by the calculation of growth curves.

Dysalotosaurus belongs to the basal Iguanodontia. This is a derived and highly diverse group of ornithopod dinosaurs, which comprises the most primitive member *Tenontosaurus* from the Early Cretaceous of North America, the European Late Cretaceous rhabdodontids, the dryosaurids including *Dysalotosaurus*, the transatlantic Upper Jurassic genus *Camptosaurus*, and all more derived large ornithopods including the famous *Iguanodon* and the hadrosaurs. *Dysalotosaurus* can be treated as the perfect intermediate taxon within ornithopods because it represents the connection between primitive ornithopods and more derived basal iguanodontians on one hand and between small and large ornithopods on the other hand. It was therefore very interesting to explore ontogenetic changes within *Dysalotosaurus* in an evolutionary and size-related context.

In 1977, *Dysalotosaurus* was synonymized with its close relative *Dryosaurus* from the Upper Jurassic of North America due to many morphological similarities. Numerous differences in skull and postcranial bones challenge this view, however. Even the morphology of the pelvic and hindlimb skeleton, which is actually relatively conservative among small ornithopods, shows more differences than between different genera of hadrosaurs or ceratopsids. Thus, the name *Dysalotosaurus* is resurrected for now and therefore also used throughout this study.

A very important first step before starting observations and analyses of ontogenetic characters was the revised interpretation of the taphonomy of the two monodominant bonebeds of *Dysalotosaurus*. Mainly due to the lack of information on the sedimentology and stratigraphy of the locality and on the spatial arrangement of the bones, it was not clear, if this mass accumulation represents the result of one or two catastrophic mass death events or just the result of attritional mortality. Several lines of evidence let now conclude that the bonebeds indeed represent a single mass death event of a *Dysalotosaurus* herd, because there are no taphonomic differences between them and there are also no traces of preburial abrasion caused by long transport or of preburial weathering due to long exposure on the surface. The two-peaked size frequency distribution, usually interpreted as the result of attritional mortality, is also only unambiguously usable for populations with one offspring per female per year. This is highly unlikely for any dinosaur. The lack of hatchlings in the size frequency distribution could also be explained by the time of the death event, which probably took place well outside the breeding season. The underrepresentation of young age classes is probably the result of slight sorting of the bones in favor of large and robust elements. Finally, the underrepresentation of mid-sized age classes is explainable by the banishment or higher mortality rate around the time of sexual maturity, as in many modern gregarious mammals. In the end, the evidence for a single mass death event dominates and possible hints for attritional mortality can be explained alternatively, so that the hypothesis of a single *Dysalotosaurus* herd could be used as the null hypothesis in all following ontogenetic studies on this dinosaur.

The ontogeny of the skull of *Dysalotosaurus* was carried out separately, because the best preserved skull, housed in the collections of the Bayerische Staatssammlung für Paläontologie and Geobiologie in Munich, was hitherto unstudied. This juvenile specimen is fully described and reconstructed. Apart from the palatine and the quadratojugal, all elements of the skull are now known and the comparison with all other preserved cranial material revealed several ontogenetic trends for the skull. The suture closure pattern, although variable in the timing, could be reconstructed. The elements of the basicranium and the parietals fuse first and the elements of the pre-orbital region fuse obviously very late or never during life. The overall skull proportions are also

changing to relatively smaller orbits, an elevated posterior skull roof, and a longer snout. This indicates that peramorphic heterochrony is a dominant evolutionary tendency in the skull shape of ornithopods, supporting the development towards larger size and full herbivory. Further juvenile ontogenetic characters could be identified during this study: (1) the basioccipital has a characteristic rhomboidal shape, with the condyle neck thicker than the condyle itself in very young individuals, (2) the frontals are very slender and long, with just a small and flat central dome, (3) the deepest point of the postorbital suture has an anterior position on the postorbital process of the jugal, and (4) the tooth number is smaller (ten compared with up to 13 in older ones) in lower and upper jaws, among others. These results were then used in two other ornithopod species. The juvenile stage of the holotype skull of *Gasparinisaura* could be independently confirmed and the example of *Thescelosaurus* has demonstrated that more than one or two characters are necessary to determine the ontogenetic stage of an extinct animal unambiguously. The intermediate stage of *Dysalotosaurus* between less derived small ornithopods and more derived and/or large ornithopods could finally be proofed by its skull ontogeny.

Numerous ontogenetic changes were found in the postcranial skeleton of *Dysalotosaurus* after numerous morphological observations and the statistical evaluation of approximately 6000 measurements. The neurocentral sutures of the vertebrae close from back to front, but the incomplete (if at all) closure in sacral and presacral vertebrae in even the largest preserved specimens demonstrates an indeterminate growth pattern for this dinosaur, as in crocodiles. This is further supported by the lack of changes of the bone surface texture, which is only significant in animals with a determinate growth pattern, such as birds and pterosaurs. Most of the ontogenetic modifications of the appendicular skeleton are a function of increasing body size and weight during growth including larger and more robust articular ends and suture surfaces and more robust attachment sites for muscles and tendons. The articular ends of long bones were well developed even in the smallest known individuals, which is a distinct sign for precocial behavior of the young. In addition, peramorphic heterochrony is the main ontogenetic modification of postcranial elements, as in the skull, but several other types of modification were also identified, such as paedomorphosis and

heterotopy. Combinations of different steps of ontogenetic modifications were also possible within a single element and obviously also alongside different steps within ornithopod phylogeny, which reveals surprisingly diverse evolutionary strategies of the actually rather conservative ornithopod bauplan. Thus, the ontogeny of *Dysalotosaurus* mirrors several morphological modifications within ornithopods, which led in at least three ornithopod lineages to larger, more graviportal, and fully herbivorous dinosaurs.

Numerous thin sections of five different skeletal elements of *Dysalotosaurus* (femur, tibia, humerus, fibula, and pubis) were produced for bone histological studies. The bone microstructure was highly variable between different skeletal elements, between ontogenetic stages, and between different parts of a single cross section. Intra-skeletal variation in bone microstructure is the consequence of differing growth rates, which are dependent on the relative size of the element and its degree of utilization. Thus, the femur of *Dysalotosaurus* has shown the highest relative growth rates due to its large size, its main weight bearing function, and its importance during locomotion. The humerus, on the other hand, has revealed relatively lower growth rates because of its smaller relative size and its low degree of utilization (no weight bearing, less important in movements).
Intra-cortical variation of a single cross section is dependent on its shape and the degree of bending of the bones long axis. This means that a more circular cross section shows less variation of its microstructure than an angular cross section. Bones with a straight long axis have also less cross sectional variation than bones with a bended long axis, because the latter experiences drift of the marrow cavity to maintain its shape during growth. By using these results on variation in the bone microstructure of *Dysalotosaurus*, one can tentatively predict relative growth rates within skeletons of other animals by just looking at the relative size and shape of the respective elements.

Another result is the confirmation of true resting lines (annuli and LAG's – lines of arrested growth) in the bones of *Dysalotosaurus*, although it was not found in an earlier study. However, they were rare and their occurrence unpredictable, so that these resting lines alone were no use for the estimation of age and the reconstruction of a growth curve. Thus, another type of not yet described growth cycles, which was frequently found within the cross sections, was used instead. In

combination with further results and findings, several key data of the life history of *Dysalotosaurus* could be reconstructed. First, the assumed precocial behavior of hatchlings is confirmed, because the already well developed articular ends of long bones were also well ossified internally. Growth curves of femora revealed that *Dysalotosaurus* grew with a moderate rate in its juvenile stage until approximately six years of age and experienced accelerated growth during its sexually immature subadult stage until reaching sexual maturity at approximately ten years of age. It further had its exponential growth phase as sexually mature adult until the 14th year of life, where the maximum growth rate was reached (approximately equates the growth rate of a marsupial mammal). Afterwards, the growth rate decelerated and finally reached asymptotic growth well after 20 years. However, the second largest femur specimen represents an estimated age of 19.5 years. None of the members of the preserved *Dysalotosaurus* herd reached the growth plateau of somatic maturity, so that none of the individuals was fully grown. As indicated by the postcranial ontogenetic study, this confirms the indeterminate growth strategy of *Dysalotosaurus*.

The fortunate discovery of medullary bone tissue, known as a storage tissue for the development of egg shells in birds, and the first discovery of a possible mark of initial sexual maturity (MISM) in five large femora led to the conclusion that the group of smaller individuals within the size frequency distribution consists of sexually immature juveniles and subadults and that the group of larger individuals consists of sexually mature adult individuals. The MISM is plotting exactly within the gap between these two peaks. This confirms the assumption, derived from the taphonomic interpretation of the two bonebeds as a mass death event of a single herd, that the young adults were either banished from the herd due to competition with the more dominant adults and/or they suffered by a higher mortality rate than older adults due to higher vulnerability to predation or higher stress levels by competing with the dominant older adults. It can therefore be assumed that some elements of the known herding behavior of living ungulate mammals were already present in this Upper Jurassic dinosaur.

The results of the bone histological study of *Dysalotosaurus* were finally combined with a relationship between abundance and consistency of resting lines in recent mammals and their

respective seasonal environment. Used on to the growth cycle pattern of sauropods, these dinosaurs can thereafter be considered as relatively insensitive to seasonal influences of their environment due to their usually large body size and high absolute growth rates. Ornithopods are a heterogeneous group, where the smaller species are less exposed to seasonal effects than the large species mainly based on differences in food demands, growth rates, and breeding strategy. In fact, large size within Ornithopoda was probably linked to a change in breeding strategy from precocial to altricial behavior. Theropods were probably territorial altogether and therefore equally susceptible to seasonal stress independently of body size.

Dysalotosaurus has turned out to be the ideal model for an intermediate stage between less derived small ornithopods and mostly more derived large ornithopods. Its ontogeny has revealed many changes in morphology and growth pattern, which have enabled ornithopods to become so extraordinarily successful throughout the Cretaceous. This includes larger body size, full herbivory with a sophisticated chewing apparatus, very high growth rates, and a social behavior probably matching that of modern ungulates.

In the end, the rather small and unimpressive dinosaur *Dysalotosaurus* was much more interesting than one would expect at a first glance and the results on its ontogeny and paleobiology have provided deep insight into otherwise completely lost aspects of a 145 million years old ecosystem. The reconstruction of the life of the past is indeed one of the most fascinating tasks in modern research, because one can help to partly revive extinct animals, and their life and death are therefore never forgotten.

Acknowledgment

This study would never have been implemented and accomplished without the support and patience of many people. First of all, I would like to thank my supervisor, Oliver Rauhut (BSPG, Munich), who initiated this project, wrote the application, and helped me in many other ways. He was always lenient and helpful, when I had yet another question and I am glad that he never got a giant black hole in his belly from my constant questioning. This is also the case for Adriana, his wife, who I thank for her honesty (in a way like this: “No, not another question! Damn, think for yourself! I have enough to do of my own!”). Oliver and Adriana introduced me into the reality of modern research, forced me to learn proper English, and showed me to get along with mountains of literature, grants and meetings. I would not be the man I am without their help and friendship.

Another important person is Martin Sander (Bonn). He introduced me into the depths of bone histology. Without him, I would never have properly understood this tricky topic with all its sometimes unmanageable variation. He also was the first, who recognized the medullary bone in a sample, which led to many important results. I am very thankful for his help and time. I also thank Nicole Klein and Koen Stein, both from Martin Sanders team in Bonn, for helpful discussions and hints as well as Olaf Dülfer (also Bonn) for his comments on the production of thin sections.

There are four other persons from the Bayerische Staatssammlung in Munich, whom I especially want to thank. This is Renate Liebreich, the preparatory, who excellently prepared this fragile juvenile skull for my work and who mended accidentally broken bones for me. The next one is Cathleen Helbig from the stone laboratory, who had an enormous pile of work to make the numerous thin sections for me. She usually works with rocks, but she managed to make this special work better than one would expect from an expert. Georg Janssen, the ex-photographer of the BSPG, was always a help, when I had problems with Photoshop and he always made excellent photos of the many specimens for me. I also thank Alexander Altenbach for his advice in basic statistics, the introduction into the software PAST, and his patience to explain to me all these abstract contexts, so that I now have at least a basic understanding of statistics.

There are many more people from the BSPG, whom I want to thank for their support, their time, and their kindness. Among them are Winfried Werner, Martin Nose, Ella Kunz, Simon Schneider, Stefan Lautenschlager, Manuela Aigelsdorfer, Richard Butler, Katrin Moser, Regina Fechner, Gertrud Rößner, Alexander Nützel, Rene Neumaier, and many more.

I also want to thank Martin Dobritz (Klinikum Rechts der Isar) and Eva Christoph (Klinikum Großhadern) for their help with the CT-scans of the juvenile skull and of some long bones of *Dysalotosaurus*, Christian Remes (now DFG) for some helpful remarks on forelimb anatomy, and Helge Schönfelder for some comments on the text of this thesis.

I would especially like to thank the curators and their colleagues in the remaining four collections, where *Dysalotosaurus* material is housed. I thank Rainer Schoch (Stuttgart) because of his kindness and support with the specimens and also because he still talks to me despite my naive stupidity. I therefore also thank the unknown preparator in Stuttgart for his effort to repair the damage. I thank Alexander Hohloch for his friendship and his helpfulness, especially for his effort to number all the specimens, which made my work so much easier. I also thank Michael Reich (Göttingen) for his help and time with the specimens. Last but not least, I want to thank Daniela Schwarz-Wings, Wolf-Dieter Heinrich, and Oliver Hampe (Berlin) for their help with the material, the first two for helpful discussions and supply of rare old papers, and especially Daniela for her time to answer my numerous questions and to give me access into the Knochenkeller and the exhibition.

Finally, I am deeply grateful to my wife, Wiete, who spend so much of her free time to play with our little Tilia, where it had actually been my turn. So, I had much more time to finish my work. She also helped me with tricky formulas and taught me how to use the Excel and Origin software properly. Without her constant support and encouragement, I never would have come to an end. All my family and friends were always there and it is good to know that they always will be.

This project was funded by the DFG-grants RA1012/4-1 and RA1012/4-2. Thank you for your trust.

This study unites the help and effort of so many wonderful people.

I am proud to be an important part of it.

Thank you all!

Table of Contents

1. General introduction

In 1906, the engineer Bernhard Sattler stumbled on pieces of a gigantic bone at the foot of the minor Tendaguru Hill located approximately 60 kilometers from the port of Lindi in the Southeast of Tanzania (formerly German East-Africa; Fig. 1.1). He would not have been dreaming at the time that his discovery was going to be the starting point of the largest, most extensive, most ambitious, and extraordinary successful paleontological expedition of the scientific history. Only one year later, Eberhard Fraas visited the site and recovered several dinosaur bones, which were named and described shortly afterwards (Fraas, 1908). The actual Tendaguru-Expedition began in 1909 and ended in 1913. Overviews on the conditions, excavations, and camp life were given first by Janensch (1914a), but the whole story was recently published by Maier (2003) in stunning detail. During four seasons of field work, 235 tons of fossil material was excavated, packed, and finally shipped to Germany (Maier, 2003).

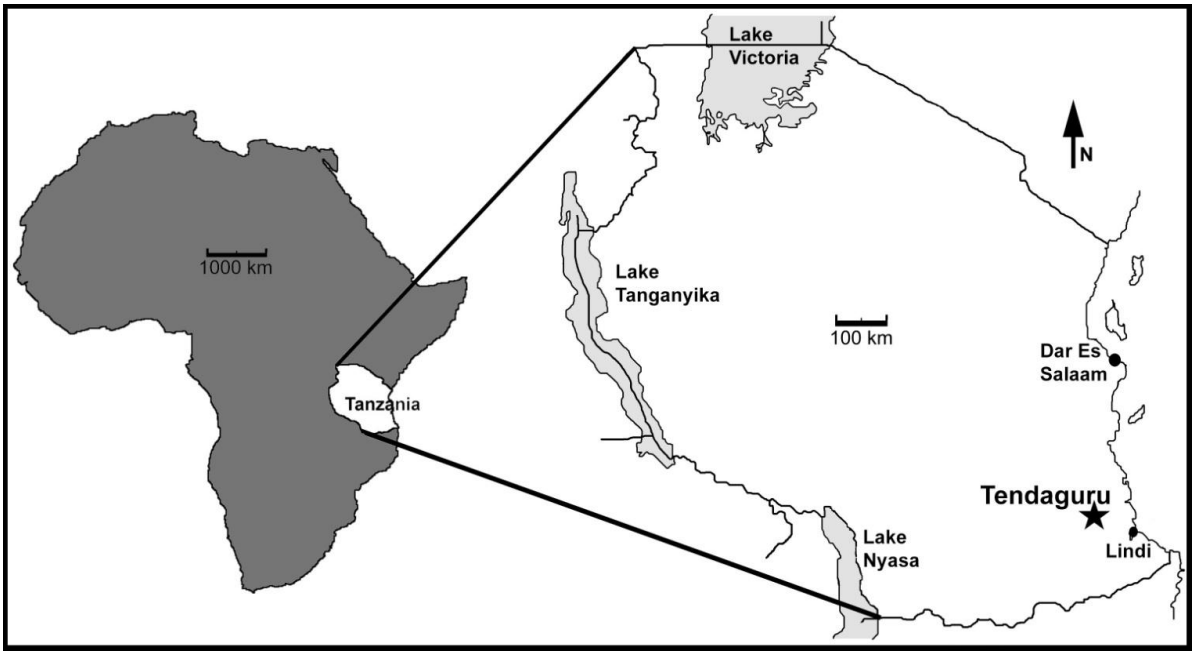

Fig. 1.1: *Approximate location of the dinosaur bearing Tendaguru area (star).*

According to the most recent revision of the stratigraphy of the Tendaguru-Formation (Bussert et al., 2009), it consists of six stratigraphic members, which are named from bottom to top Lower Dinosaur Member, *Nerinella* Member, Middle Dinosaur Member, *Indotrigonia africana*

Member, Upper Dinosaur Member, and *Rutitrigonia bornhardti-schwarzi* Member. The Dinosaur Members consist predominantly of fine-grained sediments of coastal to tidal plain origins and are the main sources for dinosaur remains (e.g. Aberhan et al., 2002; Bussert et al., 2009; Heinrich, 1999a; Janensch, 1925a). The intercalating members are dominated by sandstone and were deposited in a shallow-marine lagoon environment. Dinosaur remains are known but less common than in the Middle and Upper Dinosaur Member. The age of these transgression-regression cycles reach at least from the Middle Oxfordian (Late Jurassic) to the Hauterivian (Early Cretaceous).

Most of the dinosaur material consisted of remains of sauropod dinosaurs and of the stegosaur *Kentrosaurus*, but among them was also a vast amount of bones from a small ornithopod dinosaur, which was later named *Dysalotosaurus lettowvorbecki* by Pompeckj (1920). This can be translated as (Paul von) Lettow-Vorbeck's (a popular German General at that time) trickily catchable lizard, probably due to its apparent cursorial lifestyle. Its occurrence in the Tendaguru area, approximately 2.5km NW of the Tendaguru Hill close to the settlement of Kindope (e.g. Janensch, 1914c; 1925a; Maier, 2003), was unusual compared to the other dinosaurs, because it was found only in a single locality (named Ig and WJ, see chapter 3), but there in extraordinary numbers. In the end, more than 14000 catalogue numbers were assigned and most of the material had to be excavated in blocks due to the density of bones within the matrix of the bonebeds. The vast majority of specimens consists of isolated bones, but occasionally associated and partly articulated skeletons, e.g. skulls and series of vertebrae, were also found (Maier, 2003). Unfortunately, Pompeckj died before he could thoroughly describe the *Dysalotosaurus* specimens and the work had to be postponed. In addition, most of the already prepared material, including the few partial skeletons, was destroyed during WWII, so that the actual description by Janensch (1955) had to be carried out by using newly prepared material. However, almost every skeletal element is known from this dinosaur, often also in several ontogenetic stages, which makes *Dysalotosaurus* one of the best known small ornithopods of the world.

Dysalotosaurus was found in the Middle Dinosaur Member, which is dated as Kimmeridgian (Late Jurassic) in age (e.g. Bussert et al., 2009; see chapter 3). It belongs to the basal Iguanodontia and belongs together with *Valdosaurus* and *Dryosaurus* to the family Dryosauridae (e.g. Milner & Norman, 1984; Norman, 2004; see chapter 2). In fact, *Dysalotosaurus* was even synonymized with *Dryosaurus* due to many anatomical similarities (e.g. Galton, 1977; 1980; 1981; 1983), but this will be avoided here due to many additional facts (see chapter 2). Fragmentary material from the Middle Jurassic of England (*Callovosaurus* – Ruiz-Omenaca et al., 2007), from the Early Cretaceous of South Africa (*Kangnasaurus* – Cooper, 1985), and probably from the late Cretaceous of New Zealand and Antarctica (Agnolin et al., 2010; Hooker et al., 1991; Wiffen & Molnar, 1989; see chapter 2) demonstrates the wide stratigraphic and geographic distribution of this group. All members of the Dryosauridae are small to medium-sized ornithopod dinosaurs, which are treated as fast running and agile plant eaters (e.g. Foster, 2007; Norman, 2004; Ryan, 1997), and are therefore very similar to small *Hypsilophodon*-like ornithopods. They are, nevertheless, much more derived and closely related to medium to large sized iguanodontid ornithopods, which makes *Dysalotosaurus* and its relatives the ideal intermediate evolutionary stage between both groups.

The preservation of numerous ontogenetic stages of many bones is also a rather rare but very fortunate condition for the study of ontogeny in *Dysalotosaurus*. This was used to make assumptions about possible changes in locomotion during ontogeny (Dilkes, 2001; Heinrich et al., 1993) and to reveal the life history by using bone histology (Chinsamy, 1995; Chinsamy-Turan, 2005; Horner et al., 2009). The following extensive study attempts to adopt as many as possible different methods to extract information about morphological changes during growth, about growth rates and individual age, and, finally, about implications on ornithopod evolution in general and the life history and behaviour of *Dysalotosaurus* in particular. The combination of methods helps therefore to get a much more detailed insight into and a better understanding of ontogenetic changes in this dinosaur.

In chapter 2, the detailed systematic position of *Dysalotosaurus* is presented including some facts, which demonstrate the abolishment of the synonymy of *Dysalotosaurus* with *Dryosaurus*. The

central assumption of this study is that the two bonebeds of *Dysalotosaurus* represent a single herd. Known facts and the resulting interpretation of the taphonomy of the fossil location Ig/WJ are provided in chapter 3. The chapters 4 and 5 then describe and discuss morphological changes during ontogeny of the skull and postcranium, respectively. A combination of qualitative and quantitative methods was used here. In the latter case, multivariate statistics were avoided due to the incomplete dataset. Ratios between long bones were also not available, because the vast majority of bones were isolated, so that bivariate plots of the multivariate allometric analysis were the main method used in the end. Finally, chapter 6 deals with all aspects of the bone histology of *Dysalotosaurus* including various kinds of variation as well as the reconstruction of growth rates and curves. The conclusions combining all results are given in chapter 7.

2. The systematic palaeontology of *Dysalotosaurus lettowvorbecki*

2.1 Prior work

Soon after the first discovery of *Dysalotosaurus* fossils, Janensch recognized this taxon as an iguanodontid ornithopod (Maier, 2003:59; Reck, 1910; 1911; Fig. 2.1), which he later thought to be related to the North-American primitive ornithopod *Nanosaurus* (Janensch, 1914a:51; [he probably referred to *Nanosaurus rex*, which is known today as *Othnielosaurus*, see Galton, 2007]). Pompeckj (1920) named and diagnosed *Dysalotosaurus* first, although Virchow (1919) mentioned the name earlier in the literature. Pompeckj (1920) already classified *Dysalotosaurus* as an intermediate ornithopod taxon with a phylogenetic placement somewhere between *Hypsilophodon* and *Camptosaurus*. Later authors have placed *Dysalotosaurus* either closer to *Hypsilophodon* or to *Camptosaurus*, respectively, but the late discovery of a toothless premaxilla decided the discussion in favor of the latter (see Janensch, 1950 and references therein; Janensch, 1955:172). Thulborn (1971) even placed *Dysalotosaurus* tentatively at the base of Iguanodontia.

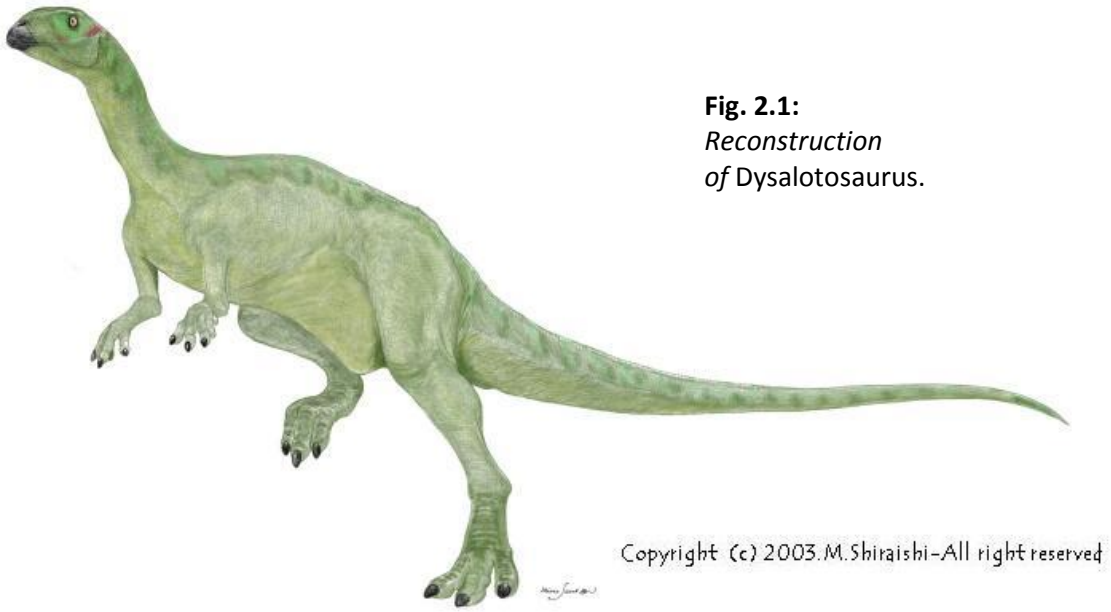

Fig. 2.1: *Reconstruction of* Dysalotosaurus.

This view was challenged by Galton (1972), because he treated hindlimb proportions (cursorial or graviportal) as more important than the presence or absence of premaxillary teeth. *Dysalotosaurus* was therefore placed into the Hypsilophodontidae. However, the following study of ornithopods from the Morrison Formation led to the preliminary conclusion that *Dysalotosaurus*, *Dryosaurus altus*, and a Lower Cretaceous ornithopod from the Lower Cretaceous of England and Niger (later named *Valdosaurus* by Galton & Taquet, 1982) could belong to their own clade within Hypsilophodontidae (Galton & Jensen, 1973). Based on numerous similarities, Galton (1977) then synonymized the genus *Dysalotosaurus* with *Dryosaurus* and proposed a Late Jurassic land connection between Laurasia and Gondwana. During the following years Galton (1980; 1981; 1983; see also Shepherd et al., 1977) specified this view. He also gave a new diagnosis for the genus *Dryosaurus* and the species *D. altus* and *D. lettowvorbecki*, and he designated the skull 'dy A' (see Janensch, 1955; chapter 4) as the neotype of the latter (Galton, 1983).

The application of the new cladistical method, which is not just based on general similarity but on the absence or presence of defined apomorphic anatomical characters, put the genus *Dryosaurus* back into the base of Iguanodontia (Norman, 1984). Milner & Norman (1984) also proposed a new family, Dryosauridae, which was again phylogenetically placed between Hypsilophodontidae and Iguanodontidae. Some of the cranial characters used to define Dryosauridae by Milner & Norman (1984) were later integrated by Sereno (1986) in a set of characters to define the whole Iguanodontia, which included *Tenontosaurus* as a more basal member than *Dryosaurus*. In addition, he named the new clade Dryomorpha, which comprised *Dryosaurus* and all descendants closer to hadrosaurs than to *Tenontosaurus*. This clade was based mainly on characters of the teeth and of the ischium. Sereno (1986:248) concluded that only *Valdosaurus* is closely related to *Dryosaurus* (he accepted the synonymy of *Dysalotosaurus* with *Dryosaurus*), which was in contrast to Cooper (1985), who argued the Cretaceous South-African *Kangnasaurus* to be a close relative of *Dryosaurus*. A partial ilium from the Upper Cretaceous of New Zealand was also referred to as a

'*Dryosaurus*-like' ornithopod (Wiffen & Molnar, 1989), but the incompleteness of the specimen and differences in the brevis shelf and postacetabular process obviously prevents an assignment beyond Ornithopoda (Agnolin et al., 2010).

Sues & Norman (1990) adopted the classification of Milner & Norman (1984) and Sereno (1986) and placed *Dryosaurus* and *Valdosaurus* into the family Dryosauridae, which is the sister group to all other Iguanodontia. They also treated *Kangnasaurus* as nomen dubium, but avoided the inclusion of *Tenontosaurus* within Iguanodontia. They defined Dryosauridae as follows: (1) premaxilla does not enclose external naris dorsally; (2) ilium with wide brevis shelf; (3) deep intercondylar groove on distal femur; (4) deep pit for M. caudifemoralis longus at the base of the 4th trochanter; and (5) vestigial metatarsal I. Together with further cranial and postcranial characters (see Galton, 1983; Milner & Norman, 1984; Sereno, 1986), the definition of this clade had become more and more stable, although some of the characters of Sues & Norman (1990) are either only known in one species (character 1) or shared by both more primitive and more derived taxa (e.g. character 3-5).

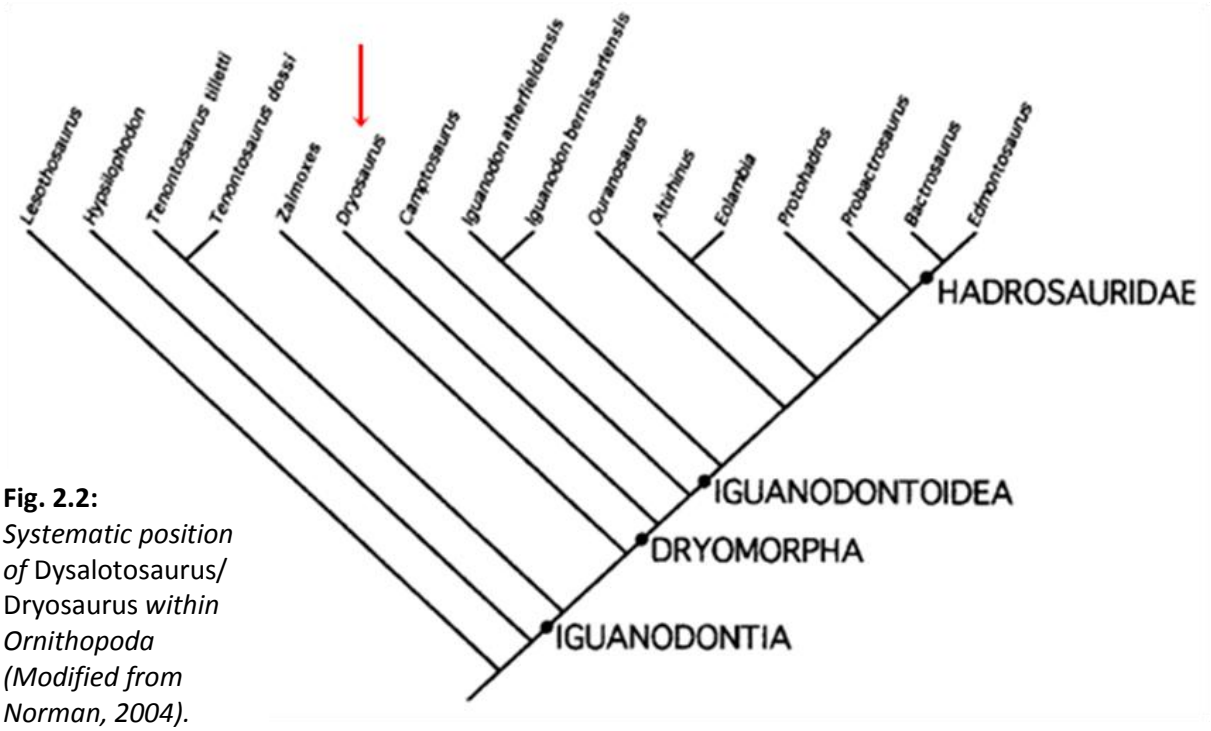

Fig. 2.2: *Systematic position of* Dysalotosaurus/ Dryosaurus *within Ornithopoda (Modified from Norman, 2004).*

Since that time, several large-scaled changes have happened to the phylogeny of Ornithopoda, such as the recognition of the paraphyly of Hypsilophodontidae and Iguanodontidae (e.g. Forster, 1997; Scheetz, 1999; in contrast to Weishampel & Heinrich, 1992), but the position of *Dryosaurus-Dysalotosaurus* within basal Iguanodontia remained stable from now on (Fig. 2.2).

Later studies naturally included more taxa than before so that the Dryosaurids are now either located between *Tenontosaurus* and *Camptosaurus* (Butler et al., 2008b; Weishampel et al., 2003) or between the rhabdodontid clade (including *Zalmoxes*) and *Camptosaurus* (Norman, 2004; Fig. 2.2). Anyway, Dryosauridae is today defined as the sister taxon to Ankylopollexia, which include *Camptosaurus* and all other iguanodontids closer to hadrosaurs than to *Dryosaurus*, and as *Dryosaurus altus* and all taxa more closely related to it than to *Parasaurolophus walkeri* (Butler et al., 2008b).

Cranial characters are naturally the most numerous characters to define the *Dryosaurus* clade, but the pelvic elements and, especially, the femur shows a unique combination of characters, which recently led to the inclusion of a 5th species into the family Dryosauridae. Ruiz-Omenaca et al. (2007) reinterpreted *Callovosaurus leedsi* (based on an isolated, well preserved femur) as the oldest member of the Dryosauridae, which is now securely known from the Middle Jurassic to the Lower Cretaceous. The femoral characters are: bowed shaft; proximally placed pendant 4th trochanter; pit for M. caudifemoralis longus well developed and separated from the 4th trochanter; anterior intercondylar groove; lateral condyle reduced and internally placed; excavation proximal to the medial condyle, which meets the medial surface of the distal end at a sharp edge (Ruiz-Omenaca et al., 2007).

2.2 On the synonymy of *Dysalotosaurus* and *Dryosaurus*

Galton (1977; 1980; 1981; 1983) based the synonymy of *Dysalotosaurus* to *Dryosaurus* mainly on the large amount of similarities between both taxa. Most differences were rather minor and even less significant than intraspecific variation of *Hypsilophodon* according to him (Galton, 1974; 1980). Differences between both dryosaurs, proving the validity of both species, included several cranial and some postcranial characters (Galton, 1981; 1983), such as the posterior extension and connection of the palpebral and premaxilla, the anterior extension of the squamosal, the dorsomedial shape of the maxilla, the shape of the trigeminal foramen, and the shape of the distal end of the humerus and radius as well as of both ends of the ulna. Differences based on length ratios of elements are less significant (Galton, 1981).

I have personally major doubts about his view, because of the number and kind of anatomical differences between the two taxa. Carpenter (1994), for instance, demonstrated that some of the morphological variations in *Hypsilophodon* are either ontogenetic or diagenetic in origin, as e.g. the presence or absence of the gap between the premaxilla and maxilla. In addition, some postcranial differences within *Hypsilophodon* turned out be clearly ontogenetic in origin, such as the differences between the scapulocoracoids and humeri of the small individual R5830 and the large individual R196 (see Galton, 1980: fig. 3C-F; chapter 5), respectively. Another source of doubt on Galton's hypothesis is the surprisingly large number of anatomical differences between both dryosaurids beyond those already noted by Galton (1980; 1981; 1983). Most of them are also not explainable by intrageneric variation. Additional cranial differences are the shape of the frontals, lacrimals, prefrontals, and of the antorbital and infratemporal fenestrae. Further detailed differences are the sutural relationship of the jugal and postorbital to adjacent elements, the portion of the jugal at the antorbital fenestra (note its constancy in *Dryosaurus*; Carpenter, 1994), and the dorsal morphology of the parietal. Even more surprising are significant differences within the postcranium in addition to Galton's observations (1981; 1983), which include both articular ends of the humerus,

the ischiadic articular surface of the pubis, the proximal ischium, morphological details on the femur, the proximal end of the fibula, the shape and articulation of the proximal tarsals, the proximal morphology of the metatarsals, and finally slight shape differences of the proximal articular ends of the first row of pedal phalanges. This itemization already contains more morphological differences than between many Late Cretaceous hadrosaurs. Hadrosaurs are extremely similar in the postcranium and most autapomorph characters are found in the skull (see e.g. Brett-Surman & Wagner, 2007; Prieto-Marquez, 2007). Without the skull, many of these taxa would probably be classified as a single genus, if one would follow Galton's interpretation. Thus, the differences between *Dryosaurus* and *Dysalotosaurus* will most likely contradict the synonymy of them as a single genus. However, further specimens of more members of the Dryosauridae are necessary to assess, how close these two taxa are related to each other and each of them to other family members, respectively.

Another source of confusion is the obvious variation between *D. altus* specimens, which can hardly be explained by ontogeny. One of the most interesting examples is the morphology of the quadrate (Fig. 2.3; see also chapter 4). This element is almost indistinguishable from *Dysalotosaurus* in the *Dryosaurus* holotype YPM 1876 (see Galton, 1983; Janensch, 1955), but the quadrate of the *Dryosaurus* skull CM 3392 has, in contrast, a concave posterior edge of the shaft and a consistent transition between the shaft and cotylar head (Galton, 1983; Hübner & Rauhut, in press.). It is therefore more similar to *Camptosaurus dispar* (see Brill & Carpenter, 2007) than to *Dysalotosaurus* (Fig. 2.3).

In addition, Galton (1983) noted that the maxillary teeth of the YPM specimens of *Dryosaurus* are also more similar to *Dysalotosaurus* than to CM 3392. Furthermore, the shapes of the ilia of different *Dryosaurus* specimens (see Galton, 1981: figs. 3E; 10) are more variable than among all specimens of *Dysalotosaurus*. More intraspecific and non-ontogenetic differences are likely to be found in the future. One possible reason for the differences among *Dryosaurus* specimens could be the presence of two chronospecies within the Morrison Formation, as recently proposed for

Camptosaurus (Carpenter & Wilson, 2008) and *Allosaurus* (Chure, 2000), or vicariance due to the wide paleogeographic distribution of this ornithopod.

Thus, the generic name *Dysalotosaurus* is resurrected for the present and is therefore also used throughout the current study on the ontogeny of the African taxon.

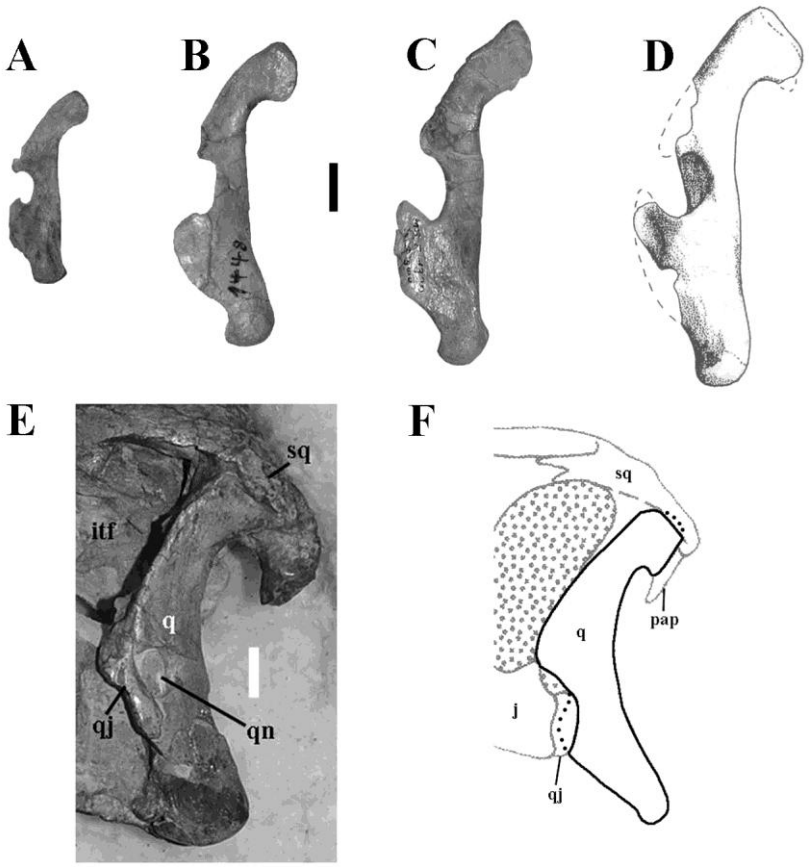

Fig. 2.3: *Lateral view of quadrates of* Dysalotosaurus *(A-C),* Dryosaurus *(D-E), and* Camptosaurus dispar *(F).* ***A*** *– Left quadrate MB.R.1326 (dy 12), slight damage above and below the quadrate notch.* ***B*** *– Left quadrate GPIT/RE/3608, upper jugal wing broken off.* ***C*** *– Left quadrate MB.R.1320 (dy B), ventral damage at cotylar head.* ***D*** *– Right quadrate of YPM 1876, reversed, modified from Galton (1983).* ***E*** *– Left quadrate of CM3392, slight damage at neck of the distal condyle, jugal wing and cotylar head slightly covered by adjacent elements.* ***F*** *– Left quadrate scheme of newly reconstructed skull, modified from Brill & Carpenter (2007).* ***Abbreviations – itf****, infratemporal fenestra;* ***j****, jugal;* ***pap****, paroccipital process;* ***q****, quadrate;* ***qj****, quadratojugal;* ***qn****, quadrate notch;* ***sq****, squamosal. Scale bars = 1cm.* ***F*** *out of scale.*

3. Taphonomy of the *Dysalotosaurus* bearing quarry Ig/WJ

The geology and stratigraphy of the Tendaguru Formation (sensu Bussert et al., 2009) has already extensively been described elsewhere (see e.g. Aberhan et al., 2002; Aitken, 1961; Bussert et al., 2009; Dietrich, 1933; Hennig, 1914; 1937) and will therefore not be repeated here. The history of the German and British Tendaguru expeditions, which both have produced *Dysalotosaurus* bones, was presented by Maier (2003) in unmatched detail. Many details of the ongoing excavation at the Ig/WJ quarry, characterized by Maier (2003), were not available from the common literature, but mainly from correspondences of Hans Reck (see below).

The Ig/WJ quarry is situated within the Middle Dinosaur Member (MDM) in the vicinity of the Kindope creek and settlement about 2.5km NW of the Tendaguru Hill (e.g. Janensch, 1925a; Maier, 2003). Werner Janensch first named the quarry Ig, after he recognized the bones coming from this site as belonging to a small iguanodontid ornithopod (Maier, 2003:59). Hans Reck renamed the quarry after Werner Janensch (WJ) in 1912 (Maier, 2003:89). The age of locality Ig/WJ and of the MDM is Upper Kimmeridgian, which is located well within the Late Jurassic (e.g. Aitken, 1961; Bussert et al., 2009; Heinrich et al., 2001; Schrank, 2005).

Fig. 3.1: *Photo of the quarry Ig/WJ showing the extension and depth of the excavations. One group of workers clear the site from overburden, another group removes the bone-bearing layers in blocks. Modified from Janensch, 1914a.*

3.1 State of the art of quarry Ig/WJ

Most of the facts are given by Janensch (1914c), but additional information was also found in publications of Bussert et al. (2009), Chinsamy-Turan (2005), Heinrich (1998; 1999a; 1999b; 2001), Heinrich et al. (2000), Hennig (1936), Janensch (1914a; 1914b; 1925b; 1955; 1961a), Maier (2003), and Zils et al. (1995).

The sediments of the Ig/WJ-quarry consist of light gray to sometimes reddish fine sandstone and siltstone with clay components and a calcareous matrix. Intra-formational, mostly green clasts of mudstone and caliche nodules occur occasionally as well. Recent research suggests that the dominant fraction of fine sand and siltstone of this quarry is also typical for most parts of the MDM (Aberhan et al., 2002; Bussert et al., 2009), which is thus not characterized mainly by sandy marls, as Janensch (1914c) described. However, the only slightly sandy silt to marl found, which fills the interior of the juvenile skull BSPG AS I 834 (see chapter 4) and the marrow cavities of broken long bones, indirectly confirms Janensch's (1914c) statement that a weaker influence of currents would result in smaller average grain size of the sediment. The intraformational clasts found sometimes within the matrix of the Ig/WJ bonebeds are indicators for their interpretation as channel lag deposits (Bussert et al., 2009). It is therefore very likely that the two bonebeds were deposited in a tidal channel and not on the surface of the coastal plain itself (pers. comm. Bussert & Heinrich, 2010).

Although the taphonomic information of the two bonebeds is highly incomplete, mainly due to hurried removal of specimens and losses during WWII, Janensch (1914c) presented several important observations. He noted the rather sharp restriction of one of the bonebeds and its distinct W-E extension. This 10 to 20cm thick layer is closely packed with bones, but the dominating large long bones (femora, tibiae, fibulae) are often parallel to each other and are orientated approximately in NW-SE direction. This point is unfortunately slightly ambiguous, because he described the long bone orientation as the same as the long axis of the whole bonebed, but the latter was orientated in

W-E direction according to him. A second bonebed was located further NW and was obviously positioned slightly below the first bonebed, separated by only a thin, fossil-free layer. It was less rich in bones and its outlines were less extensive in one direction (Janensch, 1914c). Whether the long bone orientation was the same as in the upper bonebed was not mentioned. The distribution of the two bonebeds and their spatial relationship are slightly confusing because of a correspondence of Hans Reck (published in Heinrich, 2001). He notes that the 'Ig-herd' worked by Hennig until 1911 lies beneath his 'WJ-herd' and has sharply defined borders. It is also located more to the North (Heinrich, 2001:fig. 3). This would mean on the one hand that the Ig bonebed is the lower one, with the less extended long axis and fewer bones described by Janensch (1914c). On the other hand, Janensch and Hennig were already working in both bonebeds and Janensch probably did just not know their full extent and final relationship. This would also explain Janensch's (1914c) statement of the almost complete absence of skull and hand bones and the scarcity of articulated material. There was a definite improvement during 1912 (Maier, 2003:89, 93, 95), although articulated material was also already found in 1911 (Maier, 2003:79). Janensch's (1914c) explanations therefore lead to the assumption that he mainly described the situation until the end of the 1911 season. This is also supported by a note in Maier (2003:94), where he mentioned the extension of the Ig/WJ quarry into the W, E, and S to find the outermost extent of the WJ bonebed in 1912. The occurrence of a third bonebed (Maier, 2003:92) was noted by Reck, but a confirmation and classification has to await the ongoing study of Reck's correspondence. The quantitative extension of the bonebeds is not known, but, judging from a photo from 1912 (see e.g. Heinrich, 2001:fig. 2; Maier, 2003:fig. 15), the whole quarry had an extension of several hundred square meters. The borders of the bone layers were obviously known, because radial trenches were made at the disposition of Reck in 1912 to discover their extensions (Maier, 2003:89, 94), and the bonebed WJ was obviously even completely excavated at the end of the whole campaign (Maier, 2003:95-96).

The bones are densely packed within the bonebeds, often with several bones in superposition. Apart from recent weathering due to surface exposure or close proximity to the

surface at the locality (e.g. long bones are often broken, breaks often refilled by calcareous matrix, corroded articular ends; see Janensch, 1914a; 1914c), no significant differences in the original preservation were found among the material. Bones with burning traces are not the result of preburial fire (Zils et al., 1995), but of a fire during WWII (pers. comm. Schoch, 2010). Many bones are of excellent preservation, although breakage and distortion are also common. Unidentifiable pieces and splinters are generally underrepresented, but a sampling bias cannot be excluded. Among the identifiable specimens, delicate or very long and thin bones (e.g. ribs, neural arches, elements of the skull and hand) are underrepresented compared to more robust bones (e.g. most long bones, girdle elements, vertebral centra, and phalanges of the foot; Hohloch, 2003:27; pers. obs.). Moreover, delicate processes or thin edges are often broken off (e.g. the 4th trochanter of the femur or the edges of the coracoid), but many other specimens have them well preserved and complete. Distortion, shearing or squashing is also often visible, such as in many shafts of long bones. Possible preservational differences between the two bonebeds are not determinable. Isolated bones dominate the material by far, but articulated specimens are still present in the collections (see e.g. chapter 5; Hübner, 2007; Janensch, 1955; 1961b). Skull bones also show the full range of preservation, reaching from isolated pieces to articulated partial skulls, where only the most delicate elements or outstanding processes were missing (Fig. 3.2; chapter 4).

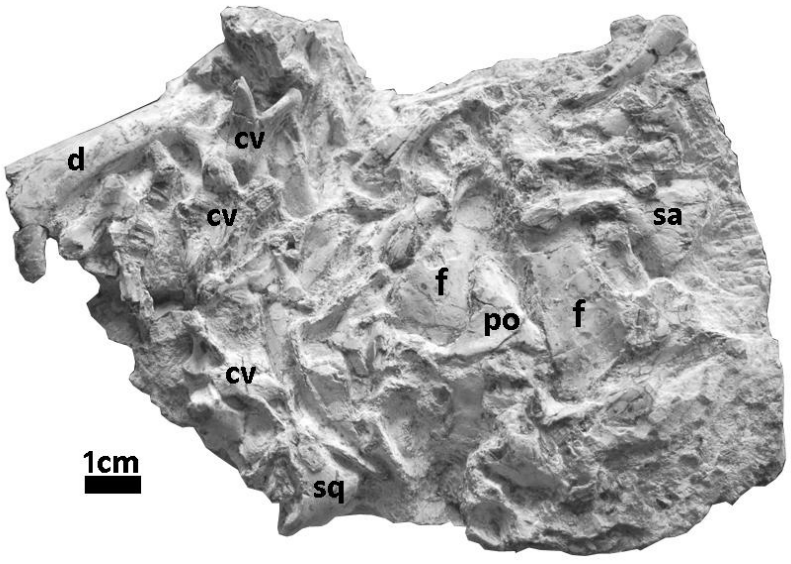

Fig. 3.2: *Associated partial juvenile skull, not yet catalogued. Some of the identified elements are labeled. Housed in the collections of the Staatliches Museum für Naturkunde, Stuttgart.* ***Abbr.:*** *cv – cervical vertebra; d – dentary; f – frontal; po – postorbital; sa – surangular; sq – squamosal.*

Most of the type material, including articulated partial skeletons, was destroyed during WWII (Heinrich, 1999a; Hübner, 2007; Maier, 2003). Another interesting preservational fact concerns the infill of the marrow cavity of long bones. Chinsamy-Turan (2005:15) noted that the infill contains silts of the same type as the surrounding matrix indicating clastic infill during burial. Half-moon-shaped precipitation of prismatic calcite also suggests that the bones may have rolled around some time before consolidation.

Dysalotosaurus was not the only taxon present in the Ig/WJ quarry, but, in contrast to the other dinosaur taxa of Tendaguru, it was found in this quarry only (Janensch, 1925a). Specimens of other dinosaurs found in Ig/WJ include *Kentrosaurus*, *Elaphrosaurus*, and a sauropod (Hennig, 1924; 1936; Janensch, 1914c; 1925b). The discovery of an articulated skull of a theropod in the upper bonebed was also reported, but if it was lost or misidentified is not known (Maier, 2003:92-93). Recent preparation of bonebed blocks in the Museum für Naturkunde Berlin further provided theropod teeth and fragmentary remains of lepidosaurs, pterosaurs, crocodiles, mammals, and several microfossils (see Heinrich, 2001 and references therein). Dietrich (1933) mentioned the rare preservation of a fresh water gastropod (*Physa* sp.).

Another important observation is the size distribution of *Dysalotosaurus* femora, which shows two distinct peaks. This was first demonstrated by Heinrich (1999a) by using femur length. This size distribution is now confirmed by the measurement of the most abundantly preserved distances among the *Dysalotosaurus* material, which includes the lateromedial widths of the femoral and tibial distal articular ends (Fig. 3.3). It is now also possible to roughly estimate the number of individuals preserved in the two bonebeds. According to 93 measured right femora (including all thin sectioned specimens), which is treated as the minimum number of individuals (MNI) for both bonebeds, the loss of many specimens during WWII, and many not usable specimens for measurements, the number of individuals was originally far beyond 100.

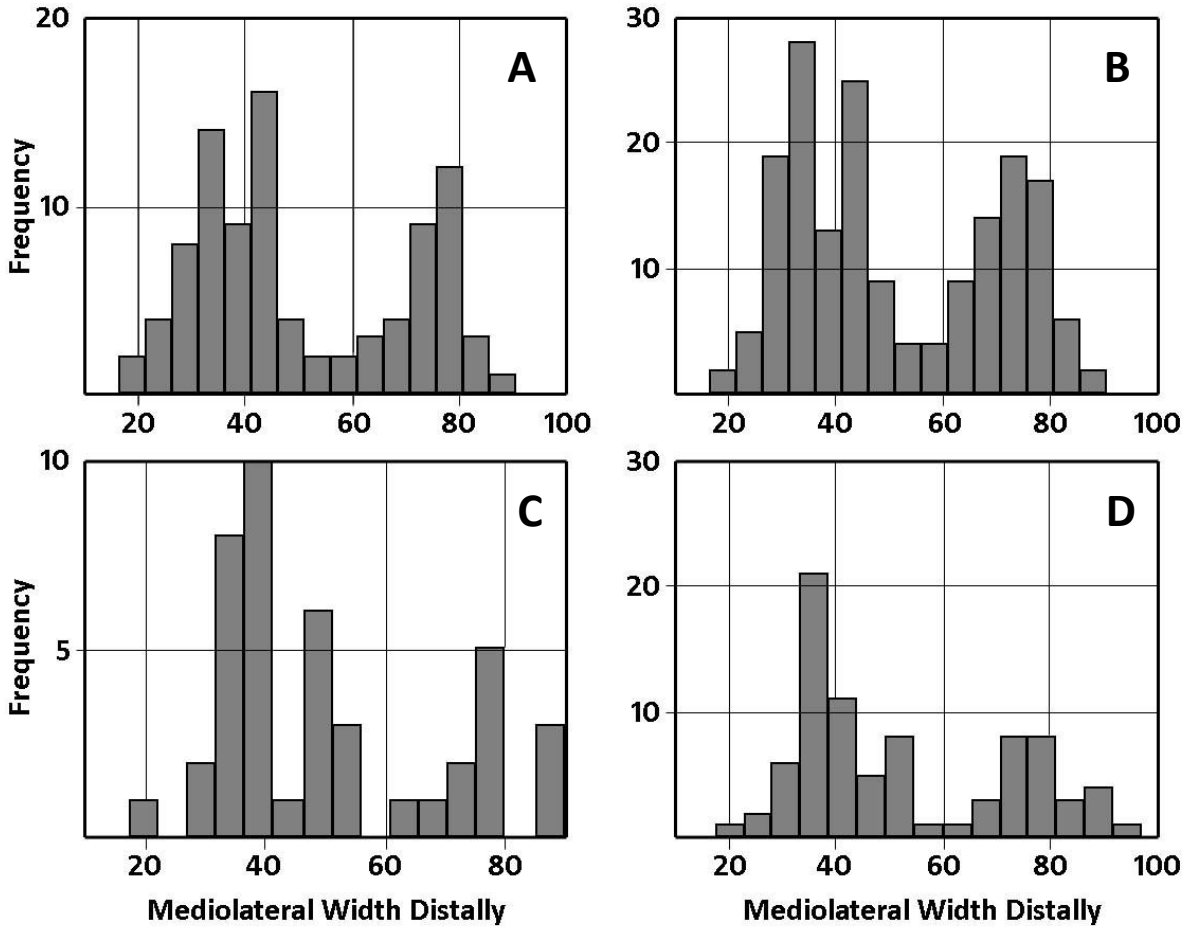

Fig. 3.3: *Size-frequency distributions of femora and tibiae calculated from the mediolateral width of their distal articular ends.* ***A*** *– Distribution of all measured right femora.* ***B*** *– Distribution of all measured femora (left and right).* ***C*** *– Distribution of all measured right tibiae.* ***D*** *– Distribution of all measured tibiae (left and right). Note the underrepresentation of mid-sized individuals.*

3.2 Discussion

Following the bonebed classification of Eberth et al. (2007), the Ig/WJ quarry contains two macrofossil bonebeds. Although many skull bones, teeth, vertebrae and phalanges are smaller than 5cm, the majority of bones are above this border. Moreover, typical microfossils, such as jaw fragments and teeth of mammals, are even rarer, since hundreds of kilos of matrix had to be dissolved to find a small number of them (e.g. Heinrich, 1998; 1999b; 2001).

The Ig/WJ bonebeds are also of multitaxic type, because, in comparison with the fossil content of the other locations within the MDM, they are rich in number of taxa. The bonebeds have

produced a minimum of four dinosaur taxa (*Dysalotosaurus*, *Kentrosaurus*, *Elaphrosaurus*, one sauropod), but a second theropod and a second sauropod taxon are likely (e.g. Heinrich, 2001; Hennig, 1936; Janensch, 1914c; 1925b; 1955; Maier, 2003:92-93). The extensive dissolution of matrix further revealed a pterosaur, a lizard, a crocodile, and three mammal taxa (Broschinski, 1999; Heinrich, 2001; Unwin & Heinrich, 1999), which extent the number of taxa to a minimum of ten. The possibly even higher number of taxa supports the classification of Ig/WJ as multitaxic bonebeds with a high diversity (see Eberth et al., 2007), especially compared with most of the other locations of the MDM. The bones of *Dysalotosaurus* also dominate over the specimens of all other taxa by far (more than 50%) in the number of identifiable specimens (NISP) and minimum number of individuals (MNI) so that the Ig/WJ bonebeds can further be classified as monodominant (see Eberth et al., 2007:114, fig. 3.2).

The first interpretation of the Ig/WJ bonebeds proposed a mass mortality event of a single *Dysalotosaurus* herd (Janensch, 1914c). Janensch based his view mainly on the mass accumulation of a high number of individuals of different ages. He further suggested that there was almost no post-mortem transport of bones due to the often excellent preservation of delicate bones and processes and the very restricted extension of the bonebeds. The adjusted orientation of many long bones were interpreted as the result of wave action and the high degree of disarticulation as the result of a reworking event (strong waves or a tide), which had reopened the first graveyard after the soft parts of the bodies had already decayed (Janensch, 1914c).

Reck (1925) challenged this view, because he never found evidence for storm deposits or other sediment layers that would indicate catastrophic events. According to him, the sediments maintained the fine clastic character throughout the profile, and the bones were rather irregularly distributed vertically. Russell et al. (1980) interpreted the mass accumulation of *Dysalotosaurus* (the *Kentrosaurus* locations as well) as the result of attritional mortality during a longer period of drought, where these animals were concentrated on spots of more plentiful vegetation und suffered augmented death by overexploitation. The remains were then concentrated by water flow once

more humid conditions had returned. Heinrich (1999a) was also more inclined to the attritional interpretation of the *Dysalotosaurus* bonebeds. He pointed out that the size distribution of femora is U-shaped, which is generally treated as the result of attritional mortality (Lyman, 1994). A catastrophic event would rather be represented by an L-shaped size distribution. In addition, an attritional scenario would also fit well to the taphonomic conditions of the sauropod localities.

The taphonomic characters of the Ig/WJ bonebeds are often unambiguous when considered separately, but some of them contradict each other at first sight resulting in the interpretation as either an attritional or catastrophic mortality pattern. It is also important to know whether the locality represents a single herd or not. Thus, the significance of each taphonomic character will be assessed separately here, in the hope to find a conclusive solution.

Number of localities and individuals: It is noteworthy that *Dysalotosaurus* is the only identifiable dinosaur taxon of the Tendaguru Formation, which is only known from a single locality, but at this place in an extraordinarily high number of individuals (e.g. Heinrich, 1999a; Janensch, 1914c; 1925a). *Kentrosaurus*, the other dinosaur taxon known from mass accumulations, is known from approximately 30 localities, including 14 from the MDM (Hennig, 1924). Sauropod taxa are known from numerous localities anyway, but even the rare theropod *Elaphrosaurus* is known from at least two localities (Janensch, 1925b). *Dysalotosaurus* is therefore a rather rare component of the dinosaur fauna of the MDM, despite its high number of individuals. This was either because this taxon was generally rarely visiting the coastal plains, or it was just too lightly built to commonly get mired in the mud, as was suggested for several sauropod and *Kentrosaurus* localities (Hennig, 1924; Janensch, 1914c; 1961a). I am not aware of any note that limb bones of *Dysalotosaurus* were found upright in the sediment or that certain skeletal complexes were in such a high degree under- or overrepresented, as would be the case, if the animals died trapped in the mud (see Hennig, 1924; Janensch, 1914c; Sander, 1992; Varricchio et al., 2008). The mass accumulation of a single dinosaur taxon usually rare or absent elsewhere in the formation (independently of the reason), indicates that it was the result of a short-term mass death event.

Abundance of taxa: As mentioned above, the Ig/WJ bonebeds are characterized as multitaxic and monodominant. Although several other taxa are represented in the bonebeds, they are only a minor component compared to the extraordinarily high number of specimens of *Dysalotosaurus*. Most of them are also highly fragmentary or often only known from single specimens. The occurrence of other dinosaur taxa can be treated as the normal 'background' macrofossils, because they were also found in numerous other localities, sometimes only a few hundred meters away (see Janensch, 1925a). The even rarer microvertebrate remains are likely to be found in other localities as well, as was shown for pterosaurs and mammals (Dietrich, 1927; Reck, 1931). So, only *Dysalotosaurus* appears to be unusual in its abundance. Monodominant bonebeds are often interpreted as either catastrophic or short-term mass death events or as multiple (attritional) death events, but at a specific site (Eberth et al., 2007). Monospecific or monodominant bonebeds of other dinosaurs are well known and most of them are interpreted as the result of a mass mortality event of a single herd (e.g. Brinkman et al., 2007; Currie & Dodson, 1984; Eberth & Getty, 2005; Hennig, 1924; Myers & Fiorillo, 2009; Rogers, 1990; Schwartz & Gillette, 1994; Varricchio & Horner, 1993). Thus, the monodominant taphonomic mode of Ig/WJ supports the interpretation as a mass death event of a *Dysalotosaurus* herd.

Deposition and spatial arrangement: One important fact is the deposition of *Dysalotosaurus* in two distinct bonebeds, separated by a thin bone-free layer (Heinrich, 2001; Janensch, 1914c). Two scenarios are proposed, which might explain this depositional setting. (1) The two bonebeds represent two mass death events of different *Dysalotosaurus* herds that happened at exact the same spot, under the same circumstances, and with the same following taphonomic history (see below). (2) The bonebeds originated from a single mass death event of a single herd.

The assumptions of the first proposal are unnecessary in the latter. The herd (or most of it) drowned within a tidal channel, probably during a spring tide. The herd was shallowly buried, but after a short time (e.g. spring tides happen nearly every two weeks) another tide or flood reopened the graveyard and swept a large part of the carcasses with it. At the return point of the tide, there

was no current at the site, so that the bone-free transitional layer could be depositing (pers. comm. Bussert, 2010). The returning tide would then finally leave the carried carcasses behind, making up the upper bonebed.

However this may be, the deposition within a tidal channel would at least explain the restricted location and extension of the bonebeds, because the much higher aquatic saturation of the channel bottom would be an ideal trap for crossing animals. Signs for mud trapping of *Dysalotosaurus* are not known (as in e.g. Sander, 1992; Varricchio et al., 2008), but the expected frequent reworking by tide currents or slight wave action within the tidal channel surely would obscure them very fast. This would partly also explain the absence of *Dysalotosaurus* anywhere else in the Tendaguru Formation. These animals were too lightly built to get mired onto the plain itself, as it was the case with the much more heavy sauropods and stegosaurs. Even if *Dysalotosaurus* individuals have died on the plain, the taphonomic environment obviously favored large and robust bones, which explains its absence elsewhere in the Tendaguru Formation (though small bones of this taxon might also go unrecognized in other localities). This pattern might also be one reason for the underrepresentation of theropod skeletal remains in the Tendaguru Formation and is similar to many other dinosaur bearing formations (e.g. Hell Creek Formation, White et al., 1998).

There is no significant vertical gradient in the grain size of the sediment surrounding the bones. Reck (1925) also noted the absence of vertical sorting of bones by size, element type, or orientation. Thus, the two bonebeds are not the result of a main flood of a river as in the *Centrosaurus* Bonebed BB43 at Dinosaur Provincial Park (Ryan et al., 2001) or the titanothere assemblage of Southern Wyoming (Turnbull & Martill, 1988), for instance. However, the sharp boundary and marked W-E extension of at least one of the bonebeds (most likely the upper bonebed WJ, see above) is probably the result of current activity within the tidal channel approximately perpendicular to the ancient shoreline. Many long bones have also roughly similar orientations. Thus, the lower, less sharply defined bonebed (Ig) would represent the original graveyard and the upper, extended, and sharply defined bonebed (WJ) would represent the parautochthonous, secondary

graveyard, which was formed by the reworking event. No information is available about differences in arrangement and degree of disarticulation between the two bonebeds. However, nearly all stages of disarticulation seemed to be present in both, reaching from nearly complete articulated skeletons to isolated single bones (e.g. Heinrich, 1999a; Janensch, 1914c; Maier, 2003).

In summary, judging from the depositional setting of the Ig/WJ quarry, the bonebeds represent the mass death of either one or two *Dysalotosaurus* herds. In the latter case, they were at least buried at the same place. It might be worth pointing out that crossing of rivers and lakes by recent gregarious ungulates can also lead to the death of more than one group within a season in approximately the same spot (e.g. Capaldo & Peters, 1995), but the 'one-event-scenario' seems more likely for the Ig/WJ quarry.

Preservation and sorting of bones: Apart from weathering due to recent exposure, the surface of the bones is well preserved and no significant preburial weathering can be detected (weathering stage 0, Behrensmeyer, 1978; Fig. 3.4). Rogers (1990) mentioned two ways of attenuated weathering: fast burial after death or mildly weathering circumstances, such as in a swamp (Behrensmeyer, 1978). The first alternative is more likely for the Ig/WJ bonebeds, because of the lack of preburial scavenging (see below), the restricted extension and sharp borders of the bonebeds, the close and often piled arrangement of bones, and the rather open and exposed paleoenvironment (Aberhan et al., 2002). However, breakage of bones is very common (Fig. 3.4), partly because of the destructive dry-wet-dry alternations of the surrounding sediment (Janensch, 1914a), especially in such clay rich deposits (Behrensmeyer, 1975:482). Many long bones, for instance, lack also at least one of their articular ends, but it cannot be excluded that this is partly the result of the split-up of blocks during excavation.

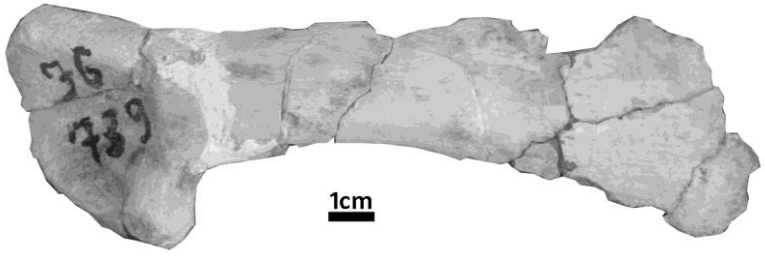

Fig. 3.4: *Left scapula MB.R.1707, demonstrating the often excellent preservation of the bone surface, but also the common breakage. Most scapulae are even only known by distal articular ends.*

Nevertheless, even broken bones are mostly well preserved and can still possess complete delicate processes. Distortion and squashing, especially of long bone shafts, is also common. The hollow marrow cavities of long bones are often either completely or partially filled with silt. In the latter case, one half of the bone is usually filled with mud, and the rest is often filled by grown minerals, mainly calcite. This mirrors the different stages of breakage of bones between completely broken off parts to only weak cracks.

Nearly all skeletal elements of *Dysalotosaurus* are known, but the overrepresentation in favor of more robust bones, such as elements of the girdles, limbs, and vertebral centra, indicates some sorting. The composition of over- and underrepresented elements seems to be similar to the Campanian bonebed at Jack's Birthday Site (Varricchio, 1995:305) and differs significantly from classic fluvial sorting patterns (e.g. Aslan & Behrensmeyer, 1996; Fernandez-Jalvo & Andrews, 2003; Voorhies, 1969). The absence of signs of preburial weathering and abrasion shows that the breakage and sorting of bones was not due to a long transport of bones. The carcasses were then either transported still intact short after drowning and deposited at a neck or barrier within the channel, or they were buried approximately at the location of death itself in a very short time. The extensive disarticulation of skeletons and the loss of many small and/or delicate bones was then induced by trampling, one or more reworking events within the channel (tidal currents or freshwater floods due to heavy rainfall, wave action), and repeated shrinkage and swelling of the clay components within the sediment because of frequent changes in the groundwater level. Signs of trampling, such as sub-parallel scratch marks (Fiorillo, 1987), are unknown, but its impact could be just attenuated by the high fraction of soft clay in the sediment (Fiorillo, 1987; Rogers, 1990:403). Trampling could also be one main reason for the common distortion and squashing of large bones (e.g. scapular blades, long bones) compared to its rarity in small and blocky bones (e.g. vertebral centra, phalanges, proximal tarsals). Scavenging is the only taphonomic factor, which can be treated as insignificant, because scratch and bite marks are unknown and teeth of theropods and crocodiles are a very rare

component of the fossil content (in contrast to e.g. the *Plateosaurus* bonebeds, see Sander, 1992; but see Turnbull & Martill, 1988:103-104).

Summing up, the preservation of the bones suggests a mixture of several taphonomic impacts on the bonebeds, where none of them can be securely excluded. These are trampling, reworking in various ways, internal sediment movements (clay fraction), and pressure of overlying sediment and densely packed other bones. In addition, preservational alteration can also be added to the taphonomic history, such as in-depth tropical weathering in more recent times, and the split-up of blocks of matrix during excavation. The close proximity of the two bonebeds and obviously absent preservational differences between them favors the mass death of only one *Dysalotosaurus* herd in a single event compared to the proposal of two events/herds. Both bonebeds are classified as autochthonous or parautochthonous. Finally, the challenge of a mass death of a herd by Reck (1925) due to the absence of storm deposits or other sedimentary signs of a catastrophic event is no longer problematic, because mass death events do not necessarily need extreme high energy impacts on the environment (e.g. Rogers, 1990; Sander, 1992; Varricchio, 1995; Varricchio & Horner, 1993).

Size-frequency distribution: The respective distribution of the most commonly preserved measurable distances in *Dysalotosaurus* (distal lateromedial width of the femur and tibia; Fig. 3.3) is similar in shape to a typical U-shaped distribution, which is often interpreted as the result of attritional mortality (e.g. Heinrich, 1999a; Lyman, 1994; Voorhies, 1969). A catastrophic mass death event is expected to have a left-skewed L-shaped size distribution representing a living population or herd. This would be in strong contrast to the sedimentological and preservational pattern for *Dysalotosaurus* discussed above, which indicate one or two mass death events. However, the application of the shape of size distributions is apparently not unambiguous, not even for large mammals. Klein (1982) has shown that the L-shape and the U-shape of size distributions fit very well to the catastrophic and attritional model, respectively, when the females of the investigated mammal species have one offspring per year. When females produce more than one offspring per year, the attritional size distribution is L-shaped as well, so that a differentiation between

catastrophic and attritional mortality is not possible anymore (Klein, 1982). The size distribution of *Dysalotosaurus* with assumed more than one or two offspring per year for each female should therefore be also less significant. Furthermore, some clearly catastrophic mammal assemblages, such as fossil rhinos of the Poison Ivy Quarry, Nebraska (Voorhies, 1985), or titanotheres from Wyoming (Turnbull & Martill, 1988), have clearly differing shapes of their size distribution. The former has a U-shaped distribution (despite of the catastrophic death by volcanic ash) and the latter a tri-modal distribution. On the other hand, the attritional assemblages of *Teleoceras* in Florida are not U-shaped, as expected, but have a peak among the young adults, especially young males (Mihlbachler, 2003).

These examples reveal that preservational biases and social habits obviously have a significant impact on the fossil size distribution. Juveniles are underrepresented in many bonebeds, because they are often less likely to be preserved due to scavenging, hydraulic transport, or they were simply born at another place or were less affected by natural traps (Heinrich, 1999a; Hulburt Jr., 1982; Klein, 1982; Kurten, 1953; Mihlbachler, 2003; Sander, 1992; Varricchio & Horner, 1993; Voorhies, 1969).

Another difference to the typical size distributions of most ungulates is the relative time of sexual maturity. In many ungulates, this takes place already after one or two years in smaller species and is only significantly delayed above 5 years in larger species (e.g. Voorhies, 1969; http://ladywildlife.com). In dinosaurs, the time of sexual maturity usually took also place after more than two years (see Lee & Werning, 2008) and this was probably also the case for *Dysalotosaurus* (chapter 6). Bearing in mind that the time of sexual maturity (or the first rutting season for young males) can lead to banishment from the herd and/or to higher stress-induced mortality (see e.g. Jarman, 2000; Jarman & Jarman, 1973; Owen-Smith, 1993; Proaktor et al., 2008; Turnbull & Martill, 1988), the resulting gap (catastrophic assemblage) or peak (attritional assemblage) within the size distribution would be further to the right in dinosaurs than in most smaller ungulates (e.g. deers) and more similar to larger ungulates (e.g. rhinos). Indeed, the death assemblage of *Dysalotosaurus* shows

a gap approximately within the medium-sized individuals, similar to a titanothere assemblage (Turnbull & Martill, 1988) and to the respective peak in an attritional *Teleoceras* assemblage (Mihlbachler, 2003).

In the end, the simple assignment of the shape of a size-frequency distribution to either a catastrophic or attritional mortality pattern is problematic. Taphonomic influence on the assemblage and social habits of the species can both lead to the under- or overrepresentation of age classes. In the case of *Dysalotosaurus*, the rather M-shaped size distribution is clearly linked to a catastrophic mortality event and not to an attritional mortality pattern. The lack of the smallest age/size class can be explained by the location of the breeding site at another location (Hulburt Jr., 1982). This is further supported by the complete absence of egg shells. The underrepresentation of small juveniles is the result of sorting in favor of larger and more robust bones. The significant gap within medium-sized individuals could represent the time of sexual maturity, which can lead in herds of modern ungulates to banishment from the herd or higher mortality due to higher stress. In a catastrophic assemblage, this would lead to the underrepresentation of this age/size class. The second peak of the size distribution of *Dysalotosaurus* is then assignable to the successful reproductive adults (see chapter 6.7.3).

3.3 Conclusions

The preservation of the ornithopod dinosaur *Dysalotosaurus* in only one location within the Tendaguru Formation in at least two adjacent mass accumulations is rather unusual, compared to the occurrence of the other dinosaur taxa from the Formation. The first proposal to explain this special preservation was the mass death of a single herd. This view was later challenged, mainly due to the lack of high-energy indicating sediments, the presence of two bonebeds, and the U-shaped size distribution, which might indicate attritional death of individuals. However, despite the serious lack of information regarding detailed sedimentological profiles, absolute dimensions of the

bonebeds, the detailed spatial arrangement of isolated bones, and stages of disarticulation, the reevaluation of the known taphonomic characters now supports the first interpretation. The preservation of the specimens indicates relatively fast burial of the carcasses without significant pre-burial transport or scavenging. No preservational difference between the two bonebeds and their close proximity to each other make the origin from a single herd more likely than the origin from two distinct mass deaths. This is further supported by the complete absence of *Dysalotosaurus* elsewhere in the Tendaguru Formation. There would also be a need for too many coincidences (short time between the events, same place, exactly the same taphonomic history) to interpret the two bonebeds as two distinct herds. Furthermore, the possible presence of a third bonebed makes the death of three herds at this location even less likely. The similarity of the size distribution of individuals to the U-shaped attritional profiles is also ambiguous, because taphonomical impacts and social habits can have a significant influence on the representation of age/size classes within the group.

Thus, the two bonebeds of *Dysalotosaurus* are most likely the remains of a single herd, which has died and was buried in a tidal channel and was split up in two bonebeds by a single strong reworking event (spring tide) shortly after death. The youngest age class is not represented, because the breeding season had not yet started and/or the breeding location was somewhere else. The underrepresentation of small age classes was induced by the preservational bias towards larger and more robust bones and the underrepresentation of medium-sized individuals was probably the result of banishment or higher mortality rate of this age class due to the time of sexual maturity.

4. Cranial ontogeny of *Dysalotosaurus lettowvorbecki* with a description of an articulated juvenile skull

4.1 Introduction

There are currently four incomplete skulls known from three German collections (Hübner, 2007). Two specimens, labelled as “dy A” and “dy B” by Janensch (1955), are kept in the Museum für Naturkunde in Berlin. Together, they provide nearly 90% of all skull elements. A disarticulated juvenile skull, housed in the Staatliches Museum für Naturkunde in Stuttgart, was recently identified (see Fig. 3.2). The juvenile skull, which is the main subject of this study, is kept in the Bayerische Staatssammlung für Paläontologie und Geobiologie in Munich. There are also many isolated skull elements kept in collections in Berlin, Göttingen, Stuttgart, and Tübingen, mainly representing elements of the upper and lower jaws, the skull roof, and the occiput.

Two authors (Galton, 1983:210; Weishampel, 1984:89) mentioned the Munich skull in their studies previously, but the specimen has neither been described nor illustrated in detail so far. However, it is significant because of its obviously juvenile growth stage and the preservation of skull elements that were formerly unknown in *Dysalotosaurus*, mainly in the mandible.

In the following chapter, a complete description of this skull is provided and is compared with all known skull elements of *Dysalotosaurus* in the light of possible ontogenetic variation. Finally, the results are used for comparison within Ornithopoda to get new insights into the ontogeny, phylogeny, and taxonomy of this group.

4.2 Material and methods

The material studied here consists of a partial, articulated skull and anterior most cervical vertebrae of a juvenile individual of *Dysalotosaurus lettowvorbecki*, kept in the collections of the Bayerische Staatssammlung für Paläontologie und Geobiologie, under specimen number BSPG AS I 834. As in the cases of material kept in collections in Stuttgart, Tübingen, and Göttingen, this material had obviously been sent for preparation from Berlin to Munich before World War II, but records of the interchange of specimens were destroyed both in Berlin and in Munich.

In addition to this specimen, the skull remains of older individuals described by Janensch (1955) were studied in the collections of the Museum für Naturkunde in Berlin, and further, mainly isolated, but sometimes associated skull remains of this taxon were examined in the collections of the Staatliches Museum für Naturkunde Stuttgart, the Institut und Museum für Geologie und Paläontologie of the University of Tübingen, and the Geowissenschaftliches Zentrum, University of Göttingen. For the description, the specimen was additionally prepared, using a combination of chemical and mechanical preparation, and computed tomography (CT) scans were performed in two hospitals in Munich (Klinikum Rechts der Isar and Klinikum Großhadern). The machines (SOMATOM Sensation 64, Siemens, with Syngo VA 11a software) were medical scanners. The obtained data provided two-dimensional image slices (0.4-mm slice intervals) with a resolution adequate to interpret the bones inside the skull (e.g. pterygoids and ectopterygoids).

To reveal possible non-obvious ontogenetic variations, which are also not determinable by using simple ratios of two variables, statistical calculations of measured distances (see Appendices I and II for details) were carried out, using multivariate allometry analyses (MAA) with the software PAST (Palaeontological Statistics, version 1.38; Hammer et al., 2001). This method is based on the allometric equation $\ln y = a(\ln x) + b$ (see Hammer & Harper, 2006:79; Huxley, 1932), where x and y are measurements, a is the allometric coefficient, and b is the arbitrary constant of integration. A relative increase of proportions to other structures (positive allometry) is represented by coefficients

larger than one, whereas coefficients smaller than one indicate a relative decrease of proportions (negative allometry). In the case of a coefficient equal to one, isometric growth of proportions is indicated. By using MAA, the automatically log-transformed data set will be subjected to principal component analysis (PCA) to get a first principal component (PC1; Hammer & Harper, 2006: 91). This PC1 can be used as a multivariate linear regression line, and thus as a size axis (in case the variation value is larger than 80%). The actual allometric coefficient (*a*) for each variable is then estimated by dividing the PC1 loading for this variable by the mean value of all PC1 loadings. A confidence interval of 95% was estimated for each coefficient. If the complete interval is different from one, the allometric coefficient of this variable is significant at $P < 0.05$. Specimens with missing values were excluded from the analyses.

The stability of significant allometric coefficients was tested by plotting the data set of the variable concerned bivariate with every other variable (i.e. measured distance) of this element. If the relative allometry of this variable is retained in comparison with either other variable, the general result of the combined data set of all variables was accepted for the analysis. However, all statistical results should be regarded with caution because the number of available specimens is mostly below ten.

The skull reconstruction of BSPG AS I 834 (Fig. 4.1C, D) was carried out using a combination of photos and CT data from the skull itself, and, in the case of incomplete or partially covered elements, by the calculation of absolute dimensions derived from other specimens of different sizes. Thus, for example, the total length of the maxilla and the total height of its laterodorsal process were calculated from known dimensions of other isolated maxillae, and the total height of the postorbital is known only from two-dimensional CT images of the skull.

Unfortunately, nothing is known about the snout region (premaxillae, nasals, lacrimals, prefrontals, palpebrals, and predentary), so the only confirmed landmarks for the reconstruction were articular facets and probable suture connections on the known elements and the arrangement

of sutures in the reconstruction of Janensch (1955) (see Fig. 4.1A, B). The dimensions and shape of the palpebral are completely speculative. The unknown quadratojugal was not illustrated.

A list of all measured skull elements, including the elements of the described skull BSPG AS I 834, and all measurements taken for allometric statistics are listed in Appendices I and II.

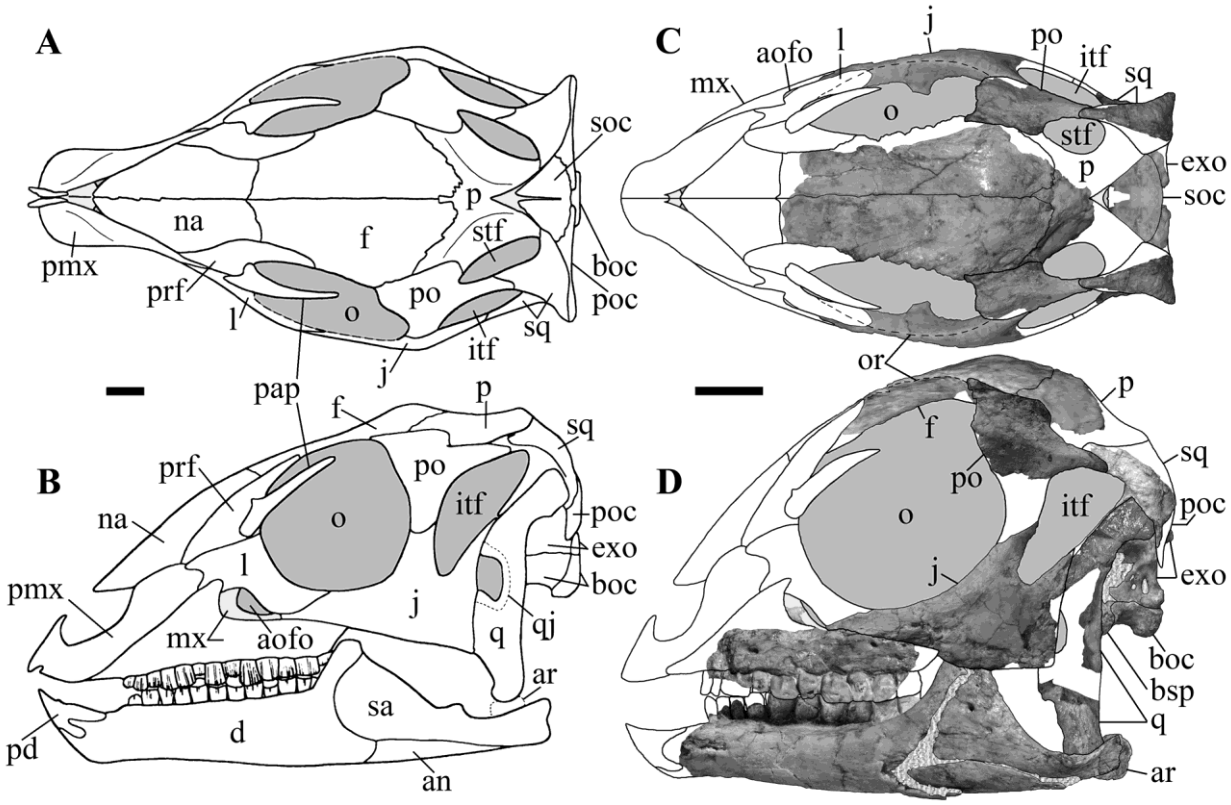

Fig 4.1: *Reconstruction and comparison of the skull BSPG AS I 834 with the reconstruction of an older individual (modified from Janensch, 1955). The reconstruction of the juvenile skull was carried out by the combination of the frontoparietal plate, the left postorbital, the left squamosal, a combination of the left and the head of the right quadrate, the left jugal, the braincase, the right maxilla, the left laterodorsal maxillary process, and, finally, the right lower jaw with the left articular. Dark grey illustrates the skull openings, light grey illustrates the inner views of, e.g. the maxilla or the frontal, and the grayish pattern on the lower jaw and the braincase illustrates sediment.* ***A*** *– Dorsal view of the skull reconstructed by Janensch (1955).* ***B*** *– Left lateral view of the skull reconstructed by Janensch (1955).* ***C*** *– Dorsal view of the reconstruction of BSPG AS I 834. For the unlabelled elements see the corresponding elements in A.* ***D*** *– Left lateral view of the reconstruction of BSPG AS I 834. For the unlabelled elements see the corresponding elements in B. Note the difference of the mandibular articulation between B and D, for example. Furthermore, Janensch (1955) indicated the unknown quadratojugal in B. This is omitted here. See the next page below for a list of the abbreviations. Scale bars = 1cm.*

Institutional abbreviations:

BSPG, Bayerische Staatssammlung für Paläontologie und Geobiologie, München; **CM**, Carnegie Museum, Pittsburgh; **GPIT**, Institut und Museum für Geologie und Paläontologie of the University of Tübingen; **GZG**, Geowissenschaftliches Zentrum, University of Göttingen; **MB**, Museum für Naturkunde, Berlin; **SMNS**, Staatliches Museum für Naturkunde, Stuttgart; **YPM**, Peabody Museum, Yale College, New Haven.

Anatomical abbreviations:

An – angular; **aofo** – antorbital fossa; **ar** – articular; **atic** – intercentrum of atlas; **atna** – neural arc of atlas; **ax** – axis (epistropheus); **boc** – basioccipital; **bsp** – basisphenoid; **co** – coronoid; **d** – dentary; **ect** – ectopterygoid; **exo** – exoccipital; **f** – frontal; **hy** – hyoid; **inat** – intercentrum of atlas; **itf** – infratemporal fenestra; **j** – jugal; **l** – lacrimal; **lf** – lacrimal facet; **lsp** – laterosphenoid; **mx** – maxilla; **na** – nasal; **o** – orbit; **or** – orbital rim; **p** – parietal; **pap** – palpebral; **pat** – proatlas; **pd** – predentary; **pf** – parietal facet; **pmx** – premaxilla; **po** – postorbital; **poc** – paroccipital process; **pof** – postorbital facet; **pra** – prearticular; **prf** – prefrontal; **prff** – prefrontal facet; **pro** – prootic; **ps** – parasphenoid; **pt** – pterygoid; **q** – quadrate; **qj** – quadratojugal; **qf** – quadrate foramen; **qw** – quadrate wing; **sa** – surangular; **saf** – surangular foramen; **soc** – supraoccipital; **spl** – splenial; **sq** – squamosal; **stf** – supratemporal fenestra; **to** – tooth; **ubr** – upper braincase; **V** – N. trigeminus; **VII** – N. facialis; **X** – N. vagus; **XIIa,p** – N. hypoglossus anterior and posterior.

4.3 Description

4.3.1 General Preservation

As preserved (Figs. 4.2 and 4.3), the skull has a total length of 67 mm, a total width of 33 mm, and a total height of 65 mm with the axis, and 55 mm without the axis. The overall aspect of skull BSPG AS I 834 implicates preservation in a nodule. All elements or parts of elements that originally extended beyond the border of this nodule were lost or broken off. In contrast, apart from surface or edge corrosion, elements located inside or aligned along the nodule borders are well preserved. Some elements unknown before, especially in the lower jaws, are preserved in this specimen,

including the articulars, splenials, prearticulars, and the right coronoid (Fig. 4.3B, D). Additionally, the relative position of paired skull elements to each other suggests an anterior displacement of the elements of the left side in comparison with the right side of the skull. The snout is completely crushed, and the lacrimals, nasals, palpebrals, predentary, prefrontals, and the premaxillae are lost. The whole braincase is displaced forward and a bit to the right (Fig. 4.2C, D). Both laterosphenoids are disarticulated from the braincase and are visible on the right side of the preserved skull (Fig. 4.3A, C). The left frontal is nearly complete and is still in articulation with the laterally eroded right frontal. Together with the articulated left anterior relict of the parietal (Fig. 4.1C), the frontals are displaced forward and collapsed into the skull, with their anterior ends pointing downwards and slightly to the right side. Thus, the dorsolateral process of the left maxilla has been broken and folded on to the right (Fig. 4.3A, C). The preserved part of the left squamosal is rotated beneath the left frontal. The left quadrate, still associated with the squamosal, is moved forwards between the left jugal and the braincase. The ventral part of the quadrate has been crushed into the posterior edge of the left surangular (Fig. 4.2A, B). There is no sign of a quadratojugal in the skull. Finally, the first cervical (atlas) is removed from the occiput and lies partly articulated with the second cervical (axis) between the posterior ends of the lower jaws (Figs 4.2C, D, 4.3B, D).

4.3.2 Dermal skull roof

Maxilla (Figs 4.1D, 4.2 and 4.3; see Appendices I and II for measurements): Both tooth-bearing main bodies of the maxillae are preserved, although slightly displaced, inclined to the left side, and more or less parallel with each other at about 30–45°. The right maxilla consists only of the incomplete tooth-bearing main body. Its dorsal processes and the posterior and anterior ends are broken off.

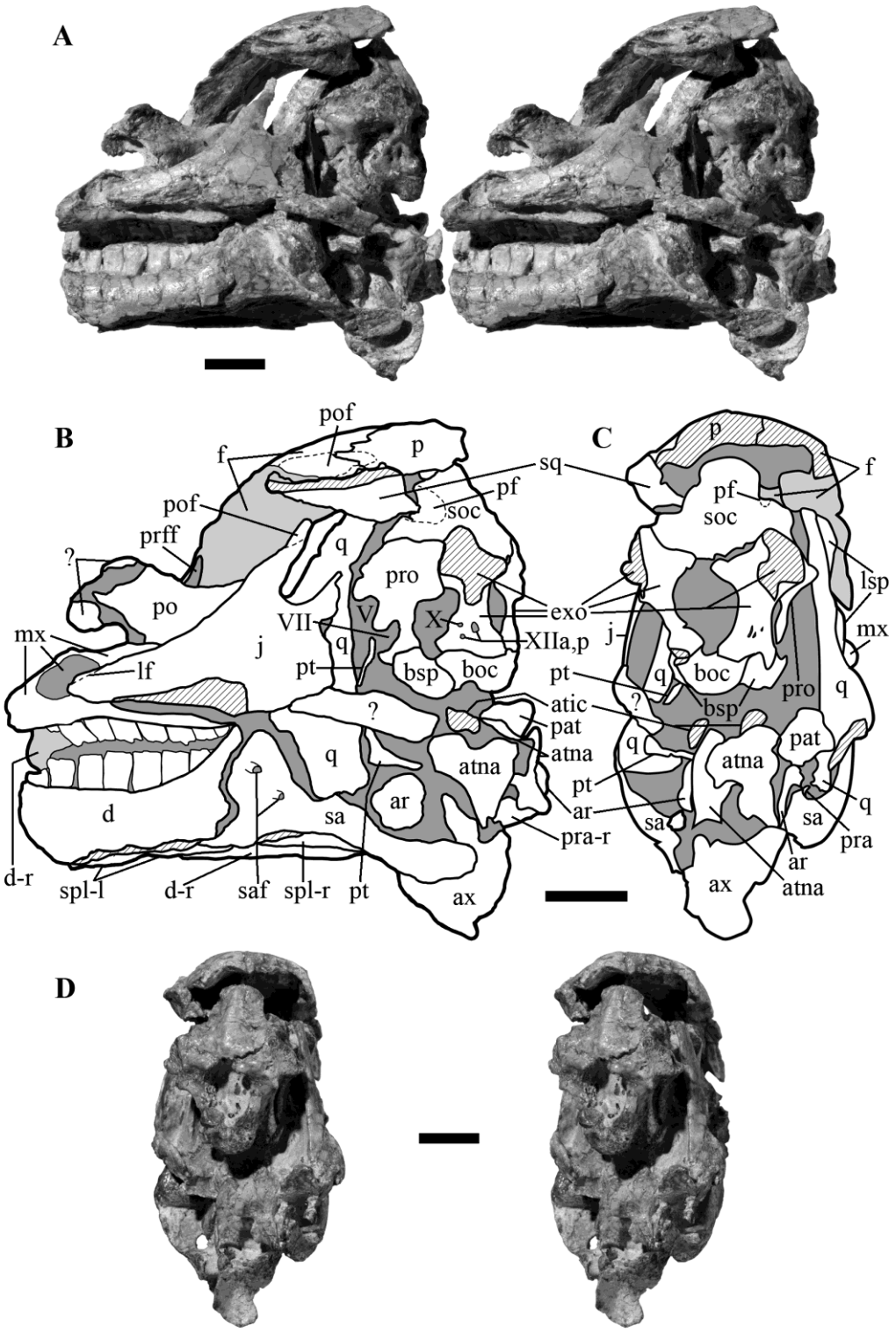

Fig. 4.2: *Stereo pairs of the skull BSPG AS I 834 and explanatory sketches. The sketches are relatively enlarged for better resolution. Dark grey illustrates sediment, light grey illustrates inner views of, e.g. the frontals or the dentaries, and hatched areas illustrate broken or corroded surfaces. The label affixes -r and -l stand for right and left of the respective element, where the distinction of each side is difficult to see.* ***A*** *– Left lateral view.* ***B*** *– Outline drawing of the left lateral view.* ***C*** *– Outline drawing of the occipital view.* ***D*** *– Occipital view. See material and methods for a list of the abbreviations. Scale bars: 1 cm.*

The posterior end, the last tooth, as well as the complete lateroventral tooth edges of the right element are sheared off. The anterior end of the maxilla is narrow, but the body abruptly widens towards the broken attachments of the lateral and medial laminae of the ascending process. A deep, dorsally opening cavern is present in this widened part between the laminae, and was probably connected posteriorly to the antorbital fossa and fenestra. As can be seen in the left element, this cavern seems to pneumatize great parts of the central maxillary body. Behind this cavern, the right maxilla bears the long and deep jugal facet. This facet widens posteriorly and is mainly dorsally directed.

A narrow groove runs along the lateral border of the antorbital fossa from the facet anteriorly, and ends in a foramen leading anteriorly into the base of the lateral ascending lamina, lateral to the cavern described above. The left maxilla lacks the anterior end and the mediodorsal process. Its isolated laterodorsal process is placed on the right maxilla, lying on the medial side and pressed down by the frontals. It is a thin sheet of bone with a pointed posterodorsal corner. As in other basal iguanodontians, except *Tenontosaurus tilletti*, this process is rather short and did not reach the nasal dorsally (Norman, 2004). The posterior end of the left maxilla is covered by the jugal and sediment, but CT images show that this part is also preserved.

There are nine teeth preserved in the right maxilla and eight in the left element. However, the complete tooth row of the right dentary (which has ten teeth, see below) suggests a similar number for the maxillae. The maxillary tooth row forms a very slightly laterally concave arch, as in many ornithischians. There are a few, irregularly spaced, large foramina on the lateral sides of the maxillae above the tooth row. Five larger foramina are present in the right element, whereas the left bears six smaller foramina. *Hypsilophodon* is similar, but has more foramina (Galton, 1974). The lateral side of the maxilla extends dorsolaterally from the tooth row, so that the dorsal rim of the maxillary body notably overhangs the tooth row laterally, but this is less obvious compared with, e.g. *Thescelosaurus neglectus* or *Zalmoxes robustus* (Galton, 1997; Weishampel et al., 2003).

Jugal (Figs. 4.1D and 4.2A, B; see Appendices I and II for measurements): The left jugal is completely preserved, whereas only the maxillary process of the right element is present, and has been removed from the skull during preparation. The main body of the left jugal has a compact, trapezoidal shape. Parts of the ventral and posterior margins are damaged. The bone is notably convex laterally, both anteroposteriorly and dorsoventrally, indicating a somewhat bulging cheek region in the articulated skull. There is no jugal boss, as present in *Zephyrosaurus* and *Orodromeus* (Scheetz, 1999; Sues, 1980). The long and slender maxillary and postorbital processes are set at an angle of approximately 110° to each other, and form the ventral and posteroventral margin of the orbit. The robust maxillary process tapers anteriorly. The lacrimal facet extends over 8 mm on the anterodorsal margin of the process. It widens anteriorly and is laterodorsally directed. Below this anteriorly descending facet, the anterior end of the maxillary process is broadened ventrally. The orientation and relative extension of the lacrimal–jugal suture is quite variable in ornithopods (see Norman, 2004; Norman et al., 2004; Weishampel, 1984). Posterior to the lacrimal facet begins the smooth and constantly concave orbital margin. The orbital margin of the jugal is broadened, so that the maxillary process of the jugal is triangular in cross section. A sharp rim separates a wider, medioventrally-extending medial surface from the lateral surface. This rim becomes less conspicuous and more rounded posterodorsally on the postorbital process.

The rounded postorbital facet, starting at the anterior side of the postorbital process with a deep, rounded depression, extends over approximately the dorsal half of this process. The lateral border of the facet ascends steeply to the posterodorsal side of the process, and is slightly twisted in itself. A slender process extends dorsally on the medial side, and was obviously completely covered by the jugal process of the postorbital in the articulated skull. The lateral part of the facet consists of a long, narrow groove along the twist described above, whereas the slender dorsal process is strongly convex and rod-like. The end of the postorbital process thus almost reaches the upper end of the infratemporal fenestra. Weishampel (1984:43) mentioned *Dysalotosaurus* as an example for a simple scarf joint between jugal and postorbital. The structure of the postorbital process in this

newly described specimen rather suggests a combination of a scarf joint ventrally and a hinge-like joint dorsally. The dorsal extension of the postorbital process is also more comparable with the described pattern in lambeosaurine hadrosaurs (Weishampel, 1984:44). The posterior half of the lateral base of the postorbital process bears a very weak depression, where the surface of the bone descends into the lower temporal fenestra.

The posterior (quadratojugal) process of the jugal is short and high. Its posterior end is considerably expanded dorsally into a long, dorsally thinning, slightly posterodorsally inclined process. Together with the postorbital process of the jugal, the quadratojugal process thus forms the entire anteroventral, ventral, and posteroventral margin of the anteroposteriorly narrow infratemporal fenestra. In basal ornithopods, such as *Hypsilophodon*, *Orodromeus*, and *Gasparinisaura*, as well as in the basal iguanodontian *Tenontosaurus*, this region is made up by the quadratojugal, so there is no contact between the jugal and the quadrate (Norman, 2004; Norman et al., 2004; see also Butler et al., 2008b: appendix 3, character 47). *Zalmoxes robustus*, *Dryosaurus altus* and all more derived iguanodontians share the general condition with *Dysalotosaurus* (Galton, 1983; Horner et al., 2004; Norman, 2004; Weishampel et al., 2003). Only *Ouranosaurus* seems to represent an intermediate condition between basal ornithopods and basal iguanodontians (see Taquet, 1976). The body of the posterior process below the infratemporal fenestra is very high, so that the ventral margin of the latter opening is placed considerably dorsal to the ventral rim of the orbit. The posterior rim of the posterior process of the jugal forms a straight, vertical margin. The ventral rim of the jugal also seems to be generally straight over its entire length, although there seems to be a slight ventrally convex extension directly below the postorbital process, although less distinct than in *Orodromeus* (Scheetz, 1999). The medial side of the jugal is mainly covered with sediment, so only the distinctive ectopterygoid process at the base of the maxillary process is visible in dorsal view.

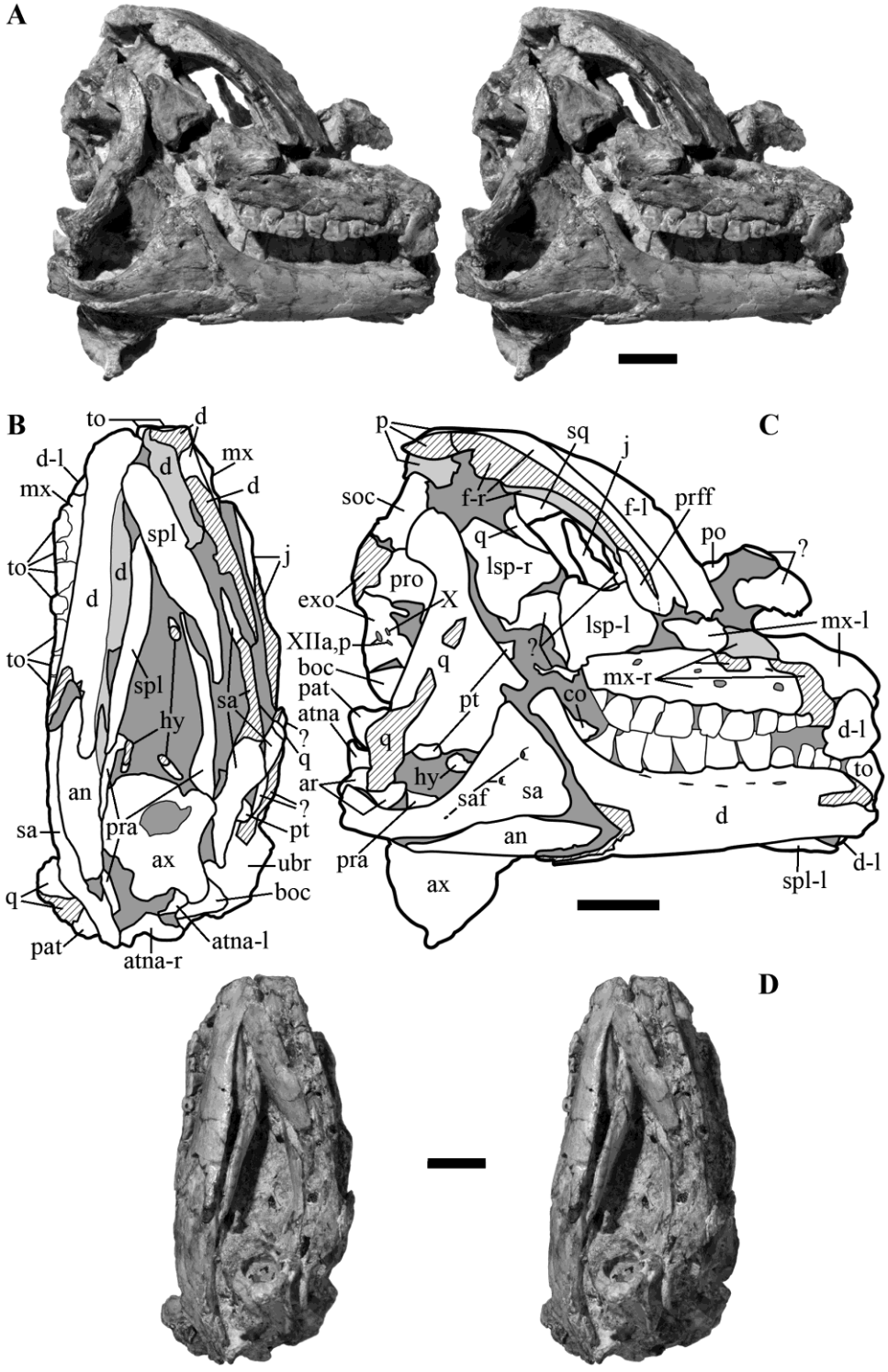

Fig. 4.3: *Stereo pairs of the skull BSPG AS I 834 and explanatory sketches. The sketches are relatively enlarged for better resolution. Dark grey illustrates sediment, light grey illustrates inner views of, e.g. the frontals or the dentaries, and hatched areas illustrate broken or corroded surfaces. The label affixes -r and -l stand for right and left of the respective element, where the distinction of each side is difficult to see.* ***A*** *– Right lateral view.* ***B*** *– Outline drawing of the ventral view.* ***C*** *– Outline drawing of the right lateral view.* ***D*** *– Ventral view. See material and methods for a list of the abbreviations. Scale bars: 1cm.*

Frontal (Figs. 4.1C, D, 4.2 and 4.3A, C; see Appendices I and II for measurements): The paired frontals are still articulated with the remaining fragment of the parietal. However, neither the frontals among themselves nor the frontals and the parietals are fused, as the sutures between the elements are clearly visible. Only the parietals seem to be fused without any visible suture.

The right frontal lacks the lateroposterior and orbital edge, whereas the left frontal is almost complete. Both have a length of approximately 40 mm, and the better preserved left frontal has a width of 11.8 mm at the posterior end of the orbital rim. The frontals become slightly narrower anteriorly, with the orbital rim forming an almost straight lateral margin. The interfrontal suture is visible as a straight median line between the two elements.

A good overview of the shape of the frontals in ornithopods and some other ornithischians in dorsal view is given by Galton (1997: fig. 9; but note that fig. 9L represents *Dryosaurus altus*, and fig. 9M represents *Dysalotosaurus*). Generally, in larger or more derived iguanodontians, such as *Tenontosaurus tilletti* (larger but less derived than *Dysalotosaurus*), *Iguanodon*, *Mantellisaurus*, or *Ouranosaurus*, the frontals are relatively shorter but transversely wider, and their participation in the orbital rim is shorter (see Galton, 1997; Norman, 1980; 1986; Ostrom, 1970; Taquet, 1976). In some hadrosaurs, the frontals are even completely excluded from the orbital rim (Horner, 1992; Horner et al., 2004).

The anterolateral corner of the frontal bears a deep groove for the contact with the prefrontal. This groove is relatively longer but less deep than in *Dryosaurus altus* (Galton, 1983, 1997). It slightly widens anteriorly and is entirely laterally directed. Posterolaterally, there is a facet for the contact with the postorbital, which extends posteriorly onto the parietal. This facet is developed as a narrow groove that undercuts the laterodorsal rim of the frontal anteriorly, and widens posteriorly to form a large, dorsally facing surface. At the frontoparietal suture, the lateral rim is slightly raised, probably in the area where the laterosphenoid met the postorbital. The frontoparietal suture forms an interdigitate, anteriorly slightly concave line, with the frontals forming

a small, lobe-shaped posterior process laterally. A small, triangular process of the parietals extends approximately 3 mm into the median suture of the frontals.

The dorsal surface of the frontals slopes posteroventrally behind the orbitae towards the supratemporal fossae. However, the supratemporal fossae (of which only the anterior end of the left depression is preserved) do not reach the frontal, but are restricted to the parietal. In contrast, the supratemporal fossa seems to cover the posterior end of the frontals in *Dryosaurus altus* and in *Lesothosaurus* (Galton, 1983; Sereno, 1991), and reaches the posterior margin of the frontal in *Hypsilophodon*, *Zalmoxes robustus*, and *Ouranosaurus* (Galton, 1974; Taquet, 1976; Weishampel et al., 2003). It seems to be excluded from the frontals in, e.g. *Thescelosaurus neglectus*, *Mantellisaurus atherfieldensis*, and *Iguanodon bernissartensis* (see Galton, 1997; Norman, 1980; 1986), as in *Dysalotosaurus*.

A small central dome is located just posterior to the orbital margin on the posterior third of the frontals, similar to a structure found in lambeosaurine hadrosaurs (Evans et al., 2007; Godefroit et al., 2004; Horner et al., 2004). As in the jugal, the orbital rim of the frontal is widened and forms a broad, ventrolaterally facing surface. The medial orbital facets of the articulated frontals form the lateral margin of a narrow, flat median surface on the ventral side of the frontals, in which the bulbi olfactorii of the brain would have been placed. The straight interfrontal suture is visible here as a thin, but deep median groove, similar to *Hypsilophodon* and *Zephyrosaurus* (Galton, 1974: fig. 6B; Sues, 1980: fig. 7B).

Parietal (Figs. 4.1C, D, 4.2; see Appendices I and II for measurements): Only the anterior most part of the left anterior wing and the central roof of the fused parietals are preserved. There is no indication of a suture between the parietals, as observed in *Orodromeus* (Scheetz, 1999) or in the juvenile skull of *Dryosaurus altus* (Carpenter, 1994). The dorsal face of the preserved left side houses a shallow, oblique depression, which deepens anteriorly. This depression represents the supratemporal fossa, the margins of which are not sharply defined. The fossa ends anteriorly

approximately 1.5 mm behind the frontoparietal suture. The anterolateral end of the parietal wing is slightly bilobate where it meets the postorbital. The posterior part of the postorbital facet of the left frontal extends 2 mm onto the dorsal surface of the parietal wing. At the medial margin of the postorbital facet, the anterior end of the parietal forms a small, pointed process between the median part of the frontal and the lateral, lobe-shaped process described above. In comparison with the main parts of the frontals, the parietals are somewhat thickened. As mentioned above, a median parietal process extends forwards into the suture between the two frontals. This process is more finger-like and much more slender than the respective process in *Hypsilophodon*. There is no anteromedian process in, e.g. *Zalmoxes robustus*, *Tenontosaurus*, *Mantellisaurus*, and *Iguanodon*, but there is a slight process-like protuberance in *Ouranosaurus* (Norman, 1980; 1986; Ostrom, 1970; Taquet, 1976; Weishampel et al., 2003; Winkler et al., 1997). The parietal of *Ouranosaurus* is also more similar to that of *Dysalotosaurus* than those of the other taxa in its dorsal shape, because it also possesses distinct anterolateral wings.

Postorbital (Figs. 4.1C, D, 4.2A, B): The left postorbital is completely preserved, although the jugal process is covered by matrix. It is completely displaced from its original position, and is positioned upright between the maxillae, approximately in the centre of the skull, as preserved. It has an anteroposterior length of 23 mm and a dorsoventral height of 22 mm (measured from CT images). The main body, the squamosal process, and the anterodorsal extension for the articulation with the frontal and parietal are visible laterally. The lateral side of the postorbital is separated from the dorsolateral part by a slight horizontal swelling, which extends from the posterior squamosal process to the orbital edge. At the point where this swelling meets the orbital margin, the latter forms a small, wide-angled process that extends 1.2 mm into the orbit. This is not as extensive as in *Dryosaurus altus*, but might be the result of ontogenetic differences, as the orbital edges of the other known postorbitals of *Dysalotosaurus* are not as smooth in this area (Galton, 1983; Janensch, 1955). A similar condition is found in *Zephyrosaurus* (Sues, 1980: fig. 7C).

Along the horizontal swelling the lateral side of the postorbital is anteroposteriorly concave and dorsoventrally convex. The stout, slightly ventrally flexed, triangular squamosal process possesses a smooth and flat dorsal facet for the contact with the anterior process of the squamosal. The ventral side bears a flat groove, which is continuous with the muscle attachment site for the M. adductor externus superficialis (Ostrom, 1961) on the squamosal, and borders the dorsal edge of the infratemporal fenestra. In *Zalmoxes robustus*, this muscle attachment is considerably larger and more anterolaterally placed (Weishampel et al., 2003).

The quadrangular dorsolateral plate of the postorbital that contacts the frontal and parietal borders the supratemporal fenestra anterolaterally. In horizontal CT slices, the deep medioposterior groove for the contact with the postorbital process of the jugal is visible in the long and slender jugal process.

Squamosal (Figs. 4.1C, D, 4.2): The preserved left squamosal lacks all of its medial part, including the parietal facet and most of the paroccipital facet. The bone is rotated about 90°, so that the almost complete ventral processes are removed underneath the left frontal. The anterior most part bears the lateroventrally placed postorbital facet. Behind this facet, the squamosal forms the posterodorsal margin of the infratemporal fenestra. From this area, a posteriorly directed triangular depression for the attachment of the M. adductor externus superficialis (Ostrom, 1961) extends onto the lateral side of the bone. In *Dryosaurus altus*, this depression seems to be much smaller and the degree of overlap between the postorbital and squamosal is larger than in *Dysalotosaurus* (Galton, 1983; Hübner & Rauhut, pers. obs.). In other ornithopods, including hadrosaurs, the postorbital–squamosal connection, as well as the size and shape of the laterodorsal depression, is quite variable, but the most unusual morphology is visible in *Zalmoxes robustus*, in which the depression is located on the postorbital and not on the squamosal (Weishampel et al., 2003).

The precotylar (ventral) process is a long, flat, and slender rod of bone that tapers anteroventrally, indicating that the quadrate was excluded from the infratemporal fenestra, as in

Gasparinisaura and in contrast to *Hypsilophodon* and *Orodromeus* (Norman et al., 2004). The head of the left quadrate is still articulated with the squamosal in the groove behind the precotylar process. The partly preserved postcotylar process frames the quadrate head posteriorly. The dorsal surface is convex anteroposteriorly. It forms an elongate, anteriorly tapering triangle in dorsal view. A distinct but flat depression is placed above the quadrate articulation on the otherwise smooth dorsal surface.

4.3.3 Palatoquadrate complex

Vomer: The very delicate, thin vomer is placed between the maxillae, adjacent to a broken anterior fragment of the left dentary. The incomplete, apparently fused anterior parts form a very thin, vertical sheet of bone. Posteriorly, this plate subdivides into two even thinner, slightly diverging branches that form a narrow V-shape in dorsal view, as is the case in *Hypsilophodon* (Galton, 1974: fig. 5C). The two posterior sheets seem to ascend posteriorly. The exact shape and borders of the bone are unclear because all visible edges are more or less corroded.

Pterygoid (Figs. 4.2 and 4.4): Both pterygoids are preserved, but are mainly just visible in the CT slices. Only the posterior border of the left element is exposed directly underneath and behind the left quadrate. The right pterygoid is still articulated with the basipterygoid process of the basisphenoid, and surrounds this process ventrally, medially, and laterally (Fig. 4D). The left pterygoid is slightly displaced anteriorly in relation to the right element. Posteriorly, the narrow, funnel-like main body widens into the vertical quadrate wing and a horizontal plate, which extends medially from the ventral end of the quadrate wing. A similarly extensive medial plate is unknown in other ornithopods. Where the two plates meet, a prominent lateroventral ridge rises to border the pterygoid flange of the quadrate ventrally, as in *Tenontosaurus dossi* (Winkler et al., 1997:334). The ectopterygoid process of the pterygoids is long and broad. In contrast to *Dryosaurus altus*, there is no anteroventral extension of this process in *Dysalotosaurus* (Hübner & Rauhut, pers. obs.; see also

Galton, 1983: fig. 2C, pl. 1). The slender and anteriorly ascending palatal ramus is triangular in cross section, with a distinct, anteriorly widening ventral groove.

Ectopterygoid (Fig. 4.4C): As with the pterygoids, the ectopterygoids are almost only visible in the CT slices. The left bone, which has a total mediolateral length of 14 mm, is slightly disarticulated from the forwards-displaced jugal and maxilla, and is additionally rotated about 30° around its mediolateral long axis. Thus, the curved, originally posteroventrally facing concavity of the strap-like mid-shaft is now opening ventrally. The posterior part of the pterygoid wing is notably elongated.

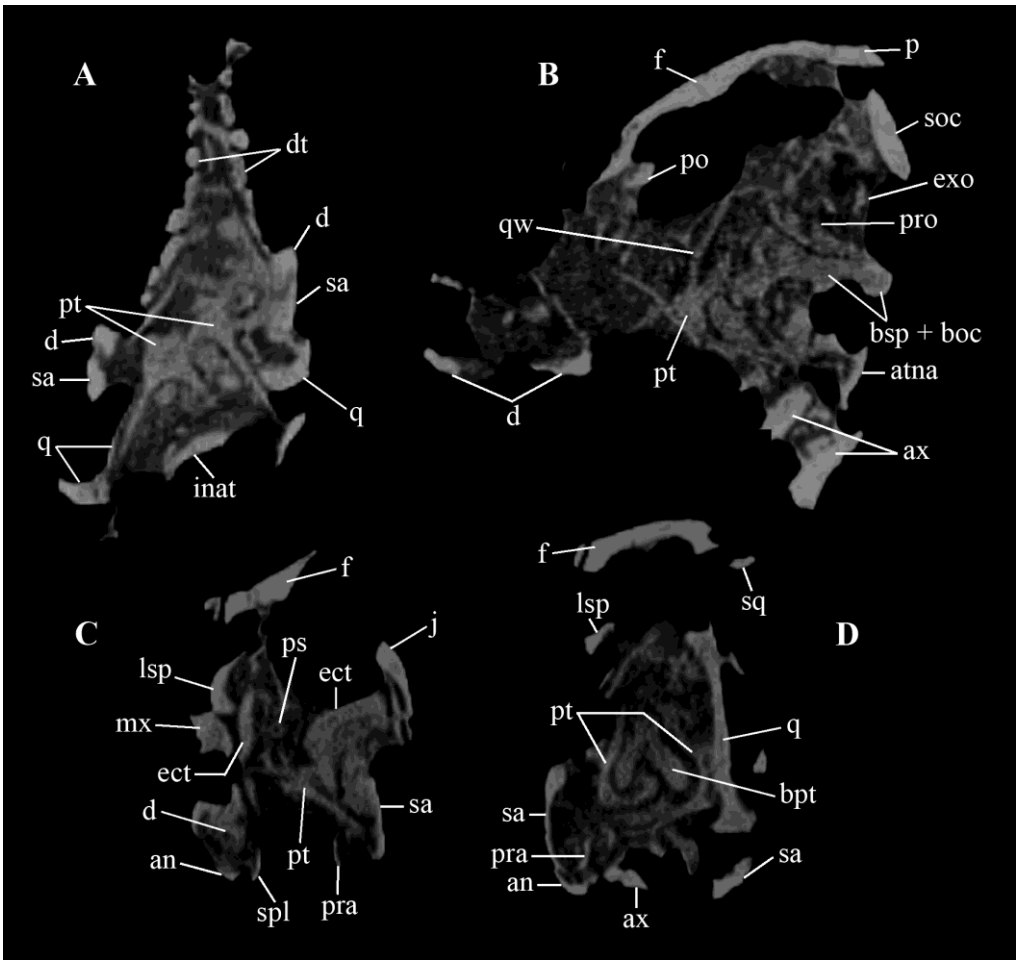

Fig. 4.4: *Computed tomography (CT) sections of the skull BSPG AS I 834.* ***A*** *– Horizontal section at the level of the dentary tooth crowns in ventral view.* ***B*** *– Sagittal section at about the sagittal midline in left lateral view.* ***C*** *- Coronal section at about the middle of the anteroposterior length in anterior view.* ***D*** *- Coronal section about 1 cm posterior to (C) in anterior view. See material and methods for a list of the abbreviations.*

The jugal wing is stout but also slightly elongated anteroposteriorly. The right ectopterygoid is completely displaced from its connections with other bones. In comparison with other ornithopods, the ectopterygoid of *Dysalotosaurus* is most similar to the respective elements in *Hypsilophodon* and *Thescelosaurus neglectus* (Galton, 1974; 1997). In derived iguanodontians and hadrosaurs, the medial part of the bone is reduced, because the pterygoid has a direct contact with the maxilla. A strap-like, anteroposteriorly-elongated anterolateral process is developed, and covers the posterolateral surface of the maxilla (see, e.g. Heaton, 1972; Norman, 1980; Godefroit et al., 2004: fig. 10C), whereas in *Dysalotosaurus* and other similar ornithopods, the lateral part of the ectopterygoid contacts primarily the medial side of the jugal, and has only a minor anterolateral projection.

Quadrate (Figs. 2.3, 4.1C, D, 4.2, 4.3, and 4.4A, B, D; see Appendices I and II for measurements): The left quadrate is well preserved, but the main part of the middle section is covered by the jugal and an indeterminable piece of bone. The cotylar head is still articulated with the left squamosal, despite the rotation of the latter bone. The entire left element is displaced forwards towards the surangular and the maxilla (Fig. 4.2A, B). The lower and upper parts of the anterolateral wing, which are separated by the quadratojugal notch, are partially visible ventrally and underneath the jugal, respectively. The right quadrate is not covered, and the dorsal head and the medial wing for the pterygoid are well preserved. Both the anterolateral wing and the distal condyle for the jaw articulation are lost (Fig. 4.3A, C), but a shallow concavity in the lateral side at approximately mid-height of the bone indicates the placement of the large quadrate foramen. The upper quadrate shaft is very slender in posterior view, whereas the lower shaft is expanded mediolaterally. The neck of the cotylar head is flattened and slightly depressed at its posterior edge. The head itself is thickened dorsally, very thin posteriorly, and forms an angle of approximately 90° with the shaft at its straight ventral edge. Starting at the ventral edge of the quadrate head, the posteromedial margin of the quadrate extends ventrally as a sharp ridge, which becomes somewhat wider ventrally.

In comparison with *Dryosaurus altus*, the quadrate of YPM 1876 (see Galton, 1983: fig. 1D, E and pl. 1, fig. 7) is very similar to the quadrate of *Dysalotosaurus*, with its straight shaft, slender cotylar neck, and in respect to the posteriorly flexed cotylar head (see Fig. 2.3). In contrast, the entire shaft of the quadrate of the holotype skull of *Dryosaurus altus* (CM 3392; see Galton, 1983) is considerably concave posteriorly, and the curvature between the shaft and cotylar head is gradual and not abrupt. This morphology is much more similar to *Camptosaurus dispar* than to *Dysalotosaurus* (compare Galton, 1983 and Brill & Carpenter, 2007). Whether the differences in quadrate morphology in *Dryosaurus altus* are a preservational or an ontogenetic feature (see Carpenter, 1994) is currently unknown. Another reason could be intraspecific evolution because of a wide stratigraphic range of the specimens, as it was recently hypothesized for *Camptosaurus* (Carpenter & Wilson, 2008).

4.3.4 Braincase

Laterosphenoid (Fig. 4.3A, C; see Appendices I and II for measurements): Both laterosphenoids are displaced from the braincase, lying with their lateral sides exposed in the area of the right orbit. The right laterosphenoid is rotated posterodorsally, so that the anterior tip is now pointing in this direction. The left element is placed with its dorsal sutural contact for the parietal facing ventrally and the tip facing anteriorly, and is thus rotated about 180° around its long axis.

The laterosphenoid is roughly triangular in outline and somewhat longer than high. The lateral surface is anteroposteriorly concave, whereas the medial surface is dorsoventrally concave. The bone thickness decreases ventrally. The sutural surface for the contact with the parietal, visible in the right laterosphenoid, is divided into two areas. A relatively smooth posterior area houses a flat lateral depression and tapers anteriorly. An elongate, deep groove, oriented slightly oblique to the long axis of the bone, forms the anterior two-fifths of the parietal articulation. At the articular contact with the prootic, a small, dorsally placed groove obviously received a small, anterior spike

extending from the dorsal part of the latter bone. This is probably the dorsal border for the ramus ophthalmicus of the trigeminal nerve, which was running anteriorly along the ventral rim of the laterosphenoid (Galton, 1983; 1989). The postorbital process of the laterosphenoid seems to be rather short and stout, but its distal articular end is corroded in both elements. In comparison, the laterosphenoid of *Zephyrosaurus* is dorsoventrally lower and the postorbital process much larger than in *Dysalotosaurus* (Galton, 1983; Sues, 1980: fig. 11). Additional differences from other ornithopods were already described by Galton (1989:223).

Parasphenoid: This bone is completely covered by sediment. Thus, only CT images are available for the description. The parasphenoid is very similar to that of dy A (MB.R.1373, Janensch, 1955), with a prominent dorsal process for the anterior restriction of the hypophysis, and a slender and tapering anterior part with a distinct dorsal groove. It is very similar to the same element in *Hypsilophodon* (see Galton, 1989:226) in its shape and orientation, whereas the parasphenoid of *Iguanodon* and *Mantellisaurus* is steeply rising upwards anteriorly (Norman, 1980; 1986).

Prootic (Figs. 4.2A, B, 4.3A, B; see Appendices I and II for measurements): Both prootics are almost complete, but are partly covered by the quadrates. The sutures to the supraoccipital and the opisthotic are unfused. The basisphenoid suture is also still visible (Fig. 4.4B). The curved crista prootica divides the broad and concave laterodorsal face from the lateral face, which bears the foramina of the N. facialis and N. trigeminus. On the left prootic, there is small, triangular groove above the large N. trigeminus foramen at the anterior edge of the crista prootica, but it is unclear if this feature represents an original character of the bone or is the result of preservation. The trigeminal foramen is very large and obviously oval in shape, although its anterior end is still covered in matrix. Thus, it cannot be said with certainty if it was completely enclosed in the prootic, although this is the case in other known prootics of *Dysalotosaurus*. The only other ornithopods with a

completely enclosed trigeminal foramen are *Dryosaurus altus* and probably *Zephyrosaurus* (Galton, 1983; 1989; Sues, 1980).

The foramen for the N. facialis is smaller than that for the N. trigeminus, but is still rather large. It is surrounded by sharp edges, except ventrally. The prootics house the ossified labyrinth posteriorly (the semicircular canals are poorly visible in CT images of the left prootic), and border the fenestra ovalis anteriorly. The fenestra ovalis is situated at approximately the same level as the trigeminal foramen, whereas the facialis foramen is slightly displaced ventrally. This constellation is quite variable in ornithopods, similar in *Dysalotosaurus*, *Zephyrosaurus* and *Hypsilophodon* (Galton, 1974; Sues, 1980), whereas these structures are more or less aligned in *Tenontosaurus dossi*, *Dryosaurus altus*, and *Probactrosaurus* (Galton, 1983; Norman, 2002; Winkler et al., 1997), and the trigeminal foramen is placed more dorsally than the foramen facialis and foramen ovalis in *Mantellisaurus atherfieldensis* (Norman, 1986). The depression of the lagenar recess is visible anteroventrally to the fenestra ovalis in the left prootic, as is the case in *Zephyrosaurus* (Sues, 1980: fig. 13). Ventrally, the prootic also forms the anterior margin of the large fissura metotica.

Basisphenoid (Fig. 4.2): Without the help of CT scans only the posterior part of this bone is visible. The surfaces of the tubera are corroded, and their original shape and extent is not clearly determinable because of slight distortions between the left and right sides. However, the tubera seem to be distinct and separated by a shallow, wide incision medially, but less prominent than the ventral part of the occipital condyle or the midline ridge of the basioccipital. The CT data reveal well-developed, lateroventrally directed basipterygoid processes (Fig. 4.4B, D), with broad, slightly anterolaterally positioned articular facets for the pterygoids, two large foramina for the right and left branch of the A. carotis interna, and the deep sella turcica for the hypophysis.

It is somewhat unclear in how far the orientation of the basipterygoid processes might be affected by deformation, but the closest similarities are found in the ornithopods *Zephyrosaurus*, *Hypsilophodon*, *Thescelosaurus neglectus*, and *Dryosaurus altus* (Galton, 1974; 1983; 1989; 1997;

Sues, 1980). *Rhabdodon* seems to have slightly anteriorly directed processes, whereas there is a slight posterior orientation in *Zalmoxes robustus* (Pincemaille-Quillevere et al., 2006; Weishampel et al., 2003). The processes are clearly posteriorly directed in *Camptosaurus dispar*, but the anteroventral direction of the pterygoid facets indicates that this might be the result of preservational artifacts (Gilmore, 1909: fig. 5).

Supraoccipital (Fig. 4.2; see Appendices I and II for measurements): The supraoccipital is complete and well preserved, and is not fused to other braincase elements. It is polygonal and wider ventrally than dorsally, and slightly inclined anterodorsally. This overall shape is very similar to that seen in the juvenile *Dryosaurus altus* skull described by Carpenter (1994: fig. 19.4B). The left side is still in articulation with the prootic and exoccipital. It forms a small part of approximately 2.5 mm of the dorsal margin of the foramen magnum. The relative contribution to the foramen magnum is similar to, e.g. *Rhabdodon*, *Dryosaurus altus*, and *Camptosaurus dispar* (Galton, 1983; Gilmore, 1909; Pincemaille-Quillevere et al., 2006). In more primitive ornithopods, such as *Hypsilophodon* and *Orodromeus* (Galton, 1974; 1989; Scheetz, 1999), the supraoccipital participation in the margin of the foramen magnum is much wider, although in *Thescelosaurus neglectus*, the exoccipitals are also very close together (Galton, 1997), and they exclude the supraoccipital completely from the foramen magnum by a thin bridge in *Tenontosaurus* (Galton, 1989; Ostrom, 1970; Pincemaille-Quillevere et al., 2006; Winkler et al., 1997). In iguanodontians more derived than *Camptosaurus*, and in hadrosaurs, the supraoccipital is always excluded from the foramen magnum by a broad exoccipital bridge (see, e.g. Horner, 1992; Norman, 1986; Taquet, 1976).

Starting at the foramen magnum, the suture with the exoccipital extends laterodorsally. The dorsal part of the posterior surface is marked by a low, broad, and rounded supraoccipital crest, which extends ventrally almost to the dorsal rim of the foramen magnum. The crest becomes narrower and more sharply defined dorsally. In the dorsal part, the lateral margins of the crest are pronounced by a narrow, very shallow groove. The dorsolateral corners of the supraoccipital flex

anteriorly to form small, almost funnel-like structures. The lateral margins of the supraoccipital are notably concave where the bone widens ventrally towards the base of the paroccipital processes.

The parietal facets are deep, U-shaped grooves in the dorsal part of the lateral margin (Fig. 4.2A, B). Between the parietal facets and the prootic suture, a small area forms a continuation of the concave dorsolateral face of the prootic. According to Sereno (1991), this part represents a separate ossification (epiotic) in *Lesothosaurus*. A small foramen for the posterior exit of the V. capitis medialis is situated on either side of the supraoccipital crest at this level, and is connected with the lateral side by a small, shallow groove.

Exoccipital/opisthotic (Figs. 4.1D, 4.2 and 4.3A, C; see Appendices I and II for measurements): The exoccipital is fused to the opisthotic without any visible suture, but not to any of the other braincase elements. Among ornithopods, a suture between exoccipital and opisthotic has only been described for *Zephyrosaurus* (Sues, 1980), although some uncertainty remains whether this might not represent a crack rather than a suture. The exoccipitals lack the paroccipital processes, but are otherwise well preserved. The bones are articulated with the prootics and the basioccipital. The supraoccipital is very slightly displaced dorsally. The exoccipitals form all the lateral and dorsolateral parts of the margin of the foramen magnum and the dorsolateral parts of the occipital condyle. The participation of the exoccipitals in the occipital condyle is similar to that found in *Dryosaurus altus* and *Camptosaurus dispar* (Galton, 1983; 1989; Gilmore, 1909), but is less extensive than that in *Thescelosaurus neglectus*, *Zalmoxes robustus*, and *Tenontosaurus* (Galton, 1997; Pincemaille-Quillevere et al., 2006; Weishampel et al., 2003; Winkler et al., 1997).

Lateral to the foramen magnum, the posterior surface of the exoccipital is slightly concave both dorsoventrally and transversely. At the dorsolateral margin of the foramen magnum, the exoccipital has a transversely elongate and dorsoventrally convex, rounded facet for the contact with the proatlas. The crista tuberalis extends from the ventral corner of the base of the paroccipital process anteroventrally, and forms the posterior wall of the fissura metotica. On the right side, the

very slender crista metotica is preserved in the angle between the paroccipital process and the crista tuberalis, and separates the smaller, elongate oval fenestra ovalis dorsally from the larger, dorsoventrally elongate fissura metotica ventrally. This morphology is very common in ornithopods and is also present in, e.g. *Zephyrosaurus*, *Rhabdodon*, *Tenontosaurus dossi*, *Probactrosaurus*, and the hadrosaur *Amurosaurus* (Godefroit et al., 2004; Norman, 2002; Pincemaille-Quillevere et al., 2006; Sues, 1980; Winkler et al., 1997).

Three nerval foramina are present in the lateral wall of the exoccipital between the crista tuberalis and a small bony strut that connects the lateral margin of the foramen magnum with the basioccipital condyle. The anterior most and slightly more dorsally placed opening is nested in the posterior wall of the crista tuberalis and probably represents the passage for the vagus nerve (X). The two remaining openings probably housed the N. hypoglossus anterior and posterior (XIIa and XIIp).

Basioccipital (Figs. 4.1D, 4.2 and 4.4B; see Appendices I and II for measurements): The ventral part of the surface of the occipital condyle is partly corroded. The sutures to the exoccipitals are clearly visible, in contrast to the almost completely closed sutures to the basisphenoid. However, the latter sutures are visible under the microscope as a thin line on the corroded lateral surface of the tubera basioccipitalia. The basioccipital forms the posterior parts of the tubera along the undulating suture with the basisphenoid. A broad, anteroposteriorly extending spur between the tubera bears a sagittal ridge. This condition is also known in *Dryosaurus altus* (Galton, 1983: fig. 1C; Hübner and Rauhut, pers. obs.), and has been described in, e.g. *Hypsilophodon*, *Tenontosaurus dossi*, and *Camptosaurus dispar* (Galton, 1974; Gilmore, 1909; Winkler et al., 1997). There is no subdivision of this ridge, as found in *Zephyrosaurus* (Sues, 1980: fig. 15A). The occipital condyle lies on approximately the same level as the basal tubera and has a short, broad neck. Its articular surface is subdivided into a posteriorly facing facet and a broad, ventrally facing area that tapers anteriorly. Thus, the ventral area of the condyle is similar to, e.g. *Zephyrosaurus* and *Camptosaurus dispar* (Gilmore, 1909; Sues, 1980) in this juvenile specimen. Only 2 mm of the ventral margin of the

foramen magnum is formed by the basioccipital, which is similar to, e.g. *Rhabdodon priscus*, *Dryosaurus altus*, and *Camptosaurus dispar* (Gilmore, 1909; Pincemaille-Quillevere et al., 2006; Hübner and Rauhut, pers. obs.), whereas in more primitive ornithopods the participation is more extensive (see, e.g. Galton, 1974).

4.3.5 Lower jaw

Dentary (Figs. 4.1D, 4.2A, B and 4.3; see Appendices I and II for measurements): Both dentaries are preserved. However, the left element lacks the whole ventral edge and the anterior third, although its isolated anterior end is displaced and rotated, and is now located above the anterior end of the right dentary (Fig. 4.3A, C). The right element is complete, except for some damage at the posterior and anterior ends.

The ventral edge of the anterior half of the dentary is slightly concave, although the anterior end of the ventral edge extends ventrally to form a slight chin, as is also present in, e.g. *Hypsilophodon* and *Orodromeus* (Galton, 1974; Scheetz, 1999), where this chin marks the posterior border of the ventral articulation for the predentary. The anterior most part of the dentary is more slender mediolaterally than the main body, and is inclined medioventrally to form one half of the spoon-like symphysis. On the ventral half of the lateral side of the anterior end there is a slight depression for the lateroventral process of the unpreserved predentary. A small, anteriorly facing foramen is present just posterodorsally to this depression.

The lateral side of the dentary is slightly convex dorsoventrally, but flexes abruptly medially at its dorsal margin to form a broad lateral shelf along the tooth row, as in all derived ornithischians (Galton, 1974). Five anteroposteriorly elongate foramina are placed along the lateral margin of the shelf. Posteriorly, the dorsal margin of the dentary extends into a large, slightly posterodorsally inclined coronoid process that is higher than the height of the body of the dentary. Its distal end is very slightly widened posteriorly. This morphology and the anteroposterior orientation are similar to

that seen in many non-ankylopollexian ornithopods, such as *Hypsilophodon*, *Thescelosaurus neglectus*, *Orodromeus*, *Tenontosaurus*, and *Dryosaurus altus* (Galton, 1974; 1983; 1997; Ostrom, 1970; Scheetz, 1999; Winkler et al., 1997). *Camptosaurus dispar* and *Ouranosaurus* represent an intermediate stage, with a short, stout, and more upright coronoid process (Gilmore, 1909; Taquet, 1976), whereas most of the derived iguanodontians possess a tall and upright process (see, e.g. *Iguanodon* and *Mantellisaurus*; Norman, 1980; 1986).

The mandible bears ten alveoli. The three anterior most alveoli bear very small and slender teeth, which are also positioned very close together (see remarks below). The medial side of each dentary is mostly covered by the splenials and sediment. In the right dentary, the splenial is somewhat displaced and reveals the Meckelian groove, which narrows anteriorly, but extends up to the symphysis (Fig. 4.3B, D), as in most non-ankylopollexian ornithopods and *Camptosaurus dispar* (e.g. Galton, 1974; Gilmore, 1909; Scheetz, 1999). In derived iguanodontians and hadrosaurs, the Meckelian groove tapers and ends well posterior to the symphysis (e.g. Horner, 1992; Norman, 1986; 1998). The ventrolateral border of the groove forms a sharp edge that originally obviously contacted the ventral margin of the splenial.

Surangular (Figs. 4.1D, 4.2 and 4.3; see Appendices I and II for measurements): Both surangulars are preserved, but the left element is strongly damaged ventrally and posteriorly. The right bone is complete apart from corrosion of the posterior edge. It is still articulated with the dentary anteriorly, with the angular lateroventrally, and with the right articular medially (Figs. 4.1C and 4.3).

The surangular is slender posteriorly, but rapidly expands dorsoventrally in the anterior direction to form a large, triangular lateral plate. The anterodorsal margin of the plate is slightly expanded transversely, indicating that a small condyle was present in this area, as in other known surangulars of *Dysalotosaurus* (Galton, 1983; Janensch, 1955), but unlike the situation in all other ornithopods, including *Dryosaurus altus* (Rauhut, pers. obs.). A large foramen is located on the lateral

side of the anterior plate in its dorsal half, just behind the edge of the dentary, and a second, smaller foramen is located approximately in the centre. Both foramina open anterolaterally. The surangular foramen *s. s.* is placed close and slightly anterior to the glenoid, and is very small. The number and relative location of foramina in the surangular varies slightly within Ornithopoda. Two anterior foramina are also found in *Hypsilophodon* and *Thescelosaurus neglectus*, apart from the surangular foramen close to the glenoid (Galton, 1974; 1997), but the smaller anterior foramen in *Hypsilophodon* has a relatively more posterior position. *Orodromeus*, *Zalmoxes robustus*, and some more derived iguanodontians, such as *Ouranosaurus* and *Altirhinus*, possess only a single anterior foramen (Norman, 1998; Scheetz, 1999; Taquet, 1976; Weishampel et al., 2003), whereas in *Iguanodon*, *Mantellisaurus*, and *Probactrosaurus* only the surangular foramen *s. s*. has been described (Norman, 1980; 1986; 2002).

The glenoid is placed on the lowest part of the bone at approximately two-thirds of its total length. It is broadened mediolaterally and bears a medial, slightly anteriorly positioned prearticular process. The dorsolateral margin of the bone flares slightly laterally at this point. The retroarticular process of the surangular is again flattened transversely for the articulation with the articular, and bends slightly medially and dorsally. Its end is slightly expanded. This is very similar to the condition in *Lesothosaurus* and *Hypsilophodon* (Galton, 1974; Sereno, 1991), and differs from the stout and dorsally more strongly curved retroarticular processes in *Zalmoxes robustus* and derived iguanodontians, such as *Iguanodon*, *Mantellisaurus*, or *Altirhinus* (Norman, 1980; 1986; 1998; Weishampel et al., 2003). The suture between surangular and dentary seems to form an almost straight, anteroventrally inclined line, although parts of the posterior border of the dentary are broken. The suture with the angular is marked as a gently concave ventral margin of the bone.

Angular (Figs. 4.1D and 4.3; see Appendices I and II for measurements): The right, almost complete angular is preserved. Its thin posterior most end is lost, but the angular facet on the surangular shows that it did not reach the posterior end of the retroarticular process. The overall

shape is that of an elongate, isosceles triangle with a uniformly convex dorsal edge. The maximum height of the angular is located exactly below the large anterior most foramen of the surangular. The broad and rounded lower edge of the posterior half of the element encloses the surangular, and therefore forms the posterior part of the ventral margin of the lower jaw. The anterior half of the angular was originally covered by the lateral wall of the dentary, but it is now partly uncovered by erosion.

The general shape and laterally visible extension on the posterolateral surface of the lower jaw is similar to many ornithopods, such as *Hypsilophodon*, *Thescelosaurus neglectus*, *Orodromeus*, and also to some more derived iguanodontians, such as *Altirhinus* (see Galton, 1974; 1997; Norman, 1998; Scheetz, 1999). In contrast, in other iguanodontians, such as *Iguanodon* and in the hadrosaurs, the angular is, if at all, only visible laterally as the ventral edge of the lower jaw below the surangular.

Whereas the posterior part of the bone is broad and rounded ventrally, the ventral edge of the anterior half is very thin, as it bears a strongly marked facet for the splenial medially. This facet starts approximately in the middle of the total length of the angular, and extends forwards and slightly laterally. Thus, the anterior half of the angular is completely enclosed by the dentary and the splenial.

Splenial (Fig. 4.3B, D): Both splenials are preserved, but they are only visible in ventral and partially in medial view. They are slightly displaced from the dentaries. The splenials form the medial wall of the Meckelian groove and overlap the anteromedial part of the angulars with a broad, ventral, finger-like process. The concave posterior end dorsal to the angular process seems to represent the border to the prearticular. Together with the dentaries, the ventral border of the splenials forms the anterior two-thirds of the ventral margin of the lower jaws.

The general shape of the splenial of *Dysalotosaurus*, its anterior extension, and the posteroventral process are very similar to the morphology in many ornithopods, such as *Hypsilophodon* and *Thescelosaurus* (Galton, 1974; 1997), including derived iguanodontians, such as

Altirhinus (Norman, 1998). It differs slightly from *Iguanodon* and *Mantellisaurus*, because a posterodorsal extension seems to be absent in the splenial of these genera (Norman, 1980; 1986).

Coronoid (Fig. 4.3A, C): In dorsal and anterior view, the right coronoid is visible medial to the coronoid process of the right dentary. The coronoid is strongly corroded and slightly displaced forwards ventrally. The corroded anterior face shows a porous internal bone structure with a larger cavity in its ventral part. The mediolateral thickness of the coronoid is 2.5 mm dorsally and 0.5 mm ventrally. Thus, it is tapering ventrally, in contrast to the coronoid process of the dentary, which becomes narrower dorsally. Originally, it probably exceeded the height of the coronoid process of the dentary dorsally, similar to *Iguanodon* and *Mantellisaurus* (see Norman, 1980: pl. III; 1986: fig. 19A), and less extensive than in *Hypsilophodon* and *Thescelosaurus neglectus* (Galton, 1974; 1997).

Prearticular (Fig. 4.3B, D; see Appendices I and II for measurements): In ventral view, the almost complete, but partially covered left prearticular is visible. The outermost anterior and anteroventral edges are corroded. The bone is slightly displaced anteriorly onto the posterior end of the medial side of the splenial, and the left articular seems to be still articulated with the prearticular. The overall shape of the bone resembles a weakly flexed, but transversely flat boomerang, with a concave dorsal edge and a straight ventral edge. Thus, the anterior and posterior ends are expanded dorsally and are higher than the central strut. This is very similar to the general morphology in *Lesothosaurus* and *Hypsilophodon* (Galton, 1974; Sereno, 1991). In contrast to the latter and *Thescelosaurus neglectus* (Galton, 1997), the posterior end covers the medial side of the articular almost completely, and reaches the posterior end of the retroarticular process, as in *Orodromeus*, *Iguanodon*, *Mantellisaurus*, and *Altirhinus* (Norman 1980; 1986; 1998; Scheetz, 1999). A small depression is present approximately in the middle of the ventral edge. The splenial facet starts 1 mm anterior from this depression at the ventral edge and ascends slightly anterodorsally.

The overall shape of the prearticular strongly resembles the left element described and illustrated in medial view by Janensch (1955: table XI, fig. 7). However, the orientation of the prearticular in BSPG AS I 834 suggests that Janensch (1955) misinterpreted the anterior and posterior ends, and thus described the splenial facet as the angular facet.

Articular (Figs. 4.1D, 4.2 and 4.3; see Appendices I and II for measurements): The right articular is still articulated with the posterior end of the right surangular, although it is slightly displaced dorsally and anteriorly. The anterodorsally thickened side of the articular is corroded at the surface, but the general features of the bone are still clearly discernable. The medial side extends slightly more anterior than the lateral side. The left articular is mainly visible in lateral view. It seems to be still articulated medially with the left prearticular, but is removed from the left surangular.
In lateral view, the articular has an oval to pentagonal shape, with a distinctive anterior corner. There is a weak, posteriorly ascending depression on the upper half of the articular for the articulation with the retroarticular process of the surangular.

Except for the anterodorsal thickened side for the articulation with the quadrate, the thickness of the whole articular 'disc' does not reach more than one millimeter. In articulation, the surangular and prearticular enclosed the articular almost completely, but the articular seems to extend beyond the retroarticular process ventrally and posteriorly in lateral view, although this might be an artifact of preservation.

The articular is similar to the same bone in *Iguanodon* and *Mantellisaurus* (Norman, 1980; 1986), but the articular surface for the quadrate is anterodorsally and not dorsally directed, and the transversely thickest part is found anteriorly, and not at mid-length.

4.3.6 Dentition

Maxillary teeth (Figs. 4.1D and 4.2A, B, 4.3A, C): There are nine teeth preserved in the right maxilla and eight teeth in the left maxilla. Most of the teeth of the right side are sheared off laterally, so that the pulp cavity is visible in some of them. A very prominent and slightly posteriorly inclined, but straight, primary ridge separates the labial face of the teeth in a wider mesial and a narrower distal part. This general morphology is very similar to that found in other basal iguanodontians, such as *Dryosaurus altus*, *Camptosaurus dispar*, *Iguanodon bernissartensis*, and *Mantellisaurus* (Galton, 1983; 2007:37, fig. 2.18A; Norman, 1980; 1986;), but differs markedly from the teeth in basal ornithopods, which usually show ridges associated with all marginal denticles and lack a pronounced primary ridge (Galton, 1997; Ostrom, 1970; Sues, 1980; Weishampel et al., 2003). Labial depressions are placed mesially and distally between the primary ridge and lower secondary ridges at the anterior and posterior tooth edges of *Dysalotosaurus*, respectively. Additional vertical ridges within these depressions, as present in *Camptosaurus dispar* (see Galton, 2007), are absent, although similar ridges have been described in adult *Dysalotosaurus* teeth by Janensch (1955). The broken surfaces of the teeth reveal a thin enamel layer extending over the whole labial face, and also encompassing the mesial and distal edges. However, enamel is absent in the lingual face, in contrast to the maxillary teeth in more basal ornithopods, including *Zalmoxes robustus* or *Tenontosaurus dossi* (Weishampel et al., 2003; Winkler et al., 1997). The teeth are closely packed, but small spaces are found between some elements. There seem to be two alternating tooth generations. Small, medially inclined wear facets are visible on the anterior most teeth of the left maxilla.

Galton (1983) noted that the maxillary teeth of the YPM specimens of *Dryosaurus altus* are more similar to those of *Dysalotosaurus* than to the teeth of the holotype skull of *Dryosaurus altus* (CM 3392). Whether this is intraspecific or ontogenetic variation, a different type of preservation, or the result of anagenetic evolution, given the wide stratigraphic distribution of this ornithopod, is currently unknown.

Dentary teeth (Figs. 4.1D, 4.2A, B, 4.3A, C, 4.4A): The dentary teeth seem to be generally similar to the maxillary teeth. However, the sculptured surface is located lingually, but it is still largely covered by sediment. The exposed lateral surface of the teeth is smooth and slightly convex anteroposteriorly. The visible laterodorsal wear facets are slightly concave. The first three dentary teeth are very slender and pencil-like when compared with the broader, more posterior teeth. In many ornithopods, the anterior teeth are more slender than the posterior teeth (e.g. *Mantellisaurus*; Norman, 1986), but this variation is not as marked, nor is the change from one tooth type to another as abrupt as in this specimen. Nevertheless, this shape difference of anterior dentary teeth is also known in *Hypsilophodon* (Galton, 1974), *Orodromeus* (Scheetz, 1999), and is probably present in the anterior most tooth in *Tenontosaurus dossi* (Winkler et al., 1997).

4.3.7 Accessory elements

Hyoid (Fig. 4.3B, D): Only the anterior and posterior ends of the left hyoid are preserved, and the posterior half is preserved of the right element. The preserved parts of the left element suggest an original length of approximately 2.1–2.3 cm. The hyoid was obviously a long and slender element with slightly expanded ends, as in other dinosaurs. The anterior end was more rounded, whereas the posterior end seems to be flattened transversely. The very slender appearance of the hyoids is similar to *Mantellisaurus atherfieldensis* (Norman, 1986), but is different from the anteriorly strongly expanded hyoids of *Iguanodon bernissartensis* (Norman, 1980) and *Ouranosaurus* (Taquet, 1976). However, the morphology of the anterior and posterior ends of the hyoids in *Dysalotosaurus* is apparently inconsistent with the morphology in other ornithopods, where the flattened end is posterior and not anterior. Whether this is a matter of preservation, of incomplete ossification, or indeed a true anatomical feature, cannot currently be decided.

4.3.8 Axial skeleton

Proatlas (Figs. 4.2 and 4.3A, D): A bony plate, preserved between the ventral end of the right quadrate and the right atlantal neural arch, is tentatively determined as the left proatlas. The oval to sub-rectangular dorsal face (now posteriorly directed) is smooth and slightly convex, and somewhat narrows posteriorly. Nevertheless, if correctly identified, the proatlas of *Dysalotosaurus* is considerably wider than in other ornithopods, such as *Hypsilophodon*, *Mantellisaurus*, and *Iguanodon* (Galton, 1974; Norman, 1980; 1986).The anterolateral edge is thickened and supports a stout ridge that extends ventrally. Together with the dorsal plate, this ridge defines a large, medioventrally concave ventral facet for the articulation with the skull. Laterally, the dorsal plate also slightly overhangs the ventral ridge, so that the two structures additionally form a much smaller, ventrolaterally concave lateral surface. The posterior part of the proatlas is a flat bony plate that would have overlapped the anterior end of the atlantal neural arch.

Atlas (Figs. 4.2 and 4.3B, D): Both halves of the neural arch of the atlas are preserved and almost complete. They are slightly disarticulated and are rotated posteroventrally from the braincase at more than 90°. At their bases, two corroded bony surfaces are visible in the matrix. The CT images demonstrate that these two surfaces belong to the lateral articular ends of the intercentrum of the atlas, which is still covered with sediment. The neural arches are broad and T-shaped in lateral view. They have a robust foot with a pronounced ventral bulge dividing the ventral articulation surface into a smaller, anteroventrally facing anterior facet for the contact with the occipital condyle, and a larger, more or less horizontal ventral facet for the intercentrum. A slightly constricted shaft connects this foot with a sub-rectangular, distinctively curved and thin, dorsolaterally facing roof. The shaft is anteroposteriorly convex in lateral view, and there is a slight depression anteriorly between the facet for the occipital condyle and the dorsal roof. The ventral border of the roof rises posteriorly and ends in a prominent posterior spike in lateral view, the end of which is broken off on either side.

In dorsal view, the anterior part of the roof of the neural arch is broad, but it narrows posteriorly. The surface of the roof is slightly twisted, so that the anterior part, which would have been overlapped by the proatlas in the articulated vertebral column, faces more laterally than the posterior part that overlapped the prezygapophysis of the axis. The posterior spike described above is restricted to the lateral part of the dorsal roof.

The neural arch of the atlas is very similar to that of *Lesothosaurus* (Sereno, 1991) and *Hypsilophodon* (Galton, 1974) in its general shape and proportions, whereas the neural arch is relatively smaller in *Iguanodon*, *Mantellisaurus*, and *Ouranosaurus* (Norman, 1980; 1986; Taquet, 1976).

Axis (Figs 4.2, 4.3 and 4.4B): The axis is located between the posterior ends of the lower jaws, and is rotated backwards and downwards at about 140°. Except for the lateral sides of the neural arch, all surfaces are corroded. The left postzygapophysis and the posterior face of the vertebral centrum are lost. The neural canal is very large and has approximately the same diameter as the centrum. The neurocentral suture is only visible in a few places, because of the generally poor preservation of the bone. It extends from the posterodorsal corner of the centrum anteriorly and slightly dorsally, and then curves ventrally again behind the prezygapophysis. The centrum seems to be short and only slightly constricted; no notable features can be made out on the corroded lateral side. The posterior end is semi-oval in shape and approximately as high as it is wide. The corroded surface of the posterior end reveals a spongy interior of the bone, with large cells separated by thin bony struts. Only the very thin cortex seems to be well ossified.

The neural arch is dominated by the convex, posteriorly rising neural spine, which forms a sharp dorsal edge. The anterior end bears a thickened knob with a rounded, dorsally oriented surface. The posterior end flares laterally towards the base of the right postzygapophysis, above which it forms a stout, laterally directed epipophyseal ridge. The posterior end of the neural arch forms a small, vertical wall between the postzygapophyses. The prezygapophyses are preserved, but

are only visible dorsolaterally of the axis. They are small, lobe-shaped processes that extend anterolaterally from the anterior end of the neural arch. With a transverse width of almost 12 mm, they account for the widest part of the axis. The more laterally oriented outer surfaces of the prezygapophyseal ends fit well into the concave medial walls of the neural arches of the atlas.

The axis of *Dysalotosaurus* is generally similar to that of other ornithopods, but a few differences are found. Most notably, the neural spine does not extend anterior to the prezygapophyses, similar to the condition in basal ornithopods, such as *Hypsilophodon* (Galton, 1974) or *Tenontosaurus* (Winkler et al., 1997), but in contrast to more advanced iguanodontians (Gilmore, 1909; Norman, 1986; Taquet, 1976; Weishampel et al., 1993). Furthermore, the neural spine is markedly convex over its entire length, whereas it is straight or even slightly concave in *Tenontosaurus* (Winkler et al., 1997), *Camptosaurus* (Gilmore, 1909), and *Ouranosaurus* (Taquet, 1976), and is only slightly convex in *Mantellisaurus* (Norman, 1986).

4.4 Discussion

The overall impression of the skull BSPG AS I 834 is that of a juvenile. The most obvious juvenile features are the relatively large orbit, the short snout, and the descending occiput. However, a closer look at this specimen has revealed additional well known juvenile features, such as open sutures (Carpenter et al., 1994; Goodwin et al., 2006; Pritchard et al., 1956), striated and very porous bone surfaces (see also Carr, 1999; Sampson et al., 1997), and a smaller number of tooth positions in the jaws (Carpenter et al., 1994). Further differences to adult or subadult skulls of *Dysalotosaurus* are discussed below.

4.4.1 Cranial anatomy of *Dysalotosaurus*

Although the complete anterior part of the skull is lost, the specimen provides some new information on the cranial osteology of *Dysalotosaurus*. Several previously unknown elements of the lower jaw are preserved in this skull (splenials, articulars, and the single coronoid). Apart from the poorly preserved vomer and coronoid, the only cranial elements of *Dysalotosaurus* that remain unknown are the palatines and quadratojugals. It is possible that at least the palatines are present and covered in matrix in the skull described here, but they could not unambiguously be identified on the CT slices.

The most important new information on the skull anatomy in *Dysalotosaurus* concerns the mandibular articulation. Janensch (1955) placed the quadrate condyle on a hypothetical, boss-like articular, so that the condyle did not touch the surangular glenoid at all (Fig. 4.1B). This was slightly changed by later authors (Galton, 1983; Norman, 2004), but, understandably, remained unresolved. The newly described articular demonstrates that the quadrate condyle rests directly on the surangular, as in all other ornithopods (e.g. Galton, 1974; Norman, 1986; 2004; Weishampel et al., 2003). The articular 'disc' is located between the retroarticular process of the surangular and the posterior end of the prearticular. Its forward projecting medial side aligns with the medially thinning quadrate condyle, and borders it medioventrally and posteroventrally (Fig. 4.1D).

4.4.2 General ontogenetic changes

Three main tendencies in ontogenetic development of the skull in *Dysalotosaurus* can be recognized.

1. All sutures of BSPG AS I 834 are visible or completely open. Nearly all displaced elements are separated along their sutural faces. Even the sutures between the braincase elements are at least visible with the microscope, with the exception of that between the exoccipitals and opisthotics. The latter suture was described by Sues (1980) for *Zephyrosaurus* and by Welles (1984) for

Dilophosaurus, but these two elements otherwise seem to fuse indistinguishably very early in ontogeny in all dinosaurs. As described by Janensch (1955:131), the sutures of the basicranium in the large skulls dy A and dy B are still open, or are at least visible, implicating that the fusion of the elements of this structure happened rather late in ontogeny.

In BSPG AS I 834, the basioccipital and basisphenoid seem to be most closely sutured, and most other specimens, in which these two elements are known, show a similar situation. In contrast, the sutural contacts and grooves for the parietal are well preserved on the supraoccipital, and implicate an unfused suture between these two elements at this ontogenetic stage. Janensch (1955) mentioned a specimen that showed fusion of the supraoccipital–parietal suture but not of the elements of the lateral braincase wall. Combined with his comments on other partial skulls (which were destroyed during World War II, and are now only known from drawings by Pompeckj, 1920), the sequence of fusion of all braincase elements seems to begin with the exoccipital–opisthotic, followed by the skull base (basioccipital, basisphenoid, and parasphenoid), the supraoccipital and parietal, and the remaining elements of the braincase. The laterosphenoids seem to be the last elements that fuse in the braincase. In BSPG AS I 834, they are both completely disarticulated, whereas all the other elements remained at least in close contact. All other known laterosphenoids of *Dysalotosaurus* are either isolated, disarticulated, or articulated, but are totally unfused to their neighbors, independent of the ontogenetic stage. However, there might be considerable variation in the sequence of fusion in the elements of the braincase in *Dysalotosaurus*, as the second largest basioccipital known (GZG V.6481) seems to have separated from the basisphenoid at its suture.

A fusion of sutures of the dermal bones is unknown, apart from the exception of the largest preserved frontals (MB.R.1319 or dy 5 in Janensch, 1955:131), which are fused with the parietal. All preorbital bones have rather smooth sutural facets, which might account for the rare preservation of, for example, the nasals and premaxillae. Many lateral dermal bones are additionally part of the so-called pleurokinetic chewing mechanism (see Norman, 1984; Norman & Weishampel, 1985; Weishampel, 1984). Thus, a fusion of the sutures of the preorbital portion and the lateral wall of the

skull is quite unlikely, and it is to be expected that these elements were unfused even in fully adult individuals (although see Holliday & Witmer, 2008, for a critical evaluation of cranial kinesis in ornithopods).

It should be mentioned that the sequence of suture fusion of a single species is not simply transferable to other species. This sequence is highly variable and depends strongly on the specific biomechanical demands of certain skull areas (Herring, 1974), and is additionally highly variable in different individuals of a species (Wang et al., 2006). Thus, dinosaurs with different skull proportions and functions may display different patterns of fusion. One example is the ontogenetic series of *Triceratops* skulls (Horner & Goodwin, 2006), where the midline suture of the nasals fuses somewhere between the juvenile and subadult growth stage certainly caused by the higher biomechanical stress in this area. However, much more research about fusion sequences and their biomechanical reasons are needed to better assess the significance of sutural fusions as an ontogenetic character.

2. The second and very notable tendency during growth is the change in the size of the orbit relative to the skull, because it influences the shape of all adjacent bones (see Fig. 4.1). In juveniles, the orbit is very large compared with the skull length (Carpenter et al., 1994; Coombs, 1982; Horner & Currie, 1994; Salgado et al., 2005), and it decreases relatively during growth (Dodson, 1975b; 1976). Thus, with the changing curvature of the orbital edge, the shapes of the surrounding bones are affected, such as, for example, the angles between different rami in the jugal and postorbital.
In the frontal, the orbital ridges on the ventral side change from strongly convex structures with a wide orbital angel in juveniles to flatter and more straight features with a narrower orbital angel in adults, in which the frontal forms a relatively smaller portion of the orbital rim (see Carpenter, 1994).

3. The third important main tendency of growth in the skull is the overall relative lengthening of the skull, and especially of the preorbital region. Although many parts of the preorbital region of the skull are missing in the specimen described here, the calculation of the total length of the lower jaw and the short maxillaries indicate a short snout in juveniles of *Dysalotosaurus* (Fig. 4.1C, D). A

pronounced increase in the relative skull length is a well-known growth phenomenon in dinosaurs (e.g. Butler et al., 2008a; Carpenter et al., 1994; Long & McNamara, 1997; Rauhut & Fechner, 2005; Salgado et al., 2005). In *Dysalotosaurus*, the occipital region is straightened, the descending parietal plateau is lifted into a horizontal position and the infratemporal fenestra is increased in height, as was also described for the closely related *Dryosaurus* (Carpenter, 1994). In a reconstructed embryonic skull of *Hypacrosaurus* (Horner & Currie, 1994: fig. 21.3), the postorbital region of the skull is also slightly declining posteroventrally, but less so than in dryosaurids. Embryonic titanosaurs have a strongly posteroventrally-sloping postorbital region of the skull (Salgado et al., 2005), but this is also still the case in adults (Curry Rogers & Forster, 2004). In other dinosaurs, including *Coelophysis* (Colbert, 1989), *Mussaurus* (Bonaparte & Vince, 1979), and *Massospondylus* (Reisz et al., 2005), embryonic or young juvenile skulls have been reconstructed with a straight postorbital region, but the reliability of these reconstructions has to be confirmed by further analyses of the respective specimens.

The ontogenetic changes of the parietal and occipital region might be related to the accommodation of larger adductor muscles. Together with the lengthening of the preorbital region and the jaws, the skull is thus changing from a short, dorsally rounded shape to a long and posteriorly ascending triangular shape. Most of these changes are probably related to increasing food intake and processing rates (longer jaws and an increase in the number of teeth) and associated biomechanical necessities (larger adductor muscles).

4.4.3 Ontogenetic variation in single elements

In the following, all individual skull elements are briefly discussed, in which ontogenetic variation was noticed. All ratios and allometric coefficients presented here are derived from the measured distances (or variables) listed in Appendices I and II. A small ‘a’, followed by a number, refers to the respective measurement in Appendices I and II. No definite ontogenetic changes were

noticed in the exoccipital, parasphenoid, squamosal, angular, vomer, coronoid, and the splenial. However, this might result from the fact that no changes were noticed in comparison with adult elements (exoccipital and angular), or because either the preservation of the juvenile remains is too poor to allow a comparison (squamosal and parasphenoid), or no comparative adult elements are known (vomer, coronoid, and splenial).

Maxilla: One of the notable ontogenetic changes in the maxilla concerns the relative height of the main body of this bone. The MAA of the main body height from the medial alveolar edge to the medial bulge (which marks the anterior end of the palatine suture; a_{66}) and the main body maximum width just before this bulge (a_{68}) results in a significant strong positive allometric coefficient for the height (a_{66} = 1.297), compared to the width (a_{68} = 0.7033). A remarkable feature of the juvenile skull BSPG AS I 834 is, furthermore, the large cavity in the base of the ascending process of this bone. Such a cavity is also present in larger specimens (e.g. MB.R.3468), but seems to be relatively smaller, which is in general accordance with the decrease in relative width of the bone. Furthermore, small maxillae have a slightly lower number of tooth positions (probably about ten, as in the dentary) compared with larger elements (11–13).

The positive allometry of the height between the alveolar edge and the medial bulge for the articulation with the palatine is probably related to higher stresses during chewing, and to provide more space for larger teeth in older individuals. It further represents an ontogenetic deepening of the pharynx, as the attachment surface for the palatine is also displaced dorsally. This might have allowed older individuals to ingest a larger quantity of food at once, compared with juveniles. The apparent reduction in relative size of the cavity in the base of the ascending process might indicate that cranial pneumaticity decreased during ontogeny in this ornithopod (if it is correctly identified as a pneumatic feature associated with the paranasal sinus system of the antorbital fenestra and fossa, see above), as has been argued for basal tetanuran theropods by Rauhut & Fechner (2005). The increasing number of tooth positions during growth is a widespread and common ontogenetic

feature in ornithopods (Brett-Surman & Wagner, 2007; Butler et al., 2008a; Carpenter et al., 1994; Tanke & Brett-Surman, 2001), although the opposite tendency is visible in tyrannosaurids and some crocodiles (Carr, 1999).

Jugal (Fig. 4.5): Only the larger left jugal of dy B (MB.R.1333) is available for an ontogenetic comparison. As noted above, the orbital edge of the small jugal of BSPG AS I 834 forms a more obtuse angle than the orbital edge of the large element. Furthermore, the orbital edge of the juvenile jugal ascends in a gradual, gently concave curve posterodorsally onto the postorbital process, whereas the edge of the large jugal performs a sharp bend at the base of this process (Fig. 4.5). Thus, the large jugal is clearly separated into an almost horizontal maxillary process and a main body with a perpendicular postorbital process. A further difference is found in the facet for the lacrimal, which ascends more steeply posterodorsally and is more laterally directed in the larger element. Thus, the degree of lateral overlap of the lacrimal on the jugal is increasing during growth.

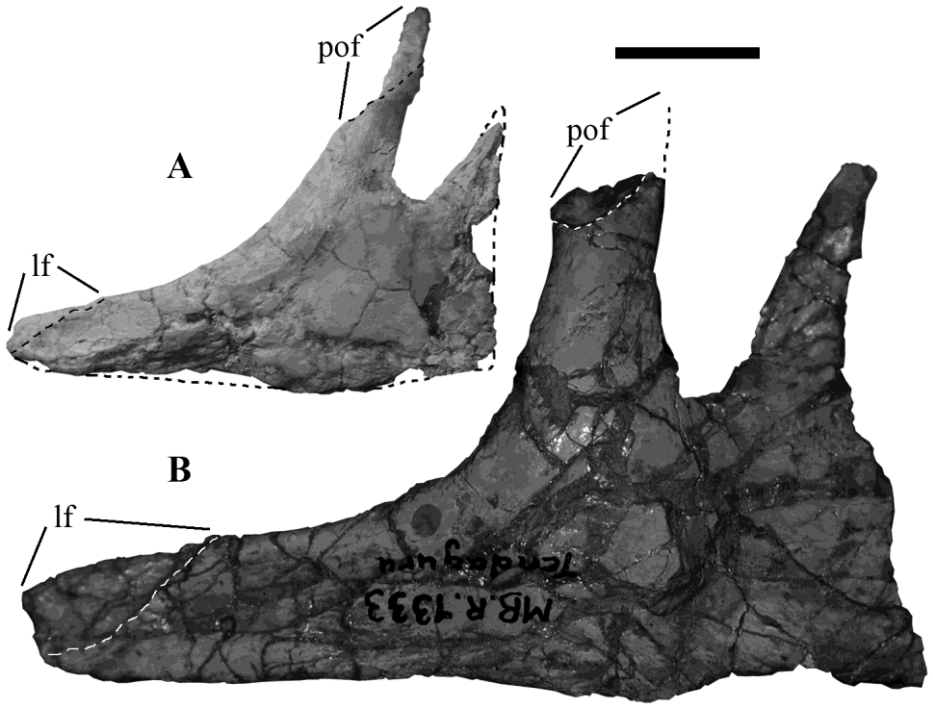

Fig. 4.5: *Comparison of two preserved jugals of* Dysalotosaurus *in lateral view.* ***A*** *– Left jugal of the juvenile skull BSPG AS I 834.* ***B*** *– Left jugal of the relatively older individual dy B (MB.R.1333). Note the ontogenetic differences of the lacrimal facet (lf) and the postorbital facet (pof). Scale bar: 1 cm.*

In addition, the anterior end of the jugal of the smaller individual is broadened mediolaterally, whereas the large jugal is flattened in this part.

The base of the postorbital process of the small jugal is shorter and more compact than the longer and more slender base of the corresponding process of the large jugal. Furthermore, the location of the lowest point of the postorbital facet is anterior in the small jugal and anterolateral in the larger element. The top of the postorbital process of the large jugal is broken off, so only the jugal facet on larger postorbitals suggests a similar shape and dorsal extent of the postorbital facet as in the small jugal.

The obviously lateral migration of the deepest point of the postorbital facet on the corresponding process of the jugal (Fig. 4.5) is also known in two other ornithopods (*Orodromeus makelai* in Scheetz, 1999: table 1; indicated in the juvenile holotype skull of *Gasparinisaura cincosaltensis* in Coria & Salgado, 1996:446; see also Salgado et al., 1997), and is therefore identified as a clear juvenile character. The observed ontogenetic increase of the overlap between jugal and lacrimal in *Dysalotosaurus* results in a more robust connection of both elements in the adult skull. Furthermore, the nearly perpendicular postorbital process in the larger specimen is related to the relative decrease of the orbit in older individuals.

Frontal (Figs. 4.1 and 4.6): The maximum width of the frontals (a_{38}), located transversely between the median suture and the posterior end of the orbital rim, increases slightly relative to the total length (a_{39}) in larger individuals. In the smallest specimen in which both measurements were available (BSPG AS I 834; Appendix I) the maximum width reaches about 30% of the total length, whereas the maximum width of the largest frontal measured (SMNSoN1; Appendix I) reaches about 41% of its total length. Thus, small frontals are relatively narrower and more elongate than large frontals. This additionally results in a wider orbital rim with a much steeper medial border ventrally in small specimens.

The central dome in the posterior part of the articulated frontals of BSPG AS I 834 and other small specimens is spatially restricted and flat. Larger frontals have a more prominent dome, which

also acquires a larger area on the dorsal surface. The relative increase of the size of the central dome is statistically significant (from an MAA of all measurements, except the total length because of too few values for a_{39}), with the maximum thickness of the frontals at the dome (a_{36}) showing a positive coefficient of 1.684. In contrast, the length of the orbital rim (a_{34}) and the width of the ventral groove for the cerebellum (a_{37}) have significantly negative coefficients (a_{34} = 0.2908; a_{37} = 0.6754). Finally, as noted above, the ventral deflection of the posterior end of the frontal is marked in small frontals, whereas large elements are more or less straight.

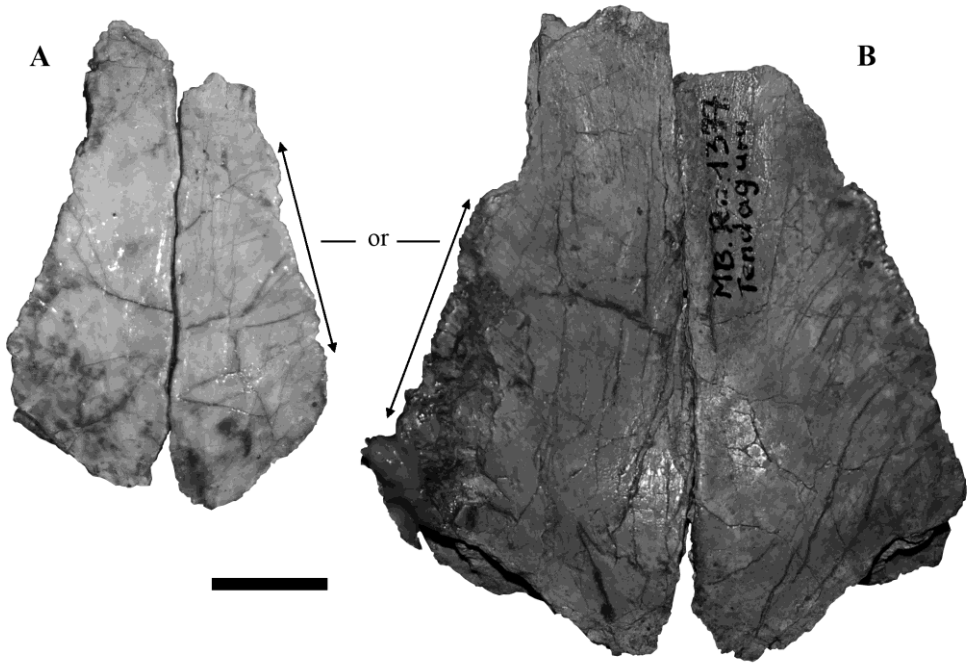

Fig. 4.6: *Comparison of associated frontal pairs of two individuals of* Dysalotosaurus*, presented in articulation in dorsal view.* ***A*** *– The smallest frontals preserved (the left frontal GPIT/RE/1595/17; the right frontal GPIT/RE/1595/15).* ***B*** *- Large frontals of the individual dy A (the right frontal MB.R.1377; the left frontal MB.R.1378). The orbital rim (or) is marked. Scale bar: 1 cm.*

Thus, two marked differences are found in the frontals of younger and older animals. The first is clearly related to the relative decrease in size of the orbit, so that the frontal width increases compared with its length and compared with the length of the orbital rim. The other difference is the interesting relative enlargement of the central dome in its height and extension. There is no sign that this is caused by an extension of the brain ventrally, as the ventral depression for the cerebellum even reduces its relative extension during growth. It is clearly a thickening of massive bone. The

influence of stress during chewing activity cannot be excluded, as long as no biomechanical analysis of the skull of *Dysalotosaurus* has been carried out. However, an analysis of a subadult ornithopod skull using finite elements by Ohashi (2006) did not indicate higher stress concentrations in the frontal area. Another possibility is the interpretation of the central dome as a feature of sexual dimorphism. Unfortunately, the very restricted sample size contains no clear signs of sexual dimorphism, so more material is needed to confirm this idea. It might be worth noting that a similar dome on the posterior part of the frontals is also present in juvenile lambeosaurines (Evans et al., 2007; Horner & Currie, 1994), but that might argue against sexual dimorphism.

Parietal: On the parietal, the margins of the supratemporal fossa are much more clearly delimited in larger individuals. The small specimens MB.R.1317 and BSPG AS I 834 have smooth and flat edges that are only clearly visible at the anteromedial margin of the fossa. As already noted above, a further ontogenetic difference seems to be the absence of a posterior process of the parietal in juveniles that contacts the supraoccipital in older individuals. The more prominent muscle attachment sites on the parietals in older individuals and an increase in anteroposterior length of the supratemporal fenestra (Fig. 4.1A, C) is again related to an enlargement of the jaw muscles in these animals during ontogeny. The development of a postparietal process at the posterior end of the parietal (Pompeckj, 1920) most probably has also helped to reinforce the posterodorsal skull roof. In adult *Dysalotosaurus*, the parietal–supraoccipital complex represents a robust frame for attaching jaw and neck muscles. That such a strengthening of the posterodorsal edge of the skull was indeed of biomechanical advantage is furthermore supported by the relatively early fusion of the suture between the supraoccipital and parietal (see above).

Postorbital: Apart from the lowest point of the jugal process, which seems to migrate from an anterior position in smaller postorbitals to an anterolateral position in larger elements, no other ontogenetic variation is determinable. The postorbital–jugal joint (see Weishampel, 1984) is one of the slightly mobile joints between two rigid skull units. The pleurokinetic skull in ornithopods

(Norman, 1984; Norman & Weishampel, 1985) consists of the rigid median elements of the skull roof and snout, and, on the other side, of the united elements of the cheek region and the palatoquadrate complex. The exact biomechanical effect of the ontogenetic lateral migration of the postorbital–jugal joint on the pleurokinetic function is unknown, but it might be related to the relative transverse flattening of the jugal.

Pterygoid: The pterygoids of the large skull dy B (MB.R.1324; MB.R.1332) have a strongly backwards pointing, hook-shaped ectopterygoid process, whereas this is only incipiently present in the small pterygoids of BSPG AS I 834. This implies a much more extensive and robust articulation with the ectopterygoid in adults. Therefore, this connection could better withstand the stronger biting forces in larger individuals.

Ectopterygoid: Apart from BSPG AS I 834, only one other left ectopterygoid, with a total mediolateral length of 26.3 mm (MB.R.1330; see Janensch, 1955), is known. The ectopterygoids of BSPG AS I 834 differ from the larger specimen mainly in the shape of their straight, very slender, and rounded mid-shafts (Fig. 4.4C). In contrast, the stout mid-shaft of MB.R.1330 is far more curved and is anteroventrally flat.

The long and straight ectopterygoid shafts of the juvenile skull BSPG AS I 834 bridged the relatively wide space between the jugal and the pterygoid caused by the large eyeballs. The stout, folded shape of the larger ectopterygoid might reflect increasing biting forces induced by the pterygoideus muscle. Ostrom (1961) and Galton (1974) suggested that at least parts of the M. pterygoideus dorsalis originate on the ectopterygoid in ornithopods, even in hadrosaurs, where the ectopterygoid is reduced to a strap-like bone (Heaton, 1972).

Quadrate: The cotylar head of a well-preserved large quadrate (GPIT/RE/3608) differs from that of smaller specimens (BSPG AS I 834; MB.R.1326) in being more hook-shaped, with a ventral

expansion of the distal part of the cotylar head (Fig. 2.3), similar to the morphology seen in *Camptosaurus dispar* (Brill & Carpenter, 2007; Gilmore, 1909). In contrast to *Dryosaurus altus* (see Carpenter, 1994), the curvature of the quadrate body is not more marked in younger animals of *Dysalotosaurus* when compared with larger individuals.

The relative expansion of the cotylar head might be related to the mobility of the quadrate cotyle in its articulation with the squamosal, maybe in relation to slight propalinal movements of the jaws during occlusion (see Ostrom, 1961; Rybczynski et al., 2008).

Laterosphenoid: The maximum posterior thickness of the laterosphenoid (a_{23}) increases relative to the posterior height (or height of the prootic contact face; a_{21}) from about 26% in BSPG AS I 834 to about 37% in the specimen GPIT/RE/9000l. The application of the MAA on the three completely measurable variables a_{21}, a_{22}, and a_{23} confirms this tendency, although the positive coefficient of a_{23} (= 1.298) is insignificant. This increase in thickness of the dorsal braincase wall might reflect the increasing strength of the deep jaw-closing muscles. Additionally, the ventral depression for the ramus ophthalmicus of the trigeminal nerve is less deep than in the respective element of dy A. The ontogenetic deepening of this depression was already observed in *Dryosaurus altus* by Carpenter (1994).

Prootic: The crista prootica becomes a sharper and more protruding edge in larger specimens. Furthermore, the thickness of all suture faces seems to increase relative to all other distances. The MAA demonstrates that the anteroventral thickness of the prootics (a_{19}) strongly increases during growth compared with all measured lengths and heights of the element, which is supported by the strong positive allometric coefficient of 2.167. However, this coefficient is still statistically insignificant, and more specimens than the six measured here are needed to test the tendency unambiguously. As in the laterosphenoid, both the increased thickness and the more strongly pronounced crista prootica probably reflect the increasing strength of the deep jaw muscles.

Basisphenoid (Fig. 4.7): The tubera basioccipitalia are very weak and smooth in the small basisphenoid MB.R.3536. In contrast, the large specimens dy A and dy B have very prominent tubera, and the posterior two-thirds of them have rugose surfaces (see Fig. 4.7A, B). The tubera in BSPG AS I 834 show an intermediate state with respect to their prominence. The degree of rugosity is unknown because of their corroded surface. Several neck muscles attach to the basal tubera (M. rectus capitis anterior and a part of the M. longissimus capitis; Ostrom, 1961), and thus the increased prominence and rugosity of these structures indicate increasing strength and mass of attaching ligaments and/or muscles. The same feature is found in other dinosaurs (e.g. Carpenter, 1982; Horner & Currie, 1994; Jacobs et al., 1994).

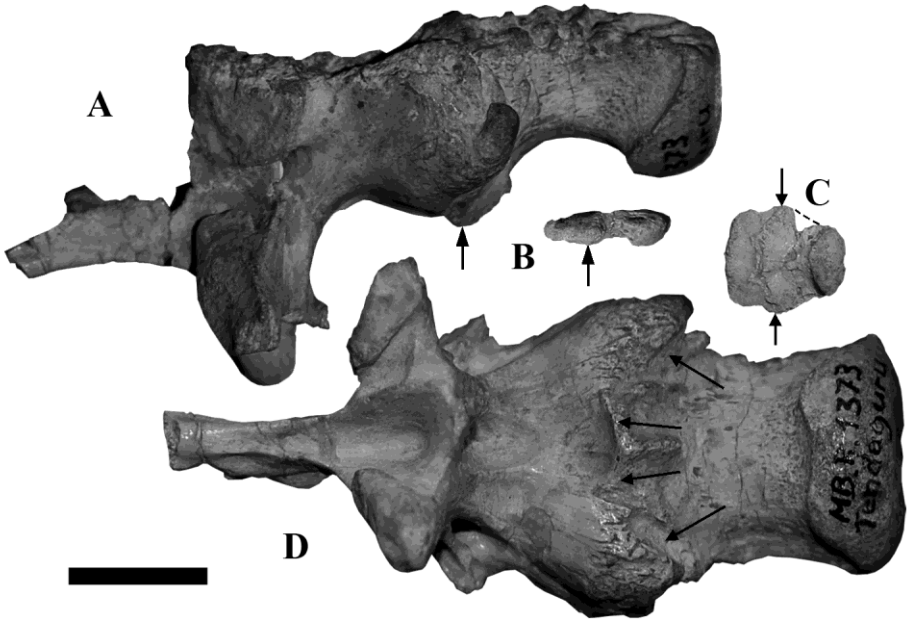

Fig. 4.7: *Comparison of the cranial base of two individuals of* Dysalotosaurus*. Small arrows indicate the location of the suture between the basioccipital and the basisphenoid. Larger arrows indicate the location of the tubera basioccipitalia. Note also the shape of the ventral lip of the occipital condyle.* ***A*** *– The large cranial base of dy A (MB.R.1373) consists of the basioccipital, the basisphenoid with the long ventral basipterygoid processes, and the anteriorly incomplete parasphenoid, in left lateral view.* ***B*** *– The smallest known cranial base (MB.R.3536) consists of the basioccipital and the posterior half of the basisphenoid, in left lateral view.* ***C*** *– Same as in B, in ventral view.* ***D*** *– Same as in A, ventral view. Scale bar: 1 cm.*

Supraoccipital: The supraoccipital crest of the large supraoccipitals of dy A (= MB.R.1372) and dy B (= MB.R.1367) is much more prominent and more sharply defined than in BSPG AS I 834, and

consists of a thin, vertical lamina. In these large specimens, this lamina connects to a posterior median process of the parietal, and helps to define two large so-called postparietal foramina between the supraoccipital and parietal (Pompeckj, 1920). The same is present in a drawing of a larger, lost skull made by Pompeckj, and reproduced by Janensch (1955: fig. 5), and is comparable with a similar but less extensive structure in *Hypsilophodon* (Galton, 1974: fig. 8). In contrast, a smaller skull (also lost) illustrated by Janensch (1955: fig. 4) is missing the posterior process of the parietal and its connection with the supraoccipital, so that only one, very large median foramen is present between the two elements. No indication of a connection between the supraoccipital crest and the parietal is present in the specimen described here, so the latter was most probably also the case in BSPG AS I 834. These changes in the morphology of the supraoccipital crest undoubtedly reflect the increasing forces applied to the posterior face of the skull by the ligamentum nuchae and M. spinalis capitis (Ostrom, 1961).

Basioccipital (Fig. 4.7): The ventral lip of the articular surface of the occipital condyle exhibits a single, rounded anterior tip in the basioccipital of BSPG AS I 834, and also in an even smaller, isolated basioccipital (MB.R.3536; Fig. 4.7C). The other three known specimens (dy A = MB.R.1373; dy B = MB.R.1367; GZG.V.6481) are all at least of double the size of BSPG AS I 834. The ventral condyle lip in these larger specimens is broadly trapezoidal in outline, and exhibits two separate anterior tips with a flat depression in between (Fig. 4.7D). The lateral height of the neck of the occipital condyle increases relative to its width from the very flat small specimen MB.R.3536 (height/width ratio of approximately 0.23) to the large dy A (height/width ratio of approximately 0.71). This ratio is 0.36 in BSPG AS I 834. Furthermore, the minimal width of the neck migrates in the small MB.R.3536 from the edge of the articular face of the condyle to the middle of the neck in the large dy A, dy B, and GZG.V.6481, so that the neck becomes relatively more slender and longer. Additionally, the ratio of the width of the occipital condyle and the width of its neck reveal an

increase of the condyle width relative to its neck (neck width/condyle width: MB.R.3536 = 1.04; BSPG AS I 834 = 0.97; dy A = 0.83; dy B = 0.81).

The most important ontogenetic differences in the basioccipital are thus visible in ventral view. In very young juveniles of *Dysalotosaurus*, the contour of the basioccipital has a condyle neck that is broader than the condyle itself (Fig. 4.7C), whereas it changes into a slender neck that is distinctly narrower than its condyle during ontogeny. This juvenile feature seems to be typical at least for ornithischians (Horner & Currie, 1994: fig. 21.10; Jacobs et al., 1994: fig. 22.2), and therefore seems to be a good indicator for very young animals. A tiny basioccipital referred to *Saurornithoides* by Carpenter (1982: fig. 2h) also seems to show this feature, although he noted in the text (p. 129) that 'the occipital condyle . . . is . . . separated from the main body by a constricted neck'. However, this statement might refer to the lateral view of the specimen, in which a neck is indeed visible (Carpenter, 1982: fig. 2g), as is the case in *Dysalotosaurus* (Fig. 4.7B). In the skull of the somewhat older juvenile BSPG AS I 834, the neck of the occipital condyle is already more pronounced, although it is still relatively shorter and broader than in adults. Other juvenile features left are the single-tipped anteroventral edge of the condyle lip and the relatively lower condyle in lateral view.

Dentary: Three size classes of dentaries can be distinguished in the available material of *Dysalotosaurus*, based on their tooth row lengths. The dentaries of BSPG AS I 834 belong to the smallest known specimens, with tooth rows of approximately 30 mm in length. Just as in the other small dentary complete enough to count the number of alveoli (GPIT/RE/1595/22), the dentaries of the small size class bear ten teeth. The intermediate size class (tooth rows of about 45 mm in length) bear between ten and 12 teeth, whereas the number of alveoli of the best-represented large size class (tooth rows of about 60–65 mm in length) varies between 11 and 13 teeth. Thus, there is a slight ontogenetic increase of tooth positions from ten to 13 (app. 30%), but, simultaneously, there is an increase of the tooth row length of more than 100%, indicating a relative broadening of the teeth during ontogeny. This broadening was not necessarily uniform along the tooth row, as indicated by

the observation that only the juvenile dentary of BSPG AS I 834 bears three very slender and rod-like teeth anteriorly, whereas all larger dentaries only possess the 'average-shaped' broader teeth. In addition, the MAA of five measured variables reveals an overall heightening of the dentary main bodies during growth, because the minimal height of the tooth-bearing part (a_{74}) increases with a positive coefficient of 1.174 (Fig. 4.8). In contrast to the negative coefficient of the maximum lateral thickness of the dentary main body (a_{72} = 0.8277), the coefficient of the body height is constantly significant in bivariate comparison with the other dentary measurements. Finally, there is a slight change of the bone surface at the articular face for the splenial. Only the largest dentaries have rough and posteriorly slight ascending striations on this surface area, whereas the smaller dentaries are very smooth.

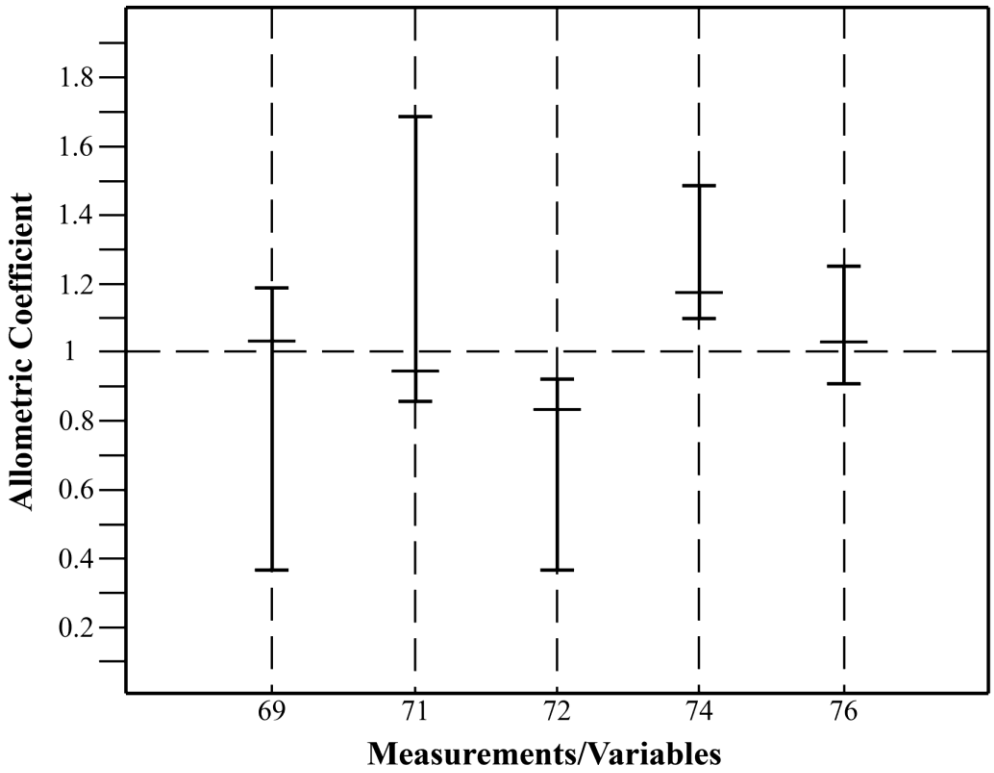

Fig. 4.8: *Diagram resulting from the multivariate allometric analysis (MAA) of five measurements of the dentary carried out by the PAST program. The allometric coefficient is marked by the broad line imbedded in the 95% intervals. The numbers of the measurements are explained in Appendix II.*

The increasing height of the tooth-bearing part of the dentary compared with its width can be explained by larger teeth in larger animals, which need longer roots for a firm anchorage. That the

teeth indeed become relatively larger reveals the comparison of the tooth row length and the tooth number. As in other ornithopods, the tooth number increases during growth (Horner & Currie, 1994; Tanke & Brett-Surman, 2001; Weishampel et al., 2003), but single teeth are also becoming relatively wider. The occurrence of slender, rod-like teeth only in small dentaries supports this tendency. The more rugose articular surface for the splenial in larger dentaries is a common ontogenetic change of articular surfaces during the increasing degree of connection between two adjacent bones (Pritchard et al., 1956).

Surangular: In the surangular, the height of the retroarticular process (a_{82}) seems to increase relative to the maximum height of the laterally visible part of the anterior plate (a_{77}), from the small surangular of BSPG AS I 834 (about 35%) to the large MB.R.1335 (about 61%). However, the retroarticular process of the large specimen is partly crushed, so it was impossible to take an unambiguous measurement of this part. Another change is the decrease of the distance between the posterior edge of the dentary facet on the surangular anteriorly (a_{81}) and the anterior end of the glenoid (marked by the tip of the lateral glenoid process), relative to the total surangular length (a_{80}). Thus, the distance from the glenoid to the retroarticular process increases from about 42% in BSPG AS I 834 to about 49% in MB.R.1335. The existence of a second small anterior foramen on the surangular plate in BSPG AS I 834 is probably just intraspecific variation, because another surangular of approximately the same size from an associated skull in the collections of Stuttgart (SMNS, unnumbered; Fig. 3.2) lacks such an additional foramen.

The increase of the height of the retroarticular process of the surangulars is probably related to a relative enlargement of the attachment sites for the M. depressor mandibulae and M. pterygoideus ventralis (Ostrom, 1961). The lengthening of the retroarticular process provides more space for the mandibular articulation itself, and might also increase the lever arm for the M. depressor mandibulae.

Prearticular: In comparison with the large isolated left prearticular (MB.R.1321; see Janensch, 1955), the splenial facet of the small element of BSPG AS I 834 is very faint and begins approximately in its central part. In MB.R.1321, this facet extends into the posterior half of the bone and is much better defined. Additionally, the plate-like, rounded ends seem to increase in height during growth. Both of these changes help to strengthen the postdentary complex of the lower jaw, both against the muscle forces acting on this structure, as well as the resulting reaction forces in the glenoid.

Dentition: As noted above, the most notable change in the dentition is a relative widening of the teeth during ontogeny. Furthermore, there is a notable difference in the relative size of the teeth in the anterior most three positions in the dentary and the rest of the tooth row in the juvenile skull BSPG AS I 834, but no such heterodonty is found in larger specimens. Unfortunately, the teeth of these three alveoli themselves are not well-enough preserved to say much about their detailed morphology, but they are certainly considerably more slender than more posterior teeth.

A similar pattern is found in other basal ornithopods. In *Agilisaurus*, three anterior teeth are cone-shaped and recurved, and also clearly differ in their function from the other dentary teeth (Barrett et al., 2005). More similar to *Dysalotosaurus*, slender and pencil-like anterior teeth are known from *Hypsilophodon* (the first three to five tooth positions, see Galton, 1974), *Orodromeus* (see Scheetz, 1999), and a single tooth in *Tenontosaurus dossi* (see Winkler et al., 1997). These teeth are more similar to the premaxillary teeth of basal ornithopods and might indicate a partially omnivorous diet in these animals (see Barrett 2000). If a similar function is inferred for *Dysalotosaurus*, this implies that this basal iguanodontian might have changed its diet during ontogeny, from partially omnivorous habits in juveniles to full herbivory in adults. However, better preserved material of these teeth is needed to test this idea.

Another probably ontogenetic difference in the teeth concerns the presence of secondary ridges on the lateral surface of maxillary teeth and the lingual surface of dentary teeth. Such ridges are absent in the teeth of BSPG AS I 834, but are present in teeth of adults (see, e.g. Janensch, 1955:

figs 14-16). Thus, the ornamentation of the enamel-bearing part of the tooth crown increases during ontogeny, as suggested by Rauhut (2001).

Neural arch of atlas: A muscle attachment site anteriorly between the lateral wall of the neural canal and the roof of the neural arch has a more prominent edge in larger specimens. Additionally, the concave anterior emargination between these parts is deeper and narrower than in small specimens. According to the position of the muscle attachment, it most likely represents the M. longissimus capitis profundus (see Tsuihiji, 2007: fig. 2B). This muscle leads anteroventrally to the posterior face of the tubera basioccipitalia (Tsuihiji, 2007), so the increasing prominence of its attachment site on the atlantal neural arch is most probably correlated with the increasing prominence and rugosity of the tubera.

4.5 Evolutionary implications

Although the large skull reconstructed by Janensch (1955: fig. 1) most probably does not represent a fully grown animal (Hübner, 2007), some of the ontogenetic variations noted provide insights into heterochronic processes in the evolution of ornithopod dinosaurs (Long & McNamara, 1997; Weishampel & Horner, 1994). Most of the rather obvious features, such as the longer snout with elongated nasals and premaxillae, the decreased relative size of the orbit, and the larger number of tooth positions (Fig. 4.1) are of peramorphic character (Long & McNamara, 1997). Norman et al. (2004:396) already pointed out that heterodontosaurids and basal euornithopods possess skulls 'not much modified from the cranial proportions observed in juveniles'. In *Dryosaurus*, this pattern is still visible, but *Camptosaurus* (Brill & Carpenter, 2007; Gilmore, 1909) already exhibits more of the derived peramorphic characters of the large iguanodontians of the Lower Cretaceous. Hadrosaurs are the final stage of this development, with extremely long and often remodeled nasals and premaxillae, and up to 60 tooth positions (Horner et al., 2004).

Similar peramorphic tendencies seem to exist in the frontals. The shortening and broadening of their dorsal shape, together with the relative decrease of the orbital rim during growth in *Dysalotosaurus* reflect the development in all ornithopods, and is even seen in sauropods (Salgado et al., 2005). Less derived '*Hypsilophodon*-like' basal ornithopods (see Norman et al., 2004), including *Hypsilophodon* (Galton, 1974) and Late Cretaceous taxa (e.g. *Thescelosaurus neglectus*; Galton, 1997), and basal, non-ankylopollexian iguanodontians (see Norman, 2004; Sereno, 1986), all possess relatively long and slender frontals, whereas all species of the Ankylopollexia have short and broad frontals. The orbital rim is more and more reduced (similar to eusauropods, see Salgado et al., 2005) until the frontals are completely excluded from the orbit in many hadrosaurs (Horner et al., 2004). At this stage, even the frontals of some young hadrosaurs seem to be excluded from the orbit, and are relatively short and broad (Horner & Currie, 1994). This is confirmed by the ratio of the frontal length and the paired frontal width, in which all non-ankylopollexian ornithopods seem to have a length to width ratio of more than one, and all ankylopollexians have a ratio of less than one. Carpenter (1994) suggested that *Hypsilophodon* (Galton, 1974) and *Zephyrosaurus* (Sues, 1980), which have a length to paired-width ratio of more than 1, are represented by immature individuals, because he also found long and slender frontals as a juvenile character in *Dryosaurus altus*. However, the ratio of the length to paired width in *Dysalotosaurus lettowvorbecki* decreases from 1.65 in BSPG AS I 834 to 1.16 in dy A. Nevertheless, no significant change of this ratio is seen in a hadrosaur (compare with Horner & Currie, 1994), and the ratio of large individuals of the non-ankylopollexian *Dysalotosaurus* remains above 1. Thus, the assumption of immaturity of *Hypsilophodon* and *Zephyrosaurus* (Carpenter, 1994) is of course possible, but their slender frontals can also be explained by their phylogenetic position inside the Ornithopoda.

The opposite tendency exists for the nasals and premaxillae, which can be attributed to their position in the skull, and is reflected by the lengthening of the muzzle noted above. All evolutionary changes from basal ornithopods on the way towards hadrosaurs seem to reflect the increased efficiency of chewing mechanisms for a higher quantity of better masticated food (Norman &

Weishampel, 1985; Scheetz, 1999; Weishampel, 1984). Similar to modern ungulates (see Carrano et al., 1999), all parts used for grabbing and chewing food (the muzzle and tooth-bearing elements) increase in size relative to the upper skull roof (e.g. the frontals), the orbitae, and the occiput. Indeed, if the change in heterodonty in *Dysalotosaurus* really reflects a change from omnivorous to fully herbivorous habits (see above), this ontogenetic change might give a glimpse into a turning point in the evolution of herbivory in ornithopods.

As discussed above, all ornithopods more primitive than iguanodontians have a somewhat heterodont dentition (more pointed and recurved premaxillary and anterior dentary teeth) that probably reflects an omnivorous diet (Barrett, 2000; Scheetz, 1999). The change noted in *Dysalotosaurus* thus reflects an ontogenetic, peramorphic change in diet from omnivorous juveniles to fully herbivorous adults that anticipates fully herbivorous diets in ankylopollexians. This change in diet might thus account for other peramorphic tendencies in the further evolution of iguanodontians, which rapidly perfect their cranial and dental morphology towards the requirements of obligate herbivory, including the marked lengthening of the snout and the formation of dental batteries with greatly enlarged tooth counts.

4.6 Taxonomical implications

Without the knowledge of the ontogenetic stage, it is always problematical to describe and name new taxa, especially considering an often poor fossil record. Only a collection of specimens of a single species or specimens of related taxa can help to evaluate diagnostic characters. Additionally, the observation of single characters to determine the ontogenetic status is not always safe: even such widely used characters as open sutures (Sampson et al., 1997) might show considerable variation arising from differing cranial functions. For example, a comparison of the frontals of illustrated specimens of *Thescelosaurus neglectus* (see Galton, 1997) would indicate that the individual with the broader and shorter frontals (plus the narrower angle of the ventromedial orbital edge) was

relatively older than the individuals with relatively narrower frontals. However, the 'younger' individual possesses a dentary with 21 alveoli, whereas the 'older' individual has only 18 alveoli. This is a clear conflict of two characters that might otherwise be used for ontogenetic determination, but the intraspecific variation of this taxon is unknown, and thus these changes could also reflect different species. The recent revision of the genus *Thescelosaurus* (Boyd et al., 2009) revealed that the 'older individual' with only 18 alveoli indeed belongs to the valid species *T. edmontonensis*, whereas the 'younger individual' with 21 alveoli is currently determined as *Thescelosaurus sp*. and therefore confirms the assumption of inter-specific variation of cranial ontogenetic characters.

The basal ornithopod *Gasparinisaura cincosaltensis* (Coria & Salgado, 1996) is a good example of a combination of characters that independently label the type skull as that of an immature individual (see also Salgado et al., 1997). Clear characters are the large orbits that make up almost one-third of the total skull length, the relatively short snout, and the descending occiput. Another possible juvenile feature is the described anterior position of the deepest point of the postorbital facet at the jugal, which is identified as a juvenile character in *Dysalotosaurus*. Of further interest is the very restricted articulation of the jugal with the lacrimal, which was noted as being 'unlike other ornithopods' (Coria & Salgado, 1996:446). The increasing overlap of both elements during growth in *Dysalotosaurus* (Fig. 4.5) indicates that this is simply another juvenile character. Finally, the antorbital fossa is located very high in the skull. Carpenter (1994) has shown in his study that the antorbital fossa migrates posteroventrally during growth in *Dryosaurus altus*. Thus, the position of this fossa in *Gasparinisaura cincosaltensis* is most probably also a juvenile character.

Of course, very large orbits and a short snout are the most apparent juvenile characters, and often point in the right direction, but one should check for additional signs of immaturity. Some basal ornithopods (Norman, 2004) and especially many birds also have very large eyes, although they obviously have reached maturity.

4.7 Conclusions

A juvenile skull of *Dysalotosaurus lettowvorbecki* was described, which has significantly increased the anatomical knowledge of this small basal iguanodontian ornithopod. Thus, all skull elements (except the quadratojugals and palatines) of *Dysalotosaurus* are now known, although some (e.g. vomer and coronoid) are just partially preserved. The mandibular articulation was reconstructed more precisely, and corresponds to that of all other ornithopods.

Furthermore, the comparison with other skull material of different growth stages has shed light onto several ontogenetic variations in the skull anatomy of this taxon. The skull BSPG AS I 834 is clearly identified as that of a juvenile by the open sutures and the relative proportions of the snout and the orbits, but several additional juvenile characters in single skull elements were found.

1. Lesser degree of overlap between the splenial and prearticular, as well as between the lacrimal and jugal.

2. In very young individuals, the basioccipital has a characteristic rhomboidal shape, with the condyle neck thicker than the condyle itself.

3. The tubera basioccipitalia are comparatively low.

4. The roof of the occiput and the parietal descend backwards, and the supraoccipital crest is low and less sharply defined than in adults.

5. A wide angle of the orbital rim at the jugals and frontals (and most likely at the lacrimals and prefrontals).

6. The frontals are very slender and long, with just a small and flat central dome.

7. The deepest point of the postorbital suture has an anterior position on the postorbital process of the jugal.

8. A smaller tooth number (ten compared with up to 13 in older ones) in lower and upper jaws, which also show a relatively smaller height of their main bodies.

Altogether, all ontogenetic characters are influenced directly or indirectly by the suture closure and by the relative change of the skull proportions, mainly because of the decrease of the size of the orbit, the lengthening of the jaws and muzzle, and the development of muscle attachment sites. The strong ontogenetic variation of the frontal width in *Dysalotosaurus* indicates that this character should be used with caution in cladistic analyses of ornithopods. Considering the large influence of the orbit size on the frontal width, the ontogenetic stage of used specimens should also be checked in analyses of other dinosaurs. However, a phylogenetic signal in frontal width seems to distinguish at least ankylopollexian ornithopods from less derived forms.

The variation of suture closure in *Dysalotosaurus* and the comparison of single characters in *Thescelosaurus neglectus* have shown that it is problematic to determine the relative growth stages of individuals of a single taxon with just one or two features. Thus, it is important to observe as many characters as possible for a more secured assessment of the growth stage, also because of heterochronic effects between different taxa. Such an evaluation was tested for *Gasparinisaura cincosaltensis*, in which several lines of evidence independently confirm the juvenile growth stage of the holotype skull.

Dysalotosaurus lettowvorbecki has opened a small window into the evolutionary pattern in ornithopod skulls. The observations on ontogenetic variation demonstrate the intermediate stage of this taxon between basal ornithopods and derived iguanodontians. Several tendencies within its ontogeny indeed anticipate later typical characters of the derived iguanodontians and hadrosaurs. These ontogenetic changes (snout lengthening, increase of tooth number, decrease of orbit size, shorter and broader frontals) are all of peramorphic character, and might, at least partially, reflect increased adaptations towards obligatory herbivory.

For the future, more detailed descriptions of ontogenetic variations in skulls are needed to find heterochronic tendencies and to solve taxonomic problems resulting from the description of animals only known from juvenile specimens. The skulls of ornithopods are the key to understand

the interrelationships between their ontogeny, taxonomy, and phylogeny, because the most important evolutionary changes in the skeleton happened there.

5. Ontogeny of the postcranium of *Dysalotosaurus lettowvorbecki*

5.1 Introduction

Recognizing the ontogenetic stage of vertebrate fossils is very important for the evaluation of phylogenetic characters, of heterochronic developments, and it has of course direct implications for the taphonomy and paleobiology of these specimens. It is also taxonomically relevant to know, how one can distinguish between closely related fossil taxa with different adult sizes. Callison & Quimby (1984) asked the question, if a specimen represents a large juvenile or a small adult, because size is only a limited tool for the assessment of ontogenetic stage (e.g. Bennett, 1995; Butler et al., 2008a; Horner et al., 2009; Rozhdestvensky, 1965; Sander et al., 2006; Weishampel et al., 2003). Size-independent criteria are therefore most important and were used more frequently in various vertebrate groups during the last decades. Qualitative characters include the degree of ossification of skeletal elements (e.g. Bennett, 1993; 1995; Brinkman, 1988; Coombs, 1986; Currie & Carroll, 1984; Galton, 1982; Horner & Weishampel, 1988; Jacobs et al., 1994; Johnson, 1977; Kear, 2007; Turvey & Holdaway, 2005), degree of suture closure (e.g. Bennett, 1993; 1995; 1996; Brochu, 1995; 1996; Chinnery & Weishampel, 1998; Coombs, 1986; Galton, 1982; Galton, 2009; Ikejiri, 2003; Ikejiri et al., 2005; Irmis, 2007; Raath, 1990; Roth, 1984), and bone surface textures (e.g. Bennett, 1993; Johnson, 1977; Tumarkin-Deratzian, 2009; Tumarkin-Deratzian et al., 2006; 2007).

Quantitative methods are mainly based on allometric relationships describing the ontogenetic and phylogenetic change of proportions (see e.g. Gould, 1966; Hammer & Harper, 2006). Most studies deal with proportions between skeletal elements and rather seldom with intra-elemental proportions (e.g. Aiello, 1981; Callison & Quimby, 1984; Colbert, 1990; Currie, 2003; Dodson, 1975a; 1975b; 1976; Hohloch, 2003; Lehman, 1990; Rinehart et al., 2009; Tidwell & Wilhite, 2005) and often combine this with biomechanical (e.g. Alexander, 1977; Bertram & Biewener, 1992; Biewener, 1983; Dilkes, 2001; Garcia & Silver, 2004; Heinrich et al., 1993) or even metabolic

approaches (e.g. Silva et al., 2006). Further developments are studies using multivariate statistics and morphometrics (see Zelditch et al., 2004) to reveal ontogenetic, intra-specific, and phylogenetic morphological changes (e.g. Bonnan, 2004; Chapman, 1990; Chapman & Brett-Surman, 1990; Chinnery, 2004; Dodson, 1975a; 1975b, 1976; Gibson et al., 1984; Weishampel & Chapman, 1990).

Morphological ontogenetic studies of ornithopods (excluding bone histology) are rather patchy, but include the whole range of methods, such as the description of ontogenetic and intra-specific variation, the comparison of body proportions, bivariate allometry, and morphometrics (Brett-Surman & Wagner, 2007; Carpenter, 1994; Chapman & Brett-Surman, 1990; Chure et al., 1994; Dilkes, 2001; Dodson, 1975c; Evans, 2007; Forster, 1990a; Galton, 1974; 2009; Guenther, 2009; Heinrich et al., 1993; Hohloch, 2003; Horner & Currie, 1994; Horner & Makela, 1979; Horner & Weishampel, 1988; Norman, 1980; Rozhdestvensky, 1965; Scheetz, 1999; Tanke & Brett-Surman, 2001; Weishampel et al., 2003). However, most of these studies deal only with one or two different methods, concentrate only on a single functional unit of the skeleton, or focus exclusively on evolutionary and heterochronic tendencies in morphology. On the other hand, many ornithopod taxa are unfortunately not well preserved or are not represented by numerous individuals of different ontogenetic stages, which hamper naturally this kind of research.

Dysalotosaurus lettowvorbecki is one of the few exceptions, where apparently dozens of individuals of a wide ontogenetic range were preserved (see chapter 3). There is only a single individual known today, where approximately 50% of the skeleton is preserved (Janensch, 1961). This individual (dy I) consists of the skull base, a complete presacral and sacral vertebral series, both girdles, one forelimb without the hand, and both femora. It unfortunately lacks a complete hindlimb, so that the only proportions between hindlimb elements could be calculated by using the sketch of a lost specimen (see Galton, 1981, tab. 5, fig. 20; Janensch, 1955, fig. 40). Other individuals were formerly preserved (Hübner, 2007; Maier, 2003), but they were obviously destroyed during World War II and are now only known from sketches (Heinrich, 1999; Janensch, 1955). The overwhelming majority of *Dysalotosaurus* bones were found isolated within the two bonebeds of the fossil location

anyway (Janensch, 1914c), so that ontogenetic changes in *Dysalotosaurus* are only evaluable among single elements.

However, the new of this study is the extensive comparison of as many distances within the individual skeletal elements as possible (strongly expanding the extent of the initial study by Hohloch, 2003), so that in the end a three-dimensional image of ontogenetic changes of elemental proportions is provided. The avoidance of multivariate statistics or shape analysis due to too many missing values or too abundant distortions of shape are thus more than equalized. Furthermore, very few of the previous studies highlighted the ontogenetic changes between more than two or three intra-elemental distances (e.g. length versus mid shaft circumference or length versus joint widths), which will be done much more intensively in this study.

5.2 Material & Methods

Most of the described ontogenetic changes within the postcranial skeleton are based upon isolated elements. Ribs were excluded from the analysis, because there were almost no complete or nearly complete specimens available for an examination and the determination of isolated ribs to their original position within the skeleton would be rather hypothetical. This is the same for the vertebrae, but at least three preserved individual series have allowed basic ontogenetic comparisons. For the analysis of the axial suture closure pattern, isolated vertebrae and further short series were used.

The sternals and the distal tarsals are not represented in this study, because there are only two or three specimens known. The pubis is also excluded, because most of the specimens were highly incomplete and none of the quantitative results were statistically significant. The exact original position of the unguals and most distal pedal phalanges is often not unambiguously determinable, because only a single articulated but incomplete pes of the small individual “dy V” is present for a comparison. Thus, only the well determinable first and second phalanges of the 2nd, 3rd, and 4th toe

were used for the description of ontogenetic changes. Finally, all bones of the carpus and manus had to be excluded from the analysis, because they are either unknown or only represented by single isolated bones, which are not clearly determinable (Galton, 1981; Janensch, 1955).

Three partial series of vertebrae are currently known from *Dysalotosaurus*, which consist of more than one morphological type (see Janensch, 1955; 1961b). The description of the sequence of neurocentral suture closure is mainly based on these individuals and is completed by observations from the overwhelming majority of isolated vertebrae. The terminology is based upon Brochu (1996) and Irmis (2007), where the neurocentral suture can be open, partially closed, or completely closed. In addition, these terms are here also used for parts of the suture on a vertebra, because the degree of suture closure is sometimes very variable even within a single vertebra.

Distinct ontogenetic stages of appendicular elements, such as the initial appearance or differentiation of a bony process, or the initial fusion of processes as in some other reptiles (e.g. Brinkman, 1988; Currie & Carroll, 1984) and in moa (Turvey & Holdaway, 2005), were not found. Thus, the classification into ontogenetic stages was abandoned due to the rather continuous change of morphologies during growth. The observed differences are mainly observed between “small” and “large” specimens of an element, which is generally in accordance with the two-peaked size-frequency distribution of the *Dysalotosaurus* herd.

Quantitative results were derived by the Multivariate Allometric Analysis (MAA) of the software PAST (Palaeontological Statistics, version 1.38; Hammer et al., 2001). Only complete or nearly complete specimens were measured, but the amount of missing values was nonetheless too high for multivariate statistics, such as Principal Component Analysis. In the end, only bivariate relationships were calculated by the MAA and were compared with each other.

5.3 Ontogeny of the axial skeleton

5.3.1 Neurocentral suture closure

The vertebral formula of *Dysalotosaurus* after Janensch (1955) contains eight cervicals, 15 dorsals, six sacrals (including a dorsosacral and a sacrocaudal vertebra) and an unknown number of caudals, which has probably included more than 40 vertebrae. In contrast, Pompeckj (1920) counted nine cervicals and Galton (1981:276) assumed a missing vertebra between the 7th and 8th position of the vertebral series of the individual "dy I", so that the count of nine cervicals is the same as in *Hypsilophodon* and *Camptosaurus*.

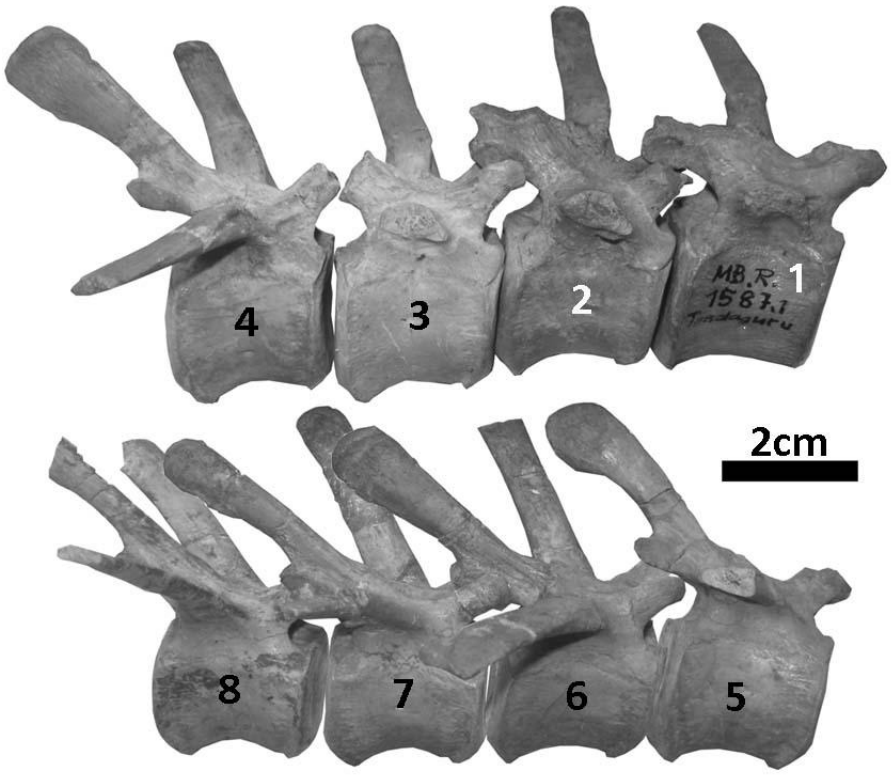

Fig. 5.1: *The preserved 8 proximal caudal vertebrae of the individual „dy II" (MB.R.1587.1-8) artificially articulated in dextral view and in natural order (position numbers 1 to 8).*

The vertebrae of the individual "dy V" (MB.R.1605.1, MB.R.1605.2, MB.R.1605.3) consist of three sacrals and six caudals, whereas the anterior most caudal vertebra is probably the sacrocaudal (Janensch, 1955). The neurocentral suture is completely open in all vertebrae and the neural arch is sometimes also disarticulated from the respective centra. The small size of "dy V" (length of second

sacral vertebral centrum = 14mm) compared to the other two individuals (31mm in "dy I" and 24mm in "dy II"; see Janensch, 1955:143) fits very well to the assumed juvenile ontogenetic stage of this individual.

The individual "dy II" is, according to its relative size, intermediate between "dy V" and "dy I". The preserved vertebral series consists of the posterior dorsal vertebrae from position seven to 15, of the complete sacrum, and the first eight caudal vertebrae (Janensch, 1955; Fig. 5.1). The neurocentral suture of the 8th caudal is only anteriorly closed on the right side. The remaining open parts of the suture are strongly interlocked (Fig. 5.2). On the left side of the centrum, the suture is partially closed anteriorly and completely closed in the remaining parts. The suture is still completely open at the anterior and posterior edges of the vertebra, where it separates the respective articular faces of the centrum from the basal "feet" of the neural arch. The right side of the 7th caudal bears a partially closed suture anteriorly, where only inclined ridges and grooves are still visible, and an irregularly running open suture in the remaining parts (Fig. 5.2). On the left side, more parts of the suture are open and there is almost no fused part as on the right side. The anterior and posterior parts of the suture at the dorsolateral edges of the articular faces of the centrum are again completely open. In the 6th caudal, only the anterior part of the right side shows first signs of sutural closure, whereas all other parts of the vertebra have completely open sutures (Fig. 5.2).

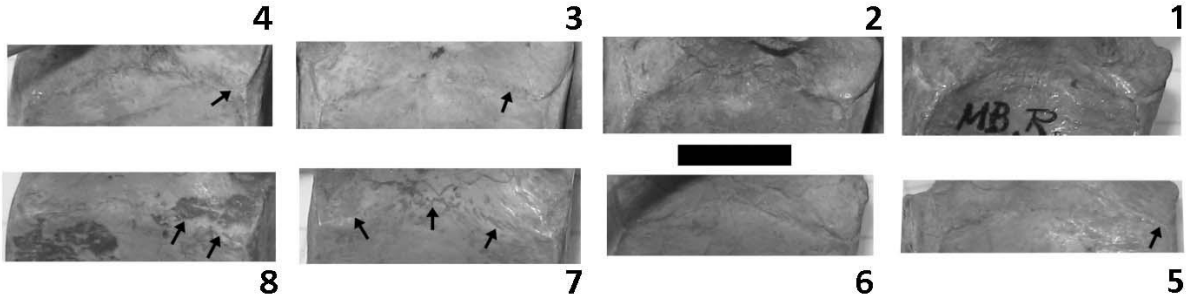

Fig. 5.2: *Detailed view of the neurocentral sutures of the proximal caudal vertebrae of Fig. 5.1 in dextral view. Arrows indicate partially or completely closed parts of the sutures. Scale bar = 1cm.*

This is similar to the 5th caudal, where only the anterior most parts of the lateral sides of the vertebra start to close. It is also similar to the 4th caudal, where only the anterior most part of the right side show signs of initial closure. The third caudal has a strong interlocking suture anteriorly on its right

side, but the rest of the suture is straight and completely open. The two anterior most caudals and all remaining sacral and dorsal vertebrae of individual “dy II” bear no sign of initial suture closure and show well visible open sutures (Fig. 5.2). The sutures between the sacral ribs and their respective vertebrae are sometimes strongly interlocked, but they are always well visible.

The individual “dy I”, on exhibition in the Museum für Naturkunde in Berlin and approximately one third larger than “dy II”, contains an almost complete presacral series lacking the atlas, probably the 8th cervical (Galton, 1981), and the last two dorsals. The individual “dy III” with the last two dorsals and all six sacrals was probably also part of individual “dy I” (Janensch, 1961b). The remaining three sacral centra (MB.R.1564), which were formerly added to “dy I” (Janensch, 1955) should therefore be treated as another individual, although the preservational association of the latter with the vertebrae of “dy I” and “dy III” is unknown. Nearly all preserved vertebrae of “dy I/dy III” have open sutures, although it is not absolutely secured for all cervicals due to lateral distortion. However, the sutures are at least partially visible in the few cervicals with obscured surfaces, so that their stage is determined open as well.

Numerous isolated vertebrae of *Dysalotosaurus* have completely closed neurocentral sutures only in the caudal series, independently of body size. Nearly all distal caudals have closed sutures. The mid caudals and proximal caudals can have all three suture types from closed to open stage, but only the largest of the latter can show completely closed sutures. All known sacral vertebrae, even the largest preserved ones, show visible sutures and most of them even lack their neural arch, which is always detached along the sutural face (Fig. 5.3A). This is also the case for most of the dorsals and cervicals. The largest almost complete isolated cervical (GPIT/RE/4225, centrum length = 42mm) and dorsal (GPIT/RE/5302, centrum length = 45mm) both bear partly visible open sutures, which let assume that none of the preserved individuals of *Dysalotosaurus* once possessed completely fused neurocentral sutures .

5.3.2 Additional ontogenetic variation of the axial skeleton

As already shown for crocodiles (Brochu, 1996), the facets for the neural arches on the larger vertebral centra of *Dysalotosaurus* have a strong relief with numerous grooves and ridges (Fig. 5.3A), whereas smaller specimens bear more smooth facets. This reflects the increasing connection between centra and neural arches during growth and is, for example, also described for the hadrosaur *Hypacrosaurus* (Horner & Currie, 1994).

Further ontogenetic changes within the axial skeleton are the more acute angle between the foot and roof anteriorly at the neural arch of the atlas (see chapter 4), where the M. longissimus capitis profundus attaches (Tsuihiji, 2007) and which connects the atlantal neural arch with the tubera basioccipitalia of the basicranium.

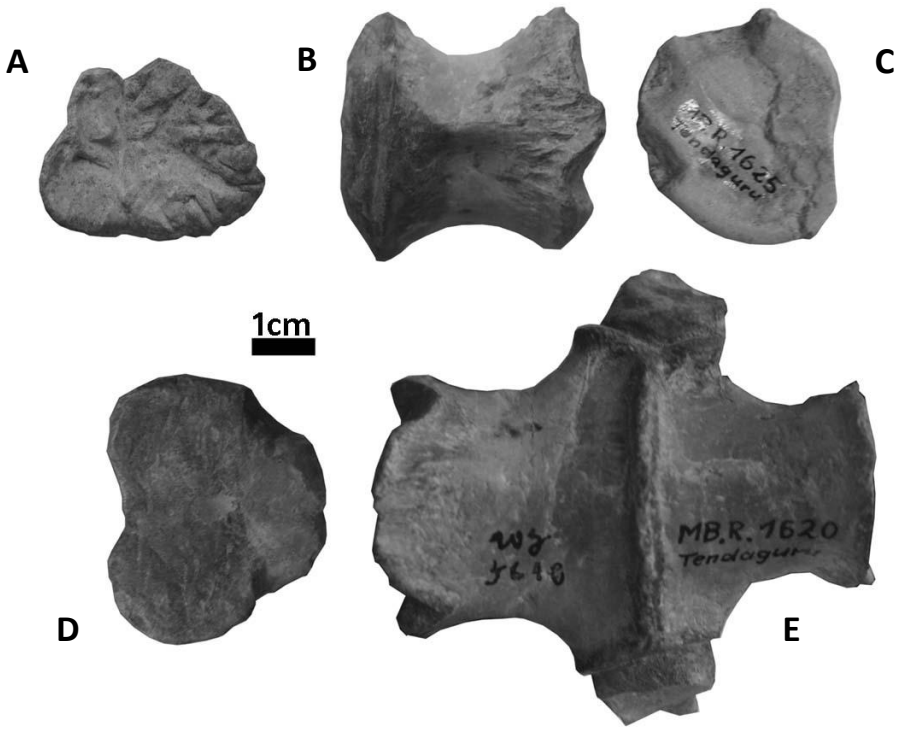

Fig. 5.3: ***A*** *– Combined right articular surface of the dorsosacral and first sacral vertebra to the first sacral rib (belongs to MB.R.1564). Note the completely intact sutural surface.* ***B-E:*** *Two vertebrae with the unusual symmetric emarginations and tongue shaped central expansions,* ***B*** *– Posterior dorsal vertebral centrum (MB.R.1625) in ventral view.* ***C*** *– The same centrum as in B in anterior view.* ***D*** *– Dorsosacral vertebra MB.R.1620 in anterior view.* ***E*** *– The same as in D in ventral view, the second sacral vertebra (the right vertebra) and the sacral ribs are still attached.*

Janensch (1955:144) has mentioned three possible ontogenetic differences between the comparable parts of the vertebral series of the smaller individual “dy II” and the larger individual “dy I/dy III”. The lateral walls of the neural canal are relatively thinner in the smaller individual “dy II” compared to “dy I/dy III”. The distance between the parapophyseal facets and the lateral end of the diapophyses is according to Janensch (1955) relatively longer in the larger individual “dy I/dy III” than in “dy II”, which also implicates a longer distance between the tuberculum and capitulum of the heads of the dorsal ribs. Finally, the anterior centrum width increases stronger in relation to centrum length in “dy I” compared to “dy II” from the 17th to the 21st position of the presacral series. The latter is tentatively confirmed for the 19th to the 23rd dorsal centrum by comparison of Janensch’s measurements of both vertebral series (1955:142-143). These measurements also demonstrate that the height of the centra generally increases during growth compared to anterior width and length, respectively, which especially regards to the first and second sacral centra. Nevertheless, these trends should be treated as very tentative, because the comparison of only two individuals can be strongly influenced by preservation.

A last and very unusual type of morphological variation concerns only two vertebral centra (Fig. 5.3B-E). The anteroventral edge of a first sacral (dorsosacral, MB.R.1620) and of a posterior dorsal centrum (MB.R.1625) bears two symmetrical emarginations and the anteroventral edge between them is tongue shaped and slightly expanded anteriorly. The emarginations of the dorsal centrum are closer together ventrally. Both centra are larger than the respective centra of “dy I/dy III” (42mm and 46mm in length compared to 38mm and 33mm in the latter, respectively; see Janensch, 1955:143). Other centra of similar size and from the same position in the vertebral series have a continuous ventral border without any sign of emarginations. Counterparts of these structures are also unknown, but the symmetrical arrangement excludes a pathological reason. As Galton (1981:276 and fig. 4J) already suggested, these emarginations represent a much firmer attachment of these vertebrae to their neighbors and, thus, an unusually high degree of co-ossification for *Dysalotosaurus*.

5.4 Ontogeny of the appendicular skeleton

None of the sutures between elements are fused in the appendicular skeleton of *Dysalotosaurus*. This regards the suture between the coracoid and the scapula, the sutures between the sacral ribs and the ilium, the sutures between the pelvic elements, and the sutures between astragalus and calcaneum as well as between both proximal tarsals and the distal tibia and fibula. All of the sutural surfaces in these bones become more rugose and distinct, and a larger relative extension, but even the largest specimens were either found isolated or, in the case of the individual "dy I", disarticulated. Differences in bone surface textures between small and large specimens were not found.

Scapula (Fig. 5.4): A general ontogenetic trend is the increasing distinctness and pronouncement of morphologies, which are insertion or origin areas for muscles and/or tendons. A distinct posteroventral depression medially at the base of the shaft becomes deeper during ontogeny with sharper anteromedial borders. A medial, shaft crossing ridge originates perpendicular to the mentioned depression and is also more pronounced in large specimens. One of these two structures are probably connected with the M. subscapularis, but the very different reconstructions for either *Maiasaura* (Dilkes, 2000:figs. 4B), *Mantellisaurus* (Norman, 1986:fig. 75B), and *Saurornitholestes* (Jasinoski et al., 2006:figs. 6D) make a secured correlation difficult. Carpenter & Wilson (2008) reconstructed the M. serratus ventralis as the muscle inserting at the posteroventral depression in *Camptosaurus*. A small but distinct bulge at the posteroventral edge of the shafts base is well visible in large specimens, but is very weak or absent in small ones. This bulge probably represents the insertion of the M. serratus superficialis (see Fig. 5.4B), which has a very similar insertional location and extend in an oviraptorosaur (Jasinoski et al., 2006:330). There are also parallel striations medially above the foramen supracoracoideum, which become stronger during growth. Finally, the distal end

of the scapular blade flares symmetrically weak in small specimens and only posteroventrally strong in large specimens (Fig. 5.4). The extension of this flaring is rather variable.

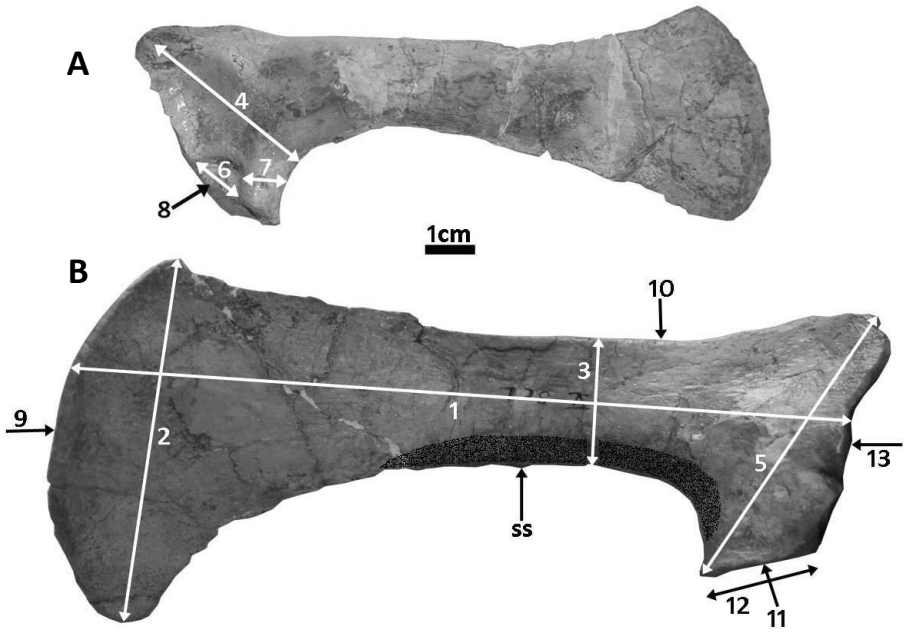

Fig. 5.4: *Scapulae of* Dysalotosaurus *demonstrating qualitative ontogenetic trends and measured distances. Arrows with only one head represent measurements perpendicular to the point of view, mostly thickness.* ***A*** *– Small left scapula GPIT/RE/5330 in lateral view.* ***B*** *– Large left scapula (dy I) in medial view. This specimen is labeled as Aststl in Appendix 3. The shaded area represents the insertional area of the M. subscapularis or M. serratus ventralis.* ***Abbr.: ss*** *– Insertional area of the M. serratus superficialis.*

Only eleven out of 35 bivariate relationships are statistically significant, but further ontogenetic trends of the scapular shape are unambiguously indicated. The shaft minimum becomes relatively thicker (a_{10}) compared to its width (a_3) and this increase in thickness is strong enough to be positive allometric against most of the other measurements – statistically significant or not. This is even more the case for the thickness of the proximal end of the scapula closely anterior to the foramen supracoracoideum (a_{13}), which obviously shows the strongest positive allometry compared to the other distances. Further significant ontogenetic trends are the deepening of the glenoid fossa ($a_{8;}$ supraglenoid fossa in Carpenter & Wilson, 2008) and the shortening of its posterior edge (a_6). This clearly results from a combination of the deeper glenoid with the larger humerus joint face (a_{11}, a_{12}) in large specimens.

Overall, attachment sites for muscles and tendons are more pronounced, the shaft becomes more robust, the contact to the coracoid is more extensive, and the glenoid is more developed with a relatively deeper fossa during growth. Finally, the proximal width of the scapular blade (a_2) increases relative to the scapular dorsoventral length (a_1).

Coracoid (Fig. 5.5): The qualitative observation provided very obvious ontogenetic trends in the general shape of this bone. The edge between the posteroventral corner for the articulation with the sternum and the articular face for the humerus is strongly concave in small specimens, but becomes less concave in large specimens. The attachment site for the scapula is rather smooth with weak ridges in small specimens and bears strong ridges and grooves in large ones (Fig. 5.5C).

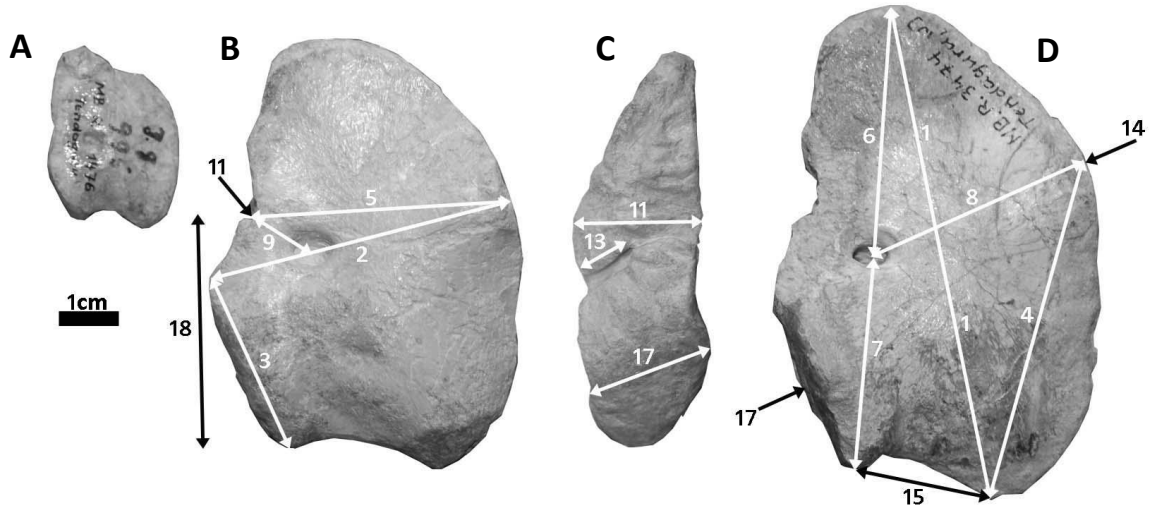

Fig. 5.5: *Coracoids of* Dysalotosaurus *demonstrating qualitative ontogenetic trends and measured distances. Arrows with only one head represent measurements perpendicular to the point of view, mostly thickness.* ***A*** *– Small right coracoid MB.R.1476 in lateral view.* ***B*** *– Large right coracoid MB.R.1485 in lateral view.* ***C*** *– Same specimen as in B, in dorsal view. Note the rough scapular face in the upper two thirds including the canal of the Fo. supracoracoideum.* ***D*** *– Large right coracoid MB.R.3474 in lateral view. The dorsolateral edge (left to the foramen) is broken off.*

In large specimens, the overall shape of the coracoid is also longer anteroposteriorly compared to its dorsoventral width. Finally, the relief of the internal side becomes much stronger during growth due to the higher elevation of the edge to the scapular attachment site, the edge to the humerus joint face, and the medial edge. Thus, large coracoids are more involuted internally than the flat small

specimens. This is also slightly the case for the external side due to the higher elevation of the border to the humerus joint face and the stronger development of two ridges running from the foramen supracoracoideum to the anteromedial corner and from this foramen to the sternal process, respectively. This effect is further intensified by the internal involution of the medial edge between these two corners.

According to Janensch (1955), the foramen supracoracoideum lies more anteriorly on the external side in small specimens. The MAA proofs that almost the opposite tendency is the case. The foramen migrates slightly anteriorly and ventrally during growth, which is confirmed by the significant positive allometry of the distances a_6 and a_7 compared to a_8, respectively (Fig. 5.6). The other two clear tendencies in shape change are the relative thickening of the humeral joint face (a_{17}) and of the scapular attachment site (a_{11}) and the extension of nearly all laterally measured distances compared to the smallest dorsoventral width (a_5), which is therefore strongly negative allometric.

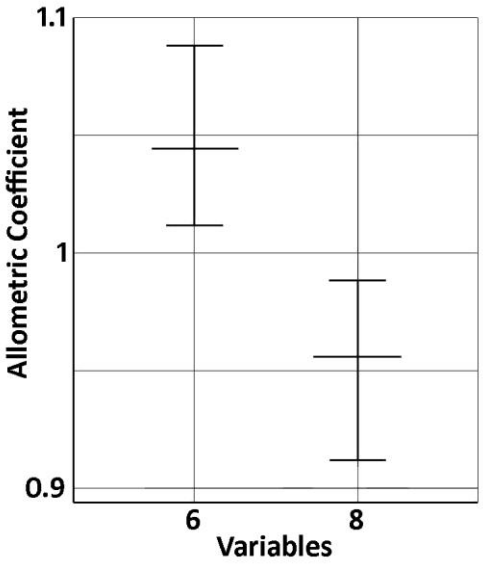

Fig. 5.6: *Bivariate plot of the measured distances/ variables* 6 *and* 8 *of the coracoid. The broadest line within the intervals represents the allometric coefficient. Both intervals are completely below or above 1 and are therefore statistically significant. Picture modified from the software PAST.*

The humeral joint face and the distance between its posterior corner and the foramen as well as the distance between both posterior corners grow almost isometric (a_3 and a_{17}; a_7 and a_{15}; a_7 and a_{18}; a_{15} and a_{18}). Nevertheless, the whole posterior half of the coracoid up to the foramen grows obviously stronger than the overall anteroposterior length of the bone, although the maximum length (a_1) is still positively allometric compared to the dorsoventral width (a_2; a_5). The observed

decreasing concavity between the two posterior corners is confirmed (a_{15} and a_{16}), but is unfortunately statistically insignificant.

In the end, the coracoid of *Dysalotosaurus* becomes more dorsoventrally slender, the humeral joint face and the scapular attachment site are more robust and elevated, and the foramen supracoracoideum migrates slightly anteriorly and ventrally. The whole bone changes from a rather flat and almost quadrangular shape to an involuted and almost half-moon-like shape during ontogeny.

Humerus (Fig. 5.7): At a first view, this element seems to grow almost isometric, but the MAA has revealed very interesting ontogenetic differences. First, the width of both articular ends (a_2; a_5) grows positively allometric compared to overall length (a_1), to width at the deltopectoral crest (a_3), and to minimum shaft diameter (a_4). The strong relative increase of the proximal width (a_2) is also the reason for the increasing medial curvature of the shaft (a_{14}). Interestingly, the thickness of the articular ends, as well as the thickness of the deltopectoral crest, grow stronger than the respective widths (a_2 to a_9; a_3 to a_{10}; a_5 to a_{12} and a_{13}), so that these parts are more robust in large specimens. Furthermore, the maximum of the deltopectoral crest is migrating slightly distally, and, finally, the medial condyle and the fossa olecranii of the distal end increase

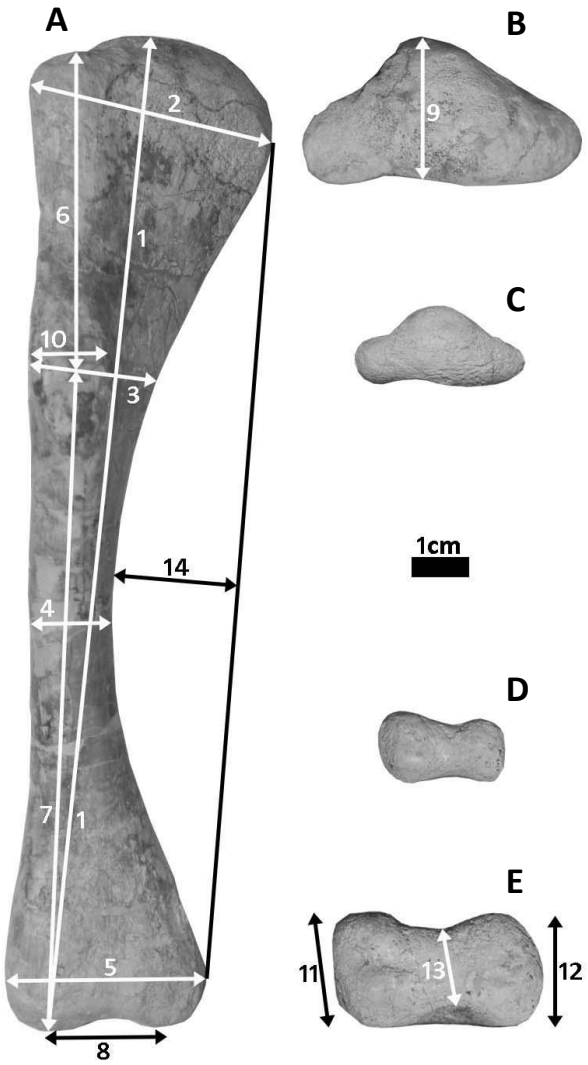

Fig. 5.7: *Humeri of* Dysalotosaurus *demonstrating qualitative ontogenetic trends and measured distances.* ***A*** *– Right Humerus SMNSoN3 in anterior view.* ***B*** *– The same as in A, in dorsal view.* ***C*** *– Right humerus SMNSoN2 in dorsal view.* ***D*** *– Same as in C, in ventral view.* ***E*** *– Same as in A, in ventral view.*

stronger relative to the lateral condyle, so that the distal joint of large specimens have two similar sized condyles and only a very flat fossa olecranii (see Fig. 5.7D-E).

Overall, the humerus becomes more robust with strong, rounded, and more even shaped articular ends, although the shaft maintains its slenderness.

Ulna (Fig. 5.8): The quantitative ontogenetic tendencies of this element are quite differentiated. The shaft gets stouter during growth compared to overall length (a_3 to a_1) for instance. The olecranon process increases stronger in size than the maximum width of the whole proximal articular end (a_7, a_9, and a_{10} compared to a_2 and a_8). Furthermore, the medial part of the distal articular end increases stronger during growth than the lateral part, which articulates with the radius (a_5 compared to a_6).

In the end, the articular ends naturally increase in size compared to the bone length, but the distinct shape change within these joints is significant. So, the olecranon process, insertional area for the triceps complex (Jasinoski et al., 2006), increases relatively, and the medial part of the distal articular end increases compared to the lateral part.

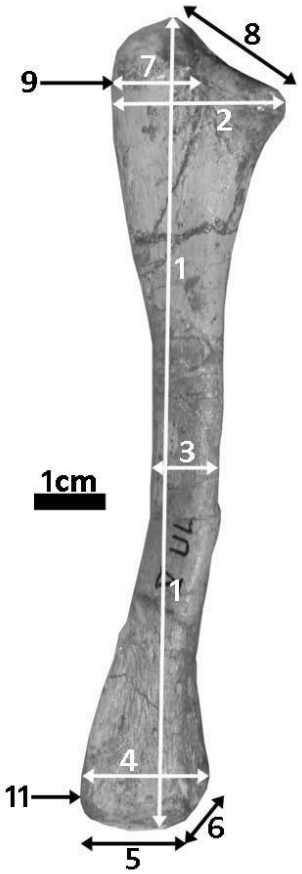

Fig. 5.8: *Ulna of* Dysalotosaurus *demonstrating measured distances. Left ulna of "dy I" in medial view. Arrows with only one head represent measurements perpendicular to the point of view, mostly thickness. This specimen is labeled as Aststl in Appendix 3.*

Radius (Fig. 5.9): Only four radii were complete enough for measurements, so that the results of the MAA should be treated as preliminary. The overall length (a_1) is negative allometric compared to most measurements of the articular ends. Furthermore, the midshaft thickness (a_3 insignificantly;

a_6 significantly) is also increasing during growth compared to the length, which gives the larger specimens a stouter appearance. The proximal end grows almost isometrically (a_2 and a_5), whereas the anterior width of the distal end (a_4) is negatively allometric compared to the respective thickness of the shaft (a_3) and the lateral width of the proximal end (a_5).

In addition and similar to the ulna, the distal end of the radius grows also inconsistently, because the whole lateral width (a_7) increases ontogenetically compared to its lateromedial counterpart (a_8). This part would fit to the respective distal part of the ulna.

In sum, the radius becomes stouter during growth, but the distal end grows strongly unequal in different views. The anterior width and the articular face for the ulna are rather negatively allometric, but the whole lateral width (a_7) increases ontogenetically compared to most of the other distances including the proximal end. So, there is the usual increase in ossification of the articular ends, but the distal articular overlap between radius and ulna maintains restricted in all ontogenetic stages.

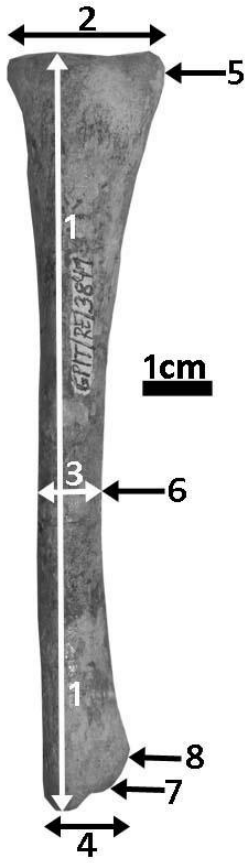

5.9: *Radius of* Dysalotosaurus *demonstrating measured distances. Arrows with only one head represent measurements perpendicular to the point of view, mostly thickness. Left radius GPIT/RE/3841 in dorsolateral view (flexor side).*

Ilium (Fig. 5.10): Several qualitative observations could be made at the ilium. First, a small, lateromedially elongated depression with a sharp anterior edge is lowered into the posteroventral end of the brevis shelf close to its junction with the main body of the postacetabular process (Fig. 5.10A). The less distinct posterodorsal counterpart is not affected during growth, but the former depression seems to be deeper and more distinct in large specimens.

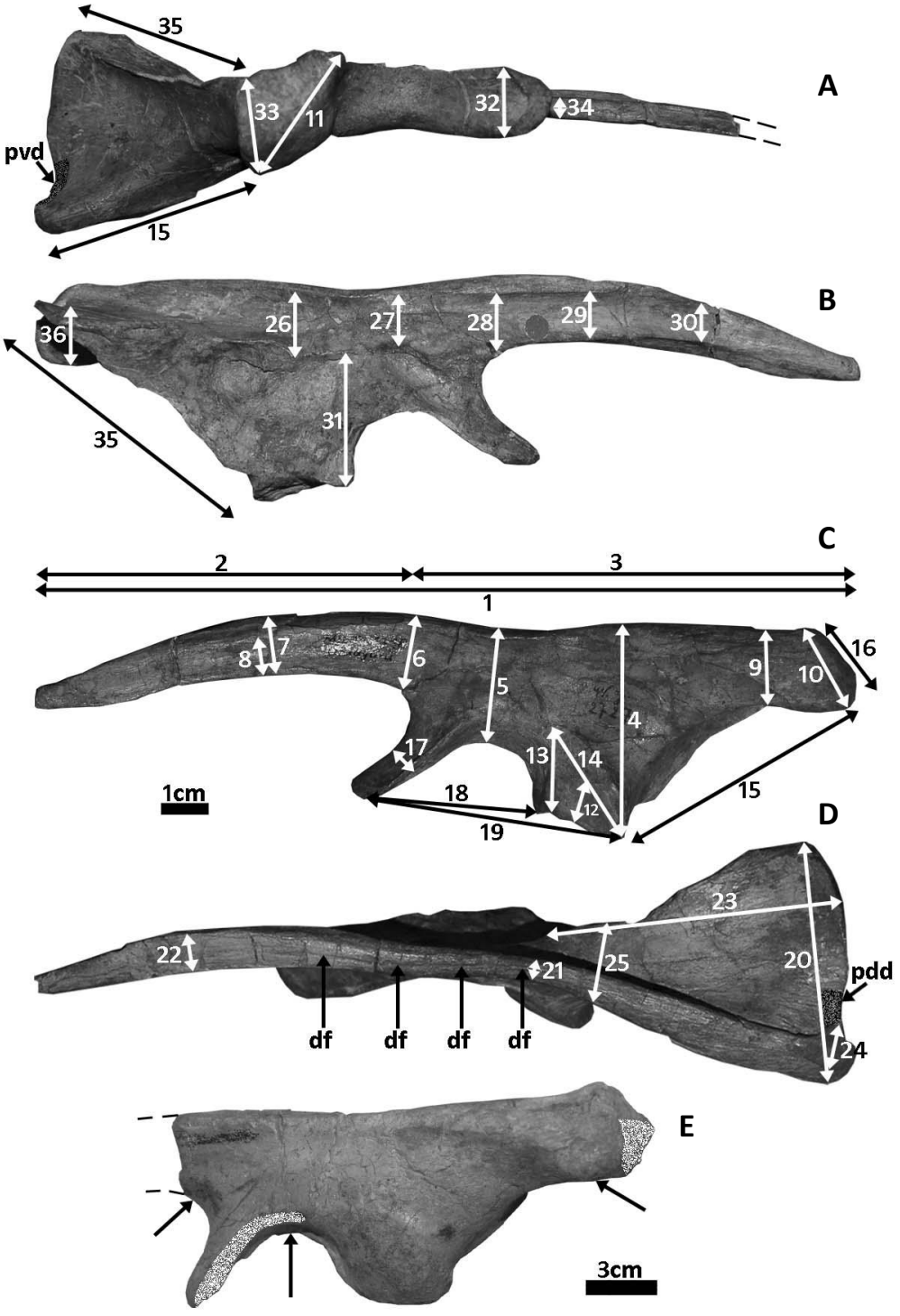

Fig. 5.10: *Illia of* Dysalotosaurus *demonstrating qualitative ontogenetic trends and measured distances.* ***A*** *– Left ilium MB.R.1718 (dy II) in ventral view.* ***B*** *– Same as in A, in medial view.* ***C*** *– Same as in A, in lateral view.* ***D*** *– Same as in A, in dorsal view.* ***E*** *– Larger partial left ilium GPIT/RE/5639 in lateral view. Note the shape differences to the smaller ilium in C (arrows without signature). Broken edges are colored in white pattern.* ***Abbr.: df*** *– dorsal furrow;* ***pdd*** *– posterodorsal depression, dark shaded;* ***pvd*** *– posteroventral depression, dark shaded.*

This structure is apparently not yet described in ornithopods, so that no specific muscle can be assigned to it. According to the reconstructions of Romer (1927), Galton (1969), and Norman (1986), it is most probably the M. iliocaudalis. Second, there is a deep and thin furrow nested within the dorsal edge of the ilium (Fig. 5.10D), which, in addition to the flattened but rough surface of the dorsal rim of the element itself, has probably served as tendinous attachment site for the M. iliotibialis. This furrow reaches beyond the level of the posterior end of the iliac peduncle in small specimens, but is obviously shorter in large specimens, because it ends well before the level of the posterior end of the ischiadic peduncle. Finally, the medial impressions for the sacral ribs on the ilium become deeper and more distinct in outline during growth.

Some outlining distances of the ilium grow nearly isometrically according to the MAA. This regards the length of the main body excluding the preacetabular process (a_3), the distance between the posterior end of the ischiadic peduncle and the posterior end of the whole bone (a_{15}), the maximum width of the brevis shelf (a_{20}), and the medial length of this shelf (a_{23}). Isometrical growth was also observed for the dorsal (a_{21}) and ventral (a_{34}) thickness of the preacetabular process at its posterior end. Significant negative allometric growth was observed for the length of the main body (a_3) compared to the height of the preacetabular posterior end (a_6), compared to the width of the ilium at the medial ridge of the ischiadic peduncle, where it is joining the brevis shelf (a_{25}), and compared to the posterior width of the ischiadic peduncle itself (a_{33}). Further negative allometry was discovered for the height of the ilium, measured at the posterior end of the ischiadic peduncle (a_4), compared to the height of the posterior end of the preacetabular process (a_6), to the minimum lateral height of the postacetabular process (a_9), and, again, compared to the posterior width of the ischiadic peduncle (a_{33}). Statistically significant are also the decreasing height above the acetabulum (a_5) compared to a_{25} (see above) and the increase of the posterior width of the ischiadic peduncle (a_{33}) compared to a formerly cartilaginous area ventrally to a triangular muscle attachment site (a_{12}). Janensch (1955) determined the M. iliofemoralis externus as the attaching muscle there, but the respective origin in *Thescelosaurus*, *Hypsilophodon*, *Mantellisaurus*, and *Maiasaura* is always

reconstructed more dorsally (Dilkes, 2000; Galton, 1969; Norman, 1986; Romer, 1927), so that this determination should be treated with caution. The last significant correlation was found for the height of the medial dorsoventrally concave depression dorsally to the level of the brevis shelf, which runs along the whole length of the ilium (probably insertion for axial muscles). The height of this depression at the anterior rim of the brevis shelf and the height centrally above the acetabulum (a_{26} and a_{27}, respectively) increase stronger than the height at the posterior end of the preacetabular process (a_{28}). The latter distance grows obviously also slower in comparison with the lateral height at the posterior end of the preacetabular process (a_6). At this level, a strongly striated dorsomedial surface is present, which probably increases its height at the expense of the adjacent medial depression. The type of muscle originating from this dorsomedial surface is currently uncertain. The M. puboischiofemoralis internus (iliofemoralis internus) can be excluded, because a separate groove is present more anteriorly at the ventromedial edge of the preacetabular process. This edge clearly marks the dorsal border of this muscle as in *Thescelosaurus* (Romer, 1927:fig. 18). The only possibilities are the axial muscle M. dorsalis trunci (see Dilkes, 2000:103) or a dorsomedial extension of the attachment site for the M. iliotibialis, which inserts on most of the dorsal edge of the ilium anyway.

Generally and by integrating the main tendencies of the remaining statistically insignificant bivariate relationships, the main body of the ilium becomes slightly lower during growth at the level of the ischiadic peduncle and at the acetabulum, whereas the posterior end of the preacetabular process becomes higher. Most of the remaining ontogenetic tendencies are summarized as progressive ossification (e.g. the increasing width of the ischiadic peduncle) or larger and more distinct muscle attachment sites. The only exception is the posterior shortening of the deep furrow on the dorsal edge. Finally, the medial arch of the acetabulum extends compared to the lateral arch (Fig. 5.10E).

Ischium (Fig. 5.11): Qualitative observation has revealed a slight deepening and medial migration of a small depression at the acetabular side of the iliac peduncle of the ischium during growth. This peduncle is also bulging more laterally in large specimens.

Nearly isometric growth was found between the anteroposterior length of the iliac peduncle (a_1) and the depth of the acetabular part of the ischium (a_5), between the anteroposterior length of the pubic peduncle (a_2) and its neck (a_{12}), between the greatest thickness of the pubic peduncle (a_4) and the thickness of the acetabular bottom (a_{19}), between the maximum anteroposterior length proximally (a_6) and the length of the neck of the iliac peduncle (a_{13}), between a_6 and the neck of the obturator process (a_{14}), and between the minimum thickness of the ischiadic blade (a_7) and the thickness of the acetabular bottom (a_{19}). Statistically significant relationships of distances have revealed very heterogeneous results for the iliac and pubic peduncles, respectively. The former becomes relatively longer compared to its width (a_1 compared to a_3), whereas the latter becomes relatively shorter compared to its width (a_2 compared to a_4). The length of the pubic peduncle (a_2) is also negatively allometric compared to the depth of the acetabular part of the ischium (a_5).

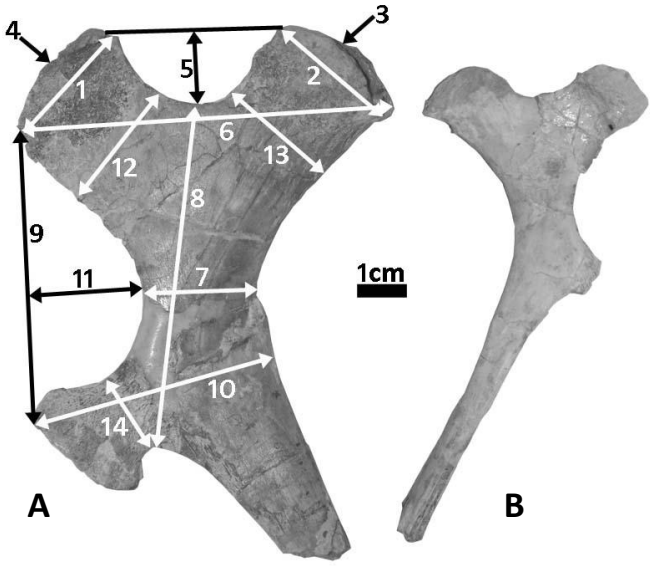

Fig. 5.11: *Ischia of* Dysalotosaurus *demonstrating qualitative ontogenetic trends and measured distances. Arrows with only one head represent measurements perpendicular to the point of view, mostly thickness.* ***A*** *– Right ischium SMNSoN2 in medial view. The pubic peduncle is partially corroded.* ***B*** *– Left ischium SMNSoN1 in medial view. The proximal part is lateromedially squeezed and the obturator process incomplete. Both specimens lack the distal end.*

On the other hand, the maximum anteroposterior length proximally (a_6) and the distance between the deepest point of the acetabulum and the ventral neck of the obturator process (a_8) are negatively allometric compared to both peduncles (a_1 and a_2). The depth of the acetabular part of the

ischium (a_5) is also positively increasing compared to the maximum anteroposterior length proximally (a_6) and the ischiadic blade (a_7) is increasing compared to the distance of a_8 (see above).

Including the implied relationships of the insignificant results, the ischium undergoes some interesting proportional changes during growth. The overall distances of the main body decrease compared to most of the other measured distances. Both peduncles increase in size compared to most of the other distances, but at least the heterogeneous change of the iliac peduncle is partially explained by the measurements themselves, because the caliper was always connected to the medially migrating depression at the neck. The negative allometry of the distance between the bottom of the acetabulum and the ventral neck of the obturator process (a_8) is either explained by the deepening of the former (a_5) or by the proximal migration of the latter. The comparison with the respective relations to the length of the iliac peduncle (a_1, see above) shows that the deepening of the acetabulum only partly explain the strong negative allometry of a_8 (almost isometry between a_1 and a_5, but strong positive allometry of a_1 compared to a_8) and a slight proximal migration of the obturator process is therefore likely. Finally, the observed medial migration of the anterior depression at the neck of the iliac peduncle fits very well with the ontogenetically shorter but broader opposing peduncle of the ilium and the increasing extension of the medial acetabular fenestra of the latter element compared to its lateral counterpart.

Femur (Fig. 5.12): Most of the qualitative morphological changes within the femur pertains muscle attachment sites. The most obvious change was observed in the structure of the large medial depression or groove, which was probably the attachment site for the M. caudofemoralis longus (Dilkes, 2000; Galton, 1969; 1981; Gatesy, 1990; Hutchinson, 2001). This depression is posteriorly and slightly dorsally directed with a sharp, steep anterior edge and a shallow, fluent posterior edge in small and medium sized femora (Fig. 5.12A). In large specimens, the inferred direction of the muscle would be strongly dorsally and slightly posteriorly directed with the steeper edge anteroventrally. The depression seems to be also relatively shallower than in smaller femora (Fig. 5.12G).

A prominent shelf or ridge runs laterally along the shaft and distally from the 4th trochanter and served most likely as attachment site for the M. adductor femoris (e.g. Dilkes, 2000). This shelf is less pronounced in small specimens and is convex posteriorly. In large specimens, it is easily recognizable due to the distinct elevation at the lateral side of the shaft (Fig. 5.12E). The shaft is also slightly concave posteriorly at this shelf. Finally, the lateral side of the distal articular end of the femur is more rounded and the anterior intercondylar groove is shallower in small specimens.

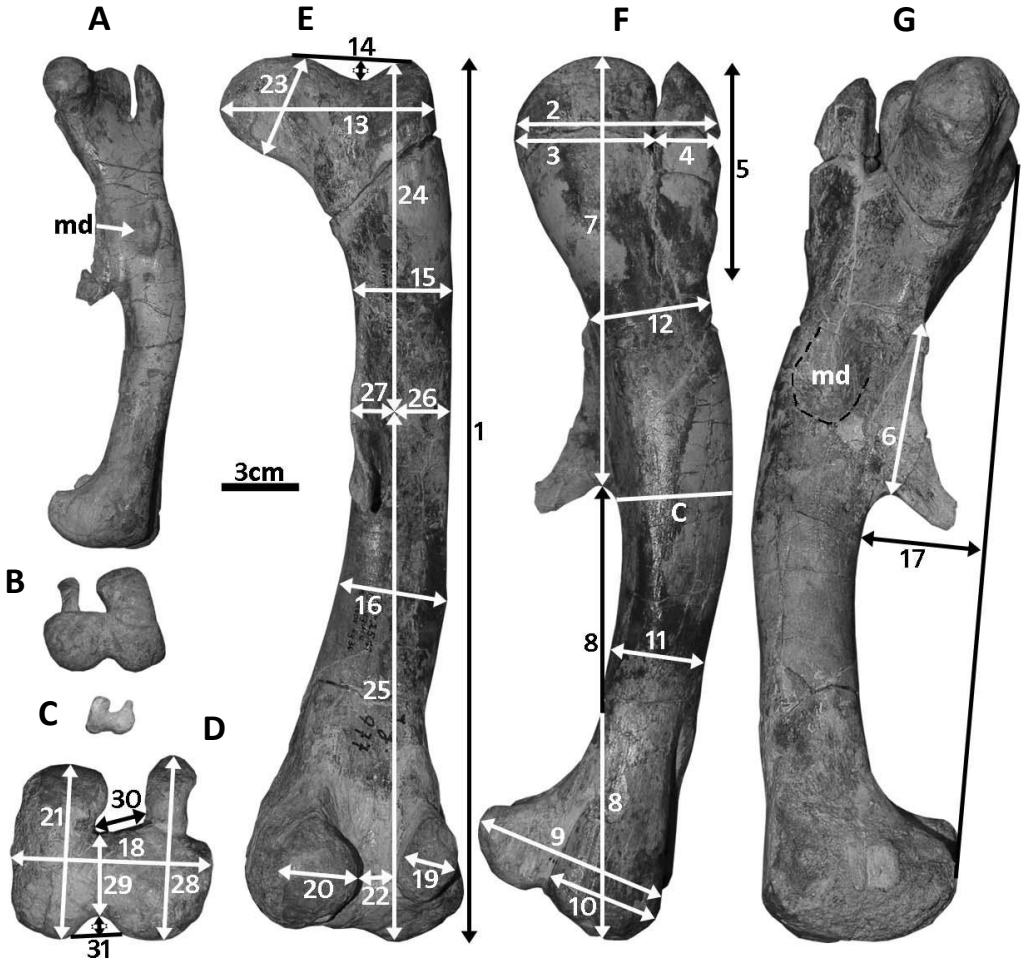

Fig. 5.12: *Femora of* Dysalotosaurus *demonstrating qualitative ontogenetic trends and measured distances.* ***A*** *– Left femur MB.R.2517 in medial view.* ***B*** *– Same as in A, in ventral view.* ***C*** *– Right femur GPIT/RE/4156 in ventral view.* ***D*** *– Right femur MB.R.2511 in ventral view.* ***E*** *– Same as in D, in posterior view.* ***F*** *– Same as in D, in lateral view.* ***G*** *– Same as in D, in medial view. Note the different depths of the anterior intercondylar groove in B, C, and D. Note the different degree of distinctiveness of the medial depression in A and G.* ***Abbr.: C*** *– Circumference;* ***md*** *– medial depression, indicated by white arrow in A and by dashed line in G.*

The surfaces of some muscle attachment sites become more rough and ridged during growth. This is especially the case for the attachment site of M. ischiotrochantericus (Carrano & Hutchinson, 2002; Dilkes, 2000; Fechner, 2009; Norman, 1986) posterolaterally at the greater trochanter, and for the attachment site of the M. iliofemoralis externus at the anteroventral base of the lesser trochanter (e.g. Romer, 1927).

One of the most significant quantitative ontogenetic changes of the femoral morphology is the negative allometry of the length (a_1) compared to most of the other measurements. The only exception is the almost isometrical relationship with the height of the medial depression (a_{34}) and with the midshaft circumference. Further isometries were found between the lengths of a_{24} and a_{25}, which meet each other at the nutritive foramen posteriorly on the shaft and laterally from the 4th trochanter, and between the anteroposterior extension of the medial distal condyle (a_{21}) and the anteroposterior median minimum of the distal articular end (a_{29}). A distal migration of the 4th trochanter is not observed and the height of its base on the shaft is even the only distance, which is negative allometric compared to overall length, although this is statistically insignificant. Other, unfortunately insignificant, results infer the slight anteroposterior thickening of the shaft (a_{11} and a_{12}) compared to the respective lateromedial distances (a_{15} and a_{16}). The strongest significant positive allometries were found for the anteroposterior maximum width of the lesser trochanter (a_4), the thickness of the femoral head (a_{23}), and for the depth of the anterior intercondylar groove (a_{31}; Fig. 5.12B-D). The thickness of the femoral head (a_{23}) is also positively allometric compared to the width of the greater trochanter (a_3). The dimensions of the lesser trochanter seem to increase stronger than the dimensions of the greater trochanter as well.

In conclusion, the femur of *Dysalotosaurus* becomes more robust during growth with relatively larger articular ends (especially the femoral head) and larger and more rough muscle attachment sites (especially lesser trochanter and anterior intercondylar groove).

Tibia (Fig. 5.13): The only qualitative ontogenetic change on the tibia was found distally on the posterolateral or lateral sharp edge of the shaft. A very small bulge rises there in large specimens, which is only detectable in medium sized specimens by touching, and completely absent in small specimens. This bulge is probably the insertional location for the M. interosseus cruris (Fechner, 2009; Gadow, 1882), although the possible attachment of M. pronator profundus cannot be excluded. Nevertheless, the orientation and position of the bulge relative to the fibula proofs the attachment of a muscle, which somehow bridges the space between the tibial and fibular shafts.

The quantitative analyses have revealed the typical significant increase of joint dimensions compared to the length of the long bone. In contrast to the already described relationships in the ulna and radius, but similar to the humerus and femur, the minimum thickness of the shaft (a_3) is almost isometric compared to the lengths of the tibia (a_1 and a_2). The other strongly negatively growing distance, even compared to the overall lengths, is the anteroposterior maximum thickness of the distal articular end (a_{18}). The latter distance shows the strongest negative allometry of all measured distances on the tibia, even compared to the minimum shaft thickness (but here only tendency, not significant).

Within the proximal articular end, the lateromedial width anteriorly at the cnemial crest (a_{10}) strongly increases during growth compared to overall anteroposterior length of this articular end (a_4), to lateromedial maximum width proximally (a_5), to the respective width of this condyle alone (a_7), and compared to the posterior width of this articular end (a_9). The latter is also positively allometric compared to a_4 and a_5. The base of the lateral condyle (a_{11}) further increases compared to its posterior width (a_7) during growth.

In comparison between the proximal and distal articular ends, the anteroposterior length proximally (a_4) is almost isometric compared to the lateromedial width between the lateral corner and the posterodistal notch for the top of the posterior ascending process of the astragalus (a_{15}).

In addition, the lateromedial maximum width proximally (a_5) is almost isometric compared to the maximum distal width lateromedially (a_{13}). The thickness of the cnemial crest (a_{10}) and the anteroposterior basic length of the lateral condyle (a_{11}) are positively allometric compared to the maximum distal width (a_{13}) and both distal thickness measurements (a_{18}, a_{19}), respectively. Within the distal articular end, the maximum width (a_{13}) decreases slightly compared to the lateral fraction of this width, which articulates with the calcaneum (a_{14}), but increases compared to the anteroposterior maximum thickness (a_{18}). The lateral articular fraction for the calcaneum (a_{14}) also increases compared to the complete lateral half of the distal joint, measured from the notch for the posterior ascending process of the astragalus (a_{15}). Again, the distal maximum thickness (a_{18}) is strongly negatively allometric in relation with all other distal measurements.

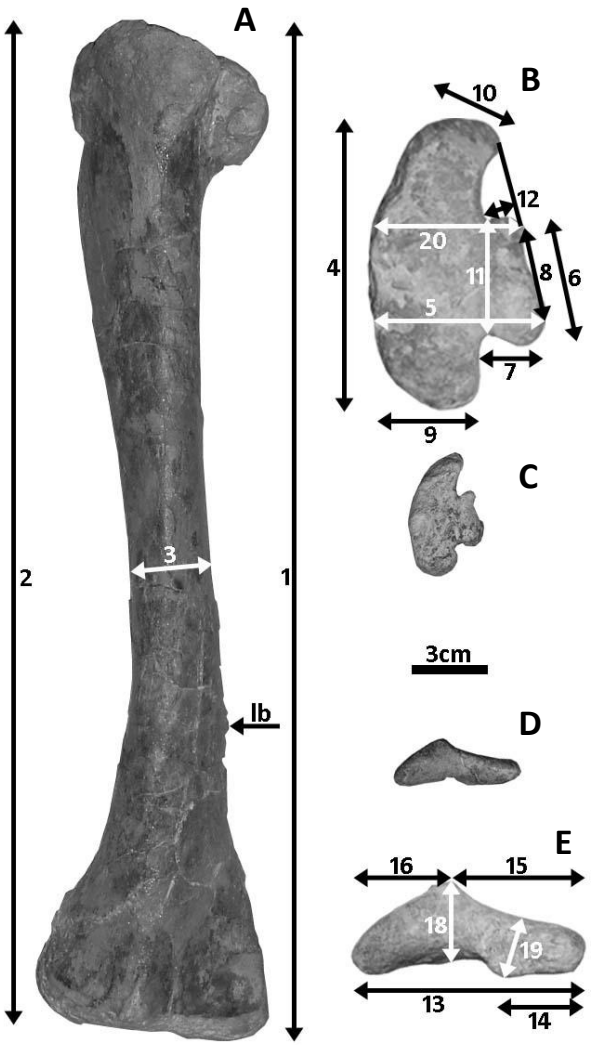

Fig. 5.13: *Tibiae of* Dysalotosaurus *demonstrating qualitative ontogenetic trends and measured distances.* ***A*** *– Right tibia R12279 in posterior view.* ***B*** *– Left tibia SMNSoN5 in dorsal view and mirrored.* ***C*** *– Right tibia MB.R.2516 in dorsal view.* ***D*** *– Same as in C, in ventral view.* ***E*** *– Same as in B, in ventral view and mirrored. Note the strong increase of the thickness of the cnemial crest between B and C.* ***Abbr.: lb*** *– lateral bulge.*

In sum, the tibia gets more robust articular ends during growth, but in contrast to e.g. the radius, ulna, and metatarsals, the shaft maintains its slenderness. The cnemial crest is the most increasing part of the whole bone (Fig. 5.13B-C), but this is not surprising due to its importance as attachment site for numerous muscles and tendons (e.g. the patella tendon). An additional

interesting fact is the positive allometry of the calcaneal articular fraction at the distal joint compared to the broad astragalus fraction.

Fibula (Fig. 5.14): Due to the frequent incomplete preservation of fibulae with only the proximal articular end and a varying adjacent part of the shaft, measurements concerning overall length, minimum shaft thickness, or distances of the distal end could not be made.

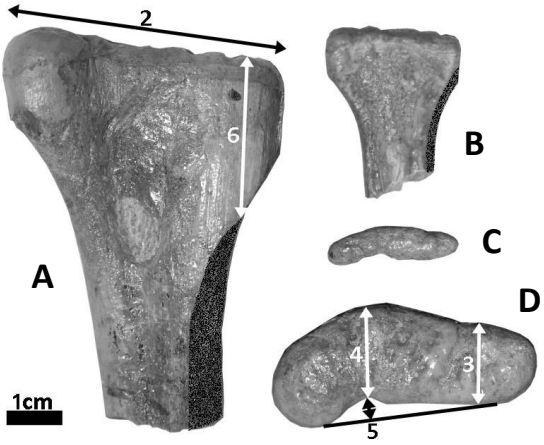

Fig. 5.14: *Fibulae of* Dysalotosaurus *demonstrating qualitative ontogenetic trends and measured distances.* ***A*** *– Proximal right fibula GPIT/RE/5109 in medial view.* ***B*** *– Proximal right fibula GPIT/RE/6841 in medial view.* ***C*** *– Same as in B, in dorsal view.* ***D*** *– Same as in A, in dorsal view. Dark shaded area represents the attachment site for the M. flexor digitorum longus.*

The proximal articular surface increases its robustness and relief during growth as in the other elements. This is confirmed by the positive allometry of its posterior and anterior thickness (a_3 and a_4, respectively) compared to its anteroposterior length (a_2). Herein, the posterior thickness (a_3) increases much less than the anterior thickness (a_4), which is very similar to the condition in the tibia. Isometric growth was observed between the anteroposterior length of the articular end (a_2) and the depth of the medial bend just posterior to the anterior proximal end (a_5) and between the posterior thickness (a_3) and the distance from the proximal articular surface to the dorsal extremity of the probable attachment site (a_6) for the M. flexor digitorum longus (Carrano & Hutchinson, 2002; Fechner, 2009; Fig. 5.14A-B).

Astragalus (Fig. 5.15): The usual ontogenetic increase of robustness and distinctiveness of possible muscle attachment sites were observed. This is the case for a strongly ridged place located anteromedially at the external surface (Fig. 5.15C). A clear determination of the respective muscle or tendon would be equivocal, but the participation of the M. extensor hallucis longus is considered.

Another attachment site consists of a relatively deep anterior fossa, which marks most likely the origin of the M. extensor digitorum brevis (Carrano & Hutchinson, 2002; Fechner, 2009; Fig. 5.15C). Ventrally and laterally, two lobes (an anterior one and a posterior one) are separated there by a deep cleft. This cleft closes successively in lateral direction, leaving a canyon-like appearance on the lateroventral surface of the bone. During growth, the two lobes merge together, but a complete fusion is never achieved (Fig. 5.15E-G).

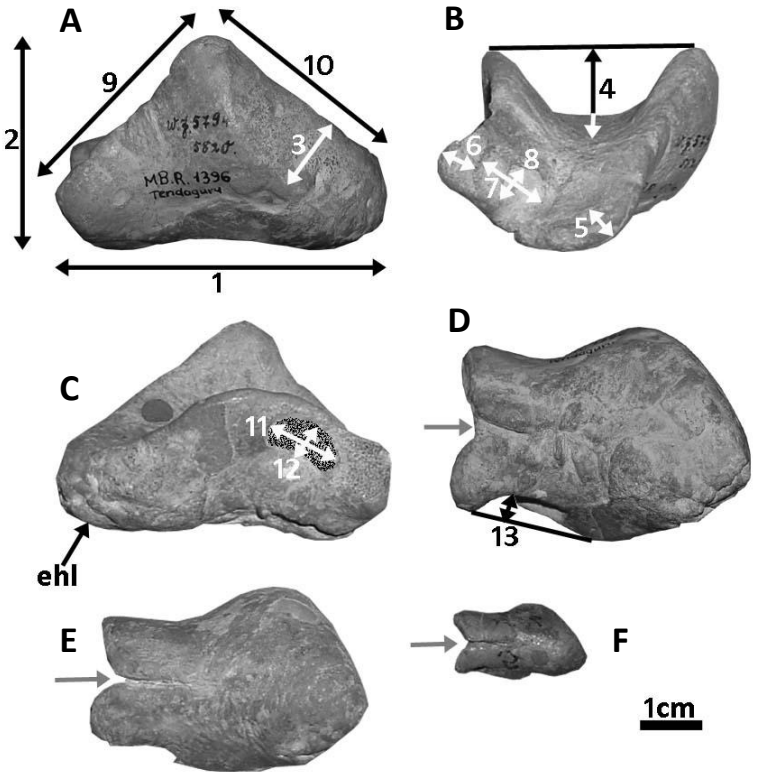

Fig. 5.15: *Astragali of* Dysalotosaurus *demonstrating qualitative ontogenetic trends and measured distances.* ***A*** *– Right astragalus MB.R.1396 in posterior view.* ***B*** *– Same as in A, in lateral view.* ***C*** *– Same as in A, in anterior view.* ***D*** *– Same as in A, in ventral view.* ***E*** *– Right astragalus MB.R.1394 in ventral view.* ***F*** *– Left astragalus MB.R.1383 in ventral view and mirrored. Note the relative extension of the lateroventral cleft relative to the total lateromedial width and its increasing ossification between E, F, and G (gray arrows). The dark shaded area in C marks the fossa for the M. extensor digitorum brevis.* ***Abbr.: ehl*** *– Attachment for M. extensor hallucis longus.*

The lateromedial maximum width (a_1) is negative allometric compared to most of the other distances, where significant results were provided with the posterior maximum height (a_2), the maximum depth between the anterior and posterior ascending processes (a_4), the thickness of the posterolateral lobe (a_5), and the lateromedial width of the anterior fossa for the M. extensor digitorum brevis (a_{11}). The only positive allometry, although insignificant, was observed to the distance between the posterolateral corner and the top of the posterior ascending process (a_9). Interestingly, the posterior maximum height (a_2) increases more slowly than the maximum depth between the anterior and posterior ascending processes (a_4; Fig. 5.15B). The lateromedial width of

the anterior fossa for the M. extensor digitorum brevis (a_{11}) is again growing relatively faster than the posterior maximum height (a_2) and is obviously one of the strongest positive allometric distances within the astragalus. The mentioned height (a_2) increases, nevertheless, stronger than the distance between the most medial point and the top of the posterior ascending process (a_{10}). The last significant result is the positive allometry of the maximum thickness medially (a_3) compared to a_{10}.

By including the insignificant tendencies, the following general ontogenetic changes have affected the astragalus of *Dysalotosaurus*. The maximum lateromedial width is decreasing relative to most of the other distances such as heights and thicknesses, so that the bone becomes more stout and robust during growth. Thereby, the posterolateral distance from the top of the posterior ascending process decreases compared to its medial counterpart and even compared to maximum width, which fits very well to the increasing fractional lateromedial width of the tibial distal end for the articulation with the calcaneum. The increasing internal depth (a_4) shows that the degree of connection to the tibia intensifies, which is also the case for the connection with the calcaneum by increasing ossification of the two lateral lobes and the increasing thickness of the posterolateral lobe. Co-ossification is, however, never achieved. The few determinable muscle attachment sites increase their robustness and sometimes even their extension, as usual.

Calcaneum (Fig. 5.16): The allometric relationships of the calcaneum basically confirm the situation seen in the tibia and astragalus. Its lateromedial width (a_6) increases strongly compared to all the other distances and, thus, extends at the expense of the astragalus. The ventral circumference of the main body (a_5) shows also positive allometry compared to anteroposterior length (a_1).
In the end, the width of the dorsal articular surfaces for the fibula and tibia increases as well as the posterior surface for the attachment site of the M. fibularis longus (Carrano & Hutchinson, 2002; Fechner, 2009; M. peroneus longus in Dilkes, 2000).

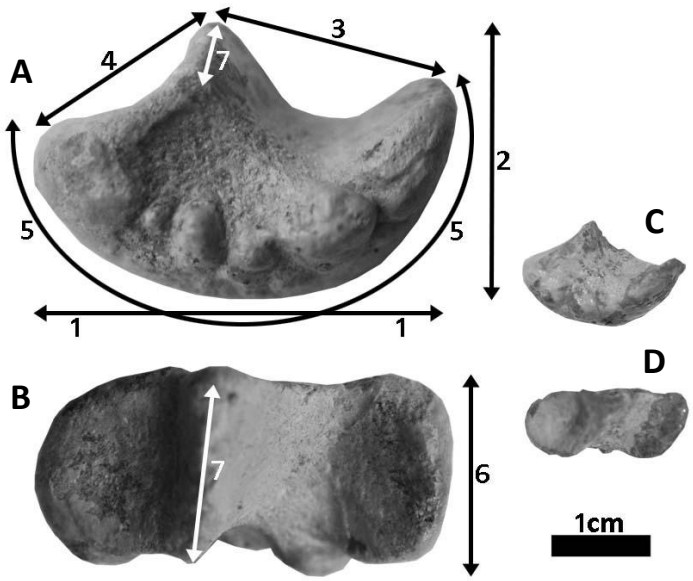

Fig. 5.16: *Calcanei of* Dysalotosaurus *demonstrating qualitative ontogenetic trends and measured distances.* ***A*** *– Right calcaneum GPIT/RE/5808 in medial view.* ***B*** *– Same as in a, in dorsal view.* ***C*** *– Right calcaneum GPIT/RE/5457 in medial view.* ***D*** *– Same as in C, in dorsal view. In the latter specimen, the dorsal process is incomplete.*

Metatarsal II (Fig. 5.17A-F): Specimens of different ontogenetic stages are very similar to each other, but the MAA has revealed some significant allometries. Again, the dimensions of the proximal and distal articular ends are positively allometric compared to the anterior and posterior maximum length (a_1 and a_2), respectively. The shaft becomes stouter due to the positive allometry of the minimum shaft thicknesses (a_5 and a_6) compared to the maximum length (a_1). The allometry of the articular ends themselves is very heterogeneous. The proximal anteroposterior length (a_3) grows stronger than the respective length distally (a_7) and the proximal anterior width (a_4) grows stronger than the distal posterior width (a_8). Some of the distal dimensions grow isometrically, such as the minimum shaft thicknesses (a_5 and a_6) compared to the distal lateromedial minimum width (a_{11}) and the distal lateromedial width anteriorly (a_9). This was also observed for the distal anteroposterior length (a_7) compared to the distal lateromedial width posteriorly (a_8). The anterior lateromedial width (a_9) distally increases, in contrast, stronger during growth than the respective posterior width (a_8) and the anteroposterior maximum and minimum lengths (a_7 and a_{10}), respectively.

Overall and including the tendencies of insignificant results, the metatarsal II becomes more robust during growth width relatively larger articular ends and a stouter shaft. The strongest ontogenetic increase experiences the anterior proximal width (a_4) and the anterior distal width (a_9). Distally, the shape of the articular end is more regular in large specimens and relatively wider

lateromedially than in small ones, which is additionally shown by the consistent (but statistically insignificant) increase of the lateromedial minimum width (a_{11}) compared to a_7 and a_8 (see above).

Metatarsal III (Fig. 5.17G-L): The overall length of this element (a_1) is negatively allometric compared to all other measured distances. The allometry of the proximal articular end is slightly heterogeneous, because the thickness of the posterior corner (a_5) increases stronger than the overall anteroposterior length (a_2). It is also significant that the anteroposterior minimum shaft thickness (a_3) is mostly negatively allometric compared to other distances (but positive in relation to a_1), but its lateromedial counterpart (a_{11}) increases much more positively compared to the anteroposterior length proximally (a_2), to the respective fractional length of a_2 (a_6), and to a_3. It is also almost isometric with the lateromedial maximum width proximally (a_4). The lateromedial minimum thickness of the shaft (a_{11}) is even one of the distances with the strongest relative growth within the mt III, although many relationships are only tendencies due to insignificant results. The distal articular end grows mainly isometrically. This is shown between the anteroposterior length of the lateral condyle (a_7) and the anteroposterior minimum length (a_8) and between the anteroposterior length of the lateral condyle (a_9), the anterior lateromedial width (a_{10}), and the posterior anteromedial width (a_{12}). The only significant ontogenetic changes were found here between a_7 (negative) and both a_9 and a_{10} (positive) and between a_8 (positive) and a_{12} (negative).

After all, the lateromedial distances of the proximal end and of the shaft minimum increase stronger than the respective anteroposterior distances, which indicates a wider and more continuous shaped (a_5 strongly positive) proximal articular end and a much wider shaft minimum. The mt III becomes therefore much more robust in anterior view, but maintains more or less the slenderness of the shaft in lateral view.

A
B
C
D
E
F
G
H
I
J
K
L
M
N
O
P
Q
R
S
T
1cm

← Fig. 5.17: *Metatarsalia of* Dysalotosaurus *demonstrating qualitative ontogenetic trends and measured distances. Arrows with only one head represent measurements perpendicular to the point of view, mostly thickness.* ***A*** *– Left metatarsal II MB.R.2526 in dorsal view.* ***B*** *– Same as in A, in medial view.* ***C*** *– Same as in A, in ventral view.* ***D*** *– Right metatarsal II GPIT/RE/3892 in dorsal view and mirrored.* ***E*** *– Same as in D, in medial view and mirrored.* ***F*** *– Same as in D, in ventral view and mirrored.* ***G*** *– Right metatarsal III SMNSoN3 in dorsal view.* ***H*** *– Same as in G, in medial view.* ***I*** *– Same as in G, in ventral view.* ***J*** *– Right metatarsal III SMNSoN1 in dorsal view.* ***K*** *– Same as in J, in medial view.* ***L*** *– Right metatarsal III GPIT/RE/6009 in ventral view.* ***M*** *– Left metatarsal IV GPIT/RE/6554 in dorsal view.* ***N*** *– Same as in M, in medial view.* ***O*** *– Same as in M, in ventral view.* ***P*** *– Left metatarsal IV GPIT/RE/5646 in dorsal view.* ***Q*** *– Right metatarsal IV MB.R.1542.1 (dy V) in medial view and mirrored.* ***R*** *– Same as in P, in ventral view.* ***S*** *– Same as in M, in anterior view.* ***T*** *– Same as in Q, in anterior view and mirrored.*

allometric compared to most of the other distances. The thickness of the shaft changes very heterogeneous during ontogeny. The lateromedial thickness at mid shaft (a_3) and the lateromedial minimum thickness (a_4) grow much stronger than their anteroposterior counterparts (a_6 and a_7, respectively). The former (a_3) increases even isometrically with one of the strongest growing distances, the lateromedial midline proximally (a_{10}). At this articular end, the thickness of the posterior corner (a_{12}) is positively allometric compared to the anteroposterior maximum length (a_8). The mainly insignificant results for the distances of the distal articular end are either positively allometric compared to shaft length (a_1, a_2) or they grow negatively allometric compared to lateromedial shaft width (a_3, a_4) and partially to the proximal end (a_{10} significantly positive, a_{17} negative). The distal distances among one another are mainly isometric (a_{14} to a_{18}; a_{15} to a_{16}; a_{16} to a_{17}; a_{16} to a_{18}; a_{17} to a_{18}).

Overall, the shaft of mt IV becomes not only more robust but also wider mediolaterally than anteroposteriorly, and the proximal end grows stronger than the distal end. The shape change of the shaft and of the proximal end suggests a more rigid articulation with mt III.

Phalanx II1 (first phalanx of the second toe) (Fig. 5.18C-D): The strongest quantitative ontogenetic increase was observed for the width and height of the proximal articular end (a_4 and a_8) compared to all remaining distances. Both distances grow almost isometric to each other. The least increase was represented by the dorsal and ventral fractional lengths measured from the proximal

end to the respective posterior beginning of the distal articular facets (a_{14} and a_{15}). This marks the significant posterior extension of these facets during growth. The total length at the sagittal plane (a_1), as well as the lengths medially and laterally (a_2 and a_3, respectively), is also strongly negatively allometric compared to most of the other distances, apart from the mentioned fractional lengths (a_{14}, a_{15}), where they are positively allometric.

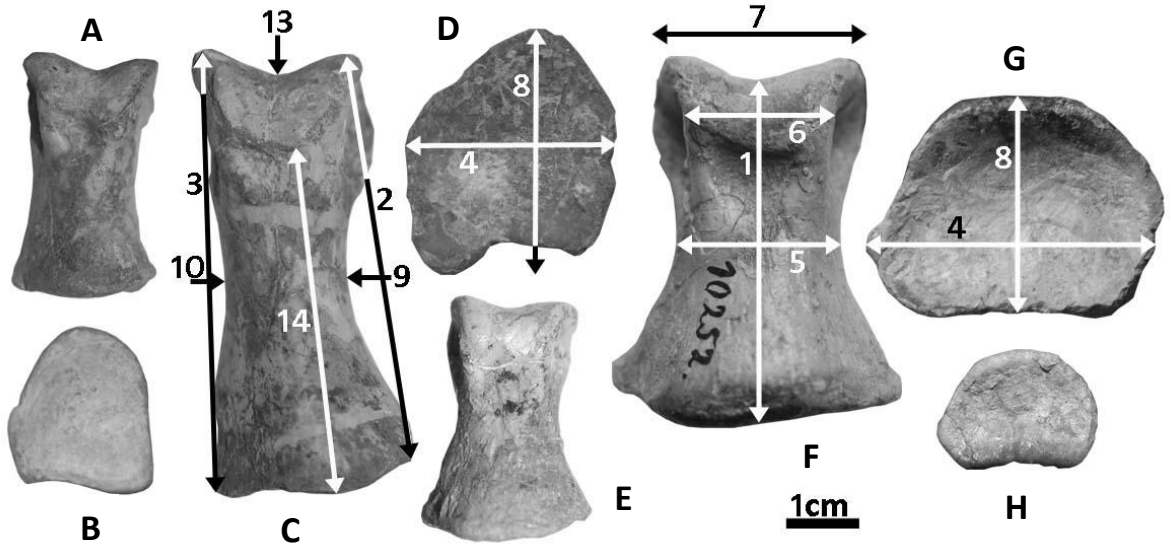

Fig. 5.18: *Phalanges of* Dysalotosaurus *demonstrating qualitative ontogenetic trends and measured distances. Arrows with only one head represent measurements perpendicular to the point of view, mostly thickness or height.* ***A*** *– Left first phalanx of the fourth toe SMNSoN2 in dorsal view.* ***B*** *– Same as in A, in proximal view.* ***C*** *– Left first phalanx of the second toe SMNSoN1 in dorsal view.* ***D*** *– Same as in C, in proximal view.* ***E*** *– Left first phalanx of the third toe GPIT/RE/3946 in dorsal view.* ***F*** *- Left first phalanx of the third toe GPIT/RE/6636 in dorsal view.* ***G*** *– Same as in F, in proximal view.* ***H*** *– Same as in E, in proximal view.*

Isometry was also observed between the dorsal condyle width (a_6) and the ventral condyle width (a_7), between the former and the height of the medial condyle (a_{11}), between the lateromedial minimum width of the shaft (a_5), the medial minimum shaft height (a_9), and the sagittal height between both condyles (a_{13}), between a_7 and a_{13}, and between the height of the lateral condyle (a_{12}) and the sagittal height between the condyles (a_{13}). There are finally slight differences between the medial and lateral side of the bone. The medial minimum shaft height (a_9) increases positively compared to the lateral shaft height (a_{10}). Unfortunately insignificant is the positive allometry of the medial condyle height (a_{11}) compared to its lateral counterpart (a_{12}).

In the end, the phalanx becomes more robust during growth with a relatively shorter shaft, wider and higher articular ends including a more extensive distal articular facet, and a slightly stronger growth of the medial shaft and the medial condyle compared to the lateral side.

Phalanx II2 (second phalanx of the second toe) (Fig. 5.19): Due to a 100 percent complete dataset, the MAA of all variables could be performed together and in addition to the bivariate plots. It confirms the condition derived by the latter that the ventral condyle width (a_7) is the only significantly increasing distance during growth. In the bivariate plots, a_7 is significant positive allometric to most of the length distances (a_1, a_2, a_3, a_{15}), to the minimum shaft width (a_5), and to the height of the lateral condyle (a_{12}). Furthermore, a_7 grows almost isometric to the proximal width (a_4), to the medial minimum shaft height (a_9), and to the intercondylar height (a_{13}). Further isometric growth was observed between the median length (a_1) and the lateral length (a_3), between the medial length (a_2) and the dorsal condyle width (a_6), between the proximal width (a_4) and the medial minimum shaft height (a_9), between the former and the intercondylar height (a_{13}), between the minimum shaft width (a_5) and the proximal height (a_8), between the dorsal condyle width (a_6) and the height of the medial condyle (a_{11}), between a_9 and a_{13}, and between the lateral minimum shaft height (a_{10}) and the height of the medial as well as lateral condyle (a_{11}, a_{12}, respectively). The only other almost significant positive allometry was observed for the proximal width (a_4) compared to its height (a_8).

Again, all length distances become in tendency shorter during growth, whereas the articular ends increase. An unusual feature is the comparatively strong positive allometry of the ventral condyle width in relation to many other distances. It is also noteworthy that the proximal width increases compared to its height, whereas it is almost isometrical in phalanx II1.

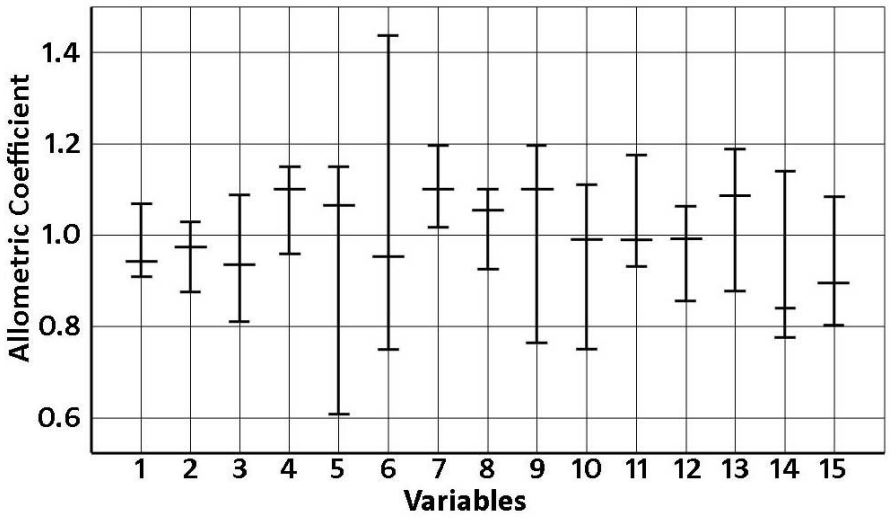

Fig. 5.19: *Multivariate plot of the MAA for all measured distances/variables of the second phalanx of the second toe. Note, that the variable 7 is the only significant, because the whole 95% interval is different from 1. Picture modified from the software PAST.*

Phalanx III1 (first phalanx of the third toe) (Fig. 5.18E-H): All length distances (a_1, a_2, a_3, a_{14}, a_{15}) are again negatively allometric compared to most of the other distances, but in comparison with the second phalanx of the second toe, the dorsal fractional length (a_{14}) is less negative than the ventral fractional length (a_{15}) and is even isometric with the sagittal length (a_1). In addition, the medial minimum shaft height (a_9) is decreasing compared to the minimum shaft width (a_5), which is another difference to the former described phalanx. Further significant results were gained for the negative allometry of a_9 compared to the heights of both condyles (a_{11} and a_{12}) and the negative allometry of the sagittal distal height (a_{13}) compared to the height of both condyles (a_{11} and a_{12}).

Many additional isometries are present, such as between the lateromedial width proximally (a_4) and the height of the lateral condyle (a_{12}), between the minimum shaft width (a_5) and the dorsal condyle width (a_6), between the latter and the sagittal distal height (a_{13}), between the ventral condyle width (a_7) and the minimum lateral shaft height (a_{10}) as well as both condyle heights (a_{11} and a_{12}), between the proximal height (a_8) and a_{12}, between the minimum lateral shaft height (a_{10}) and a_{11} as well as a_{12}, and finally between a_{11} and a_{12}.

As in phalanx II1, the shaft becomes more robust in phalanx III1 during growth with relatively larger articular ends. In contrast to the former phalanx, there is no relative increase of the medial

heights of the shaft and condyle, but an almost opposite tendency within the shaft and isometric growth of both condyles. Another difference is the relative increase of the condyles relative to the height between them, so that the distal articular end is more pronounced in large specimens.

Phalanx III2 (second phalanx of the third toe): As in the other phalanges, the length distances generally decrease during growth compared to all other distances. This is confirmed by the significant negative allometry of the median length (a_1) compared to the proximal width (a_4), the minimum shaft width (a_5), the proximal height (a_8), to the lateral minimum shaft height (a_{10}), as well as to the intercondylar height (a_{13}), and by the negative allometry of the medial length (a_2) and lateral length (a_3) compared to the height of the lateral condyle (a_{12}). The median length (a_1) is furthermore almost isometrical with a_{12}. An interesting tendency is the relative growth of the dorsal length between the condyle facet and the proximal end (a_{14}). As in the phalanges III1 and VI1, this distance slightly increases compared to its ventral counterpart (a_{15}), and as in phalanx III1, it is almost isometrical with the median length (a_1). This is in contrast to the tendency in the two described phalanges of the second toe. One of the strongest increasing distances in phalanx III2 is the proximal width (a_4), which is, apart from its relations to the lengths, confirmed by its positive allometry in relation to the lateral minimum shaft height (a_{10}) and to the intercondylar height (a_{13}). Several additional distances grow isometrically, which includes the dorsal condyle width and the intercondylar height (a_6 and a_{13}), the medial and lateral minimum shaft heights (a_9 and a_{10}), the medial and lateral condyle heights (a_{11} and a_{12}), and the dorsal length between the condyle facet and the proximal end (a_{14}).

Overall, the robustness of this phalanx is also increasing during growth, but as in the phalanges III1 and VI1 the dorsal condyle facet seems to increase its proximal extent much less compared to its ventral counterpart as in the phalanges of the second toe.

Phalanx IV1 (first phalanx of the fourth toe) (Fig. 5.18A-B): The sagittal total length (a_1) is in contrast to the other two first phalanges negatively allometric compared to the lateral total length

(a_3). In relation to the other distances, the sagittal total length decreases, except in comparison to the dorsal and ventral fractional lengths ending distally at the border of the respective articular facets (a_{14}, a_{15}). This is also true for the medial and lateral total lengths (a_2, a_3). Another significant difference to the other two first phalanges is the much weaker allometric growth of the lateromedial width proximally (a_4), which is almost isometric to the minimum shaft width (a_5), negatively allometric in relation to the dorsal condyle width (a_6), and slightly decreasing compared to the proximal height (a_8), although the latter is an insignificant tendency. A unique ontogenetic character of the phalanx IV1 is the strong positive allometry of the dorsal condyle width (a_6) compared to most of the other distances and its almost isometric growth compared to the proximal height (a_8). Further isometric growth was observed between the minimum shaft width (a_5) and the ventral condyle height (a_7) as well as with the height of the lateral condyle (a_{12}), between a_7 and the minimum medial shaft height (a_9), and between a_9 and both condyle heights (a_{11}, a_{12}). The proximal height (a_8) is the most increasing distance of the phalanx during growth.

In conclusion, and by integrating insignificant tendencies, the following ontogenetic changes of phalanx IV1 were observed. The proximal articular end becomes higher then wide, but the whole joint is still more robust compared to the shaft in large specimens. The medial height of the shaft (a_9) is the least increasing distance compared to the other two shaft distances (a_5, a_{10}), which is similar to phalanx III1, but in contrast to phalanx II1. The distal condyles of phalanx IV1 are much more perpendicular in dorsoventral orientation and are also much more distinct in large specimens. As in phalanx II1, the medial condyle slightly increases its height relative to the lateral condyle, whereas they grow isometric in phalanx III1. The distal articular facets of the condyles extend during growth again.

Phalanx VI2 (second phalanx of the fourth toe): The length distances (a_1, a_2, a_3) grow isometrical to each other, two of them are also isometrical to the intercondylar height (a_{13}) as well as to the lengths between the dorsal and ventral facets and the proximal end (a_{14} and a_{15}). The most

significant positive allometric growth compared to most of these length distances was observed for the dorsal and ventral condyle width (a_6 and a_7), for the proximal height (a_8), and for both minimum shaft heights (a_9 and a_{10}). Unusually negatively allometric is the intercondylar height (a_{13}), which is significant in relation to the proximal height and width (a_4 and a_8) and to both condyle widths (a_6 and a_7). Further interesting changes in proportion are the relative increase of the dorsal condyle width (a_6) compared to the medial minimum shaft height (a_9) and to the medial condyle height (a_{11}), the increase of the ventral condyle width (a_7) compared to the proximal height (a_8) and to a_{11}, the increase of a_8 compared to a_{11}, and the increase of the lateral minimum shaft height (a_{10}) compared to the lateral condyle height (a_{12}).

In the end, this phalanx becomes significantly stouter and robust during growth, where especially the height of the shaft increases compared to the height of the condyles. Otherwise, the condyle widths increase most of all distances.

5.5 Discussion

5.5.1 Axial skeleton

The sequence of neurocentral suture closure in *Dysalotosaurus* took place from back to front, but only the caudal series show completely fused sutures in the largest preserved individuals, whereas the remaining vertebrae maintained the open stage. Thus, even the largest known individuals were not somatically mature. The sequence and timing of the closure of neurocentral sutures is poorly known in other dinosaurs due to incomplete specimens, bad preservation, or simply lack of description in many species (Irmis, 2007). There is also no final conclusion available by using the Extant Phylogenetic Bracket (Witmer, 1995) for dinosaurs, because extant crocodiles show a posterior-anterior sequence (Brochu, 1996) and birds show an anterior-posterior sequence (Starck, 1993 [in Irmis, 2007]).

Within ornithischian dinosaurs, small ornithopods, such as *Hypsilophodon* or *Thescelosaurus*, show the crocodilian plesiomorphic condition of a posterior-anterior closure sequence (Galton, 2009; Irmis, 2007), which is now also confirmed for *Dysalotosaurus*. The preserved caudal series of the basal thyreophoran *Scutellosaurus* show this sequential type as well (Rosenbaum & Padian, 2000). Neoceratopsians seem to possess the opposite sequence, mainly due to their special syncervical vertebra (Chinnery & Weishampel, 1998; Irmis, 2007).

Within saurischian dinosaurs, the closure pattern is probably even more diverse (Irmis, 2007). The best information is known from the neosauropod *Camarasaurus*, where an anterior-posterior sequence follows after the plesiomorphic posterior-anterior condition has started, so that the dorsal vertebrae are the last in the whole sequence (Ikejiri, 2003; Ikejiri et al., 2005).

Theropods seem to show both types of sequences. Irmis (2007) has mentioned *Allosaurus* with a possible posterior-anterior sequence and *Nqwebasaurus* as a candidate for the opposite pattern. Recently, an extensive study on the abelisaurid theropod *Majungasaurus* revealed the unambiguous anterior-posterior closure sequence in this taxon (O'Connor, 2007:129). The condition in the caudal series of the respective specimen (UA 8678) was unfortunately very incompletely preserved, but at least the first five proximal caudals seem to represent the plesiomorphic posterior-anterior sequence (O'Connor, 2007:147-148 & fig. 15 therein), which implies a similar pattern as in *Camarasaurus*.

The body of evidence is still very poor for dinosaurs (Irmis, 2007), but the plesiomorphic archosaur posterior-anterior fusion sequence was probably not substituted by the derived anterior-posterior pattern in some dinosaurs. It was rather retained and the derived sequence was added to it. Interestingly, dinosaur taxa with an evident anterior-posterior fusion sequence have either comparatively large and heavy skulls (neoceratopsians), powerful necks (*Majungasaurus*; O'Connor, 2007) or very long necks (*Camarasaurus*). This would imply a biomechanical influence on the fusion pattern, but there is still much to be done to get at least an overview on the distribution of the sequence types within Dinosauria and, subsequently, on the reasons for their alteration.

All the observed or formerly documented variations in the axial skeleton of *Dysalotosaurus* are clearly the result of successive maturity and, naturally, of increasing body size and body weight. The posterior dorsal centra and sacral centra become more compact due to the relative increase of their height; the posterior dorsal ribs are more firmly attached to the vertebrae due to the longer distance between the two articular joints; at least one muscle between the atlas and basicranium becomes more firmly attached; and the lateral walls of the neural canal are increasingly ossified during growth. The latter indicates the ontogenetic relative decrease of the size of the neural canal, which is also known from other ornithopods (e.g. Chure et al., 1994; Horner & Currie, 1994). The reason of the described unusual emarginations in two vertebrae (Fig. 5.3B-E) is also a sign of increasing stiffness and co-ossification in the posterior dorsals and sacrum, although this occurs only in a small minority of individuals. The attribution of this vertebral variation to e.g. sexual dimorphism would be highly speculative. However, Galton (1974) proposed sexual dimorphism in *Hypsilophodon*, because two morphotypes of the sacrum are known from this taxon.

Increasing ossification of vertebrae in other dinosaurs include the lengthening of neural spines as in hadrosaurs (Godefroit et al., 1998; Horner & Currie, 1994), or the development of additional laminae on the vertebrae as in *Camarasaurus* (Ikejiri et al., 2005). Co-ossification of sacral vertebrae is also well known, such as in ceratopsians (e.g. Brown & Schlaikjer, 1940), hadrosaurs (e.g. Horner & Currie, 1994), thyreophorans (e.g. Coombs, 1986; Galton, 1982), sauropods (e.g. Ikejiri et al., 2005; Tidwell et al., 2005), and theropods (e.g. Raath, 1990). This is only weakly developed in *Dysalotosaurus* (Fig. 5.3E), if at all.

5.5.2 General ontogenetic trends in the appendicular skeleton

Even the smallest preserved specimens of *Dysalotosaurus* possess well developed articular ends. In contrast to hadrosaurs, it is therefore assumed that the hatchlings were precocial in behavior (see Horner & Weishampel, 1988; Horner et al., 2001; Winkler, 1994; see also chapter

6.7.3). Taphonomic implications from a study on the Proctor Lake *Hypsilophodon*-like ornithopod (Winkler & Murry, 1989) would rather indicate semi-precocial to semi-altricial behavior of this taxon at first view. However, in contrast to the possible nesting site of the hadrosaur *Maiasaura* (Horner & Makela, 1979), egg remains are completely absent, the degree of ossification of limb elements and of tooth wear is much higher, and the possible *Orodromeus* nesting site as reference for a comparison emerged as belonging to the theropod *Troodon* (Horner & Weishampel, 1996). Thus, precocial behavior is still more likely in the Proctor Lake ornithopod and the concentrated preservation of juveniles could also be the result of groups of juveniles gathered together for protection (Winkler & Murry, 1989) or just to find shade and cooling at this place.

Suture fusion within the appendicular skeleton of *Dysalotosaurus* is completely absent, although increasing stability of connection between the scapula and coracoid as well as between the astragalus and calcaneum was observed. Unfused sutures indicate that active growth is still possible, but its significance for the assessment of maturity is highly ambiguous due to high variability in the timing of fusion among reptiles (e.g. Brochu, 1995; Cole et al., 2003; Maisano, 2002). However, the extensive fusion of elements in the skeleton of pterosaurs (Bennett, 1993; 1995; 1996) is comparable with the pattern seen in birds and might be more useful for an estimation of maturity in this group than in other reptiles.

The fusion of sutures within dinosaurs is very variable. Heterodontosaurs show fusion between the scapula and coracoid, between the tibia, fibula, and the proximal tarsals, as well as between the distal tarsals and the metatarsals (Santa Luca, 1980; Norman et al., 2004; Butler et al., 2008b). This extensive fusional pattern, especially within the hindlimb, could even be treated as a possible autapomorphy of heterodontosaurs among Ornithischia. Fusion between the scapula and coracoid, between the distal tibia and the proximal tarsals, and/or between the astragalus and calcaneum occur also in several theropods, such as ceratosaurs and ornithomimosaurs (e.g. Carrano et al., 2005; Makovicky et al., 2004; Raath, 1990; Tykoski & Rowe, 2004), sauropods (e.g. Ikejiri et al., 2005; Janensch, 1961:181), thyreophorans (Galton, 1982; Galton & Upchurch, 2004; Hennig, 1924;

Vickaryous et al., 2004), and ceratopsians (Dodson et al., 2004; Hailu & Dodson, 2004). Within Ornithopoda, obviously only *Ouranosaurus* and *Oryctodromeus* seem to show fusion between the scapula and coracoid (Norman, 2004; Varricchio et al., 2007). Thus, although intra-elemental fusion is known among dinosaurs, it occurs not in all groups and, even then, not in all species. The almost complete lack of fusion in *Dysalotosaurus* therefore could be a sign of somatic immaturity even in the largest preserved individuals, but the lack of fusion in nearly all other ornithopods definitely demonstrates that the appendicular fusion pattern is inappropriate for ontogenetic assessment in this group.

Bone surface texture as a size-independent criterion to assess the ontogenetic stage was already used successfully for some small dinosaurs (Callison & Quimby, 1984), for some ceratopsian dinosaurs (Tumarkin-Deratzian, 2009), and for pterosaurs (e.g. Bennett, 1993). However, although Tumarkin-Deratzian et al. (2006) and Tumarkin-Deratzian (2009) found significant results for a dependence of intensity, type, and density of bone surface marks on ontogenetic stage, this criterion seems to be useful only in vertebrates with a determinate growth pattern (Tumarkin-Deratzian, 2003; Tumarkin-Deratzian et al., 2007). Pterosaurs do have a determinate growth pattern (Chinsamy et al., 2008) as was probably also the case for some ceratopsians (see chapter 6.8.4). Ontogenetic change of bone surface texture in *Dysalotosaurus* was not observed, which therefore implicates an indeterminate growth pattern for this dinosaur (Chinsamy, 1995; see chapter 6.7.3), as in *Alligator* (Tumarkin-Deratzian et al., 2007).

Despite the lack of sutural fusion between appendicular elements, the relative dimensions and the degree of rugosity of sutural surfaces increase during growth in *Dysalotosaurus*. This is mainly the case for the sutural surfaces between the scapula and coracoid, between the ilium and ischium, and between the astragalus and calcaneum. Likewise, articular ends, processes, and grooves for muscles and tendons become more pronounced compared to overall dimension of elements, especially compared to overall lengths and/or midshaft circumferences (e.g. the anterior intercondylar groove of the femur). Some of these processes or pits for attaching muscles even

significantly increase their surface, as seen in the olecranon process of the ulna, the lesser trochanter of the femur, the cnemial crest of the tibia, and the anterior fossa for the M. extensor digitorum brevis at the astragalus. Nearly all long bones, girdle bones, and phalanges show this pattern. Furthermore, recognizable surfaces, ridges, and small bumps, which are also clearly related to the attachment of muscles and/or tendons, become more robust and rugose, indicating firmer connections between them in larger individuals. Such small bumps or processes, for instance, are known in the scapula and tibia. All these ontogenetic tendencies are generally well known in dinosaurs including ornithopods (e.g. Brett-Surman & Wagner, 2007; Coombs, 1986; Currie, 2003:660; Currie & Azuma, 2006; Forster, 1990a; Galton, 1974; 1980; 1982; Ikejiri et al. 2005; Martin, 1994; Weishampel et al., 2003).

5.5.3 Further ontogenetic variation in single appendicular elements

Scapula: In contrast to *Tenontosaurus* (Forster, 1990a:fig. 7), the end of the scapular blade is not straight in juveniles of *Dysalotosaurus*, but as gently convex as in the larger specimens. It is much more similar to *Camptosaurus* (Carpenter & Wilson, 2008:fig.17), especially to *C. aphanoecetes*. However, a change from a more symmetrically rounded scapular distal blade in young *Dysalotosaurus* to a posteroventrally strongly flaring distal blade in larger specimens (Fig. 5.4) is not visible in both *Camptosaurus* species. This kind of ontogenetic change is very similar to *Hypsilophodon* (Galton, 1980:fig. 3C, D). Furthermore, although the relief of the proximal part of the scapula becomes more pronounced in *Dysalotosaurus* during growth, it never gets such a strong acromion process and adjacent anteroventral ridge (‘deltoid ridge’ in Brett-Surman & Wagner, 2007) as in *Camptosaurus* or *Hypsilophodon*. In this feature, it is in turn more similar to *Tenontosaurus*.

Here, the intermediate phylogenetic stage of *Dysalotosaurus* is obvious, but the ontogenetic variation in overall scapular shape is interestingly higher than in *Camptosaurus* and *Tenontosaurus* and similar to *Hypsilophodon*. Nevertheless, the strong ontogenetic and intraspecific variation of the

blade shape of the scapula in *Dysalotosaurus* does not fully explain the extraordinary differences in the respective shape between two scapulae assigned to *Zalmoxes robustus* (Weishampel et al., 2003:fig. 19). One specimen (BMNH R3814) is very similar to the scapulae of *Dysalotosaurus*, *Camptosaurus* and *Tenontosaurus* and fits nicely into the general scheme expected for basal iguanodontians. The other specimen (BMNH R3810) is only about 20% smaller, but the shape of the scapular blade looks very juvenile. *Dysalotosaurus* shows such a difference only by comparison between the smallest and largest preserved scapulae, where the smallest reaches less than 50% of the represented maximum size. Thus, it is more likely that the scapulae figured by Weishampel et al. (2003:fig. 19) either belong to different taxa, represent a generally high intra-specific variability, or these specimens are another expression of sexual dimorphism, as already suggested by the authors for the ischium of *Z. robustus*.

Coracoid: The comparison of the coracoid of *Dysalotosaurus* with *Dryosaurus altus* is difficult, because only very few specimens are known from the latter. The coracoids of the young juvenile individual are not well preserved for a comparison (Carpenter, 1994; pers. obs.) and the ontogenetic variation described by Carpenter (1994) is based upon a figure of the coracoids of the "dy I" individual of *Dysalotosaurus* itself (see Galton, 1981:fig. 6M; Carpenter, 1994:fig. 19.6M). The known coracoids of *Dryosaurus* (CM3392 not described and not adequately figured by Gilmore, 1925 and Galton, 1981; AMNH 834 obviously a younger and overall medium sized individual, see Galton, 1981:tab.2) differ from each other and from *Dysalotosaurus* mainly in the development of the sternal hook or process. In CM3392, it is longer and distinct due to a deep concavity between this process and the posteroventral beginning of the humeral articular surface (pers. obs. on the mounted skeleton). In AMNH 834, the sternal process is completely absent (Galton, 1981; Shepherd et al., 1977). The coracoids of both individuals resemble only the coracoids of the very young *Dysalotosaurus* in the almost equal dimensions of this element anteroposteriorly and dorsoventrally (Fig. 5.5A). The length of the sternal process increases only slightly in *Dysalotosaurus* during

ontogeny and the extremes found in *Dryosaurus* are not visible in any of the preserved coracoids of the former. It should therefore be tested in the future, whether the extraordinary variation in *Dryosaurus* is either the result of different preservation or whether it indicates the presence of two distinct North-American species. Ontogeny alone definitely cannot explain this degree of variation.

As already noted, the overall dimensions of the coracoid of *Dysalotosaurus* are roughly equal in small specimens, whereas it becomes anteroposteriorly longer than dorsoventrally high in large specimens (Fig. 5.5). Similar ontogenetic trends were observed in *Hypsilophodon* and *Orodromeus* (Galton, 1980; Scheetz, 1999:53). It is also probably the case in *Camptosaurus*, although the typical quadrangular overall shape of the coracoid of the latter is already present in very young individuals (Carpenter & Wilson, 2008:17D; Chure et al., 1994).

Humerus: Brett-Surman & Wagner (2007) noted for hadrosaurs the relative ontogenetic increase of the medial (ulnar) condyle of the distal humeri compared to its lateral counterpart. Exactly the same was observed in *Dysalotosaurus* (Fig. 5.7D-E) and could be an adaptation to increasing body weight or a changing biomechanical input on the medial elbow joint. An ontogenetically increasing body mass, for instance, had to be heaved up after resting on the ground (pers. comm. Remes, 2010). Another reason could be a more forceful grip of larger individuals to hold something in both hands. Anyway, the reason for this ontogenetic change is obviously the same in hadrosaurs and *Dysalotosaurus*, although the former experienced a shift from bipedality to quadrupedality during growth (Dilkes, 2001) and the latter not (see chapter 5.5.5). However, the strong variation in the distal humerus of *Dysalotosaurus*, already noted by Galton (1981), is clearly ontogenetic in nature. Similar observations were made in *Orodromeus* (Scheetz, 1999: tab. 1), where the distal condyles are, as in *Dysalotosaurus*, more distinct in juveniles than in adults.

Several further ontogenetic changes within the humerus of *Dysalotosaurus* were observed in other ornithopods. The length of the deltopectoral crest increases compared to overall humeral length also in *Orodromeus*, *Zalmoxes robustus*, *Tenontosaurus tilletti*, and *Maiasaura* (Dilkes, 2001;

Forster, 1990a; Scheetz, 1999; Weishampel et al., 2003:fig. 20). There is also an anteroposterior thickening of this crest as in *Dryosaurus altus* (see Galton, 1981:figs. 6B; 7C) and hadrosaurs in general (Brett-Surman & Wagner, 2007), which is similar to its increased pronouncement in *Orodromeus*, *Hypsilophodon*, *Tenontosaurus*, and *Camptosaurus dispar* (Carpenter & Wilson, 2008; Forster, 1990a; Galton, 1980; Scheetz, 1999). However, in the latter four genera, the deltopectoral crest is rather an anterior elevation (pointed in *Orodromeus* and *Hypsilophodon*, also in *Z. robustus*; quadrangular in *T. tilletti* and *C. dispar*) than a bulging protuberance as in *Dysalotosaurus*, *Dryosaurus*, and *Camptosaurus aphanoecetes*. Especially *Tenontosaurus* is very similar to hadrosaurs in the shape and extant of the deltopectoral crest (Dodson, 1980).

Ulna and radius: Both elements become stouter with relatively larger articular ends and a relatively thicker shaft in *Dysalotosaurus* during growth. The olecranon process of the ulna never reaches the highly pointed elevation seen in *Hypsilophodon*, *Orodromeus*, and *Z. robustus* (Galton, 1974:fig. 40; Scheetz, 1999:fig. 22; Weishampel et al., 2003:fig.21) or the distinct high shape as in more derived iguanodontians (e.g. Norman, 1980:fig. 58), but reaches a moderately higher elevation during ontogeny than *Dryosaurus* (Galton, 1981) and is most similar to *C. aphanoecetes* (Carpenter & Wilson, 2008:fig.21G) in large specimens. However, although the olecranon process expands also in dorsal view in *Dysalotosaurus*, it is in turn more similar to *Dryosaurus*, *Hypsilophodon*, and *Orodromeus* than to *C. aphanoecetes* due to the much more pronounced lateral process in the latter (Carpenter & Wilson, 2008). Hadrosaurs, stegosaurs, and *Protoceratops*, for instance (Brett-Surman & Wagner, 2007; Brown & Schlaikjer, 1940; Galton, 1982), also show ontogenetically increased robustness and elevation of the olecranon process, but especially hadrosaurs show additional differing ontogenetic tendencies. The olecranon notch for the ulna is larger in older individuals, which is not the case in *Dysalotosaurus*. Thus, the degree of articular overlap between the humerus and ulna is higher in hadrosaurs. Furthermore, the relative lengths of radius and ulna strongly increase during growth in the latter, which results in more slender elements in older individuals

(Brett-Surman & Wagner, 2007; Horner & Currie, 1994) and in the special hadrosaur forelimb proportions (long radius and metacarpals compared to relatively shorter humerus; Fig. 5.20; Appendix V) unique within ornithopods.

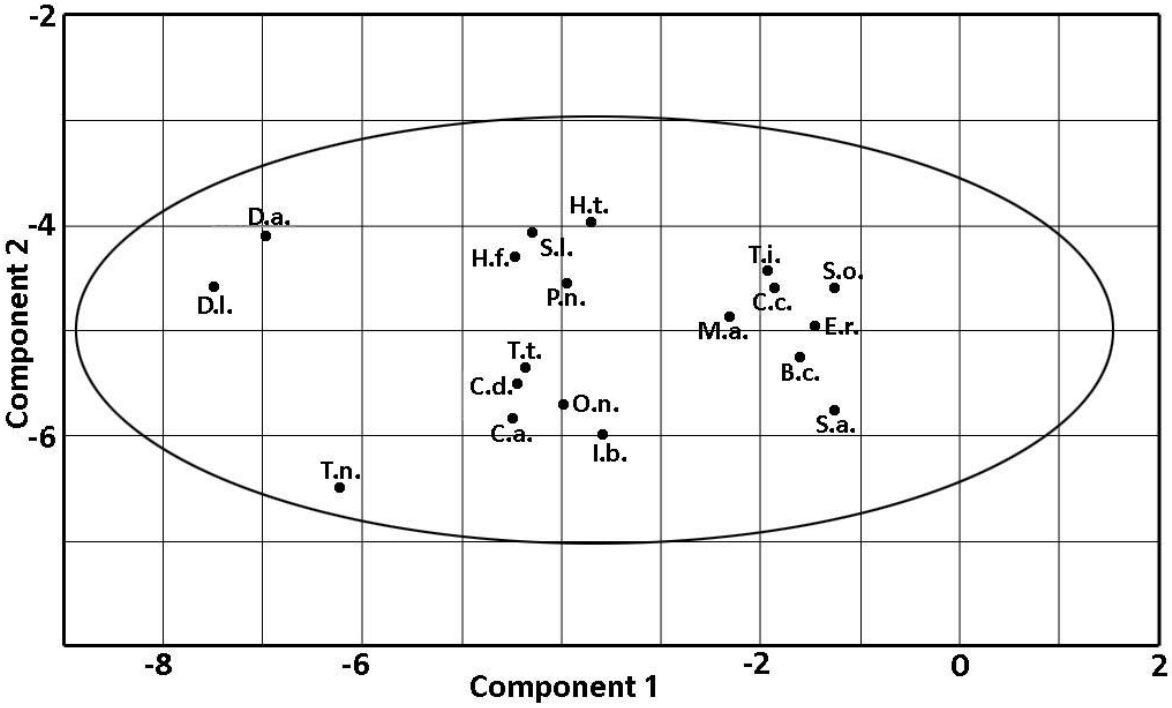

Fig. 5.20: *Resulting scatter plot of the Principal Component Analysis of all long bone ratios of several ornithopods and some other ornithischians within a 95% ellipse. The first principal component is dominated by the ratios of both the humerus and radius to the third metacarpal (Eigenvalue = 3.552; variance = 82.183%). The second principal component describes the influence of the relative length of the third metatarsal onto the distribution (Eigenvalue = 0.538; variance = 12.437%). Note the close proximity of all hadrosaurs to each other and to* Mantellisaurus*, whereas* Iguanodon bernissartensis *is more closely related to* Ouranosaurus *and all more primitive and at least facultative quadruped basal iguanodontians. Four taxa, where each is a basal member of its respective clade, are also plotting closely together. All used sources, specimens, values, and ratios are noted in Appendix V.* ***Abbr.:*** *B.c.* – Brachylophosaurus canadensis. *C.a.* – Camptosaurus aphanoecetes. *C.c.* – Corythosaurus casuarius. *C.d.* – Camptosaurus dispar. *D.a.* – Dryosaurus altus. *D.l.* – Dysalotosaurus lettowvorbecki. *E.r.* – Edmontosaurus regalis. *H.f.* – Hypsilophodon foxii. *H.t.* – Heterodontosaurus tucki. *I.b.* – Iguanodon bernissartensis. *M.a.* – Mantellisaurus atherfieldensis. *O.n.* – Ouranosaurus nigeriensis. *P.n.* – Psittacosaurus neimongoliensis. *S.a.* – Saurolophus angustirostris. *S.l.* – Scutellosaurus lawleri. *S.o.* – Saurolophus osborni. *T.i.* – Tethyshadros insularis. *T.n.* – Thescelosaurus neglectus. *T.t.* – Tenontosaurus tilletti.

Ilium: As in *Dysalotosaurus*, the main body or blade of the ilium apparently becomes also relatively longer compared to the height in *Orodromeus* and probably *C. dispar* (Carpenter & Wilson,

2008; Scheetz, 1999). Especially in hadrosaurs, the taxonomic variation of the ilium seems to be high, but ontogenetic differences are, apart from increasing robustness and larger muscle attachment sites, almost absent (Brett-Surman & Wagner, 2007; Horner & Currie, 1994). The variation of the orientation of the preacetabular process in *Hypsilophodon* (Galton, 1974) seems definitely not to have an ontogenetic origin (see measurements of ilia in Galton, 1974:tab. II). The increasing space of the acetabulum in the ilium of *Dysalotosaurus* resulted in more space for the femoral head (Fig. 5.10C, E). Unfortunately, this cannot securely be checked in other ornithopods at the moment.

Ischium: The increasing robustness of the blade and peduncles of this element were expected, but far more interesting is the medial migration of the depression at the neck of the iliac peduncle, the deepening of the acetabular fenestra (Fig. 5.11), and the slight proximal migration of the obturator process. The first ontogenetic changes are obviously linked to the increasing size of the femoral head (see below), which indicates strongly pronounced ossification of the latter. This change is clearly linked to deal with stronger forces acting on this structure in larger individuals during locomotion. It is of course not quite comparable to the situation seen in the thyreophorans *Euoplocephalus* and *Stegosaurus*, but the more spherical and more clearly delimited femoral head in large individuals of these taxa compared to their juveniles (Coombs, 1986; Galton, 1982) looks similar to the ontogenetic changes seen in *Dysalotosaurus*. No significant ontogenetic differences are visible between the two known ischia of *Dryosaurus* (Galton, 1981:figs. 10A, E), where the specimen of AMNH834 corresponds approximately to a large, medium-sized *Dysalotosaurus* individual and the holotype YPM1876 corresponds to the largest known *Dysalotosaurus* individuals (derived from femur lengths; Galton, 1981:tab. 2 and own measurements). Thus, the very shallow acetabular depression between the poorly separated peduncles in *Dryosaurus* does not have an ontogenetic reason and can therefore be treated as a clear taxonomic difference between both dryosaurids.

Femur: The deepening of the anterior intercondylar groove indicates either a thickening of the patella tendon (consisting of the united tendons of M. iliotibialis, M. ambiens, and Mm. femorotibiales) or a better fixation or guidance of this important knee extensor. This is probably a response to increasing body weight and size (Fig. 5.12B-D).

The prominence or distinction of the medial depression for the M. caudofemoralis longus varies independently of size in *Hypsilophodon* (Galton 1974). This is in contrast to *Dysalotosaurus*, in which the ontogenetic change of this depression is clearly size-related. However, within the tendency of decreasing prominence of this depression, especially of its anterior border, the intraspecific variation is too high to make founded interpretations on the reasons for this ontogenetic change. Moreover, taphonomic distortion of this region is rather abundant and complicates secured statements. Apart from that, one can definitely eliminate the insertion of the M. puboischiofemoralis internus (Norman, 1986:348-349). In most femora of all sizes, the inferred main direction of the inserting muscle is posterodorsal by varying angles, which is especially well visible in the specimens R6861 and MB.R.2517 (Fig. 5.12A) for instance. Although I have found a similar condition in the large femur MB.R.2511 (Fig. 5.12E) as described by Norman (1986), a shift of the direction of the inserting muscle from posterodorsal to anterodorsal is very unlikely and should treated as the result of intraspecific variation and general weak prominence of the edges of this depression in large femora.

The absence of the distal migration of the 4th trochanter (in contrast to *Alligator* [Dodson, 1975] and *Zalmoxes* [Weishampel et al., 2003]), the rather negative allometry of the height of its base, and the almost isometric growth and position of the medial depression indicates the relative constancy of the strength and lever arm of the M. caudofemoralis of *Dysalotosaurus* (see also chapter 5.5.5). Furthermore, the slight indication of an increase in the anteroposterior dimensions within the proximal and distal shaft compared to the respective mediolateral dimensions would be the opposite pattern seen in other dinosaurs (e.g. Bonnan, 2004:465; Carrano, 2001) and highlights the possibility that increased eccentricity in the femur takes only place in very large species. The bended femoral shaft in small cursorial dinosaurs, such as *Dysalotosaurus*, which differs significantly

from the straight shaft in large graviportal dinosaurs, may have played an important role for this differing morphology.

As noted above, the femoral head increases very strongly compared to most of the other measurements. This fits very well to the ontogenetically increasing size of the acetabulum indicated by the respective increasing dimensions in the ilium and ischium. Thus, the femoral head experienced above-average ossification, because it was the location of strong impact of stress during locomotion. Such large and separated femoral heads are typical for obligate bipedal dinosaurs (see e.g. Brochu, 2003:fig. 95; Chure, 2000:fig.145; Currie & Peng, 1993:fig. 1a; Galton, 1974:fig. 54) and are much more pronounced compared to obligate quadruped dinosaurs, although these animals also experienced a slight increase in pronouncement and separation of the femoral head during growth (Coombs, 1986; Galton, 1982).

The lesser trochanter becomes more prominent in *Dysalotosaurus* during ontogeny, which was also observed in *Zalmoxes* (Weishampel et al., 2003), but there is no sign of a closer approximation or even a tendency of fusion of it to the greater trochanter as in *Stegosaurus* (Galton, 1982), *Protoceratops* (Brown & Schlaikjer, 1940) and some hadrosaurs (Brett-Surman & Wagner, 2007; Godefroit et al., 1998). However, there is significant variation in the fusional degree between both trochanters among hadrosaur species during growth and sometimes even between the left and right side of a single individual (Brett-Surman & Wagner, 2007; Horner et al., 2004), so that a clear ontogenetic signal is not visible in this group. Hadrosaurs are also not well comparable to *Dysalotosaurus*, because at least one distinct muscle scar on the femur decreases its extension and the femoral shaft becomes less robust during growth. This is probably the result of an ontogenetic change from bipedality to facultative quadrupedality in hadrosaurs (Dilkes, 2001) and of the much more extensive cartilage caps on the articular ends in hadrosaur juveniles (Horner & Currie, 1994). This further highlights the possible differences in breeding strategy between both taxa (Horner & Weishampel, 1988; Horner et al., 2001; chapter 6.7.3).

Tibia: The most significant ontogenetic changes of the tibia are the much more robust cnemial crest (Fig. 5.13B-C), the extended base of the lateral proximal condyle, and the increasing articulation with the calcaneum at the expense of the articulation with the astragalus. The increasing robustness/thickness of the cnemial crest is also described for *Zalmoxes* (Weishampel et al., 2003) and hadrosaurs (Brett-Surman & Wagner, 2007). As in the femur, the latter show rather negative allometry of the shaft thickness resulting in less robust tibiae in adult individuals. This is also explained by larger cartilage caps on the poorly ossified articular ends in very young individuals (Horner & Currie, 1994) and by the shift from mainly bipedality in juveniles to mainly quadrupedality in adults (Dilkes, 2001). The consequences of a shift within the articulating surfaces for the proximal tarsals (more calcaneum, less astragalus) is currently unknown, but could probably related to a firmer articulation within the tibiotarsal complex.

Fibula: As in the tibia, the anterior thickness of the proximal end increases most compared to the other measured distances (Fig. 5.14C-D). It opposes the important cnemial crest of the tibia and therefore participates in providing extensive attachment sites for muscles and tendons. No other observation could be made and obvious ontogenetic trends in other ornithopods are not described or known.

Proximal tarsals: Apart from the observed increased ossification and larger and more robust muscle attachment sites, the remarkable lateromedial expansion of the calcaneum and the lateromedial shortening of the astragalus is the main ontogenetic change in the proximal tarsals. One possible explanation is the strengthening of the whole tibiotarsal complex due to increasing body weight during growth. The increasing internal depth and posterior height of the astragalus is indeed a sign of increasing overlap with the tibia. A similar lateromedial widening was found in the calcaneum of *Orodromeus* (Scheetz, 1999:tab. 1), which indicates a wider taxonomic distribution of this ontogenetic pattern. It is maybe just rarely recognized or described. The fusion of the proximal

tarsals to each other and to the fibula and tibia, as in thyreophorans (Coombs, 1986; Galton, 1982) or theropods (e.g. Raath, 1990), is never achieved, although almost fused proximal tarsals were observed in *Orodromeus* (Scheetz, 1999:tab. 1).

Metatarsals: All three elements show the expansion of most of the lateromedial dimensions compared to the anteroposterior dimensions (mt II less than the other two). Among most of the long bones, all three metatarsals even experienced the strongest increase in shaft robustness, especially in lateromedial direction, which implicates a significant higher compactness and connection within the metatarsus. Undoubtedly, this is also related to bear higher stresses during locomotion initiated by larger body mass during growth. The slightly indicated increase of the medial distal condyle of mt III compared to its lateral counterpart was also observed in *Orodromeus* (Scheetz, 1999:72). However, Scheetz (1999:93) mentioned wider mediolateral proximal dimensions compared to the anteroposterior direction in mt IV in a very young *Orodromeus*, which would reveal an opposite trend compared to *Dysalotosaurus*. Hadrosaurs experienced also an opposing trend. As in the other long bones of the hind limb, their metatarsals become less robust and elongated during growth, which was the result of strongly increasing ossification of the articular ends (Horner & Currie, 1994) and of the development of a weight supporting heel pad, which would strongly absorb a large amount of stress otherwise acting on the metatarsals (Dilkes, 2001). The opposing development of metatarsals during growth in *Dysalotosaurus* and hadrosaurs probably also mirrors the development from a digitigrade foot posture of the former to a sub-unguligrade foot posture in the latter (Moreno et al., 2007).

Phalanges: Combining the results of ontogenetic change in all examined phalanges, the relative length of the toes (the whole foot together with the metatarsals) seems to decrease in *Dysalotosaurus* during growth. Interestingly, small extant birds also have relatively longer feet than larger taxa (Gatesy & Biewener, 1991). The other ontogenetic tendencies are strongly influenced by

the position of the phalanges within the foot, because the toes have different total lengths, the phalanges have different fractional lengths, the proximal end of the toes begin at different relative positions (the third toe starts more distally than the others due to the longer mt III), and the number of phalanges increases from the second to the fourth toe. Nevertheless, some cautious ontogenetic tendencies can be verified. The dorsal condyle facet of the phalanges of the second toe increase stronger during growth than in the phalanges of the other toes, which indicate stronger extension of its phalanges compared to the others to compensate its shortness and low number of phalanges. On the other hand, the second toe can be less strongly flexed than the other toes in larger individuals for the same reasons. A further difference between the second toe and the others is the completely constant (though often statistically insignificant) relative increase of medial distances compared to its lateral counterparts. This regards the medial overall length (a_2), the medial shaft height (a_9), and the medial condyle height (a_{12}). The results of the other toes are either inconsistent or show rather isometric growth of both sides. Thus, the phalanges of the second toe become less curved medially and are more capable to bear stresses on their medial side, which is probably related to the medially located centre of mass. In addition, the medial condyles of the phalanges of the other toes are already higher than the lateral condyles in juveniles, especially in the fourth toe. The centre of pressure is aligned along the third toe (Moreno et al., 2007:60), which is confirmed by the isometric growth of both sides of the shaft and condyles within this toe in *Dysalotosaurus*. Another relatively constant tendency is the increase of the ventral condyle width (a_7), which is only negative to the dorsal width (a_6) in the fourth toe, whereas it is mainly the opposite tendency in the other toes. Together with the consistently more pronounced condyles in the fourth toe, this is most likely the result of the much better flexibility of its phalanges, mainly because of their higher number. This is probably the same situation as in *Hypsilophodon* (Galton, 1974) and *Allosaurus* (see Moreno et al., 2007:fig. 9C, D) and confirms a similar degree of digitigrade feet in *Dysalotosaurus*, and a higher degree as in *Camptosaurus*. This is also visible by the much more slender phalanges of *Dysalotosaurus*, which are also not as nearly as short distally as in *Camptosaurus* (Gilmore, 1909).

5.5.4 Evolutionary implications

Some of the ontogenetic changes found in *Dysalotosaurus* are like small windows into the evolution of ornithopods, because its small-scaled changes during growth can be found as large-scaled evolutionary tendencies within the whole group. The effect of heterochrony is obvious in some cases and reveals its importance in dinosaur evolution in general (Long & McNamara, 1997; Weishampel & Horner, 1994). Keeping in mind the morphologies of e.g. *Hypsilophodon* or *Orodromeus* as the primitive members (Galton, 1974; 1980; Scheetz, 1999) and hadrosaurs as the most derived members of ornithopods (e.g. Brett-Surman & Wagner, 2007; Horner et al., 2004), characters representing heterochronic tendencies are: the enlargement of the posterior part of the coracoid, the anteroventral migration of the foramen supracoracoideum, the distal migration of the deltopectoral crest of the humerus, the heightening of the olecranon process of the ulna, the development of a longer and lower iliac main body, the slight proximal migration of the obturator process of the ischium, the enlargement of the femoral head compared to the greater trochanter, the deepening of the intercondylar extensor groove of the femur, the more equal dimensions (dorsal or ventral view) of the astragalus, and the relative shortening of the metatarsals and phalanges. All of these ontogenetic changes are clearly of peramorphic character, as was also the case for the ontogenetic characters in the skull of *Dysalotosaurus* (see chapter 4; Hübner & Rauhut, 2010).

However, simple peramorphosis would predict later onset of maturity in hadrosaurs (Long & McNamara, 1997), but this is definitely not the case. In contrary, hadrosaurs obviously show highly accelerated growth with earlier onset of maturity (e.g. Cooper et al., 2008; Horner et al., 2000; see also chapter 6.8) and juveniles have often already similar morphologies than adults (Brett-Surman & Wagner, 2007; Horner & Currie, 1994), so that predisplacement of the mentioned ontogenetic characters is rather likely.

Other ontogenetic characters reveal that the process of ornithopod evolution was not that simple. At least two characters, the expansion of the distal scapular blade and the anterior pronouncement of the deltopectoral crest on the humerus, are obviously of paedomorphic type within basal iguanodontians. *Hypsilophodon* and *Orodromeus* show the primitive condition with the typical distally flaring scapular blade and a rather short but anteriorly high and pointed deltopectoral crest (Galton, 1980; Scheetz, 1999). This condition is still retained in *Gasparinisaura* (Coria & Salgado, 1996:fig. 6). The distal flaring of the scapular blade (especially the ventral part) is retained in all successive taxa up to *Camptosaurus* (see e.g. Carpenter & Wilson, 2008; Coria & Calvo, 2002; Forster, 1990a; Galton, 1981; Novas et al., 2004; Weishampel et al., 2003:fig. 19C) and is altered to a dorsally and ventrally expanding extension of the scapular shaft with mostly straight margins and a rectangular distal end initially within Styracosterna (see e.g. Brett-Surman & Wagner, 2007; Godefroit et al., 1998; Norman, 1980; 1986; 1998; 2002; Taquet, 1976).

The deltopectoral crest of the humerus, in contrast, is altered more often and phylogenetically much earlier. The crest is reduced to a low but robust prominence or ridge in *Notohypsilophodon*, *Thescelosaurus*, *Anabisetia*, *Talenkauen*, *Dysalotosaurus*, *Dryosaurus*, and *Camptosaurus aphanoecetes* (e.g. Carpenter & Wilson, 2008; Coria & Calvo, 2002; Galton, 1981; Martinez, 1998; Novas et al., 2004; Sternberg, 1940). Although the more sigmoidal curvature of the humerus is notable in more derived iguanodontians, the deltopectoral crest is still relatively weakly prominent, such as in *Mantellisaurus*, *Ouranosaurus*, and *Probactrosaurus* (Norman, 1986; 2002; Taquet, 1976). The almost primitive condition with a anteriorly pointed crest is known in Zalmoxes (Weishampel et al., 2003), but a new and more developed crest type with a more quadrangular shape, and forming a more acute angle to the shaft, was independently developed at least three times within Ornithopoda, such as in *Tenontosaurus*, *Camptosaurus dispar*, and Euhadrosauria (Carpenter & Wilson, 2008; Forster, 1990a; Prieto-Marquez, 2008:fig. 2.15). The dominance of the anterior projection of the deltopectoral crest in basal ornithopods was therefore broken by paedomorphosis in several more derived *Hypsilophodon*-like ornithopods and basal iguanodontians

and was reactivated in at least three independent ornithopod lineages by peramorphosis, although the distal migration of the crest was now dominant over the anterior projection. The evolution towards at least intermediate graviportal and quadruped locomotion (e.g. Carpenter & Wilson, 2008; Carrano, 1999; Dilkes, 2001; Norman, 1980) seems to be the main reason for these tendencies.

The shape of the coracoid is another example for the high variability of heterochronic effects within Ornithopoda, because there is more than one tendency included and these trends are heterogeneously distributed within this group. *Dysalotosaurus* possesses the typical half moon-shaped outline with a moderate sternal hook as in *Hypsilophodon* (Galton, 1974; 1981). It is, nevertheless, ambiguous to determine a 'primitive' condition within Ornithopoda (sensu Butler et al., 2008b), because *Orodromeus* has a dorsoventrally much wider coracoid (Scheetz, 1999:fig. 20). Such an almost circular shape is known from at least three different lineages including *Orodromeus*, *Tenontosaurus*, and *Bactrosaurus* (Forster, 1990a; Godefroit et al., 1998; Scheetz, 1999). Coracoid shapes roughly similar to *Dysalotosaurus* are of course known from *Hypsilophodon*, *Thescelosaurus*, *Dryosaurus*, *Mantellisaurus*, and *Ouranosaurus* (Galton, 1974; 1981; Gilmore, 1915; Norman, 1986; Taquet, 1976). The sternal hook is more prominent in *Gasparinisaura*, *Anabisetia*, *Tenontosaurus*, and *Iguanodon bernissartensis* (Coria & Calvo, 2002; Coria & Salgado, 1996; Forster, 1990a; Norman, 1980), which can be unambiguously explained by peramorphosis. This is expressed to an extreme in *Zalmoxes shqiperorum* (Weishampel et al., 2003) and most hadrosaurs (e.g. Brett-Surman & Wagner, 2007; Horner et al., 2004; Prieto-Marquez, 2008:fig. H6).

The development of the main body of the coracoid is a different story. *Dysalotosaurus* is one of the few ornithopods, where the coracoid has an extended anterior corner, so that the bone is distinctly longer than high even without a prominent sternal hook (Fig. 5.5). Compared to less derived ornithopods, this is a peramorphic character, which is retained to a lesser degree in *Mantellisaurus* and *Ouranosaurus*. The coracoid main body of most hadrosaurs is, in contrast, strongly reduced, which demonstrates neoteny for this part and pure dominance of the peramorphic sternal hook. *Camptosaurus* is another unique example regarding the shape of its coracoid, because

it maintains a rather quadrangular shape throughout ontogeny (see Carpenter & Wilson, 2008; Chure et al., 1994). The coracoid of the juvenile *C. dispar* (USNM2210) is similar to the juvenile coracoid of *Dysalotosaurus*, but *Camptosaurus* maintains this shape or even possesses a more quadrangular shape. It is not clear, if this represents true neoteny (Long & McNamara, 1997), but strong paedomorphosis for the coracoid of *Camptosaurus* is definitely proofed.

According to Webster & Zelditch (2005), heterochrony is just one type of modification of ontogeny throughout phylogeny, consisting of the modification of rate or timing of morphological development. A non-heterochronic modification within Ornithopoda is probably represented by the relative position of the 4th trochanter on the femoral shaft. In *Dysalotosaurus*, a distal shift of this process, as in *Alligator* (Dodson, 1975b) is unknown. In *Maiasaura*, a distinct height-increase of the base of this trochanter is observed, but there is also no sign of a distal migration. The distal migration of the 4th trochanter in other ornithopods is also not described (apart from Zalmoxes; Weishampel et al., 2003). Nonetheless, *Hypsilophodon*, *Orodromeus*, and *Gasparinisaura* are taxa showing a very proximal position of the 4th trochanter (see Coria & Salgado, 1996; Galton, 1974; Scheetz, 1999). *Parksosaurus*, *Anabisetia*, and both Dryosaurids are examples of a less proximal position (see Coria & Calvo, 2002; Galton, 1981; Hohloch, 2003:72; Janensch, 1955; Parks, 1926). Nearly all larger ornithopods including *Thescelosaurus*, *Tenontosaurus*, *Zalmoxes*, and Ankylopollexia have a 4th trochanter close to the midshaft (see e.g. Forster, 1990a; Norman, 2004; Norman et al., 2004; Sternberg, 1940; Weishampel et al., 2003). Assuming that nearly all ornithopods lack a significant distal migration of this process, heterotopy could be used as a modification pattern for the ontogeny of this process, because it modifies the location of a morphological feature without ontogenetically expressed intermediate steps (Webster & Zelditch, 2005). In addition, such a large process cannot migrate significant distances throughout ontogeny due to the need of rather constant muscle arrangements for an elevated style of locomotion, as in ornithopods. Gene mutation seems to be a better possibility to adjust the lever arm of the attaching muscles.

All the presented examples of modification of ontogeny during ornithopod evolution are united by two implications. First, the evolution of ornithopods is far more complicated as one would suggest by a first glance on their postcranial anatomy. The ornithopod skull, often the much more attended skeletal part, is not the only structure, which has experienced numerous modifications. First attempts have been made to reveal ontogenetic modifications as one factor for diversity, but event-pairing for instance (see Guenther, 2009) apparently cannot be used in all ornithopods. In *Dysalotosaurus*, modifications include larger, longer, deeper, wider structures in sometimes changing locations, but absence-presence events necessary for event-pairing are unknown.

Second, the preservation of different ontogenetic stages is very good in comparison to other dinosaur groups (e.g. Weishampel & Horner, 1994; Guenther, 2009), but there are still too few detailed studies on ontogenetic changes, especially of the postcranium. A central aim for the future should therefore be the description of these changes, because nearly every ornithopod clade has at least one taxon with a good ontogenetic record (e.g. Carpenter & Wilson, 2008; Coria & Salgado, 1996; Dilkes, 2001; Forster, 1990a; Galton, 1974; 1980; Godefroit et al., 1998; Horner & Currie, 1994; Horner et al., 2000; Kirkland, 1998; Salgado et al., 1997; Scheetz, 1999; Werning, 2005).

5.5.5 Notes on body posture and locomotion

In 1993, Heinrich et al. proposed an ontogenetic shift in body posture in *Dysalotosaurus* from quadrupedality in early juveniles (up to 150mm femur length) to bipedality in medium sized individuals (from 180mm femur length on). The significant increase of femoral bone wall thickness and maximum bending strength between these size classes was interpreted as reaction on the posterior migration of the centre of mass during growth from a position well anterior from the acetabulum in small individuals (due to their assumed relatively large head) to a position closer to the acetabulum in medium sized animals. The obviously rather abrupt increase of bending stress on the femur was then interpreted as reaction on the bipedal body posture in medium sized individuals,

while the centre of mass was still further anterior to the acetabulum. The reduction of loadings on the femur in large sized individuals, indicated by a slight decrease of relative amount of bone in the cortex and bending strength respectively, was explained by the arrival of the centre of mass at the neutral point close to the acetabulum.

Two assumptions were made by Heinrich et al. (1993) to justify their hypothesis: (1) *Dysalotosaurus* hatchlings/early juveniles had a comparatively large head compared to the body. This assumption was already challenged by Dilkes (2001), who pointed out that the skull of an early juvenile specimen of the closely related *Dryosaurus* (Carpenter, 1994) was not as nearly as large and that this would be probably also the case for *Dysalotosaurus*. A position of the centre of mass significantly anterior to the acetabulum is therefore rather unlikely. (2) The shift to bipedality should have taken place during the first months of life assuming growth rates somewhere between precocial and altricial birds. Using the data derived from the histological study (see chapter 6:Tab. 1), the calculated age for a 150mm long femur would be approximately 4.8 years and for a 180mm long femur approximately 6.8 years of age. The calculated growth rates during these years of life (not maximum rates!) are also rather close to the reptilian growth rates calculated by Heinrich et al. (1993:tab. 8) and far lower than their assumed bird-like growth rates. Thus, as these authors already noted, the abrupt changing pattern in the femora are indeed rather a classification artifact, because there are several years of time before and at least two years duration of the proposed postural transition.

Several additional observations further strengthen the doubt on a possible quadruped-biped transition. The feet of small individuals of *Dysalotosaurus*, for instance, are relatively longer than in large ones. Foot length, however, has influence on stability and duty factor during locomotion (Biewener, 1983; Gatesy & Biewener, 1991). As in small mammals and birds, relatively longer feet would increase the stability during walking and running, because relatively more ground support is given during each stride. A slightly anterior position of the centre of mass would therefore be

equalized by the longer feet in juveniles of *Dysalotosaurus*. Longer feet would also increase the duty factor, which in turn would reduce compressive and bending stresses on the bones (Biewener, 1983).

Furthermore, it is also possible that limb orientation was slightly changing in *Dysalotosaurus* during ontogeny. The limbs of small birds and mammals are more flexed and the femur is held less vertical than in larger taxa (e.g. Bertram & Biewener, 1992; Biewener, 1983; 1989; Gatesy & Biewener, 1991) resulting in a more crouched limb posture. As dinosaurs have similar scaling patterns as mammals (Carrano, 2001), it can be assumed that small dinosaurs would also have possessed a more crouched limb posture (also a more horizontal posture of the femur, but of course not nearly to such an extent as in birds) than large taxa (Carrano, 1998; Farke & Alicea, 2009). Similar variation can therefore be assumed between small and large individuals of *Dysalotosaurus*. A more crouched limb posture results in higher limb compliance and running stability, and the more horizontal femur would also help to get the feet even under a more anterior located centre of mass (Gatesy & Biewener, 1991). Thus, assuming that small *Dysalotosaurus* individuals indeed had a more anterior position of the centre of mass, the possible more crouching posture of their hind limbs would compensate it. A quadruped body posture is therefore unnecessary.

Finally, a postural shift from quadrupedality in *Dysalotosaurus* juveniles to bipedality in adults would be highly unusual among dinosaurs in an evolutionary context and among ornithopods in an ontogenetic context. In each known case, dinosaurs become either secondarily quadruped from biped ancestors (e.g. Carrano, 2001) or changed from biped juveniles to at least facultative quadruped adults during ontogeny (Dilkes, 2001; Norman, 1980). In fact, the weak distal migration of the fourth trochanter of the *Dysalotosaurus* femur (if at all) and the mainly constant bending of its shaft during ontogeny implicate similar bending stresses in juveniles and adults and therefore no sign of a postural shift (see Carrano, 1999:40 and Dilkes, 2001:1221 for additional comments). It is even not secured, if cross sectional properties are of significant value for statements on body posture at all (Farke & Alicea, 2009). The highly variable bone microstructure in *Dysalotosaurus* during ontogeny, along the shaft, and even within single femoral cross sections (see chapter 6) may also have

contributed to the variation of cross-sectional properties and possible resulting biomechanical consequences (Currey, 1984).

In addition, the increasing robustness of the long bones and phalanges in *Dysalotosaurus* during growth indicates that the juveniles were even more cursorial than the adults due to more slender and lightly built limbs. Even the adults of *Dysalotosaurus* have fulfilled all preconditions to be cursorial (see Carrano, 1999), such as the femur-tibia ratio (Galton, 1981:tab. 5; Janensch, 1955:169: fig. 40), the proximal position of the fourth trochanter on the femoral shaft, and relatively long metatarsals (Galton, 1981:tab. 5). It is also noteworthy that *Dysalotosaurus* and *Dryosaurus* have obviously a very low fore-limb/hind-limb ratio compared to many other ornithischians, which is mainly based on the reduced metacarpals of *D. altus* and on the comparatively long metatarsals (see Appendix V) in both taxa. Pompeckj (1920) described the hand of *Dysalotosaurus* in his diagnosis as weak and strongly reduced. It is therefore very likely that it was similar to the reduced hand of *D. altus*. A Principal Component Analysis (PCA), carried out from these and other long bone ratios of several ornithopods and a number of other small ornithischians (Fig. 5.20) shows that the ratios containing the relative lengths of metacarpal III and metatarsal III, respectively, are on the one hand probably unique for dryosaurids and are on the other hand strong indicators for bipedality in both taxa. Thus, as the adults of *Dysalotosaurus*, the probably even more cursorial juveniles were undoubtedly also bipedal.

In the end, the falsification of two basic assumptions of Heinrich et al. (1993), ontogenetic changes as well as constancies within the hind limb of *Dysalotosaurus*, several of its limb ratios, and the assumed higher cursoriality in juveniles suggests that the hypothesis of a postural shift from quadrupedality to bipedality during growth in this taxon should be rejected. *Dysalotosaurus* was therefore a cursorial biped throughout life.

5.6 Conclusions

In several aspects, *Dysalotosaurus* is the ideal intermediate model between small and large ornithopods as well as between basal ornithopods and ankylopollexians. The rarity of articulated specimens mostly prevented the usage of ratios for a comparison with other taxa, but the preserved extensive growth series of many postcranial elements has allowed the investigation of ontogenetic changes by using size-independent methods and criteria. The most important and most comprehensive method was the application of bivariate allometry, but qualitative observations, suture closure, and surface textures were also very helpful.

Two lines of evidence let conclude that *Dysalotosaurus* experienced an indeterminate growth pattern. First, even the largest presacral and sacral vertebrae show only incomplete fusion of their neurocentral sutures, if at all. Second, bone surface texture does not show any significant differences between large and small long bones, which is similar to *Alligator* (indeterminate growth), but different to *Branta*, centrosaurine ceratopsians, and pterosaurs (determinate growth).

As in *Hypsilophodon*, the sequence of neurocentral suture closure is from back to front in *Dysalotosaurus*. The sequences are not well known among dinosaurs though, and more studies are necessary to dissolve the often significant differences between some groups. However, the anterior-posterior fusion sequence known in some theropods, sauropods, and maybe ceratopsians, should be treated as an additional sequence and not as a substitute of the plesiomorphic posterior-anterior sequence.

Numerous ontogenetic changes were found in the elements of *Dysalotosaurus*. Many of them are common among dinosaurs and were expected, such as increasing robustness of sutural surfaces, muscle attachment sites, and articular ends. These are mainly a function of increasing body size and weight. The well ossified articular ends and presence of all important processes in the smallest long bones has revealed the possible precocial behavior of the juveniles.

The modification of time and/or rate of ontogenetic change (heterochrony) are important factors of ornithopod evolution, but the dominance of peramorphic changes are only one part of the

whole story. Single elements can be deformed by different modifications with different rates, and other modification patterns, such as heterotopy, are also possible. More data about ontogenetic changes in ornithopods are needed to get better insight in the surprisingly diverse morphological evolution of this group.

Finally, the two basic assumptions for a quadrupedal gait in small juveniles of *Dysalotosaurus*, a large juvenile skull and a short time span for the quadrupedal-bipedal shift, are disproved. Further facts, such as longer feet in juveniles, the constant bending of the femoral shaft as well as the almost constant position of the fourth trochanter, and the higher degree of cursoriality of the juveniles, let also suggest that *Dysalotosaurus* was indeed a lifelong biped animal.

6. Bone histology in *Dysalotosaurus lettowvorbecki*

6.1 Introduction

Ever since scientists worked with the remains of extinct animals, which do not have direct living descendants, it was the dream to reconstruct their life history and, at least partially, social structures and behavior. Unfortunately, it is almost impossible to obtain such fundamental information with morphological and/or statistical methods only, because absolute dates, such as age or time of maturity of single individuals, are not determinable. Size classes in a bonebed of a single species, surface texture of bones, or degree of suture closure are examples for often used tools for estimate relative age and ontogenetic status of a fossil animal, but there is always a large amount of uncertainty (e.g. Lehman, 2007; Sampson et al., 1997; Turmarkin-Deratzian, 2003). Bone histology enables the palaeontologist to partially fill this gap, because the insight into the tissue structure of an individual can provide the needed absolute data in many cases. In combination with morphological, taphonomical, and statistical data, it is possible to get a much better established and higher significant view on the life history and sometimes even on social structure and behavior of extinct species.

The following chapters deal with chances and problems by using bone histology for the reconstruction of life history parameters of extinct animals, give a short overview on the histological research in dinosaurs, and presents results and implications of the histological study of the bones of *Dysalotosaurus*.

6.2 General structure and organization of bone

In this chapter, all terms and structures of bone histology are shortly introduced, which are relevant for this study. A more complete introduction into all important aspects of bone histology is

published by Francillon-Vieillot et al. (1990), Castanet et al. (1993), Ricqles et al., 1991, and Chinsamy-Turan (2005). However, it should always be kept in mind that there is strong variability in all of the following aspects of bone organization, structures, and tissue types. Thus, it is possible to find different types of bone tissue in different elements of a skeleton, in different parts of a single bone, or even in a single cross section (Chinsamy-Turan, 2005), depending on local growth rate, ontogenetic stage, mechanical stress, and so on.

6.2.1 Spatial differentiation of bones, bone areas, and ossification types

In this study, only long and flat bones are used for histological sectioning. According to the definition of Francillon-Vieillot et al. (1990), long bones are cylindrical and elongated along a major axis and are represented mainly by the limb bones of tetrapods. Flat bones grow along a single plane or curved surface and are represented by the bones of the limb girdle, vertebral processes, and the dermal bones of the skull.

Long bones are further divided along the major axis in epiphysis, metaphysis, and diaphysis. The epiphyses represent both ends of a long bone and are the locations of growth in length. It is important to note that the uncalcified cartilage of the epiphysis is almost always not preserved in fossil bone, so that the term ‘epiphysis’ in palaeontology comprehends only the calcified cartilage at its end (e.g. Chinsamy-Turan, 2005:46; Schwarz et al., 2007). Metaphyses are the intermediate area between the epiphyses and the diaphysis and are characterized by the reduction of bone thickness to maintain the overall shape during growth. The diaphyses are located at midshaft, where the bone growths only in diameter. Long bones often possess a marrow cavity inside the shaft, which is surrounded by a wall or cortex of compact bone. Flat bones lack such a free cavity. Instead, a highly porous network of trabeculae, called cancellous or spongy bone, is sandwiched between the two opposite walls of compact bone (Francillon-Vieillot et al., 1990).

This bone structure is also present in long bones. Here, the cancellous bone dominates within the epiphyses. To increase bone length, the actively growing cartilage of the epiphyseal ends transforms into calcified cartilage, and this is successively substituted by the trabeculae of the cancellous bone. This process is known as endochondral ossification.

Further towards the centre of the long bone shaft, another kind of ossification dominates. A long bone also has to increase its thickness during growth and this is provided by apposition of compact bone onto the shafts outer surface, called periostal ossification. Schematically, layer after layer accumulates on the surface in such a way, that the periostal compact bone wall is the thickest at the diaphyseal level and decreases in thickness towards the ends of the long bone. At the metaphyseal level, the periostal ossification zone tapers and meets the perichondral surface of the epiphyses (encoche d'ossification; see Francillon-Vieillot et al., 1990). Thus, the metaphyses are a transitional zone between the endochondral epiphyses and the mainly periosteal diaphysis. In this area, a thin wall of compact bone encloses endochondral cancellous bone and, if at all present, a poorly differentiated marrow cavity.

A third kind of ossification can take place at the internal border of the compact bone wall of the long bone shaft and often encloses parts of the marrow cavity. Due to its spatial occurrence, it is called endosteal ossification. As long as external periosteal growth proceeds, the marrow cavity also increases its diameter by resorption of the internal border of the compact bone wall. When growth ceases, a band of dense endosteal bone accumulates around the marrow cavity and separates it from the periosteal compact bone wall. Another area for endosteal ossification is the metaphysis. During growth in length, the trabecular network of cancellous bone, formerly built in the epiphysis, migrates into the metaphysis. Here, the diameter of the bone is reduced by external bone resorption, because the overall shape of the bone has to be maintained. Endosteal bone now accumulates onto the trabeculae and reduces the spaces between them to stabilize the bone wall in the metaphysis (producing compact coarse cancellous bone tissue [CCCB]; Enlow, 1962). A third possibility for

endosteal ossification is the drift of the marrow cavity, where the compact bone wall is resorbed on one side of the cavity and endosteal bone accumulates on the other side (see also chapter 6.2.4).

6.2.2 Tissue structures and tissue types

Periosteal ossification is first afforded by bone cells, called osteoblasts. They produce collagenous fibrils, which are mineralized by hydroxyapatite thereafter. During this process, the osteoblasts become enclosed by the newly built bone matrix and are now called osteocytes, house in osteocyte lacunae and can communicate with each other by fine extensions enclosed in tubular canaliculi (Francillon-Vieillot et al., 1990). In fossil bone, osteocytes are often visible as numerous, dark spots in a moderate magnification.

The periosteal bone matrix itself can be divided into three main types, probably depending on growth rate (Amprino, 1947). Amongst other structures, the degree of fibrillar organization of the matrix is generally used as an indicator for growth rate (the higher the degree of organization the lower the growth rate).

Woven-fibered bone matrix (Faserknochen in German) consists of loosely packed and randomly oriented collagen fibers with numerous integrated, relatively large and often rounded osteocytes and very common vascular canals. This tissue type indicates relatively higher growth rates of the bone (e.g. Chinsamy-Turan, 2005; Francillon-Vieillot et al., 1990). Observed with a microscope under polarized light, woven-fibered matrix appears relatively dark and does not reflect the light consistently.

Lamellar bone matrix represents a completely different type of tissue. The collagen fibrils are strongly parallel in a single layer, called lamella, but the orientation differs between neighboring lamellae. Thus, there is a bright reflection under polarized light, but it appears alternately dark and light from lamella to lamella. The osteocyte lacunae are less abundant and often flattened along the lamellae. This type of matrix with its high degree of fibrillar organization indicates lower growth rates

compared to woven-fibered matrix and can be deposited as bone matrix or as infilling of primary and secondary osteons.

Parallel-fibered bone matrix is intermediate between the two former types in many aspects. As the name let assume, the collagen fibrils are generally parallel to each other, which results in completely light or dark reflection under polarized light. The osteocyte lacunae are flattened but randomly distributed (Francillon-Vieillot et al., 1990).

Further important formations in bone comprising vascular canals are primary osteons. These structures consist of bone lamellae deposited centripetally around a vascular canal. This process does not resorb previously built bone, but is integrated in the primarily accumulated bone matrix and is therefore called primary osteon. Thus, a periosteal bone tissue with primary osteons is also known as primary bone. Osteocyte lacunae, which are located within a primary osteon, are also centripetally oriented around the enclosed vascular canal and are often elongated and sandwiched between the lamellae of the primary infilling.

Primary osteons are most common in a woven-fibered matrix. The combination of this tissue with the lamellar infillings of the primary osteons leads to the widely used term fibrolamellar bone or complex (e.g. Chinsamy-Turan, 2005; Currey, 2002; Erickson, 2005; Francillon-Vieillot et al., 1990; Ricqles, 1976). The other main category (after Francillon-Vieillot et al., 1990), lamellar-zonal bone, is distinguished from fibrolamellar bone by its lamellar or parallel-fibered matrix, a lesser degree of vascularization (even absence of vascular canals is possible), and abundant zonation of the primary bone cortex. Intermediate stages are common, and the occurrence of both tissue types in a single bone is, depending on variations in growth rate, also possible. Resulting from their properties, lamellar-zonal bone indicates relatively lower growth rates than fibrolamellar bone (Amprino, 1947).

Another important structure in bone is the secondary osteon. Also known as Haversian system (see Francillon-Vieillot et al., 1990 for more details on misleading nomenclature concerning this structure), it also consists of lamellar bone, deposited centripetally around a canal, similar to primary osteons. In contrast to the latter, the lamellar infilling follows local resorption of primary

bone tissue. Thus, the lamellae of the secondary osteon are separated from the surrounding bone by a cement line and sharply cut into the former structures. It is also possible that a new generation of secondary osteons cut into osteons of a former generation. In dense haversian bone tissue, multiple generations of secondary osteons have superimposed each other and the former primary bone tissue can be completely obscured (see also chapter 6.2.4).

The last important structure, which has to be mentioned, are the Sharpey's fibers. These fibers or fiber bundles are mineralized extensions of the fibrillar attachment of muscles and tendons on the bone surface. They can be found deep in the cortex or close to the external bone surface and are easily recognized by dark thin lines under normal light and brightly reflecting areas under polarized light. Generally, Sharpey's fibers differ in orientation to the normal collagen fibrils of the bone tissue and are often oriented in a large angle to the bone surface (Currey, 2002:281). It is possible to reconstruct the former orientation of muscle and tendon forces by using these fibers. Sometimes, they are even used to reconstruct the orientation of unusual dermal plates (Buffrenil et al., 1986).

6.2.3 Patterns of vascularization

There are two main types to be distinguished, which are known as avascular/non-vascular and vascular compact bone tissue. The first type lacks any vascular canals, but it is important to note that this concerns only the periosteal bone wall and not occasionally present cancellous bone tissue. Avascular compact bone often occurs in tetrapods of very small adult body size or especially low overall growth rate and is apparently present in amphibians, reptiles, birds, and mammals (see e.g. Enlow & Brown, 1956; 1957; 1958). Avascular areas are sometimes also present in animals of larger adult body size or faster growth rate, especially when growth ceases (see chapter 6.2.5).

Vascular compact bone is more common, although the vascular density is highly variable among different tetrapods, different skeletal elements, or within single elements. Relative growth rate

seems to be the main reason for this variability (e.g. Amprino, 1947; Margerie et al., 2002; Padian et al., 2004).

Further differentiations of vascular compact bone are made by the arrangement and orientation of primary vascular canals and/or primary osteons. According to Francillon-Vieillot et al. (1990), vascular canals can be organized longitudinally (parallel to the long bone shaft), laminar (canals are arranged in circular rows in cross section), plexiform (radially oriented canals are added to the laminar pattern), radial (radially oriented canals clearly dominate), or reticular (irregular oriented canals). There is obviously no clear correlation of vascularization pattern and overall growth rate (e.g. Margerie et al., 2002; Starck & Chinsamy, 2002), although exceptions exist (Margerie et al., 2004). Similar as many of the other classifications of bone tissue types described above, two or more vascularization patterns can occur even within a single cross section of a bone.

6.2.4 Bone remodeling

Bone remodeling is a term dealing with the rearrangement and recombination of histological components (Enlow, 1962). A variety of remodeling processes combines thereby resorption of an area with apposition in another one, although it does not have to happen exactly at the time or in the same time span. There are three important processes of bone remodeling, which are significant for this study (see also chapter 6.2.1 and 7.2.2).

The first process is the relocation of the metaphysis during growth in length. Former epiphyseal areas migrate into the metaphysis, while new bone is produced close to the epiphyseal ends of the long bones. In the same manner, former metaphyseal areas migrate into the diaphysis. Despite these relocations, the bone has to maintain its overall shape. This happens by resorption of the external bone surface of the former epiphyseal area to achieve the smaller diameter of the metaphysis, where this area is now located. Certainly, the loss of external bone is compensated by apposition of endosteal bone into the internal cancellous bone. Simultaneously, metaphyseal area

migrating into the diaphysis experiences periosteal bone apposition and endosteal resorption, so that the compacted coarse cancellous bone (CCCB) of the metaphysis is successively covered by periosteal compact bone externally and resorbed by the marrow cavity internally. Intermediate stages of the metaphyseal-diaphyseal reorganization are often still observable in the shaft by sectioning a bit more distally or proximally from the diaphysis. Right inside the diaphysis, there is usually no compacted coarse cancellous bone of the metaphysis left (see sketches in Enlow, 1962).

The second process, which is often found in combination with the first one, is the lateral drift of the local axis of the bone to one side of its shaft. Especially curved long bones show this phenomenon, which is also clearly linked to maintain the overall shape of the bone. Additionally to the increase in diameter from the metaphysis to the diaphysis, the curvature of the shaft induces periostal apposition and endosteal resorption on the concave side of the shaft and periosteal resorption and endosteal apposition on the convex side of the shaft. Thus, in a cross section of such an area, one would schematically observe periosteal compact bone with a deeply cutting medullary cavity on the concave side of the shaft and a thin outer layer of periosteal compact bone combined with a thick internal part of endosteally compacted cancellous bone on the convex side of the shaft. Lateral drifting (or osseous drift; Enlow, 1962) is also the reason for the inclination of possible circumferential growth layers relative to the border of the medullary cavity. The latter has simply cut into these layers during lateral drift.

The third important remodeling process is mainly known as secondary remodeling. As the name suggests, secondary osteons are the driving force by resorption of primary compact bone and deposition into the resulting cavities. After intensive substitution, the primary compact bone can be completely remodeled by numerous generations of secondary osteons. Such secondary bone is also called Haversian bone tissue (Francillon-Vieillot et al., 1990). Animals, which are able to reach an age of multiple or even decades of years, are known to have extensive secondary remodeling (e.g. man, some other long living primates, numerous ungulates and dinosaurs etc.), where the intensity of secondary remodeling indicates relative age and is therefore also used for relative age estimation of

individuals (e.g. Horner et al., 2000; Klein & Sander, 2008; Mulhern & Ubelaker, 2003). Nevertheless, several other functional reasons of secondary remodeling, such as response to mechanical loading or healing of fractures, are discussed, especially due to interesting concentrations of clusters of secondary osteons close to insertions of muscles and tendons or inside of healing areas for instance (see e.g. Currey, 2002:368-377; Straight et al., 2009).

6.2.5 Growth patterns

Growth patterns can be divided into cyclical versus noncyclical growth and determinate versus indeterminate growth (Chinsamy-Turan, 2005; Francillon-Vieillot et al., 1990).

Cyclical growth is represented by a clear zonation of bone tissues in the periosteal compact bone, which is represented by an alternation of fast growing zones and slowly growing annuli and/or lines of arrested growth (Peabody, 1961). The fast growing zone can consist of either woven bone matrix, parallel-fibered, or even lamellar bone matrix, naturally depending on respective growth rate and ontogenetic stage. Here, vascular canals or primary osteons are usually much more abundant than in annuli or are even exclusively restricted to the fast growing zones. This part of a growth cycle is by far the widest, but the relative thickness can vary from cycle to cycle. In comparison, annuli are much narrower bands of parallel-fibered or lamellar bone matrix indicating much slower growth than the respective fast growing zone (Ricqles et al., 1991). Complete cessation of growth is marked by lines of arrested growth (LAG's). These lines, also known as resting lines (Klevezal, 1996), are hypermineralized and can be located within an annulus or at its external border (Castanet et al., 1993). There are also cases of cyclical bone, where either annuli or LAG's form the external border of a fast growing zone, respectively. At the end, one complete growth cycle consists of a fast growing zone and a completing annulus and/or LAG.

Another differentiation of growth pattern pertains determinate versus indeterminate growth. The former pattern describes animals, which build a zone of Outer Circumferential Layers

(OCL; see e.g. Chinsamy-Turan, 2005; Klevezal, 1996) at the external periphery of the periosteal compact bone wall. Another term for the very same structural pattern is External Fundamental System (EFS; e.g. Horner et al., 2000; Sander et al., 2006). OCL/EFS consists mostly of thin, poorly vascularized, or even avascular parallel-fibered or lamellar layers of bone matrix with numerous interruptions by LAG's and, thus, represent an obvious decline in growth rate. OCL/EFS is known mainly in mammals (Klevezal, 1996), birds (e.g. Ponton et al., 2004), and many dinosaurs (e.g. Chinsamy, 1990; Erickson et al., 2007). Indeterminate growth is, on the other hand, mainly known in amphibians and many reptiles (Enlow & Brown, 1956; 1957; Gross, 1934; Peabody, 1961; Ricqles, 1976) including some dinosaurs (e.g. Chinsamy, 1993). A decrease of the density of vascularization and/or thickness of growth zones are clear signs for a decreasing growth rate in these animals, but they grow throughout their life though. There is no sign of an asymptotic plateau of growth rate, as in animals with determinate growth pattern, but it is always possible that the studied individuals were not old enough (discussed in e.g. Horner & Padian, 2004) or that most of the members of a population dies before reaching their 'growth plateau' (e.g. Horner et al., 2009).

6.2.6 Aging methods for bones

Skeletochronology is a method to determine the absolute age of an animal by growth cycles in compact bone (Castanet et al., 1977). In many recent tetrapods, one growth cycle commonly represents one year of time (e.g. Castanet et al., 1993; Chinsamy-Turan, 2005; Francillon-Vieillot et al., 1990:508; Hutton, 1986; Klevezal, 1996; Klevezal & Kleinenberg, 1969; Peabody, 1961; Ricqles et al., 1991:38). Thus, this knowledge was used to estimate age in many extinct tetrapods (e.g. Botha & Chinsamy, 2000; Chinsamy, 1990; Erickson & Brochu, 1999; Erickson & Tumanova 2000; Horner & Padian, 2004; Sander et al., 2006; Varricchio, 1993). However, there are many problems with this method one have to consider before its application.

First, one has to be sure, if preserved lines are true annuli or LAG's. Resorption or reversal lines are different from LAG's or resting lines, because they are the border between the surface of an old, formerly resorbed bone tissue and newly deposited bone tissue (Francillon-Vieillot et al., 1990), for example during relocation of metaphyseal bone tissue into the diaphysis or during a change of the direction of osseous drift. A special but widely distributed type of such lines is the cementing line enclosing the lamellae of secondary osteons. Annuli and LAG's can be, thus, distinguished from resorption lines by their cyclicity (always following a growth zone), by their relatively consistent and regular appearance, and they do not separate bone tissues of different developmental origin from each other.

The next problem is to make an accurate count of the number of annuli/LAG's to get an age estimation for the respective animal. There has to be considered that the ontogenetic expansion of the marrow cavity can resorb several of the innermost growth cycles and that secondary remodeling is able to completely obscure most of the zonal primary compact bone. A possible solution is the back-calculation of the lost/obscured number of annuli/LAG's (e.g. Castanet et al., 1993:265), where the distances between successive annuli/LAG's were measured and, by using several statistical methods, the pattern of intervals were extrapolated into the marrow cavity and/or into the remodeled area (e.g. Horner & Padian, 2004; Klein, 2004; Werning, 2005). If available, the ontogenetic series of the bone of an animal and the superposition of them are another possibility to get absolute age estimates. The abundant variation in the distances between successive annuli/LAG's or the same variation between two cycles in different parts of the cross section are here less significant, because the annuli/LAG's of earlier stages are definitely known by younger specimens (e.g. Chinsamy, 1993; Erickson & Tumanova, 2000; Horner et al, 2000).

It is furthermore important to know that there is a high variability of the LAG number observed in different individuals of a population (e.g. Klevezal, 1996), between different skeletal elements of one individual (e.g. Horner et al., 2000), and sometimes even in the cross section of a single bone (e.g. Ricqles, 1983). For example, single individuals of the dinosaurs *Hypacrosaurus*

(Horner et al., 1999), *Maiasaura* (Horner et al., 2000), and *Plateosaurus* (Klein, 2004) show different numbers of preserved LAG's in different skeletal elements, which obviously depends on the general anatomical condition and specific growth pattern of each of these elements (e.g. cortical thickness, growth rate, rate of remodeling etc.).

A last important point on this topic is the assumption, whether all annuli/LAG's counted in a bone are indeed true annual layers. It is known that recent tetrapods also generate them in case of very uncomfortable environmental conditions, such as scarcity of food or illness, or during seasons of pairing or reproduction (Castanet et al., 1993). It is also possible to find double LAG's, which are consistently close together and represent a single year, and e.g. some tropical mammals can even generate two cycles in one year (Klevezal, 1996). All these deviations from the simple annual model of growth cycles are not discernable in extinct species and must be treated as sources of error in the calculation of individual age.

Amprino (1947) suggested that similar bone tissues in different animals represent similar growth rates. This assumption was used afterwards to estimate growth rate in extinct animals independently of skeletochronology (e.g. Horner et al., 2000). It is now widely accepted that adult or maximum body size seems to be one of the major factors, which have influence onto growth rate and therefore indirectly on bone tissue types (Buffrenil et al., 2008; Castanet et al., 2000; Erickson et al., 2004; Padian et al., 2004; Turvey et al., 2005). There are also differences in growth rate between different elements of a single skeleton (e.g. Buffrenil et al., 2008; Horner et al., 2000; Klein, 2004; Starck & Chinsamy, 2002) and during ontogeny (e.g. Castanet et al., 1993; Chinsamy, 1995; Horner et al., 1999; Werning, 2005). However, quantitative tests were extraordinarily rare, so that the accuracy of 'Amprino's Rule' was not exactly proofed. This was finally done by a few recent studies on some birds and reptiles, which show a clear correlation between the size and density of vascular canals within the periosteal bone matrix, but no correlation with the orientation of vascular canals (Buffrenil et al., 2008; Castanet et al., 2000; Margerie et al., 2002; Starck & Chinsamy, 2002). A correlation of growth rate with vascular orientation seems to exist only due to extreme environmental conditions,

which force an animal to generate extraordinarily high growth rates (Margerie et al., 2004). Thus, 'Amprino's Rule' can help to estimate the growth rate of an extinct species, but, as in the method of skeletochronology, the results are strongly dependent on body size, ontogenetic stage, and skeletal element and should always be considered in comparison between different individuals, populations, and species.

6.3 Bone histology in dinosaurs

Studies on bone histology of tetrapods, extant and extinct, were made at least since the beginning of the 20th century. Dinosaurs were often part of them (e.g. Enlow & Brown, 1957; Gross, 1934; Seitz, 1907), probably due to their obvious differentness compared to modern animals. These studies were always comparative and descriptive, but no further discussions on these observations were made, except in a very few cases, where, for example, the juvenile stage of a hadrosaurian dinosaur species was proofed by the histological structure found in its bone (Nopcsa & Heidsieck, 1933). All these studies were very important, though, providing important first advices on the types and variety of the histology in dinosaur bone.

Since the beginning of the seventies of the last century, a different view on the formerly as sluggish and dump considered dinosaurs took place. Dinosaurs are now considered as active, eventually endothermic, and social animals (Bakker, 1986). The following very popular and long lasting dispute on endo- or ectothermic dinosaurs (see reviews in e.g. Chinsamy and Hillenius, 2004; Norman, 1991; Padian & Horner, 2004) was also partially based upon histological evidence of dinosaur bone. The described fibrolamellar periosteal compact bone and extensive haversian remodeling was used as evidence for endothermy in dinosaurs (e.g. Bakker, 1972; Ricqles, 1974; 1976). However, Reid (1984) questioned this hypothesis in his comprehensive study on tissue types in dinosaurs, which was one of the preliminary steps to his 'intermediate' hypothesis of dinosaur physiology and metabolism (Reid, 1997). This was also derived from the rapidly increasing knowledge

on the variability of bone histology in dinosaurs, provided by a new quality of histological studies since the beginning of the nineties of the last century. Standardized samples of ontogenetic series of bones were used to discover the high variability of bone tissue types in skeletal elements and even in different sampling locations within a single bone (e.g. Chinsamy, 1990; 1993; 1995; Varricchio, 1993). Henceforward, the opinion consolidated that the simple determination of dinosaurs as either endotherm or ectotherm animals is almost impossible, because bone histology do not provide unambiguous evidence for it (Chinsamy & Hillenius, 2004; Padian & Horner, 2004). Even the occurrence or absence of resting lines in bone cortices as indicators of more reptile-like or more mammal-like metabolism, respectively (e.g. Chinsamy, 1990; 1993; 1995), is now questionable (Padian & Horner, 2004; Sander & Andrassy, 2006), because resting lines were also found in clearly endothermic and fast growing sub-recent and recent mammals (Castanet et al., 2004; Chinsamy et al., 1998; Horner et al., 1999; Klevezal, 1996; Sander & Andrassy, 2006) and in large birds (e.g. Turvey et al., 2005), which are undoubtedly endothermic.

During the last 20 years, the focus of the research in dinosaur bone histology was rather the reconstruction of the life history of single dinosaur species using qualitative and quantitative methods (see e.g. Erickson, 2005; chapter 6.2.6). The current view on dinosaur bone histology and life history is as follows. Small species have lower growth rates than large species (e.g. Padian et al., 2004). There is even evidence that dinosaurs reached their gigantic size primarily by acceleration of their absolute growth rate (Erickson et al., 2001; Sander et al., 2004), which is quite different to the pattern in the gigantic crocodile *Deinosuchus* (see Erickson & Brochu, 1999). Members of the theropod lineage have closer similarities in their fine structure to birds, whereas ornithischians seem to have more mammal-like fine structures (Rensberger & Watabe, 2000). The typical bone tissue of dinosaurs consists of fibrolamellar bone in the periostal bone wall, but there are species with either well developed cyclical or zonal interruptions (annuli/LAG's; e.g. Bybee et al., 2006; Chinsamy, 1990; Curry, 1999; Erickson & Tumanova, 2000; Erickson et al., 2007; Horner & Padian, 2004; Horner et al., 1999; Horner et al., 2000; Horner et al., 2009; Klein, 2004; Reid, 1984; Ricqles, 1983; Sander, 2000;

Sander et al., 2006; Varricchio, 1993; Werning, 2005) or with very weak to probably absent cyclicity (Chinsamy, 1995; Chinsamy et al., 1998; Klein & Sander, 2008; Sander, 2000; Sander et al., 2004; Winkler, 1994). The numbers of the cited studies already let assume that interrupted or cyclical growth is the more common growth pattern in dinosaurs. The few examples of uninterrupted/non-cyclical growth pattern belong either to small ornithopods or to sauropods. However, the variability of growth pattern in dinosaurs is so high that one can find interrupted and uninterrupted fibrolamellar bone in a single group, in a single species or even within a single individual (e.g. Horner et al., 2000; Sander, 2000; Sander & Tückmantel, 2003). It is therefore possible that the sample or ontogenetic series of a species without annuli/LAG's is too small to estimate the whole variability of its growth pattern, which probably also include interruptions in their bone tissue (e.g. Chinsamy et al., 1998; Horner et al., 2000; 2009).

The sensational identification of medullary bone in some dinosaur species, which represents a repository tissue for developing eggshells in sexually mature females, further expand the possibilities of reconstructing dinosaur life history (Lee & Werning, 2008; Schweitzer et al., 2005). The assumption of early maturation of dinosaurs well before reaching asymptotic body size (deposition of OCL/EFS, see chapter 6.2.5; e.g. Curry, 1999; Erickson, 2005; Sander, 2000) was now clearly verified in at least three dinosaur species (Lee & Werning, 2008). Thus, dinosaurs had a similar growth pattern than most modern animals except modern birds and small mammals, which are sexually mature well after somatic maturity (e.g. Chinsamy-Turan, 2005; Erickson, 2005; Lee & Werning, 2008). The latter authors also showed that dinosaurs are not simply scaled-up reptiles, because they can reach much higher relative growth rates. Further studies created e.g. mortality curves for tyrannosaurs (Erickson et al., 2004; 2006) revealing peaks of mortality at the beginning of life, during onset of sexual maturity (as in many larger modern animals) and very late in life.

Today, it becomes more and more normal to use bone histology to verify the ontogenetic stage of new species of dinosaurs (e.g. Makovicky et al., 2010; Xu et al., 2007) or to analyze the age

structure of mass accumulations of dinosaur individuals (Varricchio et al., 2008). Now, bone histology is widely accepted as a tool to get open a small window into the real life of dinosaurs.

6.4 Material and methods

6.4.1 Location and production of thin sections

The bones used for thin sectioning, were loaned from the collections in Göttingen, Stuttgart, and Tübingen. All the chosen bones (femora, tibiae, humeri, fibulae, and pubii) where already broken, lacking either the distal or proximal ends. In case of the femora, it was also possible to use isolated shafts, because the distal beginning of the fourth trochanter or the medial depression helped to clarify its orientation and the best position for the thin section. The prepubic process of the pubis represents the only non-long bone element and was chosen to highlight further variability within the skeleton of *Dysalotosaurus*. Nevertheless, it was the only pelvic element, where enough material was available. Rips were not appropriate, because almost all elements were found isolated and especially rips are difficult to sort into a specific original position.

It is important to note that it was impossible to take thin sections from the very same relative position in every element, because only incomplete specimens were used. Furthermore, it was aimed to cause as less damage as possible to the specimens, so that most of the cuts were carried out close to the broken surface of the shafts. Thus, the sections are standardized to a single interval along the bone shaft and not to a single level (Fig. 6.1). Distinct processes or expansions helped to verify the relative position of the section. Proximal femora possessed the fourth trochanter and distal femora a strong proximodistal, laterally expanding shelf. All femoral sections were made either at the base of the fourth trochanter or approximately at the proximal end of the lateral shelf. Sections from the tibia were obtained from a very distal portion of the shaft, because CT-scans revealed the thickest cortex in this part. A faint lateral knob or bulge helped to estimate the relative position (see Fig.

5.13), so that all used thin sections are located just proximal to this bulge. All available fibulae lacked the distal part including most of the shaft. These thin sections were therefore positioned very close to the proximal metaphysis. The sections from the humeri were attempted to get as close as possible to the thinnest part of the shaft. In proximal specimens, the deltopectoral crest helped to estimate the relative position. The cuts on the prepubic process of the pubii are located approximately at the level of its greatest mediolateral width.

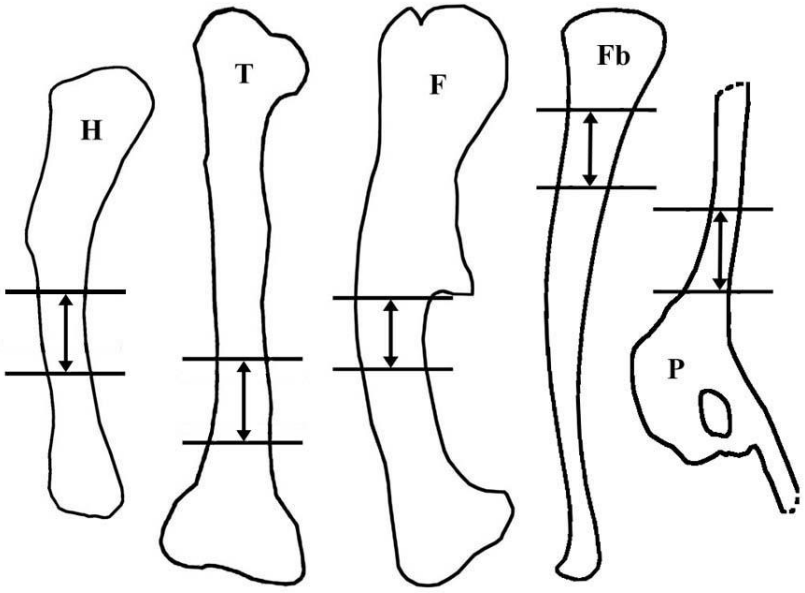

Fig. 6.1: *Intervals of cutting levels in the sampled elements.* ***Abbr.: F*** *– Femur (lateral view);* ***Fb*** *– Fibula (lateral view);* ***H*** *– Humerus (anteromedial view);* ***P*** *– Pubis (lateral view);* ***T*** *– Tibia (posterior view). Elements are not scaled.*

The bones were cross cut with a diamond powder disk on a precision saw. Due to the brittle nature of many bones, they were temporally embedded in acetone dissolvable two-component epoxy-resin (Technovit 5071) during the sawing process. The surface of the obtained and afterwards dried blocks were then ground with silicon-carbide powder (SiC) down to 600µm grain size to get a plain surface for gluing the block onto a glass slide. The hardening of the used two-component glue needed 8 to 12 hours in a splicer. In the next step, an automatic precision saw cut the glued block down to a thickness of approximately 400µm. Then, the block was put into an automatic precision grinding machine and ground with SiC powder down to the final thickness of approximately 100µm. Finally, a one-component impregnating resin was used to glue a cover slip onto the finished thin section, which needed up to 48 hours of hardening at room temperature.

6.4.2 Preservation and sorting of thin sections

The preservation of thin sections is miscellaneous and comprises extraordinarily good preservation as well as strongly obscured sections with numerous cracks and even completely lost parts. Most of the obtained thin sections showed numerous diagenetic fractures, reaching from simple thin lines to wide, crystallized fractures, which disturb the original shape of the cross section. Even the bone tissue itself was often altered by diagenetic recrystallisation or infilling of dark to opaque metal oxides. There are also samples with a conspicuous net structure of the bone tissue, obscuring most of the original vascular pattern (Fig. 6.2). It is suggested that parts of the mineral content were here dissolved during diagenesis.

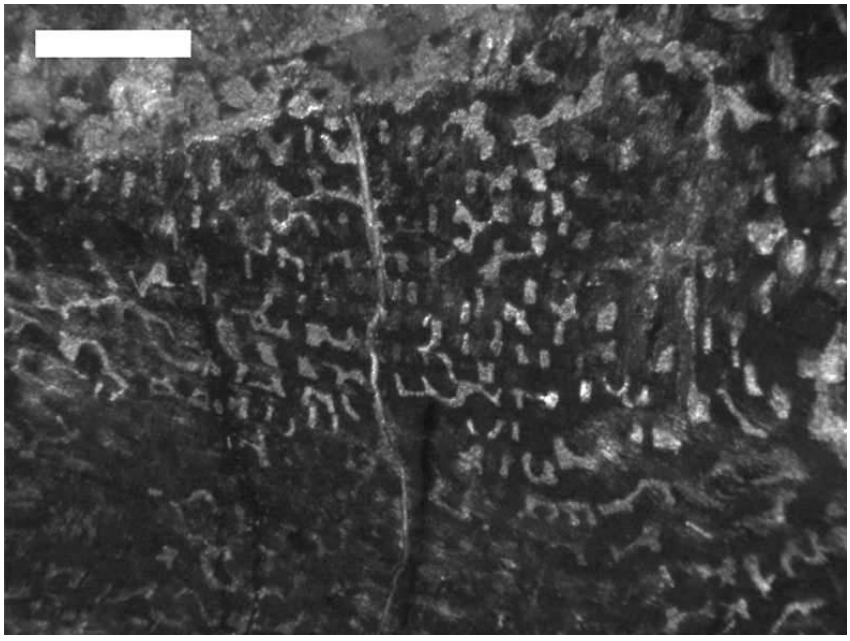

Fig. 6.2: *Detail of cross section of tibia SMNS T 13; Anterolateral unit internally; Marrow cavity at top left; Photo made under polarized light. The original vascularization is obviously altered by postmortem dissolution of bone tissue. Former primary osteons are lost during this process and the vascular canals are widened. Scale bar = 500µm.*

Dissolution and recrystallisation occur mainly in strongly broken samples and nearby strongly fractured parts. Dark colored metal oxides can obscure most of the bone walls either independently of structure or they are strongly concentrated along and inside of vascular canals. There are also occasional changes in color, which sometimes run parallel to the outer surface or of fracture surfaces and could be the result of penetrating fluids circulating inside the ambient sediments. The marrow

cavities are always filled with fine marl, large crystals or both. Chinsamy-Turan (2005:15) described some results of an unpublished study, where the mineral content of the bones of *Dysalotosaurus* was examined. It was found that the marrow cavities were often occupied by a mixture of quartz, feldspar and clay. The precipitation pattern of prismatic calcite let to the suggestion that some bones rolled around before final burial. Furthermore, multigenerational calcite precipitation indicated successive groundwater circulation in the sedimentary environment. Anyway, most of the bones experienced clastic infilling during burial (see also chapter 3).

All thin sections with at least passable preservation were described in detail. All steps beyond the description, which incorporates the count and correlation of growth cycles, were only done with femora, tibiae, and humeri. The other two sampled skeletal elements were either nearby the metaphysis (fibulae) or they had a too thin periosteal primary compact bone wall (pubii) to gain enough quantitative information.

All thin sections revealing growth cycles were sketched by using Adobe Photoshop 7.0 software. Due to the large error in taking standardized thin sections (see chapter 6.4.1), it was not possible to simply superimpose the sketches of different ontogenetic stages of a sampled skeletal element to get a complete record of all growth cycles from the smallest to the largest sampled specimen. Thus, in a first step, thin sections of the femora were sorted into four groups and the thin sections of the tibiae were sorted into two groups depending on cutting location and overall cross sectional shape. Humeri were not sorted because the overall cross sectional shape did not differ much throughout the shaft (Tabs. 1-3).

Labels	Mess 18	C	Group	Ant-post Ø	Med-lat Ø	Ant-post cavity	Med-lat cavity	BWT max	BWT min	Number growth cycles	Number LAG's/annuli	Ontogenetic stage	Age in years
GZG.V 6379	16.1	29.1	2	8.9	7.8	6.3	5.2	1.8 medial	—	1?	—	early juvenile	<1
GZG.V 6653	24.9	42.4	3	16.6	11.8	8.8	6.9	5.2 posteromedial	1.6 posterolateral	2-3	—	late juvenile	2.15
GZG.V 6467	29.3	49	1	—	—	11	10.8	3.9 medial	1.8 posterior	2-3	—	late juvenile	3.58
SMNS F 14	30.6	51	2	16.3	15.1	11.1	9.2	3.5 medial	—	3	—	late juvenile	3.98
GPIT/RE/5650	32.3	53.4	1	—	—	11.1	9.4	—	—	2	—	late juvenile	4.45
GZG.V 6665	33.3	55.2	3	19.2	17.2	8.9	9.2	7.1 posteromedial	3 posterior	2	—	late juvenile	4.79
GZG.V 6652	33.3	55	2	17.4	14.6	11.3	8.9	4.1+ medial	2.1 posterior & lateral	2	—	late juvenile	4.75
GZG.V 6590	31.6	53	2	17.3	13.3	10.4	7.8	4.3 posteromedial	2.1 posterolateral	3	1	late juvenile	4.37
GZG.V 6590 28	35.3	58	1	18.5	18.1	11.8	11.7	4.1 medial	2.2 anterolateral	3	—	late juvenile	5.31
GZG.V 6386	35.3	58	1	20.2	16.2	12.7	9.9	4.9 posteromedial	2.3 posterolateral	3	—	late juvenile	5.31
GZG.V 6211 22	41.9	68	2	—	—	14.7	11.2	—	2.3 posterior	3-4	1	subadult	7.04
GPIT/RE/3587	44.6	72	2	26	20.7	14.9	10	6.8 anterior	4 posterior	4	1	subadult	7.69
GZG.V 6381/6434	45.9	74	2	23	21	13.4	10	6 posteromedial	3.8 posterior	4	1	subadult	8
SMNS F 4	52	83.2	1	23.5	25.4	14.6	15.1	5.9 medial	3.1 posterior	4	—	subadult to adult	9.45
GZG.V 6395	70.4	111	1	—	34	20.5	14.9	12.5 posteromedial	—	7	1	adult	14
GPIT/RE/3414	70.7	111.3	1	32.2	36.8	14.6	20.6	11.4 posteromedial	5.9 anterolateral	8	1	adult	14.06
GPIT/RE/3588	72.5	114	1	33.3	37	18.7	18	11 medial	5 posterior	8	1	adult	14.58
SMNS F 1	74.1	117.7	2	39.2	35.2	19.6	17.2	13.1 medial	5.5 posterolateral	7	—	adult	15.36
SMNS F 2	77.8	122	2	38	37.2	20.1	19.1	10.8 medial	4.6 posterolateral	6	—	adult	16.37

Tab. 1: Femora. Explanation of heading-abbreviations: Mess 18 – mediolateral width at the distal end; C – Circumference of the sampled specimen; Group – the group, into which the cross section was sorted, depends on the cutting level; Ant-post Ø – Diameter of cross section in anteroposterior direction; Med-lat Ø – Diameter of cross section in mediolateral direction; Ant-post cavity – Diameter of marrow cavity in anteroposterior direction; Med-lat cavity – Diameter of marrow cavity in mediolateral direction; BWT max - Maximum of bone wall thickness; BWT min – Minimum of bone wall thickness. The age in years is derived from the growth curves.

Labels	Mess 13	Group	Ant-post Ø	Med-lat Ø	Ant-post cavity	Med-lat cavity	BWT max	BWT min	Number growth cycles	Number LAG's/annuli	Ontogenetic stage	Age in years
GPIT/RE/3795	17.3	1	6.3	—	4.6	4	1.3 anterolateral	0.9 anterior	—	—	early juvenile	<1
GZG.V 6434/6664	35.3	1/2*	12.2/12.8	14.5/12.9	6.8/5.9	7.2/5.8	4.4/4 anteromedial	2.1 lateral/2.8 anterior	2-4	—	late juvenile to subadult	3.1
GPIT/RE/5904	36.4	1	—	—	9.3	9.8	4.4 anteromedial	—	3	—	late juvenile to subadult	3.4
SMNS T 13	37.7	1	13.8	15	7.1	7.8	4.8 medial	2.1 lateral	2-4	—	late juvenile to subadult	3.8
GPIT/RE/4036	38	1	12.9	—	8.3	8.2	3.8 anterolateral	2.1 posterolateral	3	1	late juvenile to subadult	3.86
GPIT/RE/5755	38.1	2	13.3	12.6	7.2	6.3	3.8 anteromedial	2.7 anterior	3	—	late juvenile to subadult	3.91
GPIT/RE/3724	40.7	2	13.8	14.2	7.5	7.8	4 anterolateral	2.5 anterior	4	—	late juvenile to subadult	4.5
SMNS T 7	52.2	1/2*	13/12.8	—	9.2/10	9.1/—	4.8anterolateral/-medial	—	3	2	late juvenile to subadult	7.5
SMNS T 3	75.7	1	25.3	27.6	13.2	12	10.7 anterolateral	4.4 posterolateral	7	1	adult	15
GZG.V 6791	79.3	1	24	33	11.4	16.3	—	4.8 posterolateral	6	1	adult	17

Tab. 2: Tibiae. Explanation of heading-abbreviations: Mess 13 – mediolateral width at the distal end; the remaining headings as in Tab. 1. The age in years was estimated by the comparison of relative positions within the size-frequency distributions of femora and tibiae, respectively.

Labels	Cutting level	Mess 3	Ant-post Ø	Med-lat Ø	Ant-post cavity	Med-lat cavity	BWT max	BWT min	Number growth cycles	Number LAG's/annuli	Ontogenetic stage	Age in years
SMNS H 2	proximal to diaphysis	11.3	6.2	8	3.2	4.8	1.9 anterolateral	1.1 anteromedial	—	—	juvenile	1
GPIT/RE/4526	proximal to diaphysis	13.2	—	8.8	4.9	5	—	—	1	1	juvenile	2.6
GPIT/RE/4402	proximal to diaphysis	16.3	8.8	11.1	3.4	4.8	3.8 lateral	2.3 anteromedial	1	1	juvenile	5.4
GPIT/RE/4262	appr. Diaphysis	23.3	—	16.2	6.7	7.7	—	—	1	1	adult	10.8
GZG.V6569	distal to diaphysis	24.2	12.7	14.8	—	8.8	—	—	5	1	adult	11.8
GZG.V6664	proximal to diaphysis	24.8	15.2	16.3	8.1	9.1	4.2 lateral	—	4	1	adult	12.7
GZG.V6223	distal to diaphysis	26	15.3	19.6	8.2	12.5	4.2 anterior & posterior	3.1 lateral & medial	4	2	adult	15.3
GPIT/RE/4877/8929	proximal to diaphysis	30.4	16.1	20.8	7.3	11.2	5.3 anterolateral	3.2 anteromedial	4-5	3	adult	19.3
GPIT/RE/6416	distal to diaphysis	31.7	17.2	23	10	14.4	4.6 posterolateral	2.9 anterior & lateral	3-4	2	adult	>20

Tab. 3: Humeri. Explanation of heading-abbreviations: Mess 3 – mediolateral width at the deltopectoral crest; the remaining headings as in Tab. 1. The age in years was estimated by the comparison of relative positions within the size-frequency distributions of femora and humeri, respectively.

6.4.3 Conversion of growth cycles into absolute age estimates

The basic assumption is the annual character of the present growth cycles (see chapter 6.2.6), so it was the goal to correlate the cycles of all cross sections of one group of a single skeletal element, to count the final number of cycles, and to equalize them into years.

Superimposition of sketches did not lead to a significant correlation of growth cycles due to variation of the cross sectional shape and variation of the course and distances of growth cycles to each other, even within a single sorted group. Hence, another way was chosen to get a correlation, which was also carried out by using Adobe Photoshop 7.0 software.

The end of each growth cycle was marked in the sketches by a single permanent line. Dashed lines marked unsecured growth cycles due to obscured bone tissue, diffuse transition to the next growth cycle, or various splitting and fusion of several cycles. A standard location inside the cross sections, which usually revealed the best record of growth cycles, was determined for femora, tibiae, and humeri respectively. In the tibiae, two good locations were found and the final growth cycle values are averages of them.

The first step towards the correlation of cycles was the definition of an unambiguous and repeatable midpoint for every used cross section (Fig. 6.3). Femoral cross sections mostly have a triangular shape, so that two types of geometric triangles were generated. The vertices of the first triangle were set on the utmost extremity of each of the three corners of the triangular femoral cross section (Fig. 6.3A). The vertices of the second triangle were generated by three straight lines, which were placed on the external edge of the three straight walls of the triangular cross section. Each line was then graphically shifted onto the utmost extremity of the opposing corner in the cross section and the respective vertex was set. Now, the midpoint of both triangles was generated by drawing a line from each of the three vertices to the opposite straight line, so that this line separates the angle of the respective triangle corner in two equal halves. The point of intersection of these three lines is the midpoint of the triangle. In most cases, the midpoints of both triangles do not coincide. The

midpoint of a straight line, drawn between both triangle midpoints, is therefore defined (Fig. 6.3B). To minimize the possible error, a circle was additionally drawn as large as possible to fit right on the outer contour of the femoral cross section. Another straight line was created between the midpoint of this circle and the average midpoint of the two triangles. The final determined midpoint of the whole femoral cross section was then the midpoint of this last line (Fig. 6.3C).

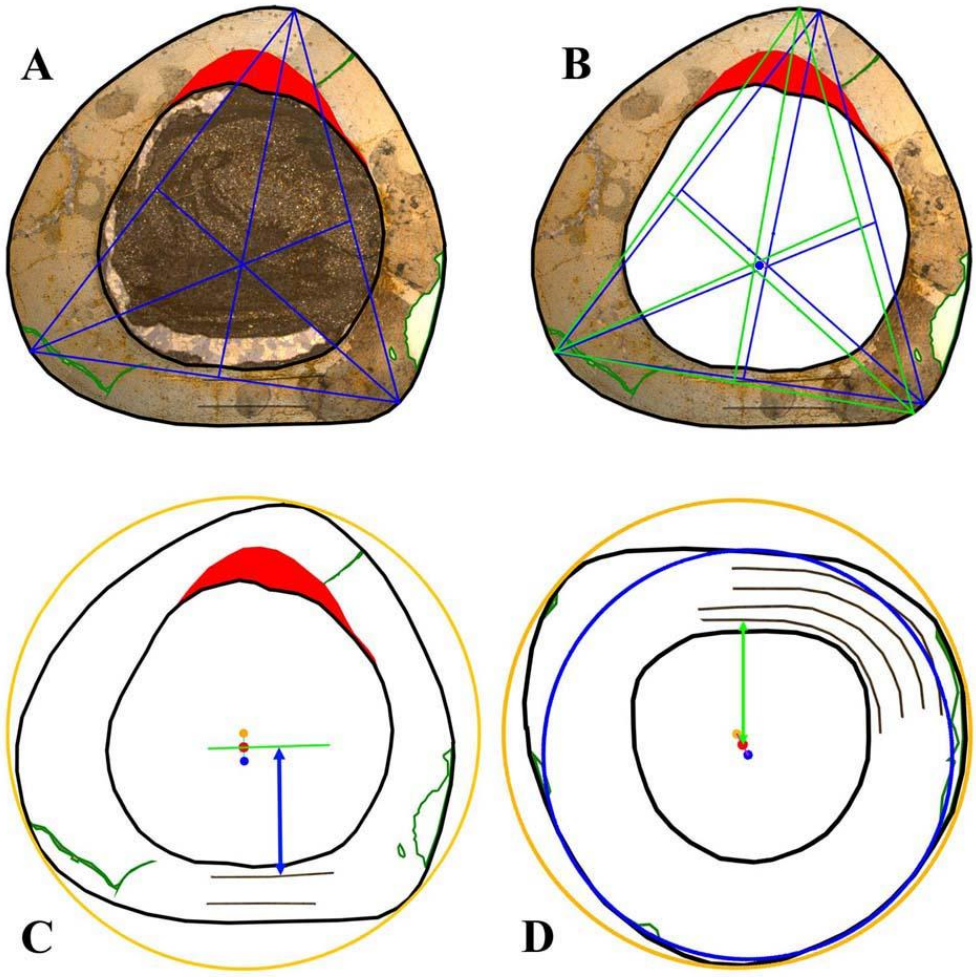

Fig. 6.3: *Sketches showing important steps to gain a standardized midpoint in cross sections for the measurement of distances between this midpoint and the external border of each growth cycle.* ***A-C:*** *Late juvenile femur GZG.V 6590 28****: A*** *– First triangle with its vertices on the utmost extremities of each corner;* ***B*** *– Second triangle with vertices extrapolated from the respective opposing straight walls. The blue point in the centre is the midpoint of both triangles;* ***C*** *– The final midpoint of the cross section is derived from the blue midpoint of the triangles and the orange midpoint of the sketched circle. The green line lies parallel to the course of the growth cycles and the distances (e.g. blue double arrow) are then measured perpendicular to the cycles in the posterolateral part of the posterior wall.* ***D*** *– Late juvenile tibia GPIT/RE/3724: The midpoints of an inner and an outer circle (blue and orange, respectively) are used to get the final midpoint (red) for measuring the growth cycle distances. All sketches are not scaled, but consistently orientated with the anterior direction to the top and the medial direction to the left. The red area in A-C represents the anterior CCCB-wedge. Lines in green mark damaged areas in the cross sections.*

The cross sectional shape of tibiae and humeri were much more oval in shape. Here, the midpoints of two circles were used to determine the midpoint of the cross section. One circle was graphically scaled down as small as possible to enclose the cross section externally and just tangent the outer edge of it. The second circle was scaled up as large as possible to tangent the outer cross sectional edge internally. The midpoint of a straight line, which was drawn between the two obtained circle midpoints, was then determined as the midpoint of the cross section (Fig. 6.3D).

During the next step, the distance between the cross sectional midpoint and each of the recorded growth cycles was measured and transformed into partial percentages of the distance between the midpoint and the outer cross sectional edge. The reference measurement for each of the cross sections, representing 100% from midpoint to outer edge, was already measured before at the respective sampled specimen. Since not the same reference measurement could be taken from each of the femora, tibiae, and humeri, regression equations were calculated with Microsoft Office Excel 2007 software to get the allometric relationship between each of these distances. At the end, all reference measurements were transformed into diaphyseal circumference and distance number 18 in femora, distance number 13 for tibiae (both means the mediolateral width of the distal end), and distance number 3 for humeri (means the width at the deltopectoral crest; Appendix IV). The data for the allometric calculation was taken from the measurement dataset of complete specimens of these long bones (Appendix V).

It is important to note that each measurement from the cross sectional midpoint to a growth cycle was taken perpendicular to the course of the latter. In all femora, the best growth record was preserved in the lateral part of the posterior wall, close to the lateroposterior corner. A straight line was drawn from the midpoint parallel to the course of the growth cycles and the measurement was then taken laterally from the midpoint and perpendicular to the course of the growth cycles (Fig. 6.3C). In all tibiae and humeri, such an additional line was not necessary and all measurements were directly taken from the midpoint. The best growth record in tibiae was preserved in anterior and medial direction and in the humeri in anterior direction only. The respective measurements from the

midpoint to the growth cycles were therefore carried out in these directions perpendicular to the course of the cycles.

A special cycle, observed in five large femora and possibly marking initial sexual maturity (MISM), was measured in the same way as the growth cycles, but was noted separately.

All measured percentages of growth cycles were then transformed, in a third step, into partial values of the reference distance of the respective cross section (representing 100%) and recorded in an Excel file. The values of each cross section were sorted in their respective group, one in humeri, two in tibiae, and four in femora. The following correlation of growth cycles was therefore done only within a single group. The still uncorrelated growth cycles of each group were related to age in years. A diagram was then created, were the x-axis represents the age and the y-axis the partial reference values of the growth cycles of each cross section of this group. Now, the correlation of growth cycles with age in years started by fitting the lowest value of all cross sections to an age of one year. The distance of successive growth cycles of every cross section in the dataset and in the diagram revealed the general distance of values between two successive years. First, all values of a single cross section were shifted, so that the smallest value fit onto a value of another cross section. In this way, the values of every single section of this group were fitted to get a single curve in the diagram, where possible outliers are minimized. It occurred especially in large or strongly obscured cross sections that the successive growth cycle values could be separated, because the large distance between them could be filled by successive values of other sections. The MISM was separately signed into the diagrams of two groups of femora.

In this way, the growth cycles of tibiae and humeri were also correlated to reveal the number of years recorded by them.

6.4.4 Calculation of body mass

Two out of four groups of sampled femora were chosen to convert their age related growth cycles into body mass estimates. The samples of the other two groups are not appropriate, because their location within the shaft is either too proximal or too distal, and their small number of recorded growth cycles only covers three to four years. In contrast, growth cycles of several samples in femoral group one and two were often placed within the same year of age during correlation. In this case, the average of all values of this year was used as the basis for the body mass calculation.

Two methods of calculating body mass by skeletal elements were considered. The first method was derived by Anderson et al. (1985; see also discussion in McNeill Alexander, 1989) by using the combined humeral and femoral shaft circumference to calculate body mass in quadruped animals. For biped animals, only the femoral shaft circumference was necessary. The following equation was therefore used for *Dysalotosaurus* femora, $W=0.16\ C_F^{2.73}$, where W is the weight and C_F is the circumference of the femur.

The second method was derived by Erickson & Tumanova (2000), known as Developmental Mass Extrapolation (DME). The basis for this body mass calculation, which emphasizes the effect of ontogeny on mass increase, is the assumption that the approximately third power of femoral length corresponds to body mass in *Alligator* (data in Dodson, 1975b) and the seagull (data in Carrier & Leon, 1992). Both species represent members of outgroups of non-avian dinosaurs (Extant Phylogenetic Bracket; Witmer, 1995), so that the ratio of femoral length to body mass could also be used for the latter, including *Dysalotosaurus*. First, the body mass of the largest available individual has to be calculated, representing the value of 100%. The largest femur specimen in the *Dysalotosaurus* material was a distal end lacking most of the shaft and the proximal end. However, the distance number 18 could be measured, so that the allometric relationship between length and distance number 18, derived from the dataset of more complete femora, helped to calculate the length of the largest femur. This was done with the Microsoft Office Excel 2007 software as well. In

the same way, the averaged and into circumference values transformed growth cycles of every year of both femoral groups were converted into their femoral length equivalences by using the calculated allometric relationship for both distances. All obtained length values were then potentized by 3. The afterwards calculated fractional percentages were finally transformed into fractional body masses of the largest femur.

The averaged value out of two in the femur group one and out of three in femur group two, belonging to the MISM, were transformed into body mass as well.

6.4.5 Establishing the growth curve

To compare the life history of *Dysalotosaurus* to other dinosaurs and recent animals, a type of growth curve had been chosen, which was already used by Erickson et al. (2001).

The calculated body mass of the averaged growth cycles was therefore plotted against their respective age in years. The equation $y = a / (1 + \exp (b * (x + c))) + d$ describes the sigmoidal course of this type of growth curve (y=body mass; x=age in years; a= largest known body mass; b, c, d= parameters to fit). The variable *a* was derived from the largest known femur with a calculated body mass of 116.53 kilograms. Only the secured growth cycle values were integrated and all unsecured values, including the values externally of the MISM, were excluded. The latter values were entered separately into the finished curve to evaluate their significance and possible age correlation. The MISM itself was included with the corresponding age of 9.5 years. A total of four curves were created, including the calculated body masses by the methods of Anderson et al. (1985) and Erickson & Tumanova (2000) for femoral group one and two, respectively. The dataset was entered into the software Microcal Origin and the non-linear curve fit function (basing on least-square regression analysis) was performed using the equation mentioned above.

6.4.6 Growth rates and age/size frequency distribution

To get yearly and daily growth rates, the calculated yearly body masses were derived by using the sigmoidal equations and the four parameters of each of the four growth curves. One version corresponds to the growth rate in a decent year (365 days) and the second version corresponds to a year in the Late Jurassic (Kimmeridge, 150 million years ago), which contained approximately 377.76 days (see Wells, 1963; Erickson & Tumanova, 2000). The maximum growth rate per day, calculated in gram, was then plotted into the diagram of Erickson et al. (2001), which was in turn formerly modified from Case (1978a).

The final step was the combination of the absolute age estimates with the size frequency distribution of the distance number 18 of all femora. First, the values of measured specimens and the sectioned samples were put together and the allometric relationships were determined for the distance number 18 and femoral circumference. The allometric relationship for the femoral circumference and length was obtained from the measured specimens with both distances preserved. Second, the calculation of age was carried out by conversion of the sigmoidal equation to x (age in years), which resulted in the following equation: $x = ln ((a / (y - d) - 1) / b + c$ (y=body mass calculated by either the method of Anderson et al., 1985, or Erickson & Tumanova, 2000; the parameters a, b, c, d were derived from each of the four growth curves). The obtained ages of the separately calculated versions for femoral group one and two for each of the measured and sectioned femora were averaged for the dataset derived from the Anderson et al. (1985) body mass calculation and for the dataset derived from the Erickson & Tumanova (2000) body mass calculation. These average age estimates were then combined with the measured or calculated circumferences and distances number 18 of the femora.

6.5 Bone histology in *Dysalotosaurus*

This chapter describes bone tissue types and structures found in the sampled bones of *Dysalotosaurus*. It follows mainly a protocol, which was made for every single thin section. The description, however, generalizes the observations for each of the elements and ontogenetic stages will be set for femora, tibiae, and humeri. The compact bone wall of the cross sections is divided into standardized units, which are derived from the spatial orientation of the whole bone in articulation. Some of these units have very special and recognizable features, which help to orientate the cross section even without the bone itself. Distances are only measured along the anteroposterior axis or the mediolateral axis (see Tabs. 1-3).

The quantitative results, derived from bivariate calculations and growth curves, are presented separately in chapter 6.6.

6.5.1 Bone histology of the femur

6.5.1.1 Description

The femoral cross section is generally triangular in shape and slightly wider lateromedially than anteroposteriorly. The shape gets more slender close to the base of the fourth trochanter and the anteroposterior distance is then wider than the lateromedial distance at this level (see Fig. 6.4A-D). The general orientation of the sections is almost constant, although most of the units are slightly displaced anti-clockwise (in right elements) in more proximal levels. One sharp corner is always directed anteriorly and the other two posterolaterally and posteromedially (in proximal sections more laterally and posteriorly, respectively). The three walls are located posteriorly (posterolaterally), anteromedially (medially), and anterolaterally and are always thinner than the corners. The thickest part of the compact bone wall is mostly the posteromedial corner, whereas the thinnest part is found either in the posterior or anterolateral wall.

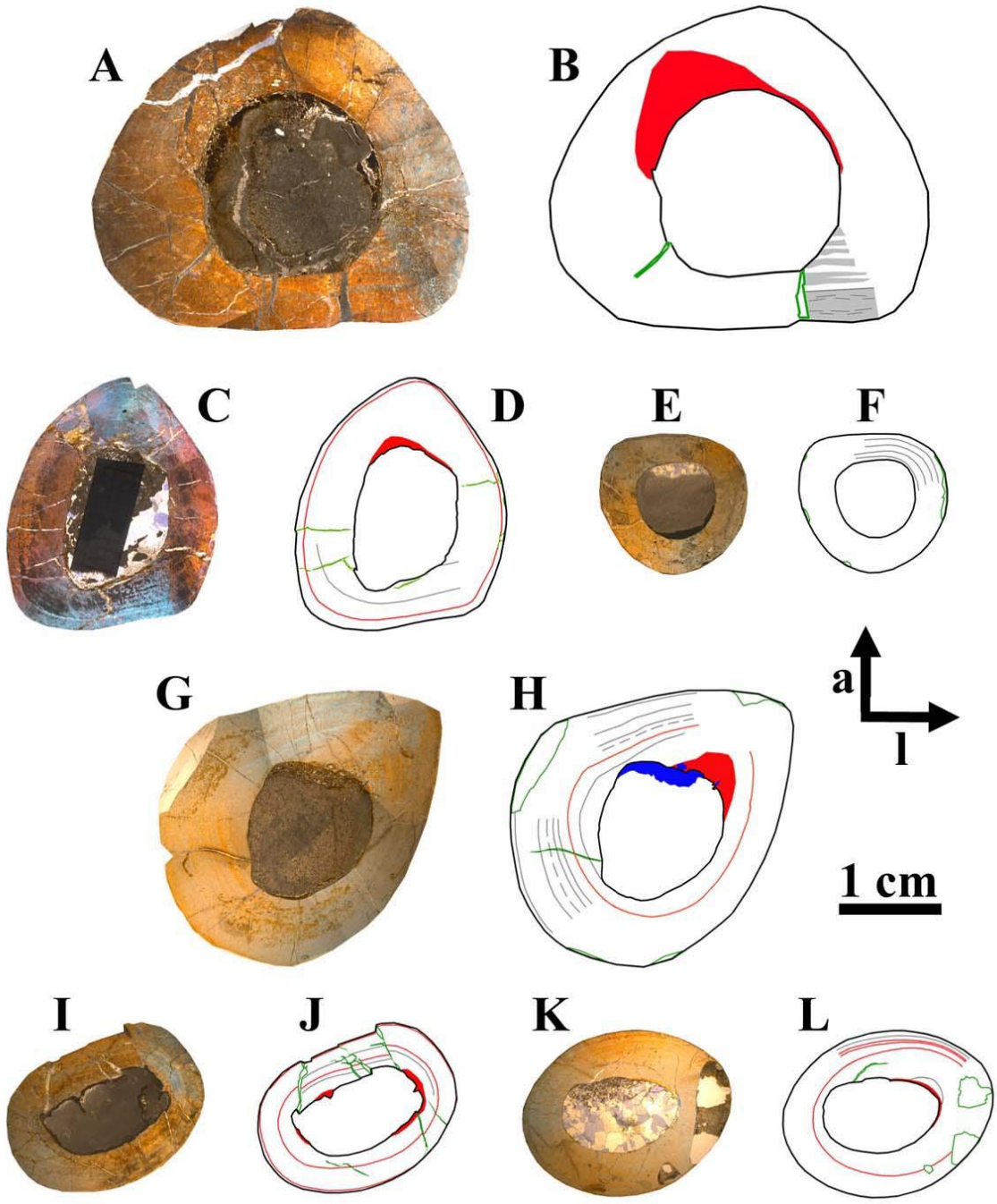

Fig. 6.4: *Representative cross sections and corresponding sketches of femora, tibiae, and humeri.* ***A-B:*** *Sexually mature adult femur GPIT/RE/3588, cut distally to the base of the fourth trochanter;* ***C-D:*** *Immature subadult femur GPIT/RE/3587, cut close to the base of the fourth trochanter;* ***E-F:*** *Late juvenile tibia GPIT/RE/3724, cut proximal to the lateral bulge;* ***G-H:*** *Sexually mature adult tibia SMNS T 3, cut close to the lateral bulge;* ***I-J:*** *Adult humerus GZG.V 6223, cut distally to the mid diaphysis;* ***K-L:*** *Adult humerus GPIT/RE/4877/8929, cut proximal to the mid diaphysis. All sections are orientated and scaled consistently. Internal red area represents CCCB (B, D, H, J) or an endosteal layer (L). Lines in green mark cross sectional damage. Growth cycles are shaded (B) or lined (D, H, J, L) in gray, LAG's are lined in red. The blue area in H represents medullary bone.*

The outer edge of the marrow cavity is well defined and mainly consistent, except internal to compact coarse cancellous bone tissue (CCCB), where undulations and caverns can occur. No spongiosa were observed within the marrow cavity. An internal fundamental system or endosteal layer was found inconsistently and with variable thicknesses. There is never a completely surrounding band, but isolated pieces, which are mainly located internal to the CCCB anteriorly and laterally. It can also occur sporadically medially and internally to the fibrolamellar primary bone wall, and it is more abundant in larger cross sections.

The compact bone wall consists mainly of two types of bone tissue. Most of the bone wall is built by fibrolamellar bone tissue with woven fibered matrix and numerous primary osteons. Compacted coarse cancellous bone (CCCB) occurs between the fibrolamellar tissue and the marrow cavity and is mostly restricted to the anterior corner and adjacent areas (Fig. 6.5A-D, G-H). In more distal sections, the amount of CCCB relative to fibrolamellar bone increases and the anterior corner can even be built entirely by CCCB. The area of this bone tissue spreads from its anterior position mainly along the lateral side of the cross section, but the thickest part of it is always located slightly anteromedial. Distally in the shaft, the average size of the innermost canals of the CCCB also increases, because of the less advanced lamellar infilling (Fig. 6.5H).

The marrow cavity has resorbed parts of the compact bone wall mainly posteromedial, posterior, and posterolateral, approximately opposite to the location of CCCB. Possible growth cycles and bone laminae are cut here, so that they disappear acute-angled into the marrow cavity on either side of the posterior bone wall (e.g. Fig. 6.4B, D).

The vascularization is very variable in size of the canals and overall density. Generally, most of the vascular canals are well developed primary osteons. Their highest density is observed in the posteromedial corner and adjacent areas. Here, they are also relatively large and the whole bone wall is mainly built by them with only a small amount of bone matrix in between. Especially in the anterior corner and lateral wall, the relative amount of bone matrix is much higher and the density of primary osteons is lower (Fig. 6.5).

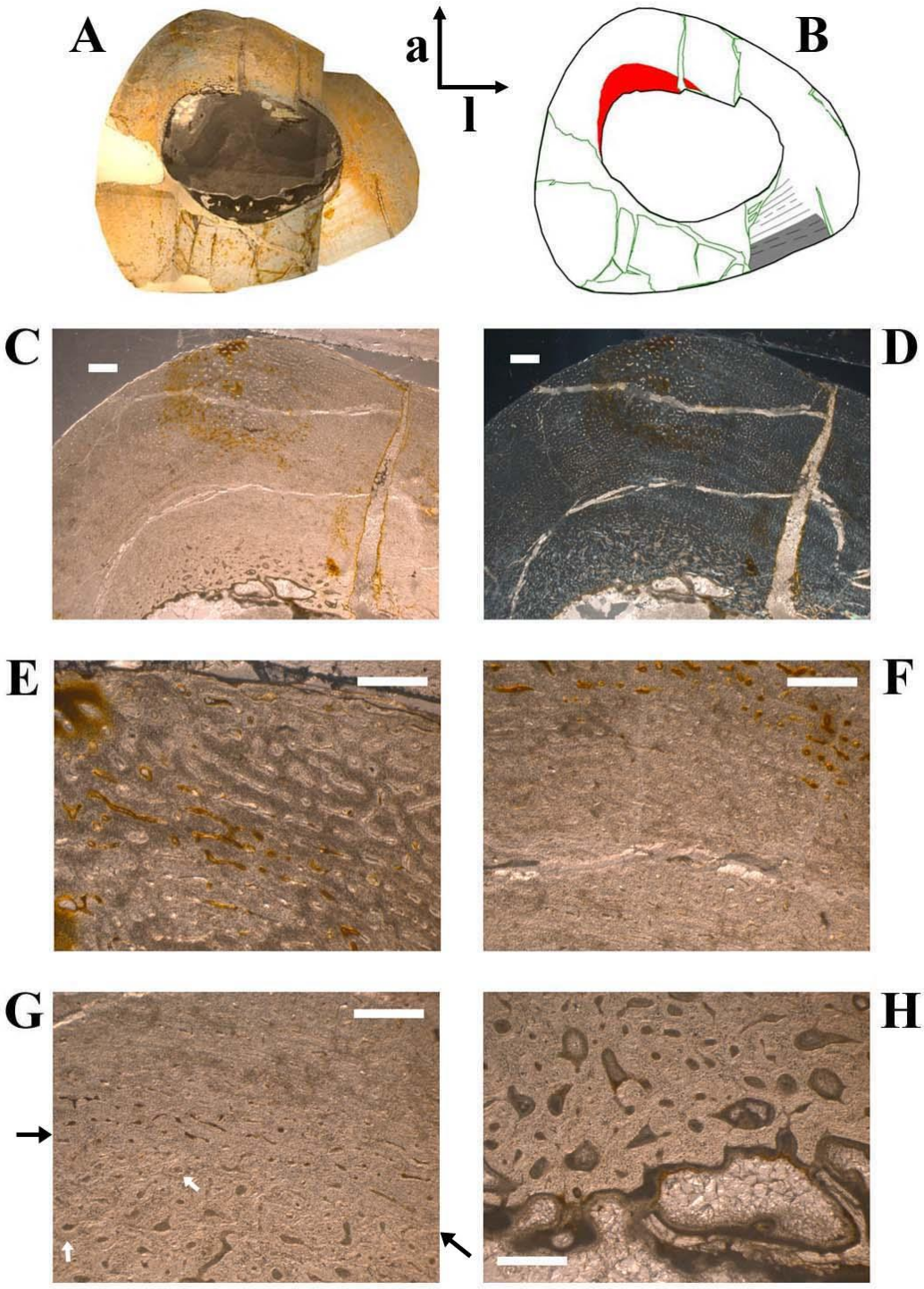

Fig. 6.5: *Sexually mature adult femur GPIT/RE/3414.* ***A-B:*** *Overview of cross section under normal light (A) and sketched (B). Red area represents the anterior CCCB-wedge, green lines mark damaged areas, and gray lines the external edge of growth cycles. The shaded area represents sexually mature adulthood.* ***C-D:*** *Overview of anterior corner under normal light (C) and polarized light (D). Note the plug-like structure in the exterior half of the bone wall. Scale bars = 1mm.* ***E-H:*** *Successive images showing details of the anterior corner starting at the periphery (E) and ending at the marrow cavity (H). All images are orientated as in A. Note the unusual vascular orientation within the plug in E, the simple vascularization in F and G, and the transition from periosteal bone tissue to CCCB (black arrows) in G with some scattered secondary osteons (white arrows). Scale bars = 500µm.*

They are also often flattened parallel to the bone laminae, compared to the mainly rounded and irregular primary osteons around the posteromedial corner.

The smallest, fairly well and longitudinally organized primary osteons are observable in the innermost areas anterolaterally, anteriorly, and anteromedially close to the CCCB. There are relatively thick cords of matrix, which isolate these osteons from each other and look like a pattern of knitting (Figs. 6.5F; 6.6A).

The organization pattern of vascular canals is relatively variable, but the laminar type is most abundant. Other patterns are observable depending on the particular area in the cross section. As a main tendency, the organization of vascular canals is high in the thin walls and low in the posterolateral and posteromedial corners (compare Figs. 6.6B, D with 6.6D, G). The anterior corner is a special case, because the actual periosteal compact bone wall is due to the internally deposited wedge of CCCB often much thinner than the other units of the bone wall. Thus, there is an especially high degree of organization. Another tendency is the general increase of vascular organization from inner parts towards the periosteal surface. In large cross sections, the inner parts reveal a mixture of longitudinal (close to the anterior corner), laminar (also anterior and as part of slow growing zones), plexiform, and even reticular patterns. The laminar type gets more and more dominant towards the outer surface until, close to it, it is the only type left (in large sections). Plexiform and reticular patterns occur also in the posteromedial and posterolateral corner, and especially the area within and adjacent to the posterolateral corner is dominated by reticular vascularization.

Moreover, the posterolateral corner represents a very special area of the bone wall (Fig. 6.6C, D). Here, vascular canals and often rather weakly developed primary osteons are larger in average and more randomly shaped and orientated. Overall, this cluster of canals ascents slightly at the edge of the marrow cavity laterally and then very steep close to the posterolateral corner, where it finally reaches the external extremity. Many of the vascular canals are even radially oriented in this direction. This area, which will be called posterolateral plug in the following text, represents a very abrupt cut within the organization of bone tissue (Fig. 6.6C, F). The general course of the posterior

growth cycles, bone laminae, and the orientation of vascular canals stops at the border of the posterolateral plug and only distinct resting lines can be tracked through it. This area is most prominent in sections close to the lateral bulge slightly distal to the midshaft and becomes less prominent towards the fourth trochanter.

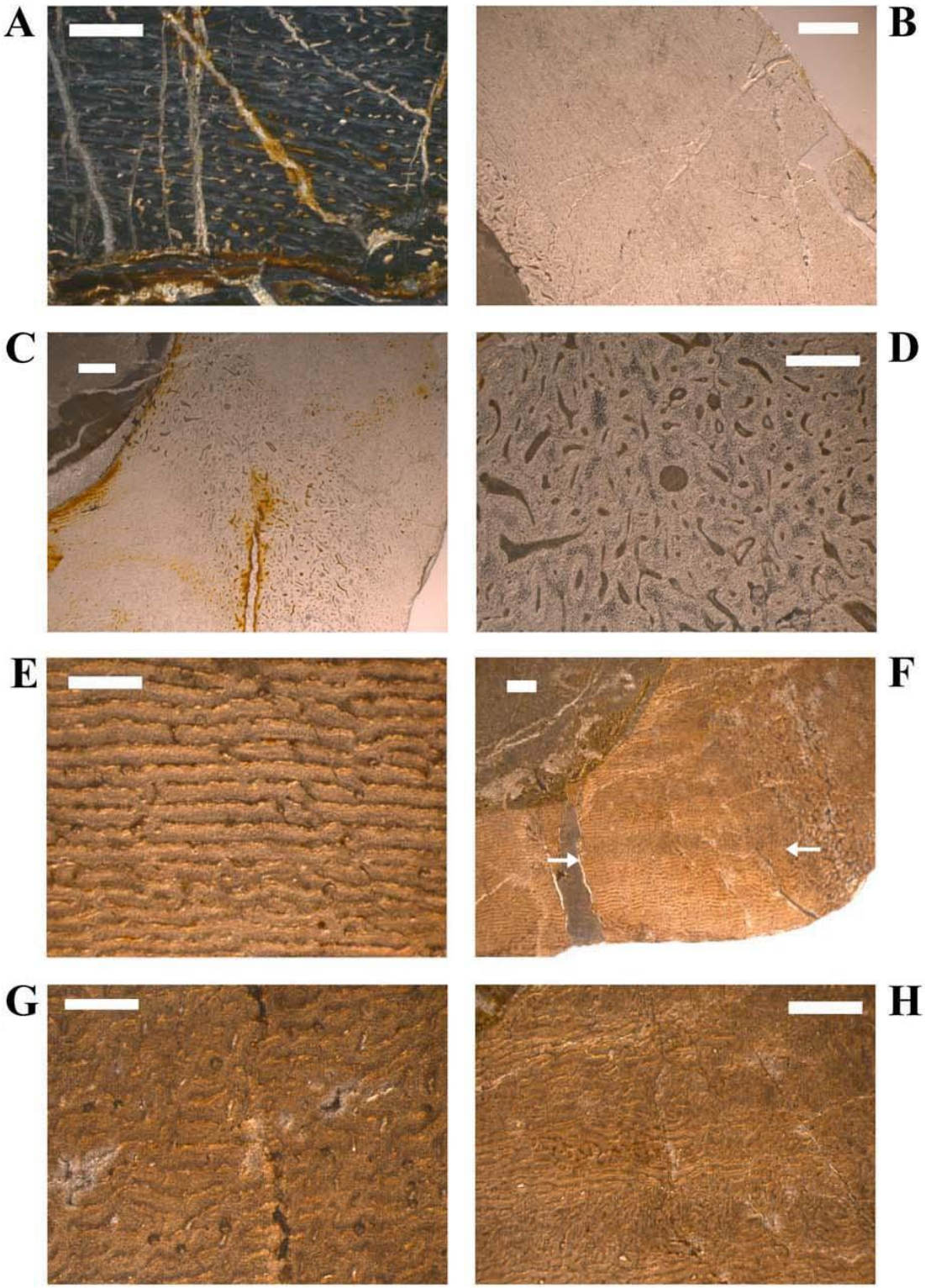

← **Fig. 6.6:** *Detailed images of sexually mature adult femoral cross sections.* ***A:*** *SMNS F 2, anterior corner, interior, showing juvenile bone tissue and the typical pattern of knitting.* ***B-D:*** *GPIT/RE/3414,* ***B*** *– Lateral wall with an anterior extension of the posterolateral plug, interior, along the border to the marrow cavity (bottom left);* ***C*** *– Overview of posterolateral plug in the respective corner;* ***D*** *– Magnification of the posterolateral plug located in the upper center of C.* ***E-H:*** *GPIT/RE/3588,* ***E*** *– Magnification of the lateral wall showing high organizational degree of mainly circumferential canals in a laminar pattern;* ***F*** *– overview of the posterolateral corner with well visible growth zones and their interruption by the posterolateral plug. Note the transition from strongly alternating zones internally to almost no alternation externally (white arrows), which is assumed to be the mark of initial sexual maturity (MISM);* ***G*** *– Magnification of the central medial corner showing weak organization of vascular canals ranging from laminar to reticular pattern;* ***H*** *– Magnification of F showing the differences in organizational degree of vascular canals between fast and slow growing zones. Scale bars = 500µm in A, D, E, G. Scale bars = 1mm in B, C, F, H.*

In sections at the base of the latter, the posterolateral plug, as well as the posterolateral corner itself, is very faint and the posteromedial corner is much more pronounced and pointed instead. A similar structure as in the posterolateral corner is not developed though.

A similar structure is sometimes visible in the outer cortex of the anterior corner in more proximal sections close to the fourth trochanter and in larger sections (Fig. 6.5C-E). This cluster, however, does not much disturb the general organization of the tissue and is also far less widespread. On the other hand, large parts of the anterior corner can also consist of brightly reflecting bone tissue with only circumferential vascular canals. In contrast to all other areas in femoral bone, parallel-fibered matrix seems to be abundant here.

The zonation pattern is highly variable. LAG's and/or annuli are present, but only in less than 50% of all sampled femora. There is additionally no correlation between size and number of LAG's and annuli, so there are medium sized femora with a LAG and large femora without one (Fig. 6.4B, D). None of the cross sections record more than one or two LAG's and/or annuli. Nevertheless, these are the only structures of growth cycles, which can be followed around most of the cross section. The other type of growth cycles is much more abundant, but also much less distinctive. It is very difficult to follow these kind of zones even along half of the cross sectional circumference. In most cases, these zones are best distinguishable in the lateral side of the posterior wall close to the posterolateral plug (Figs. 6.4A-D; 6.5A-B; 6.6F, H). This kind of growth cycles consists on one hand of weakly reflecting (of polarized light) fast growing zones with mainly longitudinal oriented collagen

fibrils as well as numerous and dense primary osteons of relatively lesser degree of organization. The fast growing zones alternate with strongly reflecting slower growing zones with mainly transverse oriented collagen fibrils and less dense and more flattened primary osteons of relatively higher degree of organization (Fig. 6.6H). The relative distances between primary osteons are larger than in the fast growing zones. The transition from the fast growing to the slow growing zone is very diffuse. The outer or external rim of these slow growing zones is the best definable of the whole growth cycle and LAG's and/or annuli mainly occur close to or directly at their outer rim (Fig. 6.7A-B). Within the anterior corner, however, the slow growing zones often merge together to a relatively uniform slow growing area throughout the periosteal compact bone wall. The slow growing zones can, in contrast, also split up during their course. Splitting occurs mainly in the transitional area from a thinner wall to a thicker corner. Inside the very thick posteromedial corner, the slow growing zones become indistinct or can even vanish and only LAG's or annuli remain. The posterolateral plug interrupts the course of growth cycles almost completely.

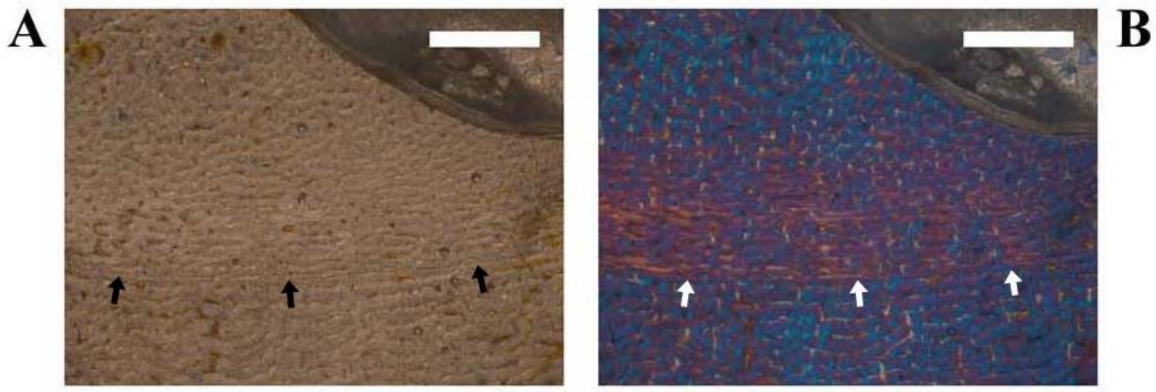

Fig. 6.7: *Sexually immature subadult femur GZG.V 6381/6434.* ***A-B: A*** *– Magnification of the interior medial corner with a single LAG (black arrows);* ***B*** *– The same as in A under polarized light combined with a λ-filter, the LAG clearly completes a growth cycle (white arrows). Marrow cavity is located at the upper right. Scale bars = 1mm.*

In five of the largest sectioned femora, there is a relatively abrupt transition between the general distinct sequence of growth cycles internally and a much more uniform area externally. It looks like a very thick slow growing zone, although a weak zonation is still recognizable (Figs. 6.4A-B;

6.5A-B; 6.6F). In a sixth specimen, there is no such a mark at all and the posterior wall bears a normal succession of growth cycles throughout its whole thickness.

Remodeling by secondary osteons is very scarce. There are only local occurrences of scattered secondary osteons, concentrating mainly on the inner part of the anterior corner along the border between the primary bone tissue and the wedge of CCCB. Isolated osteons are also present within the CCCB (Fig. 6.5G). Other isolated occurrences are located within the posterolateral plug, where clusters of scattered or several isolated secondary osteons are sometimes observable in variable distances from the external surface. Some of them could even lie very close to it. Even rarer are some isolated secondary osteons in the outer part of the anterior corner in more proximal sections. In sections of more distal cutting levels and closer to the metaphysis, secondary osteons become more abundant, especially in remaining areas of endochondral tissue, but there are never numerous generations establishing a Haversian system. However, the more distal the section was cut, the higher is the number of secondary osteons (as in a *Plateosaurus* fibula; Klein, 2004:56) and the larger is also the area occupied by CCCB.

Osteocyte lacunae are generally very abundant, although there are quite large differences in density. The highest densities were observed around the border between CCCB and the primary bone wall anteriorly and laterally, and within the posterolateral plug (Fig. 6.6D). As a matter of fact, the density of osteocyte lacunae is always higher in areas, where secondary remodeling is active. There are often also differences between the two main parts of each growth cycle and between different main units of a cross section. The fast growing zones possess relatively more lacunae than the slow growing zones. They are also much more rounded than the often flattened lacunae in the slow growing zones. The anterior corner and the walls of the cross sections possess a relatively lower density of osteocyte lacunae than the posteromedial and posterolateral corner and adjacent areas.

Sharpey's fibers are relatively common, but mainly as isolated and scattered bundles of different extent. Many are only visible by polarized reflection of their angled direction towards the external surface. Others have the appearance of a swarm of many isolated black fibers under normal

light. Some occur deep within the cortex and others close to or at the external bone surface. Although the size, orientation, and abundance are highly variable among different cross sections and even within a single section, there is a general repeatable pattern preserved. The medial side of the anterior corner often possesses fiber bundles directing medially. Following further medial along the medial wall towards the posteromedial corner, the fibers become more and more posteromedially and posteriorly directed. The posterior wall sometimes possesses posteriorly directed Sharpey's fibers. More complicated is the arrangement in the lateral side of the cross sections. Here, fiber bundles with posterior to posterolateral direction occur directly within and adjacent to the posterolateral plug in the respective corner, but soon after reaching the lateral wall, there could be fiber bundles with an anterolateral direction. The posterolaterally and anterolaterally directing fiber bundles can even cross each other along most of the lateral wall. Finally, there are sometimes small anteriorly directed fiber bundles close to the lateral side of the anterior corner.

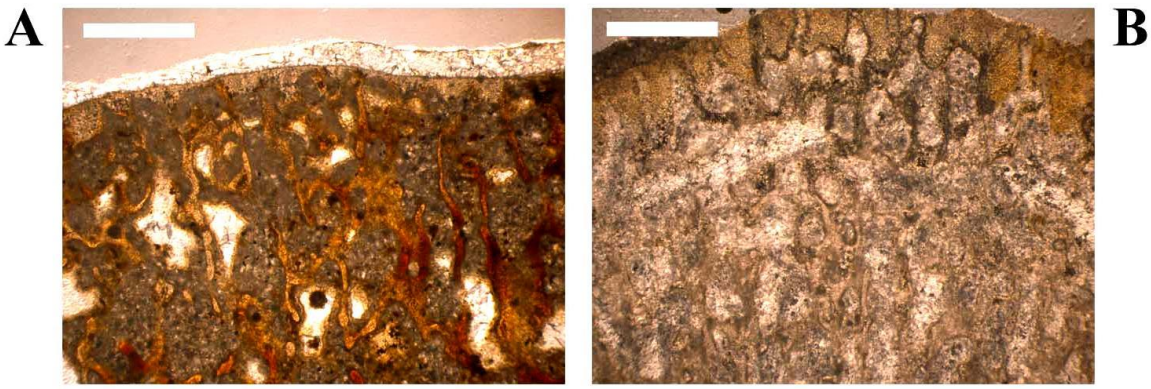

Fig. 6.8: *Longitudinal sections from the distal end of two femora. The distal side is on top. The slightly brighter foam-like structures directly at the periphery are pads of calcified cartilage. The net-like straps are endochondral trabeculae.* ***A:*** *Sexually mature adult femur GPIT/RE/3518, the calcified cartilage still builds the utmost periphery and is partially subdivided by trabecular bone;* ***B:*** *early juvenile femur GZG.V. 6379, the calcified cartilage is much thicker, but trabecular bone already comes very close to it in the centre. Scale bars = 500µm.*

Longitudinal sections of a large femur and of the smallest sampled femur (Fig. 6.8) reveal the structure of the distal epiphyseal ends of these bones. The large longitudinal section is thoroughly built by a meshwork of endochondral trabecular bone. The main direction of the bony straps is perpendicular to the plane of the preserved articular end and they are mainly parallel to each other

with numerous transverse connections. Close to the marginal rim of the epiphysis, this regular arrangement is lost in mainly randomly oriented straps. The individual thickness and length of the straps as well as the density and degree of interconnection of the trabecular meshwork decreases here distinctly. The meshwork of bony straps reaches the preserved distal end of the epiphysis, but pads of calcified cartilage are still very common and reaching up to 35µm from the distal rim into the epiphysis.

In the small femur, the pads of calcified cartilage extend up to 1mm into the epiphysis and isolated pads are also visible randomly between the straps of bone inside the epiphysis. The bony straps themselves are much thinner than in the large femur and the meshwork is much weaker developed with larger distances between the straps and less common interconnections. There is, though, a concentration of bony straps in the epiphyseal centre and it almost reaches the distal end. The endochondral ossification at the periphery of the epiphyses is, in contrast, very poor.

6.5.1.2 Ontogenetic stages in femora

Due to the highly variable features within the shaft, between different femoral cross sections, and even within a single section, ontogenetic stages are difficult to distinguish. Most of the features, such as degree of development of primary osteons, vascularization pattern, or secondary remodeling are therefore used only conditionally and the transition between successive ontogenetic stages is often smooth. The only good indicators are the number of growth cycles and the degree of development of certain structures, such as the posterolateral plug.

Stage 1 or embryonic/perinatal stage: This stage, already described in some other ornithopods (Horner et al., 2000; Horner et al., 2001; Horner et al., 2009), is not represented in the sampled femora of *Dysalotosaurus* and the overall size of other known specimens indicate that none of the preserved femora would fit into this stage.

Stage 2 or early juvenile stage (Fig. 6.9A-D): The marrow cavity is very large compared to the bone wall thickness. The internal anterior wedge, if present, consists of not yet compacted coarse cancellous bone. Especially the posterolateral corner is very weakly pronounced and the respective plug is only indicated. The periosteal compact bone tissue in this stage reveals a high amount of longitudinal vascular canals. The primary osteons are often quite isolated from each other by thick cords of well organized and relatively uniformly reflecting woven-fibered matrix (pattern of knitting). Especially in the internal part anteriorly, only simple vascular canals are present. If at all, there is only one slow growing zone developed at the external edge of the cortex.

Stage 3 or late juvenile stage: The external circumferential profile is now more pronounced and the posterolateral plug is well visible. The drift of the marrow cavity from approximately anterior to posterior is in progress, which is indicated by now well compacted CCCB of a larger anterior wedge as well as a deeper internal cut into the posterior bone wall (depends also on cutting level within the shaft). The primary osteons are more numerous and the amount of juvenile pattern of knitting is decreasing. There are first occurrences of isolated secondary osteons. Growth cycles are well distinguishable and reaching two to three in number at maximum (Fig. 6.9E).

Stage 4 or immature subadult stage: The development of the external cross sectional profile as well as of the single bone wall units (including the posterolateral plug) is now complete. The anterior wedge of CCCB is more pronounced, although this depends on the relative position within the shaft. The marrow cavity cuts deeply into the posterior wall. In the posteromedial corner and in the fast growing zones of the medial and the posterior wall, there is very few space left between the numerous and well developed primary osteons. Secondary osteons are more widespread anteriorly and can also occur in the posterolateral plug and in the external anterior plug. The number of growth cycles is three to five.

Stage 5 or sexually mature adult stage: The units of the cross sectional bone wall are strongly diversified. The anteroposterior migration of the marrow cavity interrupts up to four complete growth cycles posteriorly.

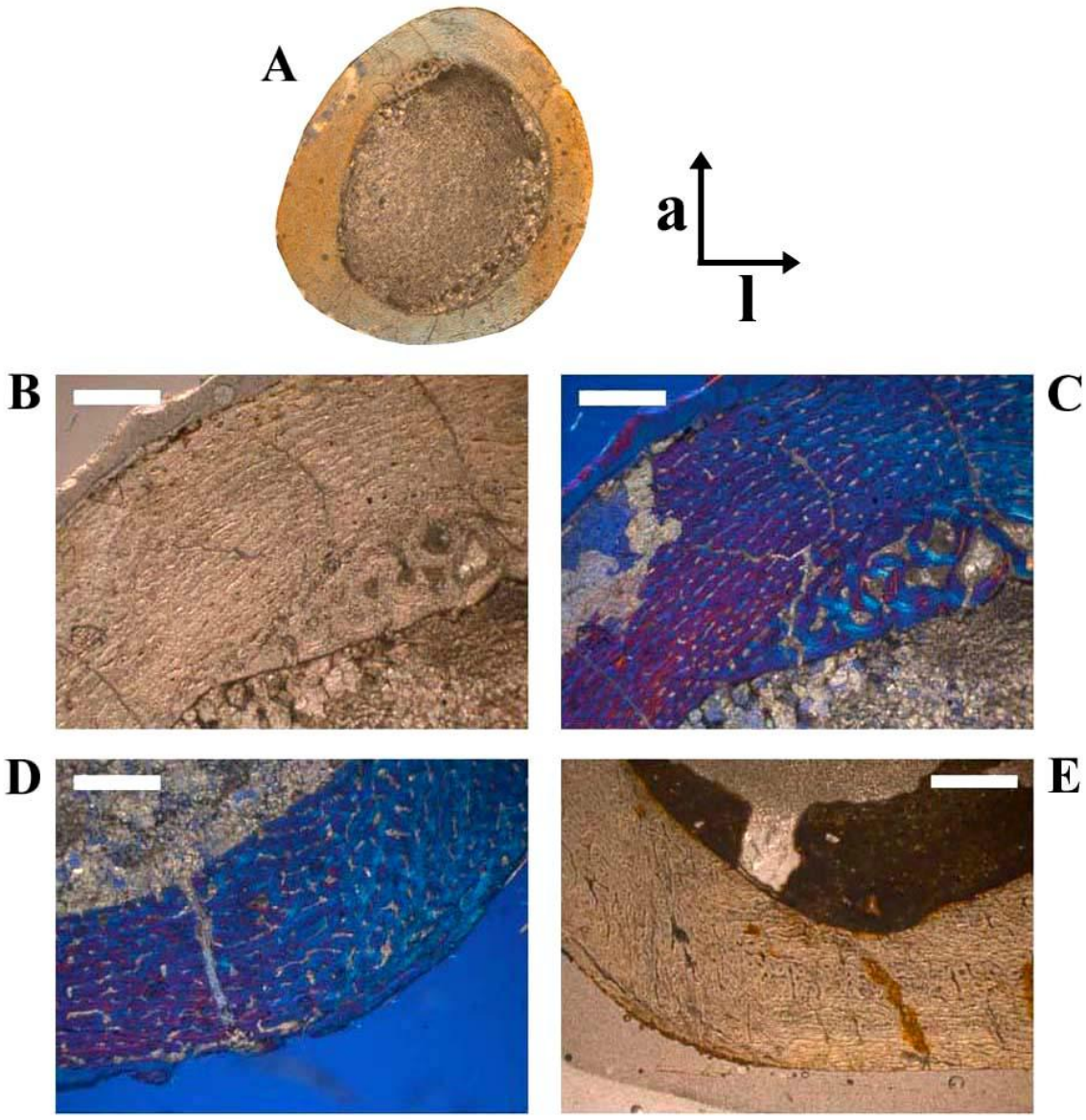

Fig. 6.9: *Cross sections of juvenile femora.* ***A-D:*** *early juvenile femur GZG.V. 6379,* ***A*** *– Overview of the whole cross section showing the weak differentiation of the sectional units;* ***B*** *– Magnification of anteromedial part of A under normal light, note the concentration of osteocyte lacunae at the border between the periosteal bone and the CCCB wedge;* ***C*** *– Same as B under polarized light combined with a λ-filter;* ***D*** *– Posterolateral corner under polarized light combined with a λ-filter, the posterolateral plug is very weak and there is no zonation.* ***E:*** *late juvenile femur GZG.V 6653 under normal light, the posterolateral plug is discernable and zonation is clearly present. All images are orientated as marked, except E, where the lateral side is on the left. A is not scaled. Scale bars = 500µm in B, C, D. Scale bar = 1mm in E.*

Secondary osteons are now numerous in clusters anteriorly and posterolaterally in different distances from the external surface. The number of growth cycles is up to nine and the transition

from well distinguishable fast and slow growing zones internally to the diffuse and more uniform wide zone externally is visible in five of the largest cross sections (Fig. 6.6F).

6.5.2 Bone histology of the tibia

6.5.2.1 Description

CT-scans have revealed the thickest periosteal cortex at approximately 30% of the shafts height, so most of the sections are located close to the little anterolateral bulge, which rises at this position (Fig. 5.13). As in the femur, the cross section can be separated into units, which help to clarify its original position in the articulated bone (Fig. 6.4E-H). The anterior wall is very straight, almost parallel to the mediolateral axis of the bone, and represents the counterpart for the articulated fibula. The anterolateral corner is often the thickest part of the cross section and is very acute angled and expanded. The anteromedial corner is less acute, but possible growth cycles change their course abruptly. The rest of the section consists of a relatively consistently curved posterior arch. This egg-like shape (Fig. 6.4G-H) becomes more and more circular proximally (Fig. 6.4E-F), but the straight anterior wall persists. The thinnest parts are either found in the anterior wall or in the lateral part of the posterior arch. The shape of the marrow cavity is more symmetrical than the external outline and the rim is almost always well defined and straight, except sometimes internal to the anterolateral corner. Here, CCCB can occur as a wedge, which extends only in the two largest cross sections far into the cortex (Figs. 6.4G-H; 6.10A, C-D). In most of the smaller sections and in the proximal ones, CCCB is absent. A slight medial shift of the marrow cavity is observed.

The internal fundamental system or endosteal layer is developed almost exclusively in medium to large sized sections with its maximum thickness in the anteromedial or anterolateral corner. There is, though, only one example, where the endosteal layer surrounds the marrow cavity almost completely. In the other sections, long pieces can be widely separated from each other.

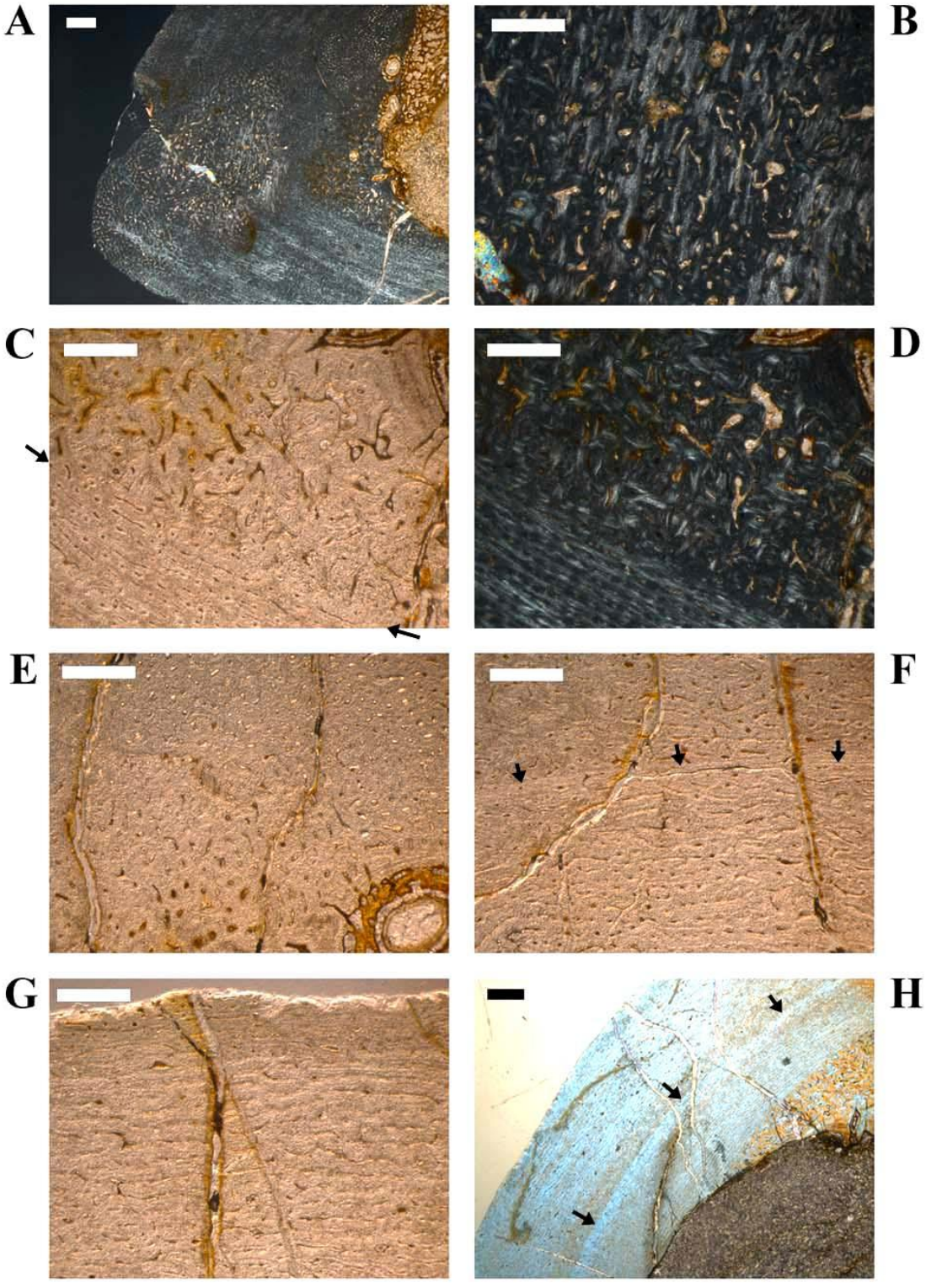

Fig. 6.10: *Sexually mature adult tibia SMNS T 3.* ***A-H: A*** *– Anterolateral corner under polarized light. Note the CCCB-wedge on the right side and the swirl-like plug structure within the bone wall. This structure is obviously inactive, because normal periosteal tissue is already deposited above it;* ***B*** *– Magnification of plug structure in A showing tissue strongly altered by bundles of Sharpey's fibers and secondary osteons;* ***C*** *– Magnification of transitional area between CCCB on the right and periosteal bone tissue on the left (arrows), image located in the lower right of A, under normal light; →*

← ***D*** *– Same as in C, under polarized light;* ***E*** *– Magnification of anterior side of anterolateral corner close to the marrow cavity (lower right) located in the upper right of A. Note the small, longitudinal, and weakly developed primary osteons typical for juvenile bone tissue;* ***F*** *– Image located exterior to E showing increasing abundance of circumferential vascular canals of laminar pattern with a single LAG in the center (arrows), marked as a red line in Fig. 4H;* ***G*** *– Image located exterior to F showing dominance of circumferential vascular canals in a laminar to sub-plexiform pattern;* ***H*** *– Lateral part of anterolateral corner, turned anti-clockwise compared to A, single LAG (arrows) completing slow growing zone (brightly reflecting bans internally), part of the CCCB-wedge on the right, under polarized light combined with a λ-filter. Scale bars = 1mm in A, H. Scale bars = 500µm in B-G.*

Similar to the femoral cross sections, the tibial cross sections consist generally of fibrolamellar bone tissue with a high density of well developed primary osteons.

There are also differences between different units of a cross section and between inner and outer areas of the bone wall. The medial part of the bone wall, and especially the anteromedial corner, is very densely packed with often relatively large primary osteons and very few amount of bone matrix in between them. Generally, the innermost areas of the medial and posterior units and sometimes also anterolateral close to the border of the CCCB consist of small, laminar organized, longitudinal osteons with relatively weak lamellar infilling. This is very similar to the innermost anterior area of femora, where early ontogenetic tissue is apparently preserved (Fig. 6.10C-E). The density of osteons also decreases slightly close to the external surface and the canals are often still open at the periphery even in the largest sectioned specimen. Less filled, but mainly larger and randomly orientated osteons are found anterolaterally approximately in the middle of the cortex. This rather circular structure is very similar in its appearance to the posterolateral plug in femora (Fig. 6.10A-B). It can even interrupt the zonation pattern. However, its extend inside the shaft is much smaller, because a bit further proximal from the lateral bulge, it vanishes almost completely and growth cycles are then rather well preserved in this corner.

The vascularization pattern is, as in femora, dominated by laminar organization, although the variability is also high. Generally, the thinner is the bone wall of a cross sectional unit the higher is the degree of organization. It is also observed that this degree increases towards the external surface and within slow growing zones. Thus, the laminar pattern dominates mainly in the anterior (Fig. 6.10F-G) and posterior to posterolateral wall, in slow growing zones, and in the outer cortex,

whereas plexiform and reticular tendencies are visible in the anteromedial, medial, and anterolateral bone walls, in the fast growing zones, and in the inner cortex (Fig. 6.11E). Reticular patterns are mainly developed in the anterolateral plug of the respective corner. The only mainly longitudinal arrangement is, as mentioned above, only preserved in the innermost parts of some cross sectional units.

Secondary remodeling is much scarcer than in femora. The only unit with preserved secondary osteons is the anterolateral corner. Scattered examples are found mainly in the outer area of the CCCB wedge and within the anterolateral plug (Fig. 6.10B). Small sections or sections from more proximal cutting levels (relative to the anterolateral bulge) are lacking secondary osteons completely.

The zonation pattern is similar to femora in having very few LAG's or annuli and mainly growth cycles consisting of fast and slow growing zones (Figs. 6.4H; 6.10A, F, H). There is also splitting and merging of slow growing zones and the number and arrangement among cross sections is very variable. In most sections, the distance between slow growing zones decreases towards the anterolateral corner and increases towards the whole medial side (Fig. 6.4H). This discrepancy of distances vanishes in more proximal sections (Fig. 6.4F). The growth cycles are best preserved in the anterior and/or medial wall and, in contrast to LAG's and annuli, they are not traceable around the bone wall. A transition from a distinct pattern of growth cycles internally to a more uniform area externally, as in five large femora, is not present.

In one of the large tibial cross sections (SMNS T3) at the anterior edge of the marrow cavity, a very special bone tissue is preserved (Figs. 6.4G-H; 6.11A-D). It is strongly cancellous with irregularly shaped caverns of various sizes. It reflects much less under polarized light. It is also clearly separated from the compact bone wall by an endosteal layer (Fig. 6.11C-D). Some of this tissue was also found inside two large caverns within the CCCB-wedge. All these features indicate that this tissue belongs to the endosteal type of tissue called medullary bone, which is already known in three other dinosaur taxa (Lee & Werning, 2008; Schweitzer et al., 2005).

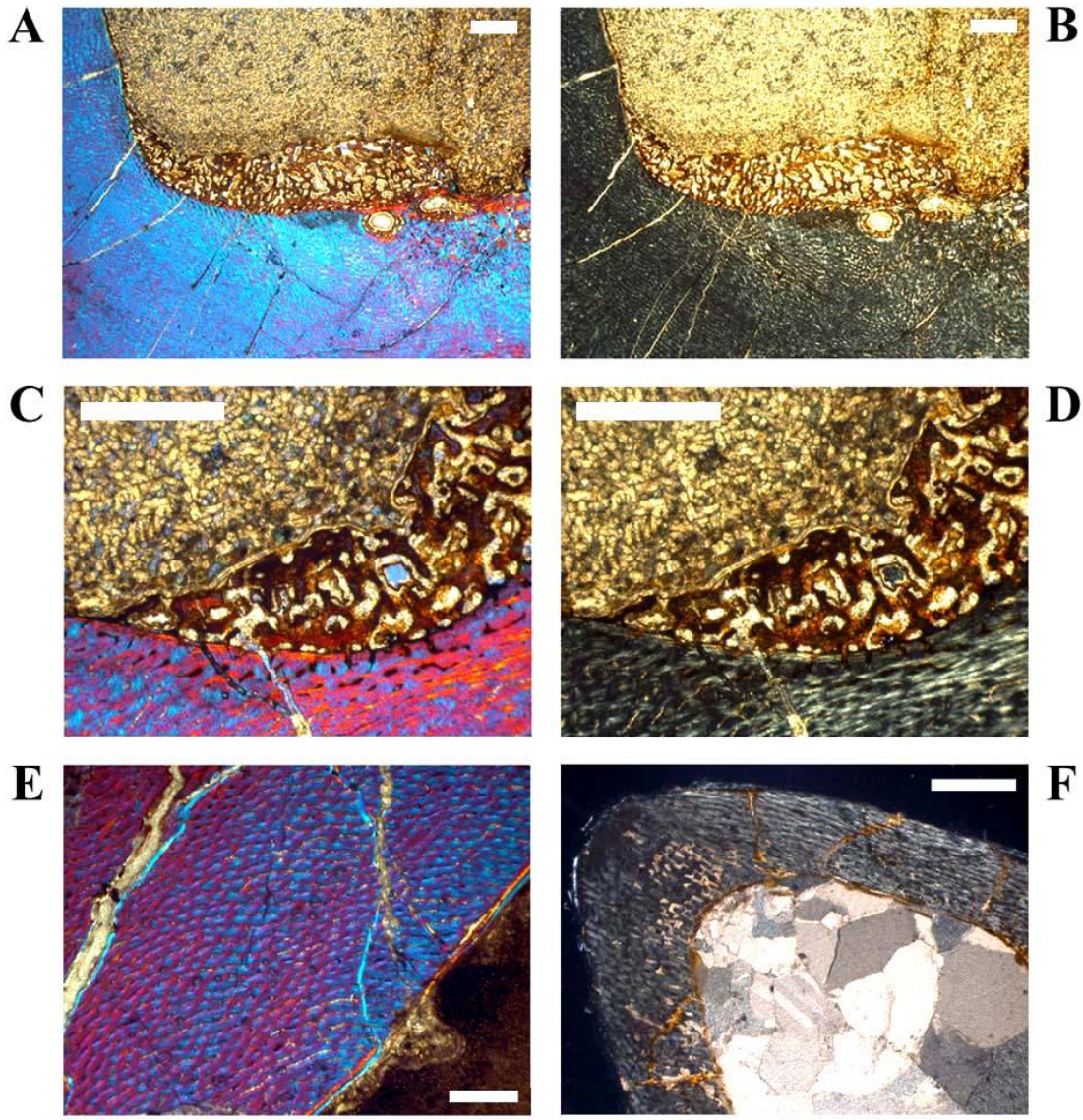

Fig. 6.11: ***A-D:*** *Sexually mature adult tibia SMNS T 3,* ***A*** *– Anterior side of the cross section, interiorly with medullary bone tissue spreading along the edge of the marrow cavity and into two large caverns within the bone wall, the wedge of CCCB begins at the central lower right, under polarized light combined with a λ-filter;* ***B*** *– Same as A under polarized light only;* ***C*** *– Magnification of A, note the thin endosteal layer separating the medullary bone from the periosteal bone wall, image slightly rotated anti-clockwise;* ***D*** *– Magnification of B, image slightly rotated anti-clockwise.* ***E:*** *Late juvenile to sexually immature subadult tibia SMNS T 7, interior posterolateral wall showing numerous well developed primary osteons in a plexiform to inclined radial pattern, the reddish band along the edge of the marrow cavity is a thin endosteal layer, the blue band represents diagenetic alteration, under polarized light combined with a λ-filter.* ***F:*** *Early juvenile tibia GPIT/RE/3795, anterolateral corner under polarized light. Scale bars = 1mm in A, B. Scale Bars = 500µm in C-F.*

Sharpey's fibers are relatively rare throughout the tibial cross sections, except in the anterolateral corner. Generally, the fiber bundles are more or less anterolaterally directed on the medial side of this corner and anteriorly directed on its lateral side. If the anterolateral plug is

present, much more directions are possible and fiber bundles are also present in the middle cortex, often only well visible under polarized light (Fig. 6.10A-B). A few weak anterolaterally directing fiber bundles are known from the anterior wall, anteriorly directed bundles from the anteromedial corner, anteromedially directed bundles from the medial wall, and laterally to posterolaterally directed bundles from the lateral wall. Most of these occur only in some of the sections.

As in the femora, the osteocyte lacunae are more abundant in the fast growing zones than in the slow growing zones. The highest density occurs in the anterolateral plug and in areas of secondary remodeling including the external rim of the CCCB wedge. The density generally decreases from the inner to the outer areas in all units.

6.5.2.2 Ontogenetic stages in tibiae

The differentiation of these stages in tibiae is more difficult than in femora, because there are fewer sections to compare with and most of the available specimens, belonging to a medium sized size range, are probably all of the same immature stage. However, the differences to the younger and older stages is significant, owing mainly to the preserved number of growth cycles, the number and distribution of secondary osteons, and the absolute size of the sampled specimens. Whereas the two younger stages belong to the group of smaller individuals in the size frequency distribution (see chapter 3), the oldest stage belongs to the group of large individuals, which are separated by a significant gap (see also chapter 6.7.3)

Stage 1 or embryonic stage: As in the femora, this stage is unknown in the tibiae.

Stage 2 or early juvenile stage: Probably only a single tibia belongs to this stage (Fig. 6.11F). The different units of the cross section differ only slightly from each other. Thus, apart from the anterolateral corner, the bone wall thickness is not very different in the whole section and there are no significant differences in the bone tissue. There is also no anterolateral plug, although the section is cut close to the expected level in the shaft. Secondary osteons, CCCB, an endosteal layer, and

resorption activity by the marrow cavity are all absent. Primary osteons are only visible medially and anteriorly, but despite of the high density, they are still under development. They are absent in the rest of the cross section, so that simple longitudinal canals in laminar arrangement dominate from the posterior bone wall to the anterolateral corner. This is very similar to the pattern of knitting observed in small femora. If at all, there is probably only the beginning of the first slow growing zone visible at the outer edge of the bone wall.

Stage 3 or late juvenile to immature subadult stage: In contrast to the former stage, these cross sections possess much better differentiated units including the anterolateral plug, which occur in the samples of the respective cutting level of the shaft. CCCB and secondary remodeling is observed in some of the sections. Resorptive activity of the marrow cavity is visible mainly anteriorly and posteromedially. The pattern of knitting with its simple arrangement of vascular canals is now only preserved in the inner cortex, whereas primary osteons are now well developed and widely distributed (Fig. 6.11E). Their density is highest anteromedially. At least two to three growth cycles are observed.

Stage 4 or sexually mature adult stage: The two largest samples belong to this stage. The cross sectional units are strongly differentiated and the bone wall thickness is highly variable. The CCCB tissue forms a large wedge, which reaches far into the cortex anterolaterally. There is a distinct swirl-like anterolateral plug incorporating most of the middle cortex and parts of the outer cortex of the respective corner. Simple juvenile vascularization is only preserved as a relict in some of the innermost parts. Secondary osteons are more abundant inside the anterolateral plug. Primary osteons are now very dense and there is only little space left for bone matrix in the thick anteromedial corner. The number of growth cycles exceeds three. Finally, medullary bone was found in one of the cross sections of this stage (see above).

6.5.3 Bone histology of the humerus

6.5.3.1 Description

The shape of the cross sections varies from a lateromedially wide and flatly oval outline distally to an almost circular oval shape more proximally (Fig. 6.4I-L). However, the shape and relative location of the marrow cavity, the relation of bone wall thickness to the size of the marrow cavity, and the arrangement of growth cycles helped to estimate the relative position of the section in the shaft of the respective humerus. Thus, cross sections taken distally from the mid diaphysis have relatively wide or large marrow cavities compared to the overall very consistent bone wall thickness (Figs. 6.4I-J; 6.12C). The cavity is also in a very central position of the cross section and has a consistently and lateromedially wider oval shape. Growth cycles are, additionally, arranged in a very consistent pattern, where the distances between each other as well as the distances to the external and internal edge of the bone wall do not vary significantly. In contrast, the external outline and the shape of the marrow cavity of the single section taken at or near the mid diaphysis (GPIT/RE/4262) are nearly circular. The bone wall is much thicker relatively to the marrow cavity and the latter lies exactly in the cross sectional centre. Nevertheless, the single preserved LAG is quite asymmetrical in its course, because it is resorbed by the marrow cavity medially and it rises up away from the cavity into the bone wall laterally. The cross sections taken proximally from the mid diaphysis have again a larger marrow cavity compared to the bone wall thickness than the mid diaphyseal section, but it strongly depends on the respective distance from the midshaft (Figs. 6.4K-L; 6.12A). In contrast to the other two cutting levels, the marrow cavity is slightly positioned medially to the cross sectional centre and it is also asymmetrical in shape. It is slightly tapering laterally because of an internally protruding low bulge of the anterolateral bone wall unit. Finally, the course of the growth cycles is also asymmetrical, so that the inner ones can be resorbed by the marrow cavity medially and they

are much closer to the external surface laterally. The distance between them is also much smaller laterally than medially.

CCCB is very rare and only visible in various units in the most distal or, anterolaterally, in the most proximal sections. More common is the preservation of an endosteal layer, although it never surrounds the marrow cavity completely. Mainly the sections cut slightly proximal to the middle of the shaft possess an endosteal layer of various thicknesses along the lateral rim of the marrow cavity (Fig. 6.4K-L) or they have a thick but short wedge of it concentrated in the anterolateral corner of the cavity (Fig. 6.12A).

The bone matrix of the primary compact bone wall consists mainly of fibrolamellar bone tissue, although the anterolateral corner can be built by brightly reflecting bone tissue of almost parallel-fibered type in some of the more proximal sections, as in the anterior corner of proximal femoral sections. However, this anterolateral plug is only visible in mid diaphyseal and proximal sections and it is much less distinct than in femora and tibiae (Fig. 6.12D).

Primary osteons are numerous and dense, but there are high numbers of relatively smaller osteons with a brightly reflecting single ring of lamellar infilling (Fig. 6.12B). Such small primary osteons are absent in femora and tibiae. The usual, well developed type of osteons is more dominating in the medial side of the humeral cross sections and within distinct fast growing zones, but both osteonal types can always be mixed up. The inner parts, as well as distinct slow growing zones, have often less well developed and/or smaller primary osteons.

The vascularization pattern is laminar dominated, but the organizational degree is increasing towards the external surface, within the thinner walls (especially anterolateral), and within the slow growing zones. The innermost part of the anterolateral or lateral unit often consists of longitudinal vascularization. There are always transitions to plexiform or even reticular patterns, especially within fast growing zones directly external to annuli or LAG's (Fig. 6.12D-E). Mainly in proximal sections, there are also large radial canals visible, which can extend throughout the whole thickness of the cortex (Fig. 6.12A).

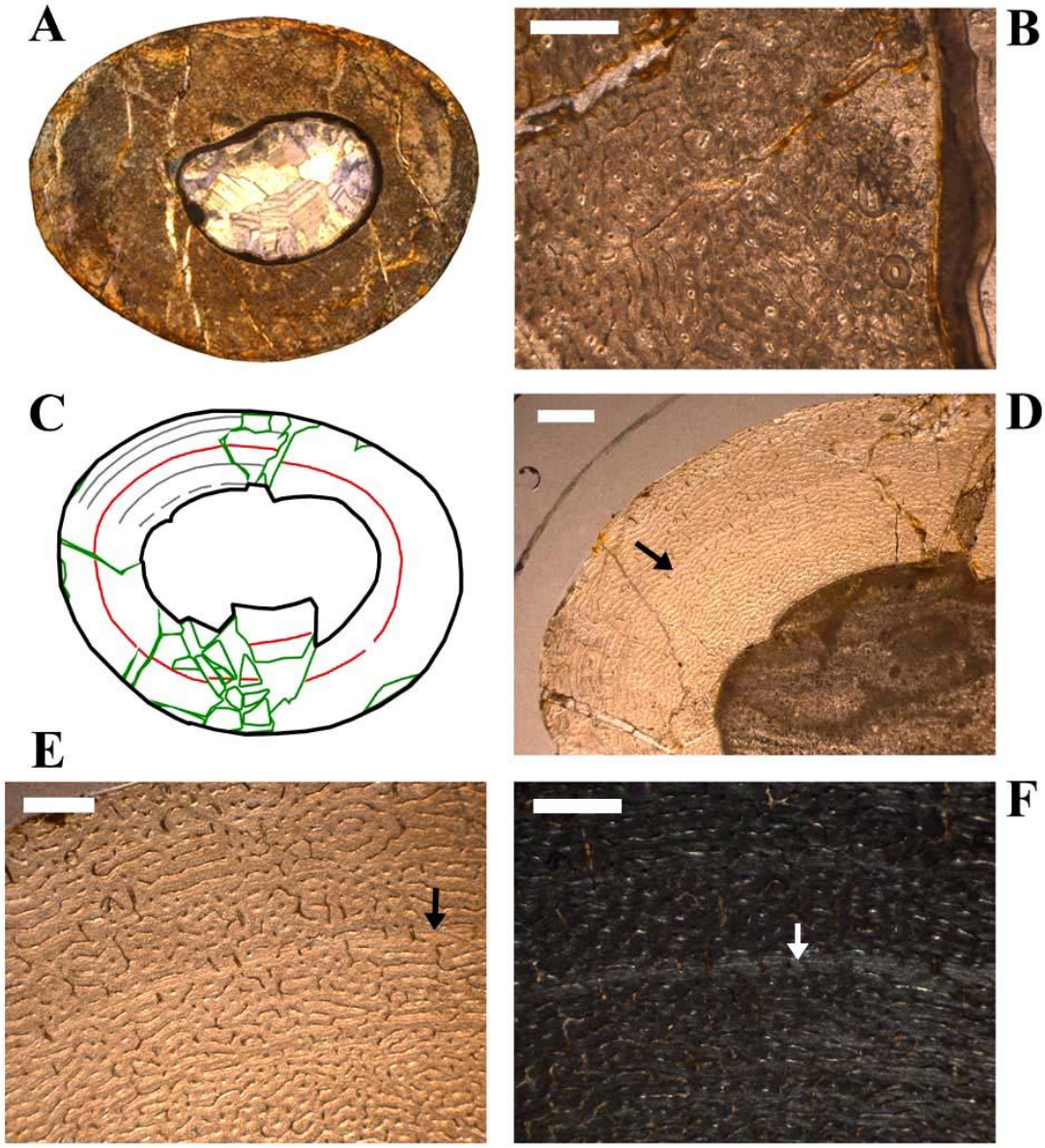

Fig. 6.12: ***A-B:*** *Juvenile humerus GPIT/RE/4402,* ***A*** *– Overview, anterior side on top and lateral side on the left. Note the wedge of endosteal lamellae anterolaterally and the inclined radial canals posteriorly;* ***B*** *– Magnification of A located anterior to the endosteal wedge, marrow cavity on the right, primary osteons are often longitudinal, very small, and filled with a single lamella, some secondary osteons are scattered close to the thin endosteal layer.* ***C-F:*** *Adult humerus GZG.V 6569, orientated as in A;* ***C*** *– Four secured growth cycles (LAG in red) and one unsecured cycle (dashed line) are preserved;* ***D*** *– Magnification of C showing the anterolateral corner. The slow growing zones immediately internal and external to the LAG (arrow) are only developed as an annulus in this cross sectional unit. They are much less distinctive in other units. Note the thick bone laminae of the plug-like structure on the left;* ***E*** *– Magnification of D showing the increasing dominance of the laminar pattern of vascular canals towards the periphery, but no significant difference within a single growth cycle. The slow growing zones are very thin and representing a rather abrupt slow-down of growth (LAG marked by arrow);* ***F*** *– Same as E under polarized light, LAG (arrow) is developed as a white line. A and C not scaled. Scale bars = 500µm in B, E, F. Scale bar = 1mm in D.*

They are strongly medially inclined, almost convoluting, and become more and more perpendicular towards the external surface closer to the medial corner. They are always more distinct and numerous in the posterior wall than in the anterior wall.

LAG's and/or annuli are more abundant than in femora and tibiae, but their distribution is still very inconsistent (Fig. 6.12C-F).

Secondary osteons are very rare. There are often some at the edge of the CCCB in most distal or proximal sections, but they mainly occur close to the internal margin of the anterolateral corner along the edge of the short endosteal layer (Fig. 6.12B) or within the anterolateral plug, if present.

As in the other long bones, osteocyte lacunae are denser within fast growing zones, in the anterolateral plug, and in the scarce areas of secondary remodeling. Sharpey's fibers are common and are similar orientated as the long radial canals with a strong medial inclination, which becomes perpendicular to the external surface in the medial corner itself.

6.5.3.2 Ontogenetic stages in humeri

The differentiation of cross sections in ontogenetic stages is much more ambiguous than in the femora and tibiae. The only unambiguous features usable for a separation are absolute size and the number of preserved growth cycles.

Stage 1 or embryonic stage: As in the other sectioned elements, this stage is not preserved.

Stage 2 or juvenile stage: The smallest sections with not more than a single growth cycle belong to this stage. The slow growing part (zone, annulus, or LAG) exists close to or at the outer rim of the bone wall. The degree of organization of the vascular canals is low, so that plexiform to sometimes reticular tissue type predominates.

Stage 3 or post-juvenile stage: All remaining cross sections belong to this stage and a further subdivision is not possible. The number of growth cycles exceeds one and the laminar vascular pattern predominates.

6.5.4 Bone histology of the fibula

Due to the scarcity of preservation of fibulae, cross sections could only be produced from levels very close to or within their proximal metaphysis. Therefore, periosteal compact bone is, if at all, often present as a thin layer surrounding parts of the bone wall externally and it is impossible to get a truthful count of growth cycles.

The overall shape of the cross sections is oval to kidney-like with very thick and strongly curved bone walls anteriorly and posteriorly, which also represent the long axis of the sections. The lateral unit is consistently convex, whereas the medial wall is distinctly concave (Fig. 6.13A). This concavity is bordered anteriorly and posteriorly by medially protruding corners, and these three structures together represent the cross sectional external shape of the attachment site of the M. flexor digitorum longus, running from the medial edge of the proximal joint distally (chapter 5.4).

Most of the thickness of the bone wall consists of already compacted coarse cancellous bone externally and not yet compacted cancellous bone internally towards the wide marrow cavity. Thus, most of the outer rim of the marrow cavity (especially in the anterior and posterior corners) is poorly defined because of wide cavernous spaces surrounded by a loose network of trabeculae. A more consistent rim was found along the thinner lateral and medial walls. Here are also the only locations, where an endosteal layer can be preserved. This band of lamellar bone is usually delicately thin laterally, much thicker medially, and especially thick posteromedially. In the cross section of the large fibula GPIT/RE/5109, possible medullary bone is preserved internal to this posteromedial thickest and partially out fanning part of endosteal layer (Fig. 6.13A-C). The medullary bone tissue also differs from the CCCB external to the endosteal layer by the lack of the brightly reflecting lamellar bone matrix typical for the latter, by the complete lack of any osteonal development, and a much higher density of osteocyte lacunae within its reticular network.

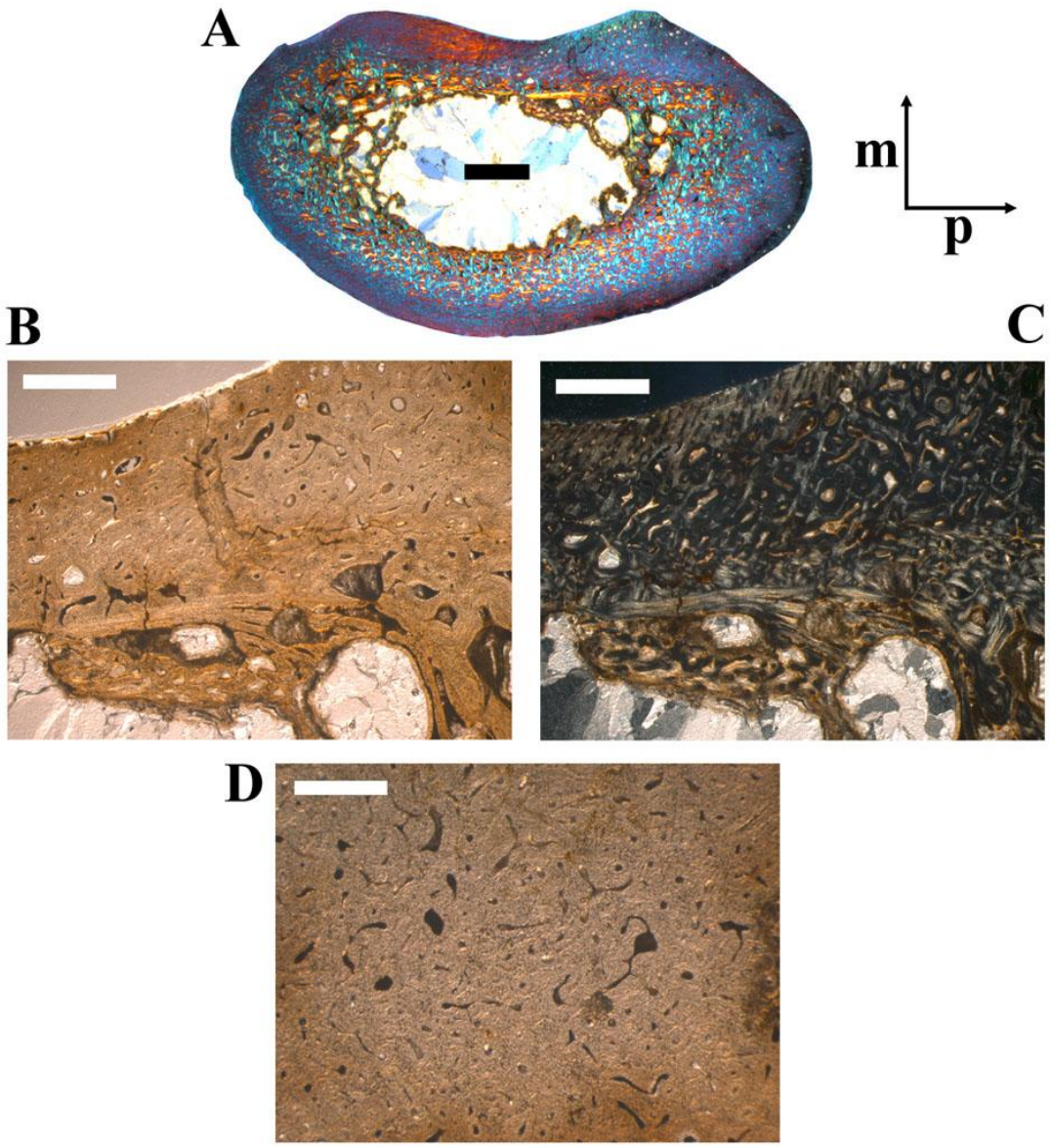

Fig. 6.13: ***A-D:*** *Fibula GPIT/RE/5109,* ***A*** *– Overview under polarized light combined with a λ-filter. The brightly reflecting and colored interior part represents CCCB;* ***B*** *– Magnification of A under normal light located at the posterior part of the medial wall showing the coarse secondary remodeling of the bone wall and the thick and fanning endosteal layer. Internal to the latter lies tissue interpreted as medullary bone;* ***C*** *– Same as in B under polarized light, the different layers of bone tissue are now well visible and start internally with medullary bone, followed towards the periphery by the endosteal layer, an anterior extension of CCCB, an inner strongly remodeled periosteal tissue, and an outer not yet remodeled periosteal tissue. Note that the latter tissue is heavily altered by Sharpey's fibers and that it has an almost metaplastic character;* ***D*** *– Magnification of the central posterior corner of A under normal light. The image is dominated by CCCB, most of the small and longitudinal vascular canals are secondary osteons. Scale bar = 1mm in A. Scale bars = 500µm in B-D.*

The thin layer of periosteal primary compact bone tissue is mainly present at the outermost area of the anterior, lateral, and posterior side of the cross sections. It consists of fibrolamellar bone

tissue, although the primary osteons are often relatively small and not very dense. Between this periosteal bone tissue and the CCCB, endochondral bone tissue often extends there with a dense, diffuse matrix and rare vascular canals. The medial wall differs strongly from the other units, because it is heavily altered by dense Sharpey's fibers, which let the area reflect very brightly under polarized light (Fig. 6.13C). They ascend more and more steeply towards the surface the closer they are to the posteromedial part of the medial wall. The bone matrix seems to be completely metaplastic in origin and the vascular canals are almost unfilled, elongated, and also orientated parallel to the Sharpey's fibers.

Secondary osteons are very common in these metaphyseal cross sections. The CCCB is not involved, but its external border and most of the endochondral tissue is, especially in the large specimens, strongly remodeled (Fig. 6.13D). Interior and mid areas of the posterior corner consist sometimes even of dense haversian tissue of at least two generations of secondary osteons. The medial wall is affected by very coarse remodeling, because the secondary osteons are less numerous and scattered. They are also much larger than in the other units and can also affect areas close to the outer surface. The inner part of the medial wall even consists almost entirely of secondary coarse cancellous bone (Fig. 6.13B-C).

High concentrations of osteocyte lacunae were always found in areas of high activity (secondary remodeling) and assumed high biomechanical stresses (medial wall close to the muscle attachment site).

6.5.5 Bone histology of the prepubic process of the pubis

In contrast to the other sampled and described skeletal elements, the prepubic process expands almost horizontally and in anterior direction. Thus, the obtained cross sections are vertically oriented and, additionally to the lateral and medial orientations within the sections, their top and bottom represent now the dorsal and ventral sides.

The sections cut directly at the maximum lateromedial width of the prepubic process, which is located in the proximal half of the process, has a wide oval shape (Fig. 6.14A). The external outline is relatively consistent apart from the lateroventral corner, which is slightly acute angled. Sections of more distal/anterior levels from the maximum width of the prepubic process have a much more triangular to lamp shade-like external outline (Fig. 6.14B). Here, the lateroventral and medioventral corners are very acute angled. The dorsal half is deeply but consistently convex, whereas the ventral rim is straight to slightly concave.

The periosteal compact bone wall is very thin compared to the overall diameter of the cross sections. There is no consistent internal margin, because there is no single large marrow cavity. This space is almost entirely filled with spongiosa. However, some of the internal cavities are quiet large, sometimes reaching the relative dimensions of a small marrow cavity. In the proximal sections, the largest of these pseudo cavities are always located in the medial half of the trabecular area and they become successively smaller towards the lateral side (Fig. 6.14A). In more distal sections, there are no significant size differences. These cavities are always of resorptive nature, because remnants of periosteal compact bone are often still preserved in some of the thicker trabeculae (Fig. 6.14C).

This periosteal compact bone consists of vascular fibrolamellar bone tissue. Well developed primary osteons are mainly visible in the dorsal and medial part of the bone wall, but they are not very dense and mostly longitudinal and only sometimes slightly plexiform (Fig. 6.14C, E). In the ventral bone wall and, in some sections, even in some dorsal and medial units, primary osteons are rarer, relatively small, and weakly developed. Here, the matrix is often almost opaque and the vascular canals are only longitudinally organized (Fig. 6.14D). Growth cycles are very rare, but in some sections there are at least one to two annuli and/or LAG's preserved in the ventral and/or dorsal unit of the bone wall.

The whole lateral bend of the bone wall is very different compared to the other units (Fig. 6.14A-B). Instead of woven matrix with vascular canals and/or primary osteons, a highly modified tissue was observed, which is very similar to the medial side in the fibular cross sections (Fig. 6.13).

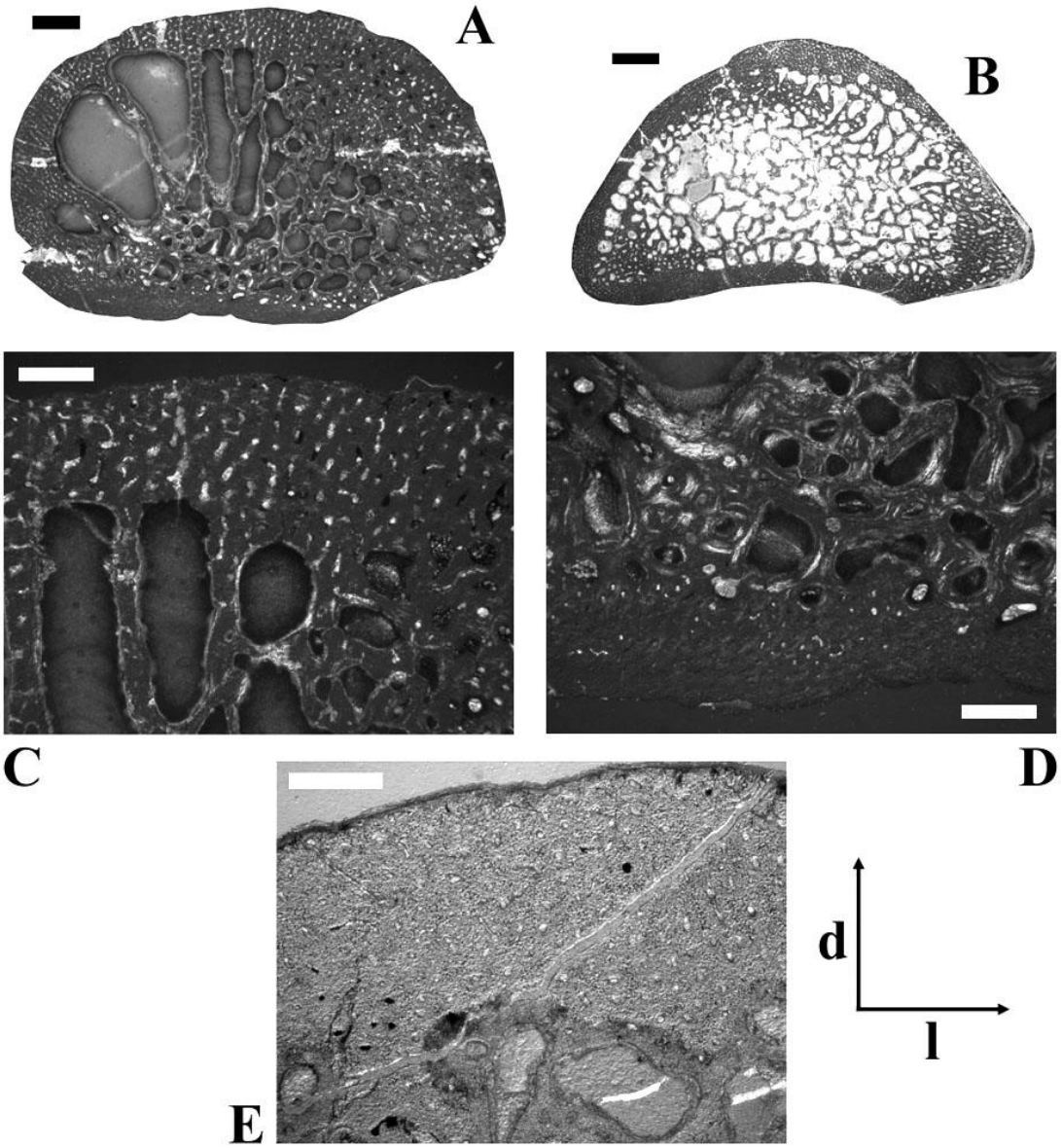

Fig. 6.14: ***A:*** *Proximal cross section of prepubic process of pubis SMNS P 17, overview under polarized light. Note the decreasing size of cavities towards the lateral side and the lateroventrally directed canals in the lateral corner.* ***B:*** *Distal cross section of prepubic process of pubis SMNS P 19, overview under polarized light. The inner space is completely trabecular. The canals in the lateral corner are directed more laterally.* ***C:*** *Magnification of A located within the dorsal centre. The trabeculae consist mainly of periosteal bone tissue with weakly developed primary osteons. The secondary lamellar deposition on the edges of the cavities has started already.* ***D:*** *Magnification of A located medioventrally showing rare vascularization of the periosteal bone wall, the internal tissue is of CCCB type in this unit.* ***E:*** *Magnification of B located within the dorsal centre under normal light. Scale bar = 1mm in A. Scale bar = 2mm in B. Scale bar = 500µm in C-E.*

The parallel-fibered or metaplastic matrix is altered by strong Sharpey's fibers and many resorptive cavities. The latter are often secondarily filled, so that large secondary osteons are

developed. The orientation of these cavities is the same as the lateroventrally directing Sharpey's fibers.

Secondary remodeling is, apart from the lateral bend, very common (Fig. 6.14C). Numerous small secondary osteons occur in the trabeculae between the large pseudo cavities as well as in the internal areas of the periosteal compact bone wall, where they are sometimes even form a dense haversian tissue. Their abundance is decreasing towards the medial side.

Sharpey's fibers are generally very common and the closer they are located to the lateroventral corner the more they are directed laterally or lateroventrally. Some fiber bundles are also directing medially and medioventrally, if they are close to the medial side.

Osteocyte lacunae are, as usual, most dense in areas of secondary remodeling and in areas occupied by numerous Sharpey's fibers, which is especially observed in the lateral bend of the sections.

6.6 Quantitative results

The combination and correlation of the fractional values of the growth cycles for each group of cross sections resulted in a quite consistent number of years represented by these cycles. Thus, the combined growth cycles in femur group one (sections from the top of the proximodistal shelf close to the middle of the shaft) represent 11 years, femur group two (sections from the base of the fourth trochanter) represent 12 years (Fig. 6.15), and tibia group one (sections close to the lateral bulge in the distal shaft) represents 11 years (Fig. 6.16). The only group for humeri represents ten years recorded by all combined growth cycles (Fig. 6.17), although several cycles were probably not recognized (compare with Tab. 3). The remaining groups three and four in femora as well as group two in tibiae contain only three to four cross sections without enough preserved growth cycles for a secured correlation. Finally, the MISM in femora always correlates with an age of approximately 9.5 years in femur group one and 10.5 years in femur group two (Figs. 6.15; 6.18).

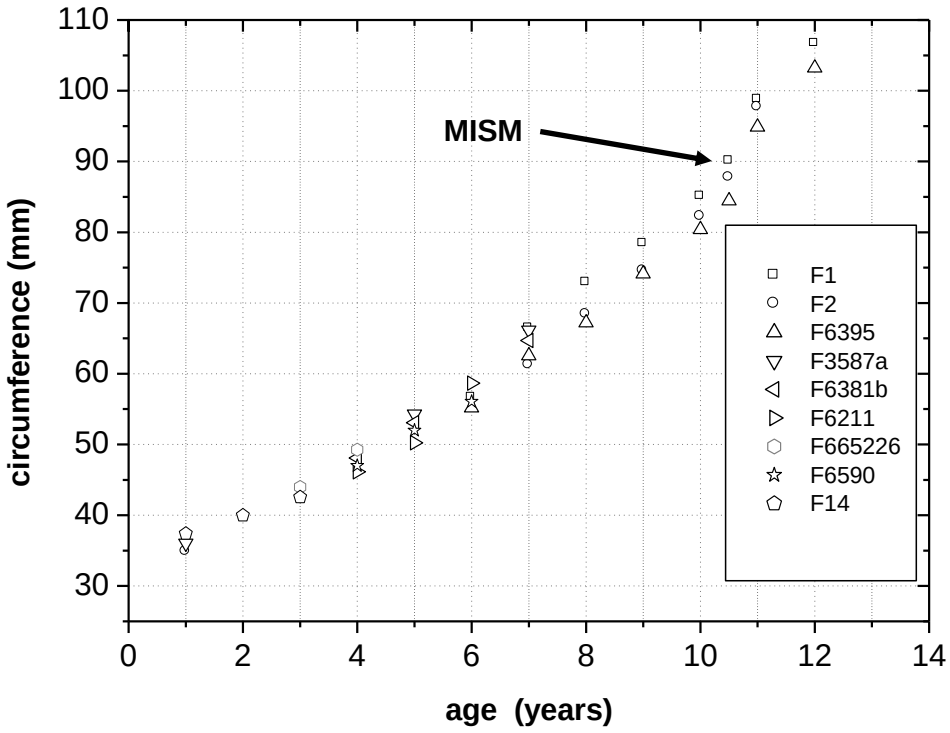

Fig. 6.15: *Fractional growth cycle values of femoral group two are correlated to age. MISM = Mark of Initial Sexual Maturity.*

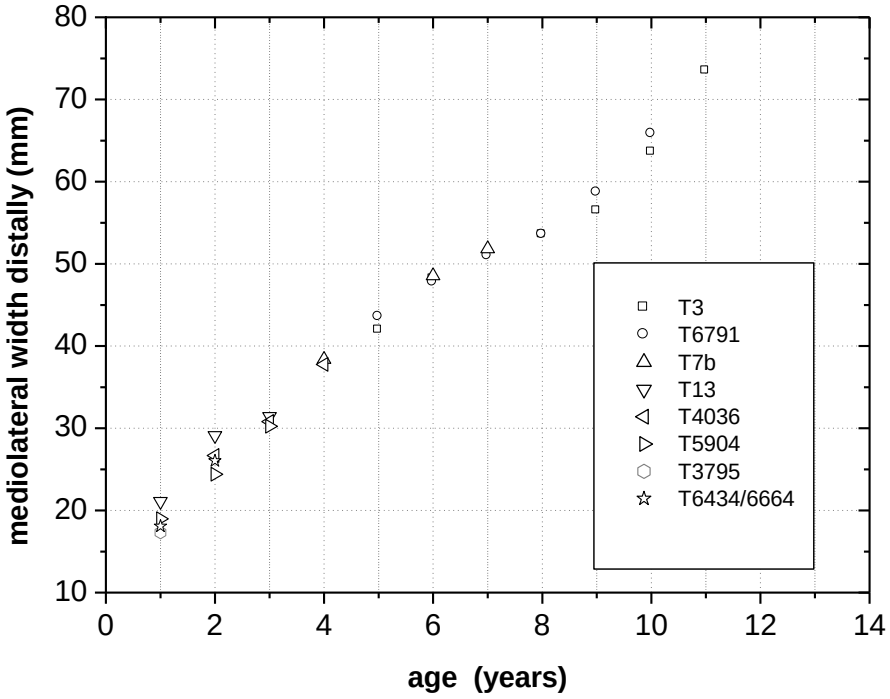

Fig. 6.16: *Fractional growth cycle values of tibia group one are correlated to age.*

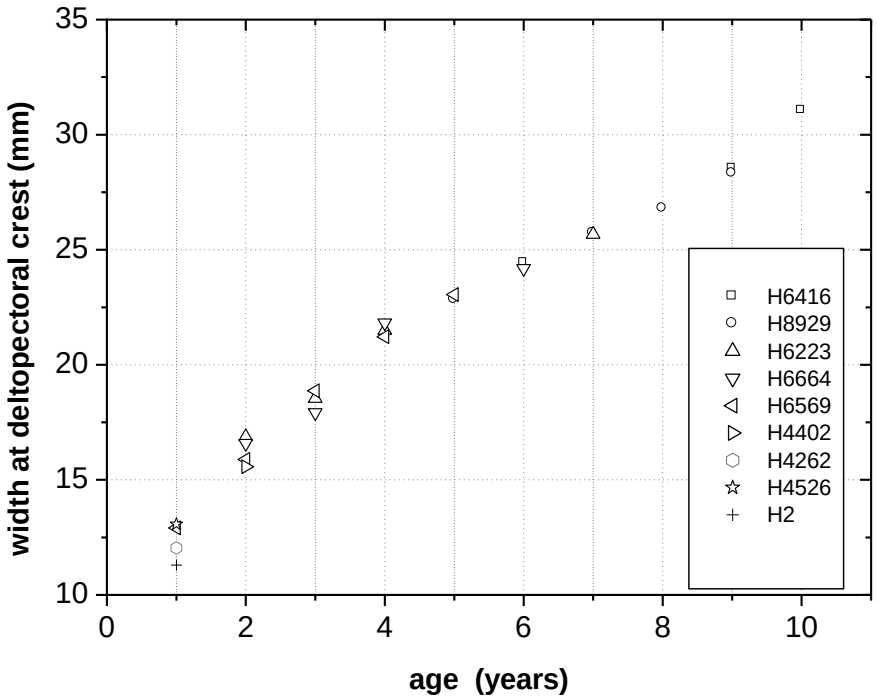

Fig. 6.17: *Fractional growth cycle values of the single group of humeri are correlated to age.*

To calculate the respective body masses for the correlated growth cycles with the Developmental Mass Extrapolation method (Erickson & Tumanova, 2000), and to finally calculate the sigmoidal growth curves, it was necessary to calculate the maximum body mass. The largest femur

specimen (MB.R.2144), which consists of a distal end of a left femur, represents a calculated body mass of 116.53kg by using the method of Anderson et al. (1985) for bipeds. In the same way, the respective body mass at the MISM was calculated with 32.44kg in average for the femur group one and 31.96kg for femur group two.

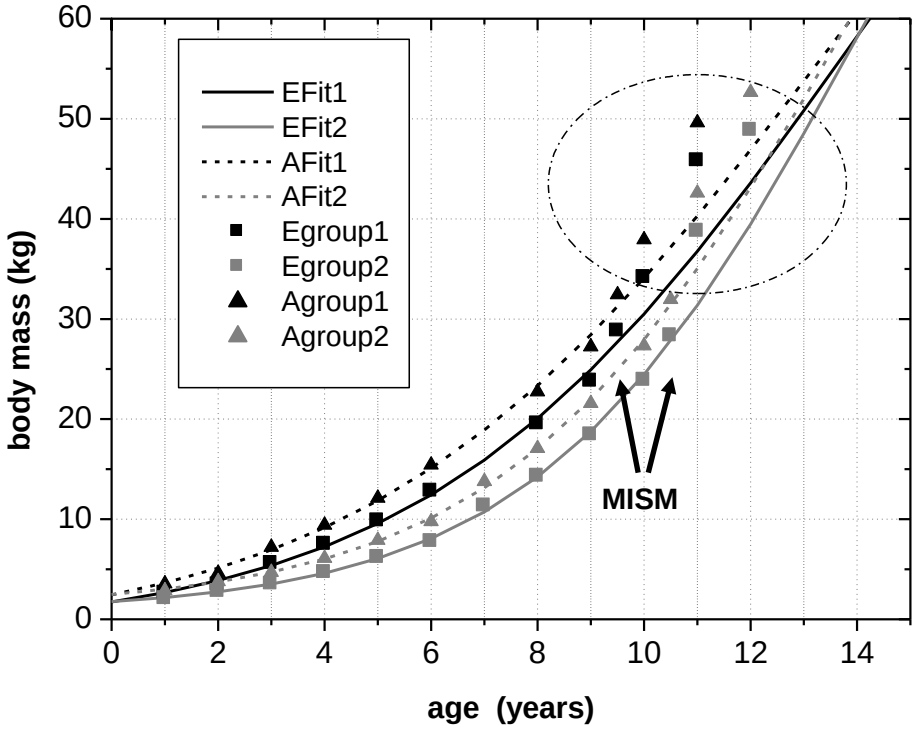

Fig. 6.18: *The nine correlated growth cycle values of femoral group one and two were combined with the values of the MISM (Mark of Initial Sexual Maturity) and used for the calculation of four growth curves. All encircled values represent unsecured growth cycles external to the MISM and were plotted into the diagram afterwards. The shift of these points onto their respective growth curves would result in a graphical change of only one additional year in age in average. Thus, 13 years are finally represented by all visible growth cycle values.* ***Abbr.: EFit1*** *– Growth curve of femoral group one, calculated with body masses derived from Erickson & Tumanova (2000);* ***EFit2*** *– Growth curve of femoral group two, calculated with body masses derived from Erickson & Tumanova (2000);* ***AFit1*** *– Growth curve of femoral group one, calculated with body masses derived from Anderson et al. (1985);* ***AFit2*** *– Growth curve of femoral group two, calculated with body masses derived from Anderson et al. (1985);* ***Egroup1*** *– Correlated fractional growth cycle values of femoral group one, the respective body masses are derived from Erickson & Tumanova (2000);* ***Egroup2*** *– Correlated fractional growth cycle values of femoral group two, the respective body masses are derived from Erickson & Tumanova (2000);* ***Agroup1*** *– Correlated fractional growth cycle values of femoral group one, the respective body masses are derived from Anderson et al. (1985);* ***Agroup2*** *– Correlated fractional growth cycle values of femoral group two, the respective body masses are derived from Anderson et al. (1985).*

By using the first nine (femur group one) to ten (femur group two) secured growth cycle values, the respective values of the MISM, and the maximum body mass, four sigmoidal growth

curves were created. The remaining growth cycle values, representing unsecured growth cycles externally to the MISM, were plotted into the curves afterwards (Fig. 6.18). The manual shift of these values by, in average, one year resulted in the ideal fit onto their respective growth curves. At the end, a total of 13 years of life of *Dysalotosaurus* are represented by the observed and correlated growth cycles in the femoral cross sections of group one and two (Fig. 6.18).

The now known values of the four parameters of each of the four growth curves were used to calculate the respective values for all known femora of *Dysalotosaurus*. The largest sampled femur (SMNS F2, group two) would therefore represent an age of 16.5 years (body mass after Anderson et al., 1985) or 16.3 years (body mass after Erickson & Tumanova, 2000). The age of the second largest femur found in the collections (R12277) would then represent an age of 19.7 years (after Anderson et al. 1985) or 19.3 years (after Erickson & Tumanova, 2000) (Fig. 6.19).

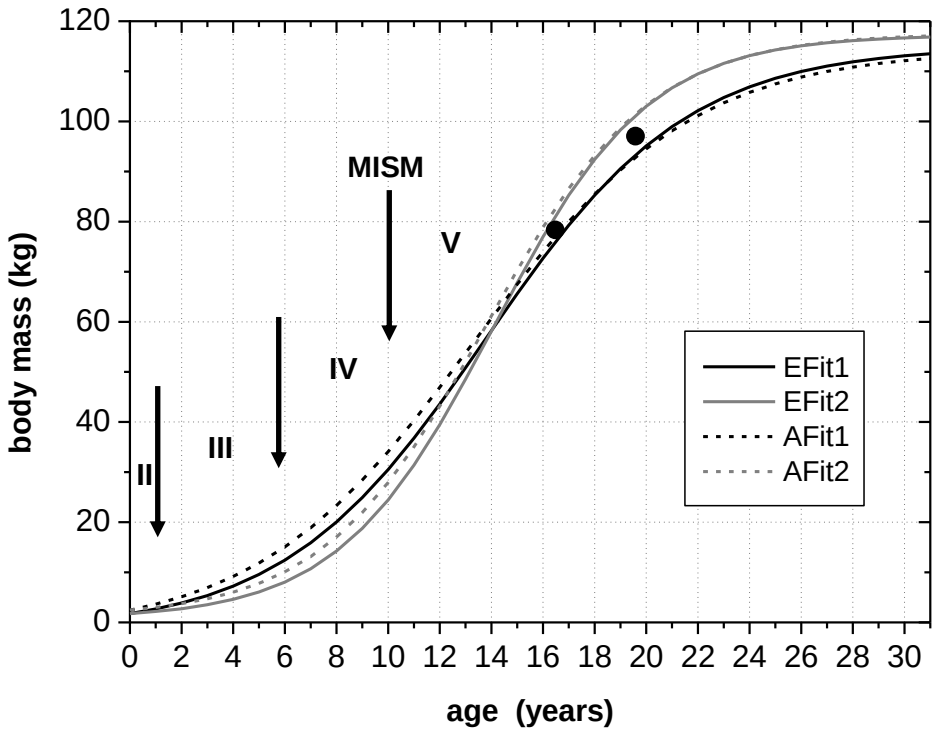

Fig. 6.19: *The four complete growth curves derived from the values shown in Fig. 6.18. Abbreviations are as in Fig. 18. The arrows separate the ontogenetic stages observed in the femoral cross sections:* ***II*** *– Early juvenile stage;* ***III*** *– Late juvenile stage;* ***IV*** *– sexually immature subadult stage;* ***V*** *– sexually mature adult stage. The black point at app. 16.5 years of age represents the largest sampled femur. The black point at app. 19.5 years of age represents the second largest preserved femur.*

The MISM is located well between the lower and middle third of the growth curves, if body mass is plotted versus age. Thus, the growth rate of body mass is still accelerating after this mark and reaches its maximum in the 14th year with a daily increase of 24 to 26 grams (for femur group two). However, by plotting the respective values of the femoral distance 18 or the midshaft circumference (representing body size) versus age, the MISM is now located very close to the centre of the curve, which is also the inflection point between accelerating and decelerating growth rate (Fig. 6.20). Finally, the relative body size of *Dysalotosaurus* at the MISM reaches 62.1% for the femur distance 18 and 63.4% for the midshaft circumference compared to known maximum body size.

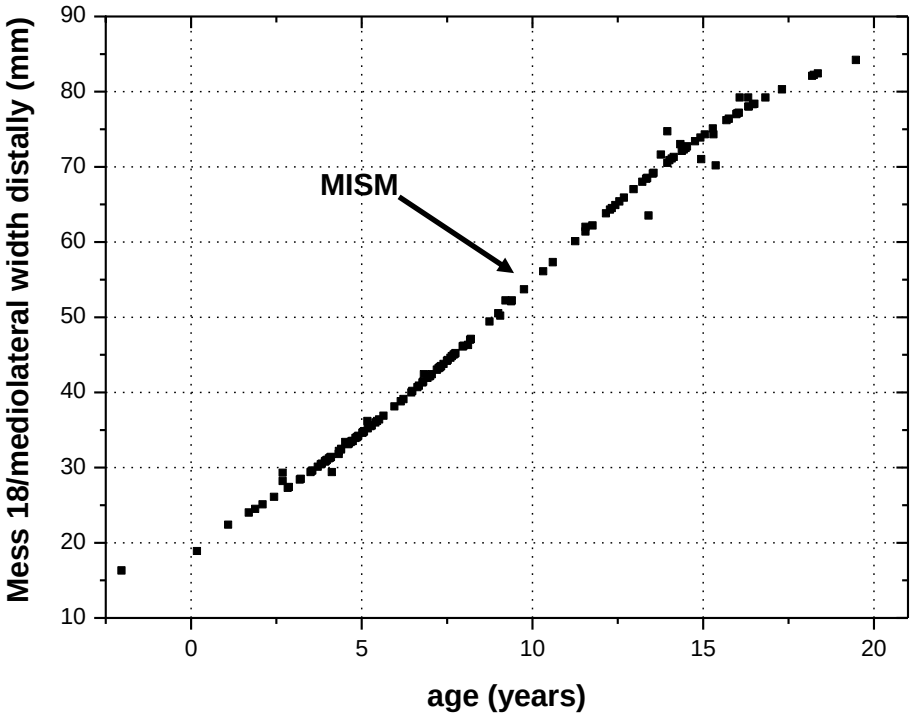

Fig. 6.20: *In contrast to the diagrams with body mass versus age, the Mark of Initial Sexually Maturity (MISM) is almost exactly positioned at the inflection point in a curve with body size versus age. Measured and calculated values of Mess 18 are combined. The age values are an average of the respective values calculated by the methods of Anderson et al. (1985) and Erickson & Tumanova (2000).*

6.7 Discussion

6.7.1 Variation of bone tissues in *Dysalotosaurus*

Variation of tissue types in *Dysalotosaurus* bones is extraordinarily widespread. It is therefore the ideal model to demonstrate, in how many ways and by which reasons bone tissues can vary between different individuals of a taxon, within an ontogenetic series, within a single animal, within a single bone, and even within a single cross section. This variation also clearly implies that comparative bone histology is only significant, when the sampling is standardized, several skeletal elements are included, and the ontogenetic stage is considered (e.g. Chinsamy-Turan, 2005; Horner et al., 1999; 2000).

Significant variation in bone tissue was found between different elements of the skeleton of *Dysalotosaurus*. The bone wall of the main weight bearing long bones (femora, tibiae) are naturally thicker than in the sampled humeri, fibulae, and prepubic processes. Interestingly, the relative growth rate is also higher in these long bones compared to the other three elements, which is inferred from the density and organizational degree of vascular canals (see e.g. Amprino, 1947; Castanet et al., 2000; Francillon-Vieillot et al., 1990; Horner et al., 2000; Margerie et al., 2002). Femora and tibiae possess a comparatively higher amount of well developed primary osteons with almost no matrix left between them and additionally more areas with plexiform or even reticular vascularization. In humeri and prepubic processes (fibulae are cut too close to the metaphysis for a judgment), the primary osteons are smaller and less well developed in average, more often longitudinal, and they are often isolated from each other by matrix (Figs. 6.12, 6.14), which indicates lower relative growth rates. Thus, as in *Maiasaura* (Horner et al., 2000) and *Plateosaurus* (Klein, 2004; Klein & Sander, 2007), different skeletal elements grow at different rates during ontogeny.

However, there has to be a reason for these different growth rates of skeletal elements. A possible explanation is the absolute size of the respective element within the skeleton combined

with the degree of utilization, which includes two components: (1) how much participate an element in bearing the body weight and (2) is it intensively used for movements, such as running, flying, or digging? In the case of the biped *Dysalotosaurus*, the femur and tibia are the largest long bones, they have to bear most of the body weight, and they are additionally intensively used for locomotion. The humerus is probably also used for grabbing food, for scratching itself, or to get up. However, this element is comparatively much smaller (in the only preserved individual 'dy I', exhibited in Berlin, app. 57% the length of its femur), has not to support the whole body weight, and has not to carry the body during locomotion. Thus, it is less densely vascularized and has a relatively thinner bone wall. The sampled prepubic process is even more different to the femur and tibia regarding density of vascularization and bone wall thickness, because it serves only as muscle attachment site and is not involved in active movements or in bearing the body weight.

Similar tendencies are visible in other tetrapods, but it strongly depends on their respective skeletal bauplan. The humerus of the therapsid *Diictodon* obviously reached higher relative growth rates than its femur (Ray & Chinsamy, 2004), because it was probably used for digging in addition to weight bearing. This is also observed more extensively in the common mole (*Talpa europea*) by Enlow & Brown (1958), where the large humerus is well vascularized and the much thinner cortex of the smaller tibia is almost avascular indicating much slower relative growth rates. It is not as simple in birds and pterosaurs, because the weighing of active forelimbs, mainly for flying, against weight bearing hindlimbs is highly speculative. However, there are at least indications that the absolute size of bones (e.g. small bones compared with large bones in pterosaurs [Ricqles et al., 2000:373]; radius of the king penguin chick compared to the other bones [Margerie et al., 2004]) is correlated with relative growth rate in these groups, which is also seen in some dinosaurs (see e.g. Horner et al., 2000; Klein, 2004). Although there are obviously no subsumable differences in the vascularization pattern between elements in recent ratite skeletons, their flightless habit almost predict the much lower growth rates for the forelimb elements compared to the long bones of the hindlimb (Castanet et al., 2000). This is also comparable to biped dinosaurs, such as *Allosaurus* (see e.g. Bybee et al.,

2006:fig. 2) and *Dysalotosaurus*, or facultative quadruped dinosaurs with a strong size difference between fore- and hindlimbs, such as *Scutellosaurus* (Padian et al., 2004).

It is furthermore important to note that the bones of the stylopodium (humerus, femur) have mostly higher relative growth rates than the more distal bones of the zeugo- and autopodium, because the latter are often not only smaller in overall size but they also can share possible weight bearing or muscle activity among each other. Thus, the absolute forces acting on each of them are probably smaller than on the single humerus and femur. This is suggested for e.g. the less vascularized radii and ulnae compared to the humeri and femora in *Thrinaxodon* (Botha & Chinsamy, 2005) and to the femora in *Scylacops* (Ray et al., 2004), and for the ulnae of *Allosaurus* and *Tenontosaurus* compared to the other sampled bones of the respective studies (Bybee et al., 2006; Werning, 2005). Nevertheless, whenever bones of the zeugo- and autopodium are fused (e.g. to the tibiotarsus and tarsometatarsus in birds), are much more prominent than their neighbors (e.g. the tibiae in many dinosaurs), or are exclusively used for especially powerful movements (e.g. the wing phalanges of pterosaurs), their relative growth rates should be more comparable to the bones of the stylopodium (see Castanet et al., 2000; *Dysalotosaurus*; Ricqles et al., 2000; respectively). In all these cases, the fused bones are, of course, additionally larger than usual. In the end, the relative size of a bone in a skeleton reveals its importance in weight bearing and/or movement and its relative growth rate compared to other elements is therefore predictable to a certain degree.

In an evolutionary context, the more frequent or intensive use of an element, which leads to a better blood flow and higher apposition rate (see Starck & Chinsamy, 2002), would result in higher growth rates, so that this element could become larger during evolution. However, the simple enlargement of skeletal elements is only one possibility. The other one is the fusion of adjacent elements, which probably is also related to higher growth rates. On the other hand, less frequent or intensive use of elements would result in less intensive blood flow, apposition rate, and therefore growth rate. This was probably the way, how flightless birds have evolved only small and mostly useless wings.

The differences between certain units of single cross sections are also very obvious, although cross sections with very consistent outlines (especially distal and mid diaphyseal humeri; see chapter 6.5.3.1; Fig. 6.4) reveal much less variation of bone tissues. The strongest differences were found in sections with irregular outlines and acute corners, such as in femoral sections (Figs. 6.4-6.6), in distal tibial sections (Figs. 6.4G-H; 6.10A), and in prepubic sections (Fig. 6.14). Some of the intrasectional variation is caused by differences in bone wall thickness. Most affected are the sections of femora and distal tibiae. Here, the thicker posteromedial and posterolateral corners (femora) as well as the anteromedial corner and medial bend (tibia) have a higher density of additionally large and weakly organized primary osteons with only rare space left for bone matrix between them (Figs. 6.6; 6.11E). The collagen fibrils in these areas are hardly organized, so that there is only a weak consistent reflection under polarized light. The osteocyte lacunae are more numerous and less organized and, finally, the slow growing zones are getting weaker and the distances between them are larger than in the thinner bone wall units (see below; Fig. 6.4H, L)). In the latter, in the anterior corner of femora, and in the anterolateral corner of tibiae, the opposite trend of the noted features of the thick bone wall units takes place (Figs. 6.5C-G; 6.6A, B, E; 6.10C-G). Some of the cross sectional variation, found by Horner et al. (2009:741) in the largest sampled femur of *Dryosaurus altus*, might also be caused by the reasons found in *Dysalotosaurus*.

The tendency of higher relative growth rate in thicker bone wall units of a section is overlapped in femora, distal tibiae, and proximal humeri by another source for variation in the bone tissue. As mentioned above, only the external portion of the anterior corner in femora (except for the most proximal levels), of the anterolateral corner in distal tibiae, and seldomly of the anterolateral corner in proximal humeri consists of periosteal fibrolamellar bone. In contrast, the internal portion consists of a wedge of CCCB (femora, tibiae) or of endosteal lamellae (mainly humeri). The external periosteal portion in these units possesses well organized (longitudinal to laminar) primary osteons, which are also well separated from each other by matrix (Figs. 6.5F-G; 6.9B-C; 6.10C-F). Osteocyte lacunae are less dense than in other units and the collagen fibrils are

highly organized in a mainly transverse direction, so that the matrix reflects polarized light more consistently. Additionally, all preserved or visible growth cycles (including LAG's/annuli) are closer together (Fig. 6.4H, L), and in femora, the slow growing zones can even merge together. The exclusively periosteal fibrolamellar bone wall of the opposite side of the cross sections (posterior bend in femora, medial sides in distal tibiae and proximal humeri) is distinctly resorbed internally by the marrow cavity, the osteocyte lacunae and the well developed and less organized primary osteons are very dense, and the distances between growth cycles are much wider (Figs. 6.4B, D, H, L; 6.5B; 6.6F-G; 6.7; 6.9E). Thus, the latter units were deposited by much higher relative growth rates than the former units.

These differences of growth rates of opposing units in cross sections are well explained by the drift of the marrow cavity towards the side with the suggested higher relative growth rate. The combination with the bending orientation of the respective long axes of the bone shafts (see Fig. 6.1) indicates that the marrow cavity always drifts from the convex side of the shafts long axis to the concave side to maintain the overall bone wall thickness during growth. The convex side of the long axis is located anteriorly in femora and laterally in distal tibiae and proximal humeri, respectively. This also explains, why there is still unresorbed CCCB left in the mentioned units of relative slow growth, because this usually metaphyseal tissue type is necessary for a consistent bone wall thickness during ontogeny (Enlow, 1962). For the same reason, juvenile bone tissue, with small longitudinal primary osteons and the typical knitting pattern of the surrounding matrix, is still preserved here in the internal areas of the periosteal portion even in large cross sections (Figs. 6.6A; 6.7C-D). The typical intrasectional variation caused by osseous drift is well described in Enlow (1962) for rats and monkeys and is also shown by Buffrenil et al. (2008: fig. 2E) for *Varanus* and by Castanet et al. (1993: fig. 13) for the small lizard *Gallotia*. In contrast, this typical variation is rarely described in detail in fossil tetrapods, although it is documented in the multituberculate mammal *Nemegtbataar* by Chinsamy & Hurum (2006:330; figs. 6, 7) and indicated in the dinosaurs *Scutellosaurus* (Padian et al., 2004:556; fig. 2) and *Psittacosaurus* (Erickson & Tumanova, 2000), for instance. As a result,

cortical drift is supposed to be the normal case in long bones with a bend long axis (Enlow, 1962; Francillon-Vieillot et al., 1990) and should be considered before histological sampling, because it has a strong influence on the microstructure and, therefore, on estimated growth rates. This phenomenon should especially be kept in mind in cases, where only parts of a cross section are preserved or obtained.

The described special bone tissue of the posterolateral plug in femora (Fig. 6.6C, D, F), in the anterolateral corner in tibiae and humeri (Figs. 6.10A-B; 6.12D), the medial wall in fibulae (Fig. 6.13A-C), and the lateroventral corner in prepubic processes (Fig. 6.14A-B), are suggested to be the result of muscle and/or tendon forces acting on these cross sectional units. This is indicated by the relationship of these special structures with external processes or attachment sites for muscles. The tissue structures also display the potential orientations of the acting muscle forces, because Sharpey's fibers are most abundant in these units, and the vascular canals are often oriented in a certain dominant direction. Furthermore, these plugs are very restricted to the other units by sharp borders and contain increased secondary remodeling. The mainly scattered secondary osteons are sometimes even developed close to the external surface, which is very unusual for the 'normal' bone tissue in *Dysalotosaurus*, independently of ontogenetic stage.

Such unusual restricted areas in cross sections are already mentioned for the femur in *Hypsilophodon* and described for the femur in *Iguanodon* (Reid, 1984:642-643; figs. 19, 22 therein). He has also found sharply delimited and more strongly remodeled areas (also visible in *Hypacrosaurus* [Horner et al., 1999: fig. 1D]) in possible connection with muscle attachment sites. As in *Dysalotosaurus*, these special areas can also be sharply restricted to a certain level in the shaft and can soon vanish over a very short distance within the shafts long axis. Otherwise, only sparse notes were made on these plug-like structures in the literature, mostly as areas with unusually intensive secondary remodeling almost reaching the external surface (e.g. Horner et al., 1999; 2000; Horner et al., 2009; Varricchio, 1993; Werning, 2005). Horner et al. (2000) already noted the possibility of

muscle action as a reason for these above-average remodeled areas, which was already pointed out by Currey (1984).

The number, relative distances, and developmental degree of growth cycles are highly variable in *Dysalotosaurus*. Their number is naturally strongly influenced by ontogeny (the larger/older the more; see chapter 6.5), but it is in addition obviously a function of primary bone wall thickness. This can be seen between different elements of the skeleton. The thickest primary bone walls observed in the samples are developed in femora and tibiae with 12.5 and 11mm, respectively. These elements preserve the highest number of growth cycles, which counts up to nine in the largest sections alone and up to 12 after ontogenetic correlation of the relative distances in all sections (see chapter 6.4.3). Humeri, which have a maximum primary bone wall thickness of 5.3mm in the sampled specimens, have only up to five cycles in a single section and up to ten after the correlation. The much thinner primary bone wall in the prepubic process can preserve only two cycles at maximum. It is furthermore observable that the relative distances between growth cycles are also dependent on the cutting level within the shaft, because the average thickness of the periosteal bone wall is increasing towards the mid diaphysis and the portion of CCCB at the total bone wall thickness is here insignificant (Enlow, 1962; Francillon-Vieillot et al. 1990). The resulting differences in the course of calculated growth curves derived from these distances are even stronger between cutting levels than between different methods for calculating body masses (Fig. 6.19).

In contrast to the results of Chinsamy (1995), there are indeed LAG's and/or annuli preserved in *Dysalotosaurus*, but they are rather rare, especially in femora (Tab. 1). They are slightly more abundant in tibiae and prepubic processes and most abundant in humeri (Tabs. 2; 3). There is also no distinct pattern, which would predict the occurrence of LAG's/annuli, because a medium-sized femur, for instance, can possess a single LAG and a large femur none at all (Fig. 6.4B, D). In tibiae and humeri, the number of LAG's increase with increasing bone wall thickness, but this is the same pattern as for all growth cycles, and LAG's are only part of them (see e.g. Fig. 6.12C-F). Interestingly, some of the prepubic processes, with their extremely thin relative primary bone wall, possess more

LAG's/annuli as the thick-walled femora. Together with the observed occurrence and distribution of LAG's/annuli in the other sampled skeletal elements, the growth pattern in *Dysalotosaurus* seems to be very dependent on relative growth rate, environmental conditions, and specific life history of a single individual. Thus, LAG's/annuli are only developed in worse situations for a single individual (e.g. injury, disease, additional stress due to competition and/or reproduction) or bad environmental conditions (long draughts, scarcity of food, catastrophic events). Furthermore, LAG's/annuli are more likely developed in skeletal elements of relatively slower growth rate (humeri, prepubic processes) than in elements with relatively higher growth rates (femora, tibiae), which was already suggested by Horner et al. (2000) for *Maiasaura*.

The relatively random and rare formation of clearly defined resting lines is in striking contrast to the pattern seen in many other dinosaurs. In theropods (e.g. Chinsamy, 1990; Erickson et al., 2007; Horner & Padian, 2004), mainly primitive and/or smaller sauropodomorphs (e.g. Klein, 2004; Sander et al., 2006), and some ornithischians studied (e.g. Erickson & Tumanova, 2000; Horner et al., 1999; 2000; Werning, 2005), LAG's/annuli occur much more regularly and not as an exception, as in *Dysalotosaurus*. Especially large and derived sauropods have much weaker cycles, such as polished lines (Sander, 2000) or zonal differences in vascularization (Curry, 1999; Ricqles, 1983; Sander et al., 2004), which are assumed to be annual markers as well.

None of these studies have mentioned such a kind of growth cycles found here. Their identity as possible annual markers is now, however, unambiguously proved. Despite the often relatively weak appearance, the repeatable and rhythmic occurrence of faster and slower growing zones is striking. As known from true resting lines, (1) their preserved number increases with related body size of the sampled individual and is quite constant (with a maximum deviation of 2) throughout a single ontogenetic stage of a certain element (see also Tabs. 1-3); (2) The thickness of the slow growing zones is relatively constant, regardless of the fluctuations in thickness of bone wall units in a cross section, whereas the fast growing zones become thicker in the thick bone wall units and thinner in the thin bone wall units; (3) the zonation becomes weaker in thicker bone wall units and

more distinct in thinner units of a cross section; and (4) the plot of the maximum growth rate with age, which is derived from the correlated growth cycles under the assumption of their annual signal, fits almost perfectly into the linear regression line of maximum growth rates developed for dinosaurs (Erickson, 2005; Erickson et al., 2001; see also Lehman & Woodward, 2008; see Fig. 6.21). The obviously cyclical fluctuations found in juvenile *Maiasaura* (Horner et al., 2000) and in the holotype of *Hypacrosaurus* (Horner et al., 1999) are probably another kind of growth cycles, but their significance as annual markers is questioned by these authors and has still to be proved.

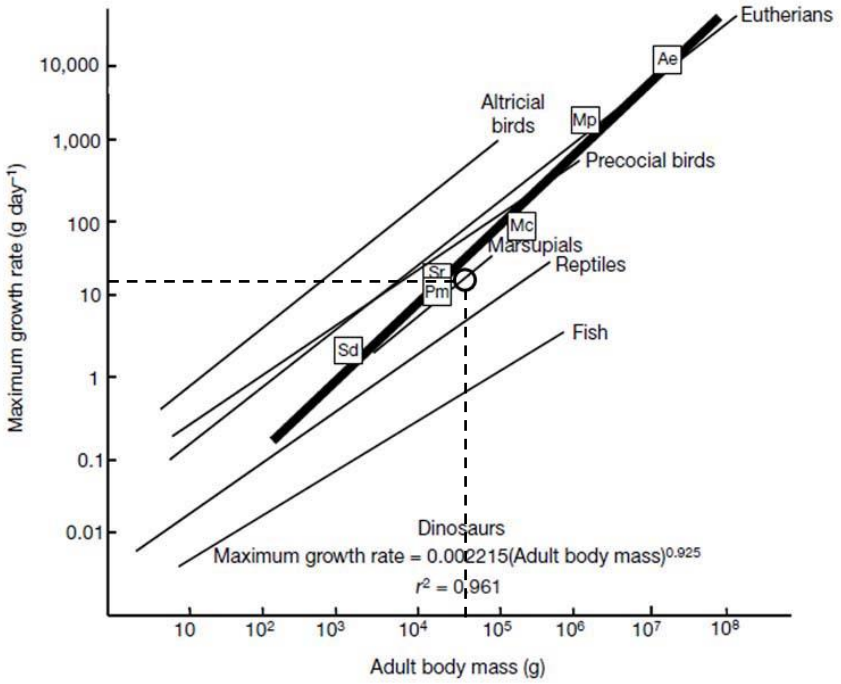

Fig. 6.21: *By comparing the maximum growth rate of* Dysalotosaurus *with other dinosaurs and recent animals, it is located close to the regression line for dinosaurs and is very similar to large marsupial mammals (modified from Erickson et al., 2001).* ***Abbr.: Sd*** – Shuvuuia deserti*;* ***Pm*** – Psittacosaurus mongoliensis*;* ***Sr*** – Syntarsus rhodesiensis*;* ***Mc*** – Massospondylus carinatus*;* ***Mp*** – Maiasaura peeblesorum*;* ***Ae*** – Apatosaurus excelsus*.*

It is important to note, however, that the type of growth cycles described for *Dysalotosaurus* probably exists in a wider range of taxa, because the cyclicity between differently oriented collagen fibrils is also mentioned in *Alligator* by Lee (2004:205; see also figs. 2J-L; 3I-K; 4 therein), and is probably present in an extinct crurotarsian (pers. comm. Bronowicz, 2009) and another ornithopod (pers. comm. Werning, 2009). Thus, this kind of growth cycles will probably be observed in much

more tetrapods in the future and should provide age estimations especially in taxa with an otherwise poor record of resting lines.

6.7.2 Correlation and comparison of ontogenetic growth stages

Since all the sampled elements are isolated and microstructural details vary between different elements of a skeleton, the correlation of ontogenetic stages in femora, tibiae, and humeri of *Dysalotosaurus* is only preliminary.

Nevertheless, the second ontogenetic stage of all three elements (early juvenile or juvenile stage; Figs. 6.9A-D; 6.11F; the first or embryonic to hatchling stage is not represented) is well comparable, because each of the respective sections belongs to the smallest available specimens and is located close to or at the left margin within the respective size-frequency distributions (Fig. 3.3). Furthermore, the vascular canals are often longitudinal and the development of primary osteons is incomplete in some cross sectional units of femora and tibiae. In the smallest humeri, there are much more primary osteons with complete lamellar infilling, although many of them are rather small. There is also only a single slow growing zone/annulus/LAG close to or directly at the outer periphery of the bone wall. Secondary osteons are rare or absent (depends also on cutting level within the shaft) and possible histological differences between sectional units are very weak (Fig. 6.9A, D). This correlated juvenile stage is similar to the stage of large nestlings in *Maiasaura* (Horner et al., 2000), to the stage of small juveniles in *Orodromeus* (Horner et al., 2009), and is located in between the perinate and juvenile stage of *Dryosaurus* (Horner et al., 2009).

The correlation of the following stages is more difficult, because there are different numbers of distinguishable stages in femora, tibiae, and humeri. The third and fourth stage of femora (late juvenile [Fig. 6.9E] and immature subadult stages [Figs. 6.4C-D; 6.7]) are here correlated with the third stage of tibiae (late juvenile to immature subadult stage [Figs. 6.4E-F; 6.11E]), and the last stage of humeri (post-juvenile stage [Figs. 6.4I-L; 6.12]). Individual cross sections in humeri are only

assignable to either immature subadult or mature adult stages by their absolute size within the size-frequency distribution (Tab. 3). To summarize these late juvenile to immature subadult stages, the respective cross sections of femora, tibiae, and humeri possess more than one growth cycle (up to five in the fourth femoral stage); the vascular pattern of vascular canals is now dominantly laminar to plexiform (see also intrasectional variation above); primary osteons are abundant throughout and well developed; secondary osteons, plug structures, and indications for osseous drift are present; and the cross sectional units are well diversified (generally less prominent in humeri). The closest similarities to described growth stages of other ornithopods were found to the large juvenile and subadult stages in *Orodromeus* (Horner et al., 2009), to the juvenile and smallest subadult stages in *Dryosaurus* (Horner et al., 2009), and to the juvenile stage in *Maiasaura* (Horner et al., 2000). Both the late juvenile stage and immature subadult stage of *Dysalotosaurus* femora are, moreover, similar to the subadult stage in *Orodromeus* and to the small subadult stage in *Dryosaurus*.

The last represented ontogenetic stage is named here sexually mature adult stage. This does not mean skeletal or somatic maturity, because none of the sampled specimens show an External Fundamental System (EFS; Chinsamy-Turan, 2005; Erickson, 2005). The differentiation to the next younger stages is unambiguous in femora and tibiae. In humeri, only the absolute size and the respective position within the general size-frequency distribution are helpful (Tab. 3). Generally, the cross sectional units are well diversified and there are strong differences in bone wall thicknesses (in humeri less distinct, as usual). Growth cycles are numerous (up to nine in femora, seven in tibiae, five in humeri), but they can be interrupted by strongly developed plug structures within the cortex (Figs. 6.4B, H; 6.6F; 6.9E; 6.10A). Primary osteons are mature, numerous, and very dense in most areas. Secondary osteons are more numerous than in the former stage and are represented around the CCCB wedge and in the plug structures (Figs. 6.5G; 6.10B). Osseous drift is highly advanced (but depends especially in humeri on cutting level of cross section). This ontogenetic stage is comparable to the subadult stage in *Orodromeus* and the medium sized subadult femur of *Dryosaurus* (Horner et

al., 2009). It does not match the subadult stage in *Maiasaura* due to the lack of extensive remodeling in the deep cortex and the lack of the starting EFS (Horner et al., 2001).

Generally, the ontogeny of the bone histology in *Dysalotosaurus* is most similar to *Dryosaurus* (Horner et al., 2009) regarding overall size of skeletal elements as well as the respective cross sectional dimensions, vascularization pattern, and degree of secondary remodeling.

Orodromeus reveals a vascularization pattern, which is usually found in skeletal elements of *Dysalotosaurus* with relatively lower growth rates, such as in sectional units of humeri or prepubic processes (Figs. 6.12B; 6.14 C, E). There, rather isolated, mainly longitudinal, and smaller primary osteons are common, which are well described for *Orodromeus* (Horner et al., 2009; Padian et al., 2004). LAG's are also more common as in *Dysalotosaurus* and an EFS is known, which indicates nearly cessation of growth in the somatically mature adults. It confirms that this ornithopod, which has reached a smaller maximum body size than *Dysalotosaurus*, grew with a lower overall growth rate than the latter genus (for other examples see e.g. Case, 1978b; Castanet et al., 2000; Erickson et al., 2001; Padian et al., 2004).

The opposite case is the much larger *Maiasaura*. The vascularization pattern is not very different, but the much thicker primary bone walls experienced much more intensive secondary remodeling. Large and widespread resorption cavities or dense Haversian bone, which can obscure the primary bone in the deeper cortex, is completely unknown in the sampled elements of *Dysalotosaurus*. The intensity of secondary remodeling is therefore probably not only an indicator of individual age and longevity (e.g. Klein & Sander, 2008; Sander, 2000), but also an indicator of maximum body size and, therefore, overall growth rate (Ricqles, 1976). This is probably the case in primates (compare e.g. Castanet et al. [2004] and Burr [1992] with Mulhern & Ubelaker [2003], see also Singh et al. [1974]), ornithopods (see above), and sauropodomorphs (compare e.g. Klein [2004] with Klein & Sander [2008]). The comparison of the largest sampled femur of *Dysalotosaurus* with the largest femur of *Dryosaurus* (49cm length; see Horner et al., 2009), which show much more extensive secondary remodeling, either confirms this assumption, or the latter was indeed

individually older than the former (Klein & Sander, 2008). This femur is even larger than the largest preserved, but not sampled, *Dysalotosaurus* femur, which has a calculated length of 38cm. Together with the observations of increasing secondary remodeling within the ontogenetic stages of *Dysalotosaurus*, the influence of individual age on remodeling intensity is probably most important, but the other factors mentioned above should obviously also kept in mind.

Finally, Horner et al. (2009) described that the largest *Dryosaurus* femur was still actively growing, because it lacks an EFS and has therefore belonged to a somatically subadult individual. Thus, it is suggested that none of the known individuals of *Dysalotosaurus* were somatically mature.

6.7.3 The life history of *Dysalotosaurus*

The embryonic or perinatal ontogenetic stage is not preserved in *Dysalotosaurus*, but the longitudinal section of the smallest known femur (see chapter 6.5.1; Fig. 6.8B), which belongs to the early juvenile stage, is very distinctive regarding possible behavior of hatchlings. Endochondral trabecular bone reaches almost the preserved surface of the calcified cartilage zone (see Reid, 1997: fig. 29.5) in the centre of the distal femoral end and starts to separate the pads of calcified cartilage from each other (Fig. 6.8B). In the deeper parts, only isolated small pads of calcified cartilage were preserved within connections of transverse and longitudinal struts of endochondral trabeculae.

This structure is very similar to the structures described for younger stages of *Orodromeus* and *Troodon* (Horner et al., 2001), although these pads reach naturally much deeper at this early ontogenetic stage than in the described sample of *Dysalotosaurus*. It is also in strong contrast to the situation seen in some hadrosaurs (Horner et al., 2001), where pads of calcified cartilage are not constricted to the preserved epiphysis, but reach through the whole metaphysis into the diaphysis. Endochondral bone is much rarer and apparently lacks transverse struts crossing the long tubular structures, which consist of connected cartilage canals and marrow processes. In the large nestling of *Maiasaura* (Horner et al., 2000), thin coatings of endochondral bone are under development along

the wall of the marrow processes, but noticeable transverse struts were only observed deeper within the metaphysis. Since large nestlings of *Maiasaura* are here tentatively correlated with the early juvenile stage of femora in *Dysalotosaurus*, the possible behavior of hatchlings of *Dysalotosaurus* are supposed to be different to *Maiasaura* and other hadrosaurs, but similar to *Orodromeus* and *Troodon*. In combination with the morphological observation that even the smallest known long bones, especially of the hindlimb, have well ossified and developed articular ends and bony processes (Horner & Weishampel, 1988, see also chapter 5.4.2), the hatchlings of *Dysalotosaurus* were most likely precocial. Thus, they could follow their parents short after hatching, but experienced rather moderate growth rates compared to the probably semi- to fully altricial hadrosaurs (Horner et al., 2001). By the way, the precocial behavior is also assumed for the closest relative of *Dysalotosaurus*, *Dryosaurus altus*, whereas an embryo of the larger taxon *Camptosaurus* was probably altricial similar to *Maiasaura* (Chure et al., 1994).

These moderate growth rates are well visible in the four growth curves, where body mass is plotted against age for femora (Fig. 6.19). The early and late juvenile stages of this element cover the moderately sloping part of the growth curves up to approximately six years of age. Following the growth curves further upwards, the sexually immature subadult stage of the thin sections correlates with the age of six up to ten years. The latter date is here proposed to be the time of achievement of sexual maturity and therefore separates the immature subadult members of the *Dysalotosaurus* herd from the sexually mature individuals. This hypothesis was derived from five out of the six sampled large femora, which belong to the most mature histological ontogenetic stage observed (see chapter 6.5.1.1). A sharp mark (Mark of Initial Sexual Maturity – MISM) is visible in these cross sections (Figs. 6.4B; 6.5B; 6.6F), which represents the beginning of a relatively consistent exterior growth pattern and separates the latter from the interior usually distinct cyclical growth pattern. Only weak zonation is recognizable in this exterior zone and the general appearance is similar to the slow growing zones regarding the mainly transversely oriented and well organized collagen fibrils and the orientation and organization of vascular canals. This outer zone apparently represents an overall slow-down of bone

apposition rates, which interestingly starts in each of the five concerning femora at almost the same relative position within the cross sections and is therefore found between 9.5 and 10.5 years of age in the growth curves (Figs. 6.15; 6.18; 6.19). Thus, this mark represents not an individual event, but a real physiological signal and it indicates an important change in the life history of *Dysalotosaurus*.

The achievement of sexual maturity is the most probable possibility to explain this change in growth pattern. Several other reasons confirm this assumption. (1) This event is commonly combined by a slow-down of growth rate in many other tetrapods (e.g. Andrews, 1982; Chinsamy et al., 2008; Erickson, 2005; Lee & Werning, 2008; Sander, 2000); (2) The timing of sexual maturity lies well before somatic maturity as in other dinosaurs (e.g. Erickson et al., 2006; 2007; Klein, 2004; Lee & Werning, 2008; Sander 2000); (3) This event plots in diagrams with body size versus age almost exactly at the curves point of inflection (Lee & Werning, 2008; but see below); (4) The preservation of medullary bone tissue in a large fibula and a large tibia (Figs. 6.11A-D; 6.13B-C), which plot well within the group of large individuals in the size-frequency distributions as the described large femora (Fig. 3.3; Tab. 2), show that this group contains sexually mature individuals; and (5) By correlating the respective value of this mark with femoral size, the mark plots well within the gap between the dominating groups of small and large individuals of the *Dysalotosaurus* herd (Fig. 6.22).

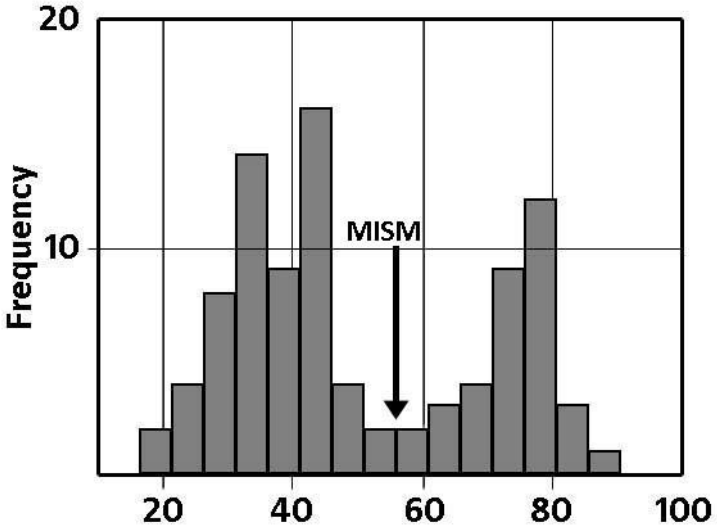

Fig. 6.22: *Size-frequency distribution of all measured right femora (see also Fig. 3.3). The Mark of Initial Sexual Maturity (MISM) is located at the mediolateral width of the distal articular end (Mess 18) of app. 56.5mm.*

This gap shows the underrepresentation of individuals and is probably the result of banishment and/or increased mortality of this size class. In recent and at least temporarily gregarious ungulate

mammals, mainly young males suffer increased mortality around the time of sexual maturity, because they are driven out of the herd very early by prime-aged males (e.g. Impala; Jarman & Jarman, 1973) or leave the herd by oneself (e.g. Kudu; Owen-Smith, 1993). They are therefore more vulnerable to predators and have higher stress levels due to their low rank within bachelor herds. In other species, young males suffer high mortality during their first participation in the rut (e.g. bighorn sheep; Jorgenson et al., 1997 and rhinos; Mihlbachler, 2003). Young females also have higher mortality rates due to low experience in reproduction, high reproduction costs and competition with prime-aged females (e.g. red deer; Proaktor et al., 2008). Higher mortality rates resulting from early sexual maturity were also suggested for the tyrannosaur *Albertosaurus* (Erickson et al., 2006). Thus, the position of the mark right within the gap of the size-frequency distribution confirms the assumption that it is indeed the Mark of Initial Sexual Maturity.

However, there is an antagonism between the apparent decrease in bone apposition rate observed in the cross sections at this mark and its relative position within the growth curves (body mass versus age; Fig. 6.19). There, it is located within the lower third of the exponential growth phase and growth rate is accelerating even after this mark up to the fourteenth year of life with its maximum growth rate in body mass. This is similar to other dinosaur taxa, where the time of sexual maturity is strongly indicated by the occurrence of medullary bone (Lee and Werning, 2008) and/or increased midlife mortality (Erickson et al., 2006). The time of sexual maturity presented in Lee & Werning (2008) for *Tenontosaurus* (8 years) and *Allosaurus* (10 years) is located, as in *Dysalotosaurus*, within the lower third of the exponential growth phase and not at the curves point of inflection, where growth rate reaches its maximum. In the case of *Tyrannosaurus*, the estimate of 18 years is indeed close to the inflection point, which is similar to *Albertosaurus* (compare Erickson et al., 2004 with Erickson et al., 2006), although the exact time of sexual maturity is probably an upper bound for *Tyrannosaurus* (Lee & Werning, 2008).

It is suggested that the phenomenon of contradicting features in *Dysalotosaurus* is an effect of allometric scaling between increasing body mass and increasing body size (including bone

apposition), where the ratio would be 8:1 (compare also Box 3a with 3b in Erickson, 2005). Furthermore, the scaling effect of body mass is neutralized by plotting a variable representing body size versus age (Fig. 6.20), where the time of sexual maturity in *Dysalotosaurus* is indeed located almost exactly at the curves point of inflection. It should also be noted that the described mark is completely absent in all large tibiae and humeri of respective position within the size-frequency distributions. This indicates an only moderate slow down of bone apposition rate, which is probably not visible in elements of slightly lower relative growth rates compared to the rates in femora.

Finally, the relative body size at time of sexual maturity compared to maximum known body size in *Dysalotosaurus* is approximately 62 to 64%, which is strikingly similar to the remarked 60% to the recorded maximum size known in *Albertosaurus* (Erickson et al., 2006) and close to the estimated value of 70% in *Barosaurus* (Sander, 2000). Thus, the paradoxon between decelerating bone apposition and still accelerating body mass in *Dysalotosaurus* in young sexually mature adults is treated here as rather insignificant.

The location of the largest sampled femur (SMNS F2 – group two) within the growth curves is well below the estimated asymptote at approximately 16.4 years of age (Fig. 6.19). Additional features of still active growth are the open vascular canals at the periphery, well vascularized tissue in the external bone wall areas, and the complete absence of an EFS. The second largest known femur (R12277) is also located still below the asymptotic level of the growth curves, which would indicate somatic maturity, nearly cease of growth, and the formation of an EFS. However, the largest known femur specimen used as indication for maximum body size and mass, respectively, could not be sampled for thin sections and the evidence for an EFS is not proofed. The absence of this external structure in a much larger femur of the closely related taxon *Dryosaurus altus* (Horner et al., 2009) let assume that this species obviously grew to larger body sizes than *Dysalotosaurus* and that both taxa most likely experienced indeterminate growth, as Chinsamy (1995) already suggested.

Anyway, although many of the *Dysalotosaurus* individuals could be reproductively active for more than five years, almost none of them obviously reached somatic maturity. One reason is the

relative small body size (especially compared to the sauropods) and the lack of any additional defensive structures (as in *Kentrosaurus*), which made *Dysalotosaurus* highly vulnerable to most of the contemporaneous predators. This could also be the reason, why sexual maturity was reached not until the ninth year of life. The cost of reproduction was too high for these smaller individuals, because they were too vulnerable to predation. Furthermore, there seems to be a strong intraspecific competition within the herd. This is partially indicated by the high mortality around time of sexual maturity and could be another reason for the long time until active reproduction and for the prolonged exponential growth phase in sexually mature adults. Body size, and especially body mass (indicating strength or fitness), were probably the driving forces to compete with each other. Larger/stronger individuals had a more dominant role within the herd, and therefore a better chance for reproduction, than smaller/weaker individuals. Thus, fast and extended indeterminate growth was probably a survival advantage for *Dysalotosaurus*.

6.8 Implications for and speculations on the growth pattern in other dinosaurs

Dysalotosaurus belongs to one of the groups of dinosaurs, where annuli/LAG's as representatives of a zonal bone tissue are rather scarce, completely absent, or are replaced by less obvious growth cycles. This regards several small ornithopods and many sauropods (Chinsamy, 1995; Chinsamy et al., 1998; Curry, 1999; Horner et al., 2009; Klein & Sander, 2008; Ricqles, 1983; Rimblot-Baly et al., 1995; Sander, 2000; Sander et al., 2004; Winkler, 1994). On the other hand, large ornithopods, other ornithischians, prosauropods, and all theropods (independently of body size), which were histologically sampled up to date and are also more derived than *Herrerasaurus* (see Chinsamy, 1995; Chinsamy-Turan, 2005), showed a relative consistent growth pattern with annuli/LAG's representing the usual kind of growth cycles (e.g. Bybee et al., 2006; Chinsamy, 1990; 1993; Erickson & Tumanova, 2000; Erickson et al. 2007; Horner & Padian, 2004; Horner et al., 1999; 2000; Klein, 2004).

Klevezal (1996) has found a relationship between the abundance and uniformity of these resting lines and environmental conditions in recent mammalian populations, which could partially explain the sorting of dinosaurs into such multiform groups. Populations inhabiting regions with strong seasonality of temperature, but also humidity or food supply, consists mainly of individuals with distinct and weakly variable resting lines in their bone microstructure (mostly two-phase annual rhythm). In contrast, populations of the same species, but inhabiting more friendly regions, can consist of a high amount of individuals with only weakly developed resting lines and a higher variability in number (poly-phase annual rhythm). However, there are always individuals of a population stepping out of the line and even could possess the growth pattern common in the other population, respectively. Thus, it is always likely that a single fossil specimen represents the usual growth pattern of its population, but it is also possible that it represents the anomalous minority of its population. An unusual growth pattern found in a single specimen should therefore be treated with caution, as was already emphasized for the case of a single studied femur of a polar ornithopod (Chinsamy et al., 1998; Horner et al., 2009; see below).

The regular development of resting lines in highly seasonal regions is advantageous compared to irregular cyclicity, because the former is synchronized to the seasonal changes of environmental conditions. Irregular or asynchronous growth is disadvantageous in strongly seasonal regions, because growth phases reaching into harsh times cost naturally more energy than arrested growth. Poly-phase growing individuals have therefore to fit their growth regime to the seasonal conditions or die. In less seasonal regions, it does not matter, which growth regime an individual possess, because the effects on its energy balance is not so disadvantageous and the variability of growth patterns in the population is therefore much higher (Klevezal, 1996).

The results for *Dysalotosaurus* have shown that the abundance and development of resting lines depends either on relative growth rate (resting lines in faster growing femora are less abundant) and harsh environmental conditions (by far not all growth cycles are completed by a resting line). For the Tendaguru region with its reconstructed seasonal change of humidity (Aberhan

et al., 2002), long droughts would be such harsh times followed by a shortage of food and water. This is also indicated by the depositional area of the Tendaguru Beds, which are very unlikely to be the usual habitat for the preserved dinosaurs.

6.8.1 Sauropoda

Many of the already studied Tendaguru sauropods possess an inconsistent growth pattern without typical resting lines (excluding the EFS in the largest individuals) and have often developed polish lines as an alternative pattern, although these lines show only a slow-down in the growth rate and not an interruption (Sander, 2000). Altogether, there is much variability in the presence or absence, number, or relative distances of resting and/or polish lines, even within a single species, such as in *Barosaurus* or *Brachiosaurus*. In the case of *Barosaurus*, sexual dimorphism is suggested as the main reason for the differences between the two morphs (Sander, 2000), but this is probably rather the result of interspecific variation (Remes, 2009). *Janenschia*, with its regular development of polish and resting lines, is also not a remarkable exception, because only two bones could be sampled by Sander (2000) and it is therefore not automatically a secured representative of the whole population of this taxon. Furthermore, even in clearly defined annual seasons, different species can have different growth patterns, although they are living in the same region. This is, for example, evident for some tropical ungulates (Klevezal, 1996). Sauropods from other regions also fit into this scheme, because true resting lines in long bones are the exception in most of the species (Klein & Sander, 2008:251) and possible growth cycles are mainly represented by modulations of the vascularization (Curry, 1999; Lehman & Woodward, 2008; Ricqles, 1983). The only exception is the dwarf sauropod *Europasaurus*, which obviously had a much lower growth rate than its giant relatives (Sander et al., 2006). Body size and, consequentially, extraordinarily high growth rates in sauropods (e.g. Erickson et al., 2001; Lehman & Woodward, 2008; Padian et al., 2001; Sander et al., 2004) seem to be the main factor for the scarcity of a consistent development of regular resting lines in this

group, as it was also suggested for other smaller dinosaurs during their initial fast growing stage (Horner et al., 2000; Padian & Horner, 2004). This is supported by the decrease of abundance and consistency of resting lines in skeletal elements of *Dysalotosaurus*, which grow relatively faster than other elements. Furthermore, sauropods were due to their large body size less affected to changes in temperature (Chinsamy & Hillenius, 2004), and temperature was a minor seasonal factor during most of the Mesozoic anyway (Farlow et al., 1995). Shortage of food as a result of seasonal draught was also probably not strongly affecting on general sauropod growth rates, because they probably fed on everything they could get without competition of lower browsing ornithopods and thyreophorans and they were also capable to avoid harsh environmental conditions by migration (Upchurch et al., 2004). Thus, sauropod populations should be, and obviously are, generally highly variable in their growth pattern, which is comparable to recent mammalian populations living under weakly pronounced seasonal conditions (Klevezal, 1996).

6.8.2 Theropoda

With the probable but not thoroughly studied exception of the basal taxon *Herrerasaurus* (Chinsamy-Turan, 2005:162), theropods are the dinosaur group with the most uniform growth pattern regarding the occurrence and consistency of resting lines. This is also very unusual, because the range of body size within theropods is comparable to ornithopods (see below). The large tyrannosaurids and *Allosaurus* possess an abundant development of resting lines (Bybee et al., 2006; Erickson et al., 2006; Horner & Padian, 2004) just as much smaller sampled theropods (Chinsamy, 1990; Chinsamy et al., 1998; Erickson et al., 2007; Varricchio, 1993; Varricchio et al., 2008). This growth pattern is obviously completely independent of body size and might be induced by phylogeny. However, this is the case for most vertebrates (Castanet et al., 1993; Chinsamy-Turan, 2005; Erickson, 2005). The variation in the development of resting lines in mammals (Klevezal, 1996), as well as in sauropods and ornithopods (see above and below, respectively), has shown that this

basic growth pattern is often modified due to different body sizes, seasonal factors, and specific nutritional demands. The relative consistent development of resting lines in nearly all theropods is therefore assumed to reflect a collective external factor, which affects all taxa independently of size or habitat and is furthermore unique for this group.

The best possible explanation is assumed to be territoriality for nearly all species of theropods (e.g. Tanke & Currie, 1998). The overwhelming majority of modern terrestrial avian or mammalian carnivores are territorial animals. The polar bear or many sea birds are some of the few exceptions. Home-range size increases with metabolic needs and carnivores with a large proportion of flesh in their diet have larger home-ranges than omnivores or insectivores (Gittleman & Harvey, 1982). The large predators among theropods were exclusively meat eaters (Fastowski & Smith, 2004) as most of the top-predators today (except Ursidae) and possessed therefore very large home-ranges. Anyway, Hebblewhite & Merrill (2007) have shown that migration of potential prey has influence on their predation risk. Carnivores are almost never migrating with their prey (Bell & Snively, 2008), though, and in a seasonal environment, they almost certainly have to suffer periods of starvation or they have to traverse their home-ranges more often than in good, prey rich seasons (as e.g. the wild dog; Gittleman & Harvey, 1982). This seasonal fluctuation in stress and food supply probably affects predators of almost the whole size range, because the diet of most medium-sized to small theropods has consisted mainly on meat as well (Fastowski & Smith, 2004). Thus, almost all theropods were influenced by seasonal shortage of prey due to their assumed territoriality, and this could have resulted in the consistent development of resting lines as the best growth pattern to save energy during these regular bad times. In the end, this assumed liability of theropods to food shortage is well comparable to the effects of strong seasonality in modern mammalian populations (Klevezal, 1996).

Body size is treated here as another factor influencing the regular development of resting lines in theropods. Although small theropods should have the smallest home-ranges and the highest potential to find prey (especially as an insectivore or omnivore), the overall growth rate is certainly

very low and an additional seasonal slow-down in growth rate would sooner result in the development of resting lines. For the smallest theropods, maximum body size therefore dominates probably over seasonal environmental influences. At the other end of the scale, large theropods would have needed higher numbers of prey, which additionally was more difficult to catch. They probably had also much larger home-ranges than smaller theropods. Their large body sizes (and therefore maximum growth rates) would rather predict the scarcity of resting lines. However, as in large ornithopods, resting lines are regularly present in large theropods and the seasonal influence on growth pattern seems to dominate over body size effects.

6.8.3 Ornithopoda

The growth pattern in ornithopods seems to be a bit more consistent at the first view, because LAG's are now also known in *Dysalotosaurus* (in contrast to Chinsamy, 1995), as well as in *Orodromeus* and *Dryosaurus altus* (Horner et al., 2009; Scheetz, 1999). *Dysalotosaurus* and *Dryosaurus altus* are phylogenetically intermediate between *Orodromeus* (one of the most primitive ornithopods *sensu* Butler et al., 2008b) and *Tenontosaurus* (primitive basal iguanodontian; Butler et al., 2008b; Weishampel et al., 2003) on one side and the hadrosaurs *Maiasaura* and *Hypacrosaurus* on the other side. Only the first five taxa were studied in an ontogenetic context including several specimens and/or individuals (this study; Horner et al., 2000; Horner et al., 2009; Scheetz, 1999; Werning, 2005). The bone histology of *Hypacrosaurus* is only published for the somatically mature holotype individual and embryonic to perinatal specimens (Cooper et al., 2008; Horner et al., 1999; 2001). The Proctor Lake ornithopod is too scarcely described for a comparison (Winkler, 1994). The bone histology of three other ornithopods is only known from single specimens (Chinsamy et al., 1998) or without bearing an ontogenetic background (Reid, 1984), which is therefore not securely representative. Only *Gasparinisaura* is currently under study by using multiple elements and some ontogenetic stages (Cerda & Chinsamy, 2008), but just one femur seems to show a distinct cyclical

growth pattern. This is expressed by zones of fibrolamellar bone alternating with bands of poorly vascularized lamellar bone, but true LAG's were not found.

LAG's are obviously more common in ornithopods than previously thought, however, and completely azonal bone is rather unlikely (in contrast to e.g. Chinsamy, 1995; Chinsamy et al., 1998; Chinsamy-Turan, 2005). LAG's occur in *Orodromeus*, *Dysalotosaurus*, *Tenontosaurus*, and *Maiasaura* at first in the late juvenile stage (this study; Horner et al., 2000; Horner et al., 2009; Werning, 2005). In *Dysalotosaurus*, LAG's are very rare and close to the periphery at this stage (except in humeri). The first LAG in *Tenontosaurus* is also not consistently developed in all specimens and is sometimes substituted by a band of differing orientated collagen fibrils (Werning, 2005). In *Dryosaurus altus*, LAG's were found in all three subadult femora, but at non-overlapping relative positions indicating at least three different growth cycles for the two smaller specimens and up to 15, if one include the largest femur and calculate the possible number of LAG's by back counting (Horner et al., 2009). Unfortunately, most of the inner cortex of this largest femur is secondarily remodeled, so this cannot be checked. If *Dryosaurus* is indeed similar to *Dysalotosaurus* in its growth pattern, which is implicated by relative growth rates (similar vascularization pattern) and the absence of an EFS, than the number of developed LAG's would be still relatively rare in the large femora of *Dryosaurus*, despite the potentially high number of growth cycles. In *Dysalotosaurus*, ten out of 14 femora from the sexually immature subadult and sexually mature adult stage bear one (in one case two) LAG or annulus, respectively (in Tab. 1 six out of nine, excluding the femora not used for the age calculations), but these resting lines represent at least three to four non-overlapping positions, which confirms a very inconsistent and highly variable growth pattern. It is therefore possible that Chinsamy (1995) sampled just accidentally such specimens, where LAG's are not developed among the other growth cycles. However, azonal growth is definitely disproved for *Dysalotosaurus*.

Orodromeus differs from both *Dysalotosaurus* and *Dryosaurus* by its lower overall growth rate (see above) and the presence of an EFS in the largest individuals (Horner et al., 2009). Another difference is the quiet consistent development of LAG's in the tibiae and femora of subadult and

adult individuals. This could be the consequence of overall lower growth rates in *Orodromeus* (Horner et al., 2009). The development of LAG's is more likely, because the seasonal slow-down in growth starts from an already lower level than in *Dysalotosaurus* and *Dryosaurus*. However, *Orodromeus* seems to be rather an exception among small to medium sized ornithopods regarding its growth pattern (see below).

The age of *Orodromeus* at the beginning of somatic maturity is estimated by Horner et al. (2009) with five to six years. This is relatively short for a dinosaur of this size, because other small dinosaur taxa, such as *Psittacosaurus* or some small theropods, reached ages of at least nine and eight to 18 years, respectively (Erickson & Tumanova, 2000; Erickson et al., 2007). Scheetz (1999:87) described four additional bands of highly reflecting bone tissue alternating with weakly reflecting darker bands in a juvenile femur of *Orodromeus*, which is also illustrated in Horner et al. (2009:fig. 2C). At a first glance, it has some similarities to the alternation of fast and slow growing zones in *Dysalotosaurus*, although such a suggestion should be treated with caution. Anyway, if these bands are assumed to be annual cycles, than the age of *Orodromeus* would be about ten years at time of reaching somatic maturity. This would fit much better to the estimated ages of other small dinosaurs.

The three larger ornithopods *Tenontosaurus*, *Maiasaura*, and *Hypacrosaurus* developed much higher numbers of LAG's in the subadult and adult stages than *Dysalotosaurus* and *Dryosaurus* before reaching somatic maturity (Werning, 2005; Horner et al., 1999; 2000). They experienced very high growth rates during the juvenile stages (e.g. Horner et al., 2000), as the comparison of the growth curve of *Tenontosaurus* also shows in comparison to the averaged growth curve of *Dysalotosaurus* (Fig. 6.23). Thus, all three large ornithopods had higher initial and juvenile growth rates and reached their asymptotic growth plateau relatively earlier than most of the smaller ornithopods.

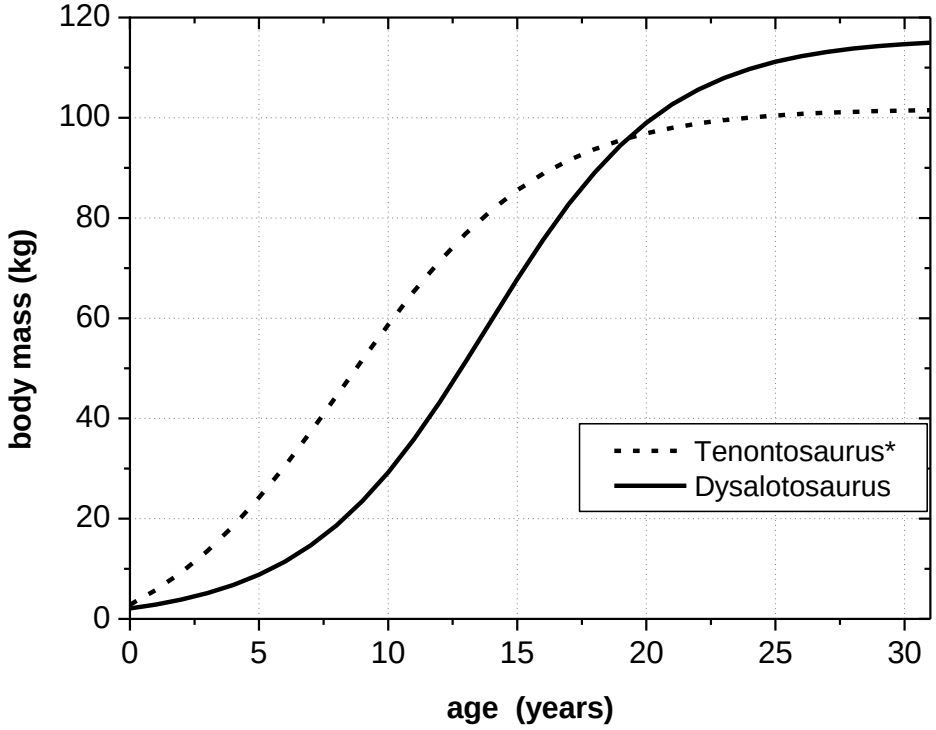

Fig. 6.23: *Comparison of growth curves of* Tenontosaurus tilletti *(derived from Lee & Werning, 2008:tab. 2) and* Dysalotosaurus lettowvorbecki*. *Note that the maximum body mass of* Tenontosaurus *is app. ten times higher than in* Dysalotosaurus*. Thus, for a better comparison, the body mass values of* Tenontosaurus *were divided by 10 and then used for the growth curve calculation.*

The application of the above mentioned relationship between strength of seasonality of environmental factors and occurrence and uniformity of resting lines (Klevezal, 1996) is in ornithopods obviously not linked to body size in the same way as in sauropods (dependent on growth rates and body size alone, see above). The abundance of numerous resting lines in subadults and adults of larger ornithopod taxa indicate higher seasonal stress than in the medium-sized *Dysalotosaurus* and *Dryosaurus*. Another example is the absence of resting lines in the small Proctor Lake hypsilophodont ornithopod compared to the occurrence of such lines in a large hadrosaur of the same locality (Winkler, 1994). The zonation in just a single femur of *Gasparinisaura* (assuming that the others lack it; Cerda & Chinsamy, 2008) probably represents similar intra-specific variation of cyclical growth patterns than in *Dysalotosaurus*, although LAG's are even completely unknown.

This indicates that most small ornithopods had probably less seasonal environmental stress than large ornithopods and that different growth patterns exist in large and small taxa, respectively. Two reasons are proposed for these differences.

(1) *Food demands and migration:* Small ornithopods were mostly selective low-browsers (Norman et al., 2004) and probably not able for supra-regional migration (Bell & Snively, 2008). They needed much lower absolute amounts of food than large ornithopods, which would also have a weaker effect on their growth rates during dry (or cold) seasons than in large taxa. The latter also cleared their local habitat of food much faster than small ornithopods, not only because of their higher absolute food demands, but also due to their much more effective chewing ability (e.g. Carrano et al., 1999; Norman & Weishampel, 1985), and their partly assumed gregarious behavior (e.g. Carrano et al., 1999; Forster, 1990b; Horner & Makela, 1979; Horner et al., 2004). For many of them, migration was therefore essential to survive and this meant additional seasonal stress.
Furthermore, some small ornithopods were probably able to endure bad times by specialized adaptations, such as the fossorial *Oryctodromeus* (Varricchio et al., 2007; see also Martin, 2009), to which larger ornithopods were unable to do so (Bell & Snively, 2008).

In conclusion, higher food demands and seasonal migration of large ornithopods could be one reason for the much more consistent development of resting lines in their long bones compared to small ornithopods. Exceptions are maybe the ornithopods *Telmatosaurus* and *Zalmoxes*, which are treated as secondarily downsized taxa due to their restricted island habitat (Redelstorff et al., 2009).

(2) *Breeding strategy and courtship/rut: Dysalotosaurus*, *Orodromeus*, and other smaller ornithopods were probably precocial as hatchlings (see chapters 5.4.2 and 6.7.3; Horner et al., 2001; Winkler, 1994), whereas hadrosaurs were mainly altricial (Horner & Makela, 1979; Horner et al., 2000; 2001). Parents of precocial offspring (small ornithopods) just have to care for the eggs and have to protect and lead the young within the herd. The latter task was probably also managed by other adult members of this herd, so that the individual stress of single adults was even lower. Altricial behavior means the possibility of extraordinary high juvenile growth rates on the one hand,

but also more stress for the caring adults on the other hand. Parents of an altricial offspring have to feed their young and have to protect them against other adults of the colony and against carnivores of all sizes. Colonial nesting is also a stress factor in itself, because many individuals are concentrated in a comparatively small area. In addition, at least the sexually dimorphic lambeosaurine hadrosaurs could have had a seasonal rut or courtship (Carrano et al., 1999), which also would mean higher seasonal stress for sexually mature adults. Thus, the large hadrosaurs have suffered much more stress as sexually mature adults, but their altricial behavior equalized this disadvantage due to the ability to outgrow other dinosaurs as juveniles, especially all contemporaneous theropods (Cooper et al., 2008). The growth pattern of *Tenontosaurus* (Lee & Werning, 2008; Werning, 2005; Fig. 6.23) is similar to hadrosaurs, so that altricial behavior can be assumed as well. Thus, altricial behavior was probably one of the key strategies within Ornithopoda to become large in a short time and the resulting growth pattern (higher juvenile growth rates and earlier achievement of sexual and somatic maturity compared to small ornithopods) reflects this seasonally much more stressful strategy by the regular development of resting lines in sexually mature adults.

As a last point and with the information on the bone histology of other ornithopods at hand, the unusual pattern of the polar ornithopod (Chinsamy et al., 1998) can now be reevaluated. There are three possibilities to explain the unusual azonal growth pattern in this femur, although a dark polar winter would implicate well developed growth cycles. (1) It is just an insignificant single sample. It is therefore at least likely that it represents a minority of its population and further studies might reveal growth zones in the bone of this taxon. (2) The sampled individual could be not more than one year old. Polar penguin chicks, for instance, grow extremely fast (even among birds) to reach the necessary body size before the beginning of the winter season (Margerie et al., 2004). This is also possible for the polar ornithopod, because it has to reach a specific body size before its first winter. The vascularization pattern of the femur (mainly longitudinal primary osteons) would actually indicate lower growth rates, but Starck & Chinsamy (2002) have shown that growth rates, inferred from a vascularization pattern, can be highly variable. Another indication for this hypothesis is the

structure of the lamellar bone tissue at the periphery, which looks like an EFS. LAG's, found usually closely spaced there, are not visible (Chinsamy et al., 1998: fig. 1C). This means that this peripheral structure is either an EFS in its first year of development or it represents a thick first annulus, which was deposited during the first winter of its life and the animal died at the end of this winter season. (3) As in most of the other small ornithopods, it was hardly affected by the dark season, because it rarely experienced food shortage, had a precocial behavior or it possessed a certain ability to optimize its chance to survive (see Bell & Snively, 2008; Martin, 2009; Varricchio et al., 2007). The contrasting cyclical growth pattern of the contemporaneous *Timimus* is probably partially the result of territoriality (see chapter 6.8.2).

It is important to note that the remarks on the reasons for different growth patterns in ornithopods are tentative hypotheses. The variability of growth patterns, especially in smaller ornithopods, is striking and ontogenetic histological studies of more taxa are urgently needed to strengthen or disprove them. Nevertheless, the occurrence and/or consistency of resting lines in ornithopods is obviously dependent on a mixture of absolute growth rates (which depends on maximum body size), relative growth rates (depends on the sampled skeletal element and its ontogenetic stage), the degree of seasonality of the respective habitat, and the liability of the taxon to seasonal effects including temperature, humidity, food supply, migration, and behavior (e.g. precocial or altricial breeding strategy). Phylogeny plays a rather unimportant role, as already indicated by Werning (2005).

6.8.4 Other ornithischians

There are still too few studies on other ornithischians to draw secured conclusions. However, neoceratopsians seem to have evolved similar strategies in growth pattern and paleobehavior as large ornithopods (*Tenontosaurus* and probably all ankylopollexians), because they also experienced higher juvenile growth rates and earlier achievement of sexual and somatic maturity compared to

smaller basal ceratopsians (see Erickson & Tumanova, 2000; Erickson et al., 2009; Lee, 2006; Reizner & Horner, 2006). Several large neoceratopsians are also assumed to show gregarious behavior (e.g. Currie & Dodson, 1984; Lehman, 2007; Rogers, 1990; Ryan et al., 2001), although this interpretation should still be treated with caution (Dodson et al., 2004; Rogers, 1990). However, seasonal migration of neoceratopsians has probably taken place between coastal and inland environments (Brinkman et al., 1998) and seasonal stress due to mating and reproduction is very likely (Dodson et al., 2004 and references therein). Thus, the similar growth pattern of large ornithopods and most neoceratopsians is another evidence for their similar paleobiology and paleobehavior. Unfortunately, neoceratopsian hatchlings are still very rare to test possible altricial behavior.

Thyreophorans are also rarely studied, but Padian et al. (2004), Redelstorff and Sander (2009), and Stein & Sander (2009) have shown for the primitive thyreophoran *Scutellosaurus,* the derived stegosaur *Stegosaurus*, and derived ankylosaurs, respectively, that this group had a very distinctive growth pattern. Their overall slower growth rate compared to all other dinosaurs of similar body size is partly explained by their ability of active protection against predators (Redelstorff & Sander, 2009).

6.9 Conclusions

The large amount of specimens, representing a wide range of ontogenetic stages, offered the unique occasion to learn more about the modes and reasons of variation in bone tissues and allowed deep insight into the growth pattern and life history of the ornithopod dinosaur *Dysalotosaurus*.

Variation within the bone tissue was mainly found between different skeletal elements and between different units of single cross sections. The former is the result of different relative growth rates, which are dependent on the individual size of a certain element and its degree of utilization within the skeleton. Skeletal elements with a large absolute size, with main weight bearing functions, and elements intensively used for movements (e.g. for locomotion) experience higher relative

growth rates than other elements. Some elements have of course combined these characters, which explain the highest growth rates in the femur for instance. Accordingly, the only predictable model on the occurrence of true resting lines (LAG's and annuli) in *Dysalotosaurus* is their increasing abundance in skeletal elements with lower relative growth rate compared to other elements. The number of growth cycles naturally increases during ontogeny, but this definitely is not the case for true resting lines. The extraordinary variation in the development of resting lines in *Dysalotosaurus* eliminates prediction of their existence and relative number in skeletal elements of different ontogenetic stages.

Intra-cortical variation in bone tissue, and thus growth rate, is mainly the result of osseous drift and variation in bone wall thickness during growth. Some relationships between the direction of osseous drift, bone wall thickness, variation in bone tissue, and resulting intra-cortical growth rates, can now be better defined:

1. In the case of a long bone with a bended long axis, osseous drift takes place from the convex to the concave side of this long axis.
2. Relative growth rates, mainly derived from the organizational degree and the density of vascular canals, are lower on the convex side of the bended long axis and higher on its concave side.
3. Growth rates are also relatively higher in thicker cross sectional units than in thinner units.
4. Variation in bone tissue (and thereby relative growth rate) within a cross section decreases the more consistent and round the transverse shape of a bone is. A shaft with a triangular transverse outline contains much more variation than a shaft with a circular transverse outline.
5. In the case of partial sampling of a bended long bone, the part with the best potential record of ordinary bone tissue, and possible growth cycles, is the flat wall on its concave side.

The bone histology of *Dysalotosaurus* is most similar to *Dryosaurus altus* in respect of ontogenetic stages, rarity of resting lines, variation of bone tissues, low degree of secondary remodeling, and the absence of an External Fundamental System in the largest specimens. This confirms the close relationship and a similar growth pattern and general life style of these taxa.

Specimens of the assumed precocial hatchlings are not preserved. Nevertheless, a new type of growth cycles could be used to reconstruct almost the whole life history of *Dysalotosaurus*, despite of the scarcity and variability of resting lines. Growth curves of femora, which were derived by this alternation of fast and slow growing zones, revealed that *Dysalotosaurus* grew with a moderate rate in its juvenile stage until approximately six years of age, experienced accelerated growth during its sexually immature subadult stage until reaching sexual maturity at approximately ten years of age, and had its exponential growth phase as sexually mature adult until the 14th year of life, where the maximum growth rate was reached. Afterwards, the growth rate decelerated and finally reached asymptotic growth well after 20 years. However, the second largest femur specimen represents an estimated age of 19.5 years. None of the members of the preserved *Dysalotosaurus* herd reached the growth plateau of somatic maturity, which was already indicated by the suggested absence of an EFS.

The group of large individuals within the size-frequency distribution obviously consists of sexually mature adults, because medullary bone was found in a tibia and a fibula of this size range. The time of initial sexual maturity was discovered as a mark (MISM) in five large femora representing a slow-down of bone apposition rates.

Indeterminate growth, combined with delayed sexual maturity, is assumed to represent the optimal growth strategy of *Dysalotosaurus* to withstand intra-specific competition and its high liability for predation.

The results of the bone histological study of *Dysalotosaurus* were finally combined with a relationship between abundance and consistency of resting lines in recent mammals and their respective seasonal environment. Sauropods are thereafter considered as relatively insensitive to seasonal influences of their environment due to their usually large body size and high absolute growth rates. Ornithopods are a more heterogeneous group, where the smaller species are less exposed to seasonal effects than the large species mainly based on differences in food demands, growth rates, and breeding strategy. In fact, large size within Ornithopoda was probably also linked

to a change in breeding strategy from precocial to altricial behavior. Theropods were probably territorial altogether and were therefore equally susceptible to seasonal stress, independently of body size.

Dinosaurs well may be developed resting lines, because all their ancestors possessed them, but this basic growth pattern was often derived in several ways later during evolution. Then, a mixture of body size, behavior, food demands, and seasonal fluctuations overprinted the predetermined growth pattern in various dinosaur groups originating from their phylogenetic origin.

7. Final conclusions

The fortunate preservation of thousands of bones in different ontogenetic stages has made the basal iguanodontian ornithopod *Dysalotosaurus lettowvorbecki* the ideal model for the study of morphological and histological changes during growth. It is further advantageous that obviously a single herd was shortly buried after a mass death event and conclusions about some aspects of behavior can therefore be drawn.

The paleoclimate during deposition of the Middle Dinosaur Member, among the other units of the Tendaguru Formation, was alternating between dry and wet seasons in a subtropical to tropical climate. The depositional area, probably once a tidal flat, was not the preferred habitat for the dinosaurs due to the scarcity of vegetation, shelter, and hiding places, but they were definitely forced to wander on the flats to find fresh water during the dry seasons. Some sauropods and stegosaurs got mired in the mud, but the *Dysalotosaurus* herd was probably trapped in a tidal channel by a tide and perished by drowning. A single reworking event split them up into two accumulations afterwards, which become later the two known bonebeds Ig and WJ, 2.5km in the northwest of Tendaguru Hill. The underrepresentation of young individuals is partially the result of local reworking, but the complete absence of the youngest age class, as well as of egg shell remains, let assume that the herd had died far from possible nesting grounds and well outside the breeding season. This is supported by the discovery of medullary bone in two large long bones, which lasts only for a few weeks at most to serve as a store for the developing eggs in a sexually mature female. Thus, the breeding season would probably have started soon after the time of death of the herd. Breeding is most often placed into the beginning of the wet season to supply the young with food and water, which further let assume that the *Dysalotosaurus* herd died at the end of the dry season or at the beginning of the wet season. The age of the youngest preserved individuals of the herd (slightly less, or equal to, a year) supports this hypothesis as well.

Ontogenetic variation in the skull of *Dysalotosaurus* was mainly influenced by the suture closure pattern, by the relative decrease of the orbits, by the relative increase of the pre-orbital region, and by the increasing development of muscle attachment sites. Further variation includes the number of tooth positions, the degree of overlap between cranial elements, and the shape of the basioccipital, for instance. Nevertheless, the variation in suture closure and the conflicting ontogenetic features in two specimens of *Thescelosaurus* show that more than one or two single characters are necessary to evaluate the ontogenetic stage of an individual, which was independently proofed for the holotype skull of *Gasparinisaura*.

Ontogenetic features of the postcranial skeleton of *Dysalotosaurus* comprise the posterior-anterior neurocentral suture closure pattern, the narrower neural canal, the increasing robustness of muscle attachment sites and articular ends of long bones, and many more detailed intra-elemental changes. Most of them are clearly linked to increasing body size and weight. A formerly proposed shift from quadruped to biped locomotion during growth was not supported though, and *Dysalotosaurus* was obviously a lifelong biped cursorial animal.

Peramorphic heterochrony seems to be the main evolutionary tendency within ornithopods, as demonstrated by both the cranial and postcranial ontogeny of *Dysalotosaurus*. However, by integrating the results of the bone histological study, this was achieved only by the dryosaurids due to delayed sexual maturity. The large bodied ornithopods (*Tenontosaurus*, hadrosaurs, probably all remaining ankylopollexians as well) all show accelerated growth rates and earlier sexual maturity compared to dryosaurids, which would mean predisplacement of ontogenetic features. One of the best examples is the deepening of the anterior intercondylar groove of the femur. The increasing body size or weight was accompanied by the deepening of this groove during evolution and the higher growth rates made the large and more derived ornithopods reach also a more advanced developmental stage of this feature in an earlier ontogenetic stage. The second important evolutionary tendency is the shift from a mainly biped locomotion in small ornithopods to facultative quadruped locomotion in large ornithopods. This is demonstrated by the diverse modifications of

ontogeny, which can include paedomorphosis and heterotopy apart from the dominant peramorphosis.

The variation of microstructures within the bones of *Dysalotosaurus* is remarkable. Variation was observed between individuals, between different bones of the skeleton, between levels within a bone, between ontogenetic stages, and between different units of a single cross section. Despite of these, the life history of this dinosaur could be reconstructed, mainly with the help of a special type of growth cycles. The combination with external morphology has revealed that *Dysalotosaurus* had a precocial breeding strategy. It further reached sexual maturity at approximately ten years of age and the oldest individuals of the preserved herd were not much older than 20 years. Indeterminate growth is confirmed by the lack of completed neurocentral suture closure, by the uniformity of bone surface textures and by the lack of an External Fundamental System probably even in the oldest individuals. The underrepresentation of mid-sized individuals within the *Dysalotosaurus* herd is explained by the time of sexual maturity, which has obviously resulted in the banishment from the herd or a higher mortality risk at this age. It also separates the two peaks within the size-frequency distribution in a group of immature juveniles and subadults and a group of sexually mature adults.

Dysalotosaurus has turned out to be as the ideal model for an intermediate stage between less derived small ornithopods and mostly more derived large ornithopods. Its ontogeny has revealed many changes in morphology and growth pattern, which have enabled ornithopods to become so extraordinarily successful throughout the Cretaceous. This includes larger body size, full herbivory with a sophisticated chewing apparatus, very high growth rates, and a social behavior probably matching that of modern ungulates. Most small and large ornithopods can further be divided by their breeding strategy (precocial versus altricial respectively) and by their liability to various seasonal stress. However, *Dysalotosaurus* is, probably as *Dryosaurus*, also unique within Ornithopoda, because it belongs to the only group of small taxa nested well within the almost thoroughly large bodied basal Iguanodontia. Its growth pattern is additionally marked by delayed sexual and somatic maturity, which is comparable to *Tyrannosaurus* in relation to other smaller tyrannosaurs, for instance. This

could be another strategy to become larger without changing its breeding strategy, or it was simply advantageous to become larger as long as possible to be most successful in life.

In the end, many fortunes initiated this study and pushed it on, but the numerous new results have given deep insight into a 145 million year old ecosystem and one of its inhabitant. It has also proofed that there is no need for gigantism, large steak-knife teeth, or numerous threatening spikes to be fascinating. In any case, the reconstruction of the life of an extinct animal opens a small window into the past, initiates a connection with the present, and gives the scientist the impression to help this animal to life again. Its story is uncovered and, thus, never forgotten.

References

Aberhan M, Bussert R, Heinrich W-D, Schrank E, Schultka S, Sames B, Kriwet J, Kapilima S. 2002. Paleoecology and depositional environments of the Tendaguru Beds (Late Jurassic to Early Cretaceous, Tanzania). Mitteilungen aus dem Museum für Naturkunde Berlin, Geowissenschaftliche Reihe 2: 201-205.

Agnolin FL, Ezcurra MD, Pais DF, Salisbury SW. 2010. A reappraisal of the Cretaceous non-avian dinosaur faunas from Australia and New Zealand: evidence for their Gondwanan affinities. Journal of Systematic Palaeontology 8(2): 257-300.

Aiello LC. 1981. The allometry of primate body proportions. Symposia of the Zoological Society of London 48: 331-358.

Aitken WG. 1961. Geology and palaeontology of the Jurassic and Cretaceous of southern Tanganyika. Geological Survey of Tanganyika Bulletin 31: 1-144.

Alexander R McN. 1977. Allometry of the limbs of antelopes (Bovidae). Journal of Zoology, London 183: 125-146.

Alexander R McN. 1989. Dynamics of dinosaurs and other extinct giants. New York: Columbia University Press, 167 pp.

Amprino R. 1947. La structure du tissu osseux envisagèe comme expression de differences dans la vitesse de l' accroisement. Archives de Biologie 58: 315-330.

Anderson JF, Hall-Martin A, Russell DA. 1985. Long-bone circumference and weight in mammals, birds and dinosaurs. Journal of Zoology, London 207: 53-61.

Andrews RM. 1982. Patterns of growth in reptiles. In: Gans C, Pough FH, eds. Biology of the Reptilia. London: Academic Press, 273-320.

Aslan A, Behrensmeyer AK. 1996. Taphonomy and time resolution of bone assemblages in a contemporary fluvial system: the East Fork River, Wyoming. Palaios 11: 411-421.

Bakker RT. 1972. Anatomical and ecological evidence of endothermy in dinosaurs. Nature 238: 81-85.

Bakker RT. 1986. The dinosaur heresies: new theories unlocking the mystery of the dinosaurs and their extinction. New York: Morrow, 481 pp.

Barrett PM. 2000. Prosauropod dinosaurs and iguanas: speculations on the diets of extinct reptiles. In: Sues H-D, ed. Evolution of herbivory in terrestrial vertebrates: perspectives from the fossil record. Cambridge: Cambridge University Press, 42-78.

Barrett PM, Butler RJ, Knoll F. 2005. Small-bodied ornithischian dinosaurs from the Middle Jurassic of Sichuan, China. Journal of Vertebrate Paleontology 25: 823-834.

Behrensmeyer AK. 1975. The taphonomy and paleoecology of Plio-Pleistocene vertebrate assemblages east of Lake Rudolf, Kenya. Bulletin of the Museum of Comparative Zoology 146: 473-578.

Behrensmeyer AK. 1978. Taphonomic and ecologic information from bone weathering. Paleobiology 4: 150-162.

Bell PR, Snively E. 2008. Polar dinosaurs on parade: a review of dinosaur migration. Alcheringa 32: 271-284.

Bennett SC. 1993. The ontogeny of *Pteranodon* and other pterosaurs. Paleobiology 19: 92-106.

Bennett SC. 1995. A statistical study of *Rhamphorhynchus* from the Solnhofen Limestone of Germany: year-classes of a single large species. Journal of Paleontology 69(3): 569-580.

Bennett CS. 1996. Year-classes of pterosaurs from the Solnhofen Limestone of Germany: taxonomic and systematic implications. Journal of Vertebrate Paleontology 16(3): 432-444.

Bertram JEA, Biewener AA. 1992. Allometry and curvature in the long bones of quadrupedal mammals. Journal of Zoology 226: 455-467.

Biewener AA. 1983. Allometry of quadrupedal locomotion: the scaling of duty factor, bone curvature and limb orientation to body size. Journal of Experimental Biology 105: 147-171.

Biewener AA. 1989. Mammalian terrestrial locomotion and size – Mechanical design principles define limits. BioScience 39(11): 776-783.

Bonaparte JF, Vince M. 1979. El hallazgo del primer nido de Dinosaurios Triasicos, (Saurischia, Prosauropoda), Triasico Superior de Patagonia, Argentina. Ameghiniana 16: 173-182.

Bonnan MF. 2004. Morphometric analysis of humerus and femur shape in Morrison Sauropods: implications for functional morphology and paleobiology. Paleobiology 30(3): 444-470.

Botha J, Chinsamy A. 2000. Growth patterns from the bone histology of the cynodonts *Diademodon* and *Cynognathus*. Journal of Vertebrate Paleontology 20: 705-711.

Botha J, Chinsamy A. 2005. Growth patterns of *Thrinaxodon liorhinus*, a non-mammalian cynodont from the Lower Triassic of South Africa. Palaeontology 48(2): 385-394.

Boyd CA, Brown CM, Scheetz RD, Clarke JA. 2009. Taxonomic revision of the basal neornithischian taxa *Thescelosaurus* and *Bugenasaura*. Journal of Vertebrate Paleontology 29(3): 758-770.

Brett-Surman MK, Wagner JR. 2007. Discussion of character analysis of the appendicular anatomy in Campanian and Maastrichtian North American hadrosaurids – Variation and ontogeny. In: Carpenter K, ed, Horns and beaks: ceratopsian and ornithopod dinosaurs. Bloomington: Indiana University Press, 135-170.

Brill K, Carpenter K. 2007. A description of a new ornithopod from the Lytle Member of the Purgatoire Formation (Lower Cretaceous) and a reassessment of the skull of *Camptosaurus*. In: Carpenter K, ed, Horns and beaks: ceratopsian and ornithopod dinosaurs. Bloomington: Indiana University Press, 49-68.

Brinkman DB. 1988. Size-independent criteria for estimating relative age in *Ophiacodon* and *Dimetrodon* (Reptilia, Pelycosauria) from the Admiral and Lower Belle Plains Formations of west-central Texas. Journal of Vertebrate Paleontology 8: 172-180.

Brinkman D, Ryan MJ, Eberth DA. 1998. The paleogeographic and stratigraphic distribution of ceratopsids (Ornithischia) in the Upper Judith River Group of western Canada. Palaios 13: 160-169.

Brinkman DB, Eberth DA, Currie PJ. 2007. From bonebeds to paleobiology: Applications of bonebed data. In: Rogers RR, Eberth DA, Fiorillo AR, eds, Bonebeds – Genesis, analysis, and paleobiological significance. Chicago/London: The University of Chicago Press, 221-264.

Brochu CA. 1995. Heterochrony in the crocodylian scapulocoracoid. Journal of Herpetology 29(3): 464-468.

Brochu CA. 1996. Closure of neurocentral sutures during crocodilian ontogeny: implications for maturity assessment in fossil archosaurs. Journal of Vertebrate Paleontology 16: 49-62.

Brochu CA. 2003. Osteology of *Tyrannosaurus rex*: Insights from a nearly complete skeleton and high-resolution computed tomographic analysis of the skull. Society of Vertebrate Paleontology Memoir 7, 138 pp.

Broschinski A. 1999. Ein paramacellodides Lacertilier-Fragment aus dem Oberen Jura von Tendaguru/Tansania. Mitteilungen aus dem Museum für Naturkunde Berlin, Geowissenschaftliche Reihe 2: 155-158.

Brown B, Schlaikjer EM. 1940. The structure and relationships of *Protoceratops*. Annual of the New York Academy of Science 40(3): 133-266.

de Buffrenil V, Farlow JO, Ricqles A. 1986. Growth and function of *Stegosaurus* plates: Evidence from bone histology. Paleobiology 12: 459-473.

de Buffrenil V, Houssaye A, Böhme W. 2008. Bone vascular supply in monitor lizards Squamata: Varanidae: Influence of size, growth, and phylogeny. Journal of Morphology 269: 533-543.

Burr DB. 1992. Estimated intracortical bone turnover in the femur of growing macaques: Implications for their use as models in skeletal pathology. The Anatomical Record 232: 180-189.

Bussert R., Heinrich W-D., Aberhan, M., 2009*. The Tendaguru Formation (Late Jurassic to Early Cretaceous, southern Tanzania): definition, palaeoenvironments, and sequence stratigraphy. Fossil Record 12(2):141-174.*

Butler RJ, Porro LB, Norman DB. 2008a. A juvenile skull of the primitive ornithischian dinosaur *Heterodontosaurus tucki* from the 'Stormberg' of southern Africa. Journal of Vertebrate Paleontology 28: 702-711.

Butler RJ, Upchurch P, *Norman DB.* 2008b. *The phylogeny of the ornithischian dinosaurs. Journal of Systematic Palaeontology 6 (1): 1-40.*

Bybee PJ, Lee AH, Lamm E-T. 2006. Sizing the Jurassic theropod dinosaur *Allosaurus*: assessing growth strategy and evolution of ontogenetic scaling of limbs. Journal of Morphology 267(3): 347-359.

Callison G, Quimby HM. 1984. Tiny dinosaurs: are they fully grown? Journal of Vertebrate Paleontology 3: 200-209.

Capaldo SD, Peters CR 1995*.* Skeletal Inventories from Wildebeest drownings at Lakes Masek and Ndutu in the Serengeti Ecosystem of Tanzania. Journal of Archaeological Science 22: 385-408.

Carpenter K. 1982. Baby dinosaurs from the Late Cretaceous Lance and Hell Creek formations and a description of a new species of theropod. Contributions to Geology, University of Wyoming 20: 123-134.

Carpenter K. 1994. Baby *Dryosaurus* from the Upper Jurassic Morrison Formation of Dinosaur National Monument. In: Carpenter K, Hirsch KF, Horner JR, eds, Dinosaur eggs and babies. Cambridge: Cambridge University Press, 288-297.

Carpenter K, Wilson Y. 2008. A new species of *Camptosaurus* (Ornithopoda: Dinosauria) from the Morrison Formation (Upper Jurassic) of Dinosaur National Monument, Utah, and a biomechanical analysis of its forelimb. Annals of Carnegie Museum 76: 227-263.

Carpenter K, Hirsch KF, Horner JR. 1994. Summary and prospectus. In: Carpenter K, Hirsch KF, Horner JR, eds, Dinosaur eggs and babies. Cambridge: Cambridge University Press, 366-369.

Carr TD. 1999. Craniofacial ontogeny in Tyrannosauridae (Dinosauria, Coelurosauria). Journal of Vertebrate Paleontology 19(3): 497-520.

Carrano MT. 1998. Locomotion in non-avian dinosaurs: integrating data from hindlimb kinematics, in vivo strains, and bone morphology. Paleobiology 24(4): 450-469.

Carrano MT. 1999. What, if anything, is a cursor? Categories versus continua for determining locomotor habit in mammals and dinosaurs. Journal of Zoology, London 247: 29-42.

Carrano MT. 2001. Implications of limb bone scaling, curvature and eccentricity in mammals and non-avian dinosaurs. Journal of Zoology, London 254: 41-55.

Carrano MT, Hutchinson JR. 2002. Pelvic and hindlimb musculature of *Tyrannosaurus rex* (Dinosauria: Theropoda). Journal of Morphology 253: 207-228.

Carrano MT, Janis CM, Sepkoski JJ Jr. 1999. Hadrosaurs as ungulate parallels: Lost lifestyles and deficient data. Acta Paleontologica Polonica 44 (3): 237-261.

Carrano MT, Hutchinson JR, Sampson SD. 2005. New information on *Segisaurus halli*, a small theropod dinosaur from the Early Jurassic of Arizona. Journal of Vertebrate Paleontology 25(4):835-849.

Carrier D, Leon LR. 1990. Skeletal growth in the California gull (*Larus californicus*). Journal of Zoology, London 222: 375-389.

Case TJ. 1978a. On the evolution and adaptive significance of postnatal growth rates in the terrestrial vertebrates. **Quarterly Review of Biology** 53: 243-282.

Case TJ. 1978b. Speculations on the growth rate and reproduction of some dinosaurs. Paleobiology 4: 320-328.

Castanet J, Meunier FJ, de Ricqles A. 1977. L'enregistrement de la croissance cyclique par le tissu osseux chez les vertebres poikilothermes: donnees comparatives et essai de synthese. Bulletin Biologie de France et Belgique 111: 183-202.

Castanet J, Curry Rogers K, Cubo J, Boisard J-J. 2000. Periosteal bone growth rates in extant ratites (ostriches and emu). Implications for assessing growth in dinosaurs, **Compte rendu de l'Academie des Sciences Paris**, Sciences de la vie 323: 543-550.

Castanet J, Francillon-Vieillot H, Meunier FJ, de Ricqlès A. 1993. Bone and individual aging. In: Hall BK, ed. Bone. Volume 7: Bone growth - B. Boca Raton: CRC Press, 245-283.

Castanet J, Croci S, Aujard F, Perret M, Cubo J, de Margerie E. 2004. Lines of arrested growth in bone and age estimation in a small primate: *Microcebus murinus*. Journal of Zoology, London 263: 31-39.

Cerda IA, Chinsamy-Turan A. 2008. Bone histology of *Gasparinisaura cincosaltensis*, a basal ornithopod dinosaur from the Upper Cretaceous of Patagonia. Ameghiniana 45(4): 24R.

Chapman RE. 1990. Shape analysis in the study of dinosaur morphology. In: Carpenter K, Currie JR, eds. Dinosaur systematics: Approaches and perspectives. Cambridge: Cambridge University Press, 21-42.

Chapman RE, Brett-Surman MK. 1990. Morphometric observations on hadrosaurid ornithopods. In: Carpenter K, Currie JR, eds. Dinosaur systematics: Approaches and perspectives. Cambridge: Cambridge University Press, 163-177.

Chinnery BJ. 2004. Morphometric analysis of evolutionary trends in the ceratopsian postcranial skeleton. Journal of Vertebrate Paleontology 24(3): 591-609.

Chinnery BJ, Weishampel DB. 1998. *Montanoceratops cerorhynchus* (Dinosauria: Ceratopsia) and relationships among basal neoceratopsians. Journal of Vertebrate Paleontology 18(3): 569-585.

Chinsamy A. 1990. Physiological implications of the bone histology of *Syntarsus rhodesiensis* (Saurischia: Theropoda). Palaeontologica Africana 27: 77-82.

Chinsamy A. 1993. Bone histology and growth trajectory of the prosauropod dinosaur *Massospondylus carinatus* Owen. Modern Geology 18: 319-329.

Chinsamy A. 1995. Ontogenetic changes in the bone histology of the Late Jurassic ornithopod *Dryosaurus lettowvorbecki*. Journal of Vertebrate Paleontology 15(1): 96-104.

Chinsamy-Turan A. 2005. The microstructure of dinosaur bone – Deciphering biology with fine-scale techniques. Baltimore/London: Johns Hopkins University Press, 195 pp.

Chinsamy A, Hillenius WJ. 2004. Physiology of nonavian dinosaurs. In: Weishampel DB, Dodson P, Osmólska H, eds. The Dinosauria. Second edition. Berkeley: University of California Press, 643-659.

Chinsamy A, Hurum JH. 2006. Bone microstructure and growth patterns of early mammals. Acta Palaeontologica Polonica 51(2): 325-338.

Chinsamy A, Codorniu L, Chiappe L. 2008. Developmental growth patterns of the filter-feeder pterosaur, *Pterodaustro guinñazui*. Biology Letters 4: 282-285.

Chinsamy A, Rich T, Vickers-Rich P. 1998. Polar dinosaur bone histology. Journal of Vertebrate Paleontology 18: 385-390.

Chure DJ. 2000. A new species of *Allosaurus* from the Morrison Formation of Dinosaur National Monument (UT-CO) and a revision of the theropod family Allosauridae. PhD Thesis. New York: Columbia University, 909 pp.

Chure DJ, Turner C, Peterson F. 1994. An embryo of *Camptosaurus* from the Morrison Formation (Jurassic, Middle Tithonian) in Dinosaur National Monument, Utah. In: Carpenter K, Hirsch KF, Horner JR, eds, Dinosaur eggs and babies. Cambridge: Cambridge University Press, 298-310.

Colbert EH. 1981. A primitive ornithischian dinosaur from the Kayenta Formation of Arizona. Museum Northern Arizona Bulletin 53: 1-61. (cited in Appendix 5)

Colbert EH. 1989. The Triassic dinosaur *Coelophysis*. Museum of Northern Arizona Bulletin 57: 1-160.

Colbert EH. 1990. Variation in *Coelophysis bauri*. In: Carpenter K, Currie JR, eds. Dinosaur systematics: Approaches and perspectives. Cambridge: Cambridge University Press, 81-90.

Cole A, Fedak T, Hall B, Olson W, Vickaryous M. 2003. Sutures joining ontogeny and fossils. The Palaeontological Newsletter 52: 29-32.

Coombs WP Jr. 1982. Juvenile specimens of the ornithischian dinosaur *Psittacosaurus*. Palaeontology 25 (1): 89-107.

Coombs WP Jr. 1986. A juvenile ankylosaur referable to the genus *Euoplocephalus* (Reptilia, Ornithischia). Journal of Vertebrate Paleontology 6(2): 162-173.

Cooper LN, Lee AH, Taper ML, Horner JR. 2008. Relative growth rates of predator and prey dinosaurs reflect effects of predation. Proceedings of the Royal Society B doi:10.1098/rspb.2008.0912, Published online.

Cooper MR 1985. A revision of the ornithischian dinosaur *Kangnasaurus coetzeei* Haughton, with a classification of the Ornithischia. Annals of the South African Museum 95: 281-317.

Coria RA, Calvo JO. 2002. A new iguanodontian ornithopod from Neuquen Basin, Patagonia, Argentina. Journal of Vertebrate Paleontology 22(3): 503-509.

Coria RA, Salgado L. 1996. A basal Iguanodontian (Ornithischia: Ornithopoda) from the Late Cretaceous of South America. Journal of Vertebrate Palaeontology 16 (3): 445-457.

Currey JD. 1984. Comparative Mechanical Properties and Histology of Bone. American Zoologist 24: 5-12.

Currey JD. 2002. Bones – Structure and mechanics. Princeton/Oxford: Princeton University Press, 436 pp.

Currie PJ. 2003. Allometric growth in tyrannosaurids (Dinosauria: Theropoda) from the Upper Cretaceous of North America and Asia. Canadian Journal of Earth Science 40(4): 651-665.

Currie PJ, Azuma Y. 2006. New specimens, including a growth series, of *Fukuiraptor* (Dinosauria, Theropoda) from the Lower Cetaceous Kitadani Quarry of Japan. Journal of the Paleontological Society of Korea 22(1): 15-27.

Currie PJ, Carroll RL. 1984. Ontogenetic changes in the eosuchian reptile *Thadeosaurus*. Journal of Vertebrate Paleontology 4(1): 68-84.

Currie PJ, Dodson P. 1984. Mass death of a herd of ceratopsian dinosaurs. In: Reif WE, Westphal F, eds, Third Symposium on Mesozoic Terrestrial Ecosystems, Short Papers. Tübingen: Attempto Verlag, 61-66.

Currie PJ, Peng JH. 1993. A juvenile specimen of *Saurornithoides mongoliensis* from the Djadokhta Formation (Upper Cretaceous) of Northern China. Canadian Journal of Earth Sciences 30: 2224-2230.

Curry KA. 1999. Ontogenetic histology of *Apatosaurus* (Dinosauria: Sauropod): New insights on growth rates and longevity. Journal of Vertebrate Paleontology 19(4): 654-665.

Curry Rogers K, Forster CA. 2004. The skull of *Rapetosaurus krausei* (Sauropoda: Titanosauria) from the Late Cretaceous of Madagascar. Journal of Vertebrate Paleontology 24: 121-144.

Dalla Vecchia FM. 2009. *Tethyshadros insularis*, a new hadrosauroid dinosaur (Ornithischia) from the Upper Cretaceous of Italy. Journal of Vertebrate Paleontology 29(4): 1100-1116. (Cited in Appendix V)

Dietrich WO. 1927. *Brancatherulum* n. g., ein Proplacentalier aus dem obersten Jura des Tendaguru in Deutsch-Ostafrika. Centralblatt für Mineralogie, Geologie und Paläontologie, B 10: 423-426.

Dietrich WO. 1933. Zur Stratigraphie und Paläontologie der Tendaguruschichten. Palaeontographica Supplement VII, 2. Reihe, Teil 2: 1-86.

Dilkes DW. 2000. Appendicular myology of the hadrosaurian dinosaur *Maiasaura peeblesorum* from the late Cretaceous (Campanian) of Montana. Transactions of the Royal Society of Edinburgh – Earth Sciences 90(2): 87-126.

Dilkes DW. 2001. An ontogenetic perspective on locomotion in the Late Cretaceous dinosaur *Maiasaura peeblesorum* (Ornithischia: Hadrosauridae). Canadian Journal of Earth Sciences 38: 1205-1227.

Dodson P. 1975a. Relative growth in two sympatric species of *Sceloporus*. *American Midland Naturalist* 94(2): 421-450.

Dodson P. 1975b. Functional and ecological significance of relative growth in *Alligator. Journal of Zoology, London* 175: 315-355.

Dodson P. 1975c. Taxonomic implications of relative growth in lambeosaurine hadrosaurs. Systematic Zoology 24(1): 37-54.

Dodson P. 1976. Quantitative aspects of relative growth and sexual dimorphism in *Protoceratops*. Journal of Paleontology 50 (5): 929-940.

Dodson P. 1980. Comparative osteology of the American ornithopods *Camptosaurus* and *Tenontosaurus*. **Memoirs de la Societe Geologique de France** 139: 81-85.

Dodson P, Forster CA, Sampson SD. 2004. Ceratopsidae. In: Weishampel DB, Dodson P, Osmólska H, eds. The Dinosauria. Second edition. Berkeley: University of California Press, 494-513.

Eberth DA, Getty MA. 2005. Ceratopsian bonebeds: occurrence, origins, and significance. In: Currie PJ, Koppelhus EB, eds, Dinosaur Provincial Park: A spectacular ecosystem revealed. Bloomington: Indiana University Press, 501–536.

Eberth DA, Shannon M, Noland BG. 2007. A bonebeds database: Classification, biases, and patterns of occurrence. In: Rogers RR, Eberth DA, Fiorillo AR, eds, Bonebeds – Genesis, analysis, and paleobiological significance. Chicago/London: The University of Chicago Press, 103-220.

Enlow DH. 1962. A Study of the Post-Natal Growth and Remodeling of Bone. American Journal of Anatomy 110: 79-101.

Enlow DH, Brown SO. 1956. A comparative histological study of fossil and recent bone tissues. Part I. The Texas Journal of Science 9: 405-439.

Enlow DH, Brown SO. 1957. A comparative histological study of fossil and recent bone tissues. Part II. The Texas Journal of Science 9: 186-214.

Enlow DH, Brown SO. 1958. A comparative histological study of fossil and recent bone tissues. Part III. The Texas Journal of Science 10: 187-230.

Erickson GM. 2005. Assessing dinosaur growth patterns: a microscopic revolution. Trends in Ecology and Evolution 20(12): 677-684.

Erickson GM, Brochu CA. 1999. How the "terror crocodile" grew so big. Nature 398: 205-206.

Erickson GM, Tumanova TA. 2000. Growth curve of *Psittacosaurus mongoliensis* Osborn (Ceratopsia: Psittacosauridae) inferred from long bone histology. Zoological Journal of the Linnean Society 130: 551-566.

Erickson GM, Curry Rogers K, Yerby SA. 2001. Dinosaurian growth patterns and rapid avian growth rates. Nature 412: 429-433.

Erickson GM, Currie PJ, Inouye BD, Winn AA. 2006. Tyrannosaur life tables: An example of nonavian dinosaur population biology. Science 313: 213-217.

Erickson GM, Makovicky PJ, Currie PJ, Norell MA, Yerby SA, Brochu CA. 2004. Gigantism and comparative life-history parameters of tyrannosaurid dinosaurs. Nature 430: 772-775.

Erickson GM, Makovicky PJ, Inouye BD, Zhou C-F, Gao K-Q. 2009. A life table for *Psittacosaurus lujiatunensis*: initial insights into ornithischian dinosaur population biology. The Anatomical Record 292: 1514-1521.

Erickson GM, Rogers KC, Varricchio DJ, Norell MA, Xu X. 2007. Growth patterns in brooding dinosaurs reveals the timing of sexual maturity in non-avian dinosaurs and genesis of the avian condition. Biology Letters doi:10.1098/rsbl.2007.0254, Published online.

Evans DC. 2007. Ontogeny and evolution of lambeosaurine dinosaurs (Ornithischia: Hadrosauridae). PhD Thesis. Toronto: University of Toronto, 497 pp.

Evans DC, Reisz RR, Dupuis K. 2007. A juvenile *Parasaurolophus* (Ornithischia: Hadrosauridae) braincase from Dinosaur Provincial Park, Alberta, with comments on crest ontogeny in the genus. Journal of Vertebrate Paleontology 27: 642-650.

Farke AA, Alicea J. 2009. Femoral strength and posture in terrestrial birds and non-avian theropods. The Anatomical Record 292: 1406-1411.

Farlow JO, Dodson P, Chinsamy A. 1995. Dinosaur biology. Annual Review of Ecology and Systematics 26: 445-471.

Fastovsky DE, Smith JB. 2004. Dinosaur paleoecology. In: Weishampel DB, Dodson P, Osmólska H, eds. The Dinosauria. Second edition. Berkeley: University of California Press, 614-626.

Fechner R. 2009. Morphofunctional evolution of the pelvic girdle and hindlimb of Dinosauromorpha on the lineage to Sauropoda. PhD Thesis. Munich: Ludwig Maximilians Universität, 197 pp.

Fernandez-Jalvo Y, Andrews P. 2003. Experimental effects of water abrasion on bone fragments. Journal of Taphonomy 1(3): 147-163.

Fiorillo AR. 1987. Trample marks: Caution from the Cretaceous. Current Research in the Pleistocene 4: 73-75.

Forster CA. 1990a. The postcranial skeleton of the ornithopod dinosaur *Tenontosaurus tilletti*. Journal of Vertebrate Paleontology 10(3): 273-294.

Forster CA. 1990b. Evidence for juvenile groups in the ornithopod dinosaur *Tenontosaurus tilletti* Ostrom. Journal of Paleontology 64(1): 164-165.

Forster CA. 1997. Phylogeny of the Iguanodontia and Hadrosauridae. Journal of Vertebrate Paleontology 17(3): 47A.

Foster J. 2007. Jurassic West: The dinosaurs of the Morrison Formation and their world. Bloomington: Indiana University Press, 387pp.

Fraas E. 1908. Ostafrikanische Dinosaurier. Palaeontographica 55:105-144.

Francillon-Vieillot H, de Buffrénil V, Castanet J, Géraudie J, Meunier FJ, Sire JY, Zylberberg L, de Ricqlès A. 1990. Microstructure and mineralization of vertebrate skeletal tissues. In: Carter JE, ed. Skeletal biomineralization: Patterns, processes and evolutionary trends. New York: Van Nostrand Reinhold, 471-530.

Gadow H. 1882. Beiträge zur Myologie der hinteren Extremität der Reptilien. Morphologisches Jahrbuch 7: 329-466.

Galton PM. 1969. The pelvic musculature of the dinosaur *Hypsilophodon* (Reptilia: Ornithischia). Postilla 131: 1-64.

Galton PM. 1972. Classification and evolution of ornithopod dinosaurs. Nature 239: 464-466.

Galton PM. 1974. The ornithischian dinosaur *Hypsilophodon* from the Wealden of the Isle of Wight. Bulletin of the British Museum of Natural History, Geology 25 (1): 1-152.

Galton PM. 1977. The ornithopod dinosaur *Dryosaurus* and a Laurasia-Gondwanaland connection in the Upper Jurassic. Nature 268: 230-232.

Galton PM. 1980. *Dryosaurus* and *Camptosaurus*, intercontinental genera of Upper Jurassic ornithopod dinosaurs. Mémoires de la Société Géologique de France (N. S.) 139: 103-108.

Galton PM. 1981. *Dryosaurus,* a hypsilophodontid dinosaur from the Upper Jurassic of North America and Africa. Postcranial skeleton. Paläontologische Zeitschrift, 55(3/4): 271-312.

Galton FM. 1982. Juveniles of the stegosaurian dinosaur *Stegosaurus* from the Upper Jurassic of North America. Journal of Vertebrate Paleontology 2: 47-62.

Galton PM. 1983. The cranial anatomy of *Dryosaurus*, a hypsilophodontid dinosaur from the Upper Jurassic of North America and East Africa, with a review of hypsilophodontids from the Upper Jurassic of North America. Geologica et Palaeontologica 17: 207-243.

Galton PM. 1989. Crania and endocranial casts from ornithopod dinosaurs of the families Dryosauridae and Hypsilophodontidae (Reptilia: Ornithischia). Geologica et Palaeontologica 23: 217-239.

Galton PM. 1997. Cranial anatomy of the basal hypsilophodontid dinosaur *Thescelosaurus neglectus* Gilmore (Ornithischia: Ornithopoda) from the Upper Cretaceous of North America. Revue de Paléobiologie 16(1): 231-258.

Galton PM. 2007. Teeth of ornithischian dinosaurs (mostly Ornithopoda) from the Morrison Formation (Upper Jurassic) of the western United States. In: Carpenter K, ed. Horns and beaks: ceratopsian and ornithopod dinosaurs. Bloomington: Indiana University Press, 17-47.

Galton PM. 2009. Notes on Neocomian (Lower Cretaceous) ornithopod dinosaurs from England - *Hypsilophodon*, *Valdosaurus*, "*Camptosaurus*", "*Iguanodon*" - and referred specimens from Romania and elsewhere. Revue de Paleobiologie 28: 211-272.

Galton PM, Jensen JA. 1973. Skeleton of a hypsilophodontid dinosaur (*Nanosaurus* (?) *rex*) from the Upper Jurassic of Utah. Brigham Young University Geology Studies 20: 137-157.

Galton PM, Taquet P. 1982. *Valdosaurus*, a hypsilophodontid dinosaur from the Lower Cretaceous of Europe and Africa. Geobios 15: 147-159.

Galton PM, Upchurch P. 2004. Stegosauria. In: Weishampel DB, Dodson P, Osmólska H, eds. The Dinosauria. Second edition. Berkeley: University of California Press, 343-362.

Garcia GJM, da Silva JKL. 2004. On the scaling of mammalian long bones. The Journal of Experimental Biology 207: 1577-1584.

Gatesy SM. 1990. Caudofemoral musculature and the evolution of theropod locomotion. Paleobiology 16: 170-186.

Gatesy SM, Biewener AA. 1991. Bipedal locomotion: effects of speed, size and limb posture in birds and humans. Journal of Zoology, London 224: 127-147.

Gibson AR, Baker AJ, Moeed A. 1984. Morphometric variation in introduced populations of the common myna (*Acridotheres tristis*): An application of the jackknife to principal component analysis. Systematic Zoology 33: 408-421.

Gilmore CW. 1909. Osteology of the Jurassic reptile *Camptosaurus*, with a revision of the species of the genus, and a description of two new species. Proceedings of the U.S. National Museum 36: 197-332.

Gilmore CW. 1915. Osteology of *Thescelosaurus*, an orthopodous dinosaur from the Lance Formation of Wyoming. Proceedings of the United States National Museum 49: 591-616.

Gilmore CW. 1925. Osteology of ornithopodous dinosaurs from the Dinosaur National Monument, Utah. *Camptosaurus medius*, *Dryosaurus altus*, *Laosaurus gracilis*. Memoirs of the Carnegie Museum 10: 385-409.

Gittleman JL, Harvey PH. 1982. Carnivore home-range size, metabolic needs and ecology. Behavioural Ecology and Sociobiology 10: 57-63.

Godefroit P, Bolotsky YL, van Itterbeek J. 2004. The lambeosaurine dinosaur *Amurosaurus riabinini* from the Maastrichtian of far eastern Russia. Acta Palaeontologica Polonica 49: 585-618.

Godefroit P, Dong Z-M, Bultynck P, Li H, Feng L. 1998. Sino-Belgian Cooperative Program. Cretaceous Dinosaurs and Mammals from Inner Mongolia: 1) New Bactrosaurus (Dinosauria: Hadrosauroidea) material from Iren Dabasu (Inner Mongolia, P.R. China). Bulletin del l'Instut Royal Des Sciences Naturelles de Belgique, Sciences de la Terre 68: 1-70.

Goodwin MB, Clemens WA, Horner JR, Padian K. 2006. The smallest known *Triceratops* skull: new observations on ceratopsid cranial anatomy and ontogeny. Journal of Vertebrate Paleontology 26(1): 103-112.

Gould SJ. 1966. Allometry and size in ontogeny and phylogeny. Biological Review 41: 587-640.

Gross W. 1934. Die Typen des mikroskopischen Knochenbaues bei fossile Stegocephalen und Reptilien. Zeitschrift der Anatomie und Entwicklungsgeschichte 103: 731-764.

Guenther MF. 2009. Influence of sequence heterochrony on hadrosaurid dinosaur postcranial development. The Anatomical Record 292: 1427-1441.

Hailu Y, Dodson P. 2004. Basal Ceratopsia. In: Weishampel DB, Dodson P, Osmólska H, eds. The Dinosauria. Second edition. Berkeley: University of California Press, 478-493.

Hammer Ø, Harper DAT. 2006. Paleontological data analysis. Oxford: Blackwell Publishing.

Hammer Ø, Harper DAT, Ryan PD. 2001. PAST: Paleontological statistics software package for education and data analysis. Palaeontologia Electronica 4 (1): 1-9.

Heaton MJ. 1972. The palatal structure of some Canadian Hadrosauridae (Reptilia: Ornithischia). Canadian Journal of Earth Sciences 9: 185-205.

Hebblewhite M, Merrill EH. 2007. Multiscale wolf predation risk for elk: does migration reduce risk? Oecologia 152: 377-387.

Heinrich RE, Ruff CB, Weishampel DB. 1993. Femoral ontogeny and locomotor biomechanics of *Dryosaurus lettowvorbecki* (Dinosauria, Iguanodontia). Zoological Journal of the Linnean Society 108: 179-196.

Heinrich W-D. 1998. Late Jurassic mammals from Tendaguru, Tanzania, East Africa. Journal of Mammalian

Evolution 5 (4): 269-290.

Heinrich W-D 1999a. The taphonomy of dinosaurs from the Upper Jurassic of Tendaguru (Tanzania) based on field sketches of the German Tendaguru Expedition (1909-1913). Mitteilungen aus dem Museum für Naturkunde in Berlin, Geowissenschaftliche Reihe 2: 25-61.

Heinrich W-D. 1999b. First haramiyid (Mammalia, Allotheria) from the Mesozoic of Gondwana. Mitteilungen aus dem Museum für Naturkunde Berlin, Geowissenschaftliche Reihe 2: 159-170.

Heinrich W-D. 2001. New records of *Staffia aenigmatica* (Mammalia, Allotheria, Haramiyida) from the Upper Jurassic of Tendaguru in southeastern Tanzania, East Africa. Mitteilungen aus dem Museum für Naturkunde Berlin, Geowissenschaftliche Reihe 4: 239-255.

Heinrich W-D, Bussert R, Aberhan M, Hampe O, Kapilima S, Schrank E, Schultka S, Maier G, Msaky E, Sames B, Chami R. 2001. The German-Tanzanian Tendaguru Expedition 2000. Mitteilungen aus dem Museum für Naturkunde Berlin, Geowissenschaftliche Reihe 4: 223-237.

Hennig E. 1914. Beiträge zur Geologie und Stratigraphie Deutsch-Ostafrikas. Archiv für Biontologie 3(3): 1-72.

Hennig E. 1924. *Kentrurosaurus aethiopicus* – Die Stegosaurier-Funde vom Tendaguru, Deutsch-Ostafrika. Palaeontographica Supplement VII, 1. Reihe (1), Lieferung 2: 100-253.

Hennig E. 1937. Der Sedimentstreifen des Lindi-Kilwa Hinterlandes (Deutsch-Ostafrika). Palaeontographica Supplement VII, 2. Reihe, Teil 2: 99-186.

Herring SW. 1974. A biometric study of suture fusion and skull growth in peccaries. Anatomy and Embryology 146: 167-180.

Hohloch A. 2003. Biometrische Analyse zum Postcranialskelett von *Dryosaurus lettowvorbecki* und Vergleich zu *Hypsilophodon foxii* (Dinosauria, Ornithopoda). Diploma thesis. Tübingen: Eberhard Karls Universität, 116 pp.

Holliday CM, Witmer LM. 2008. Cranial kinesis in dinosaurs: intracranial joints, protractor muscles, and their significance for cranial evolution and function in diapsids. Journal of Vertebrate Paleontology 28: 1073-1088.

Hooker JJ, Milner AC, Sequeira SEK. 1991. An ornithopod dinosaur from the Late Cretaceous of West Antarctica. Antarctic Research 3: 331-332.

Horner JR. 1992. Cranial morphology of *Prosaurolophus* (Ornithischia: Hadrosauridae). With descriptions of two new hadrosaurid species and an evaluation of hadrosaurid phylogenetic relationships. Museum of the Rockies Occasional Papers 2: 1-119.

Horner JR, Currie PJ. 1994. Embryonic and neonatal morphology and ontogeny of a new species of *Hypacrosaurus* (Ornithischia, Lambeosaurinae) from Montana and Alberta. In: Carpenter K, Hirsch KF, Horner JR, eds, Dinosaur eggs and babies. Cambridge: Cambridge University Press, 312-336.

Horner JR, Goodwin MB. 2006. Major cranial changes during *Triceratops* ontogeny. Proceedings of the Royal Society B 273: 2757-2761.

Horner JR, Makela R. 1979. Nest of juveniles provides evidence of family structure among dinosaurs. Nature 282(5736): 296-298.

Horner JR, Weishampel DB. 1988. A comparative embryological study of two ornithischian dinosaurs. Nature 332: 256-257.

Horner JR, Padian K. 2004. Age and growth dynamics of *Tyrannosaurus rex*. Proceedings of the Royal Society of London B 271: 1875-1880.

Horner JR, Weishampel DB. 1996. Correction to: A comparative embryological study of two ornithischian dinosaurs (1988). Nature 383: 103.

Horner JR, Padian K, de Ricqles A. 2001. Comparative osteohistology of some embryonic and perinatal archosaurs: developmental and behavioral implications for dinosaurs. Paleobiology 27: 39-58.

Horner JR, de Ricqles A, Padian K. 1999. Variation in dinosaur skeletochronology indicators: implications for

age assessment and physiology. Paleobiology 25(3): 295-304.

Horner JR, de Ricqles A, Padian K. 2000. Long bone histology of the hadrosaurid dinosaur *Maiasaura peeblesorum*: growth dynamics and physiology based on an ontogenetic series of skeletal elements. Journal of Vertebrate Paleontology 20(1): 115-129.

Horner JR, Weishampel DB, Forster CA. 2004. Hadrosauridae. In: Weishampel DB, Dodson P, Osmólska H, eds, The Dinosauria. Second edition. Berkeley: University of California Press, 438-468.

Horner JR, de Ricqles A, Padian K, Scheetz RD. 2009. Comparative long bone histology and growth of the 'Hypsilophodontid" dinosaurs *Orodromeus makelai*, *Dryosaurus altus*, and *Tenontosaurus tilletti* (Ornithischia: Euornithopoda). Journal of Vertebrate Paleontology 29(3): 734-747.

Hübner TR. 2007. *Dryosaurus lettowvorbecki* – A hoard of options. Hallesches Jahrbuch für Geowissenschaften Beiheft 23: 137-139.

Hübner TR, Rauhut OWM. 2010. A juvenile skull of *Dysalotosaurus lettowvorbecki* (Ornithischia: Iguanodontia), and implications for cranial ontogeny, phylogeny, and taxonomy in ornithopod dinosaurs. Zoological Journal of the Linnean Society. In press.

Hurlburt Jr. RC. 1982. Population dynamics of the three-toed horse *Neohipparion* from the Late Miocene of Florida. Paleobiology 8(2): 159-167.

Hutchinson JR. 2001. The evolution of femoral osteology and soft tissues on the line to extant birds (Neornithes). Zoological Journal of the Linnean Society 131: 169-197.

Hutton JM. 1986. Age determination of living Nile crocodiles from the cortical stratification of bone. Copeia 1986(2): 332-341.

Huxley JS. 1932. Problems of relative growth. London: MacVeagh.

Ikejiri T. 2003. Sequence of closure of neurocentral sutures in *Camarasaurus* (Sauropoda) and implications for phylogeny in Reptilia. Journal of Vertebrate Paleontology 23(3): 65A.

Ikejiri T, Tidwell V, Trexler DL. 2005. New adult specimens of *Camarasaurus lentus* highlight ontogenetic variation within the species. In: Tidwell V, Carpenter K, eds. Thunder-Lizards: the Sauropodomorph Dinosaurs. Bloomington: Indiana University Press, 154-186.

Irmis RB. 2007. Axial skeleton ontogeny in the Parasuchia (Archosauria: Pseudosuchia) and its implications for ontogenetic determination in archosaurs. Journal of Vertebrate Paleontology 27: 350-361.

Jacobs LL, Winkler DA, Murry PA, Maurice JM. 1994. A nodosaurid scuteling from the Texas shore of the Western Interior Seaway. In: Carpenter K, Hirsch KF, Horner JR, eds, Dinosaur eggs and babies. Cambridge: Cambridge University Press, 337-346.

Janensch W. 1914a. Bericht über den Verlauf der Tendaguru-Expedition. Archiv für Biontologie 3(1): 17-58.

Janensch W. 1914b. Übersicht über die Wirbeltierfauna der Tendaguru-Schichten, nebst einer kurzen Charakterisierung der neu aufgeführten Arten von Sauropoden. Archiv für Biontologie 3(1): 81-110.

Janensch W. 1914c. Die Gliederung der Tendaguru-Schichten im Tendaguru-Gebiet und die Entstehung der Saurier-Lagerstätten. Archiv für Biontologie 3(3): 227-261.

Janensch W. 1925a. Die Grabungsstellen der Tendaguru-Gegend. Palaeontographica Supplement VII, 1. Reihe (1): 17-19.

Janensch W. 1925b. Die Coelurosaurier und Theropoden der Tendaguru-Schichten Deutsch-Ostafrikas. Palaeontographica, Supplement VII, 1. Reihe (1): 1-97.

Janensch W. 1950. Die systematische Stellung des Ornithopoden *Dysalotosaurus* aus den Tendaguru-Schichten. Neues Jahrbuch für Geologie und Paläontologie Monatshefte 1950: 286-287.

Janensch W. 1955. Der Ornithopode *Dysalotosaurus* der Tendaguruschichten. Palaeontographica Supplement VII, 1. Reihe, Teil 3: 105-176.

Janensch W. 1961a. Die Gliedmaßen und Gliedmaßengürtel der Sauropoden der Tendaguruschichten. Palaeontographica, Supplement VII, l. Reihe (3): 177-235.

Janensch W. 1961b. Skelettrekonstruktion von *Dysalotosaurus lettowvorbecki*. Palaeontographica Supplement VII, 1. Reihe, Teil 3: 237-240.

Jarman PJ. 2000. Dimorphism in social Artiodactyla: Selection upon females. In: Vrba ES, Schaller GB, eds, Antelopes, deer, and relatives – Fossil record, behavioral ecology, systematic, and conservation. New Haven/London: Yale University Press, 171-179.

Jarman PJ, Jarman MV. 1973. Social behavior, population structure, and reproduction potential in impala. East African Wildlife Journal 11: 329-338.

Jasinoski SC, Russell AP, Currie PJ. 2006. An integrative phylogenetic and extrapolatory approach to the reconstruction of dromaeosaur (Theropoda: Eumaniraptora) shoulder musculature. Zoological Journal of the Linnean Society 146: 301-344.

Johnson R. 1977. Size independent criteria for estimating relative age and the relationships among growth parameters in a group of fossil reptiles (Reptilia: Ichthyosauria). Canadian Journal of Earth Sciences 14: 1916-1924.

Jorgenson JT, Festa-Bianchet M, Gaillard J-M, Wishart WD. 1997. Effects of age, sex, disease, and density on survival of bighorn sheep. Ecology 78(4): 1019-1032.

Kear BP 2007. A Juvenile pliosauroid plesiosaur (Reptilia: Sauropterygia) from the Lower Cretaceous of South Australia. Journal of Paleontology 81(1): 154-162.

Kirkland JI. 1998. A new hadrosaurid from the upper Cedar Mountain Formation (Albian–Cenomanian: Cretaceous) of eastern Utah - the oldest known hadrosaurid (lambeosaurine?). In: Spencer GL, Kirkland JI, Estep JW, eds. Lower and Middle Cretaceous Terrestrial Ecosystems. New Mexico Museum of Natural History Bulletin 14: 283-295.

Klein N. 2004. Bone histology and growth of the prosauropod dinosaur *Plateosaurus engelhardti* Meyer 1837 from the Norian bonebeds of Trossingen (Germany) and Frick (Switzerland). PhD Thesis. Bonn: Rheinische Friedrich-Wilhelms-Universität, 128 pp.

Klein N, Sander PM. 2007. Bone histology and growth of the prosauropod dinosaur *Plateosaurus engelhardti* (von Meyer 1837) from the Norian bonebeds of Trossingen (Germany) and Frick (Switzerland). Special Papers in Palaeontology 77: 169-206.

Klein N, Sander PM. 2008. Ontogenetic stages in the long bone histology of sauropod dinosaurs. Paleobiology 34(2): 247-263.

Klein RG. 1982. Patterns of ungulate mortality and ungulate mortality profiles from Langebaanweg (Early Pliocene) Elandsfontein (Middle Pleistocene), south-western Cape Province, South Africa. Annals of the South

African Museum 90(2): 49-94.

Klevezal GA. 1996. Recording structures of mammals: Determination of age and reconstruction of life history. Rotterdam: Balkema, 274 pp.

Klevezal GA, Kleinenberg SE. 1969. Age determination of mammals from annual layers in teeth and bones. Jerusalem: Translated from Russian by Israeli Program for Scientific Translations Press, 128 pp.

Kurten B. 1953. On the variation and population dynamics of fossil and recent mammal populations. Acta Zoologica Fennica 76: 1-121.

Lee AH. 2004. Histological organization and its relationship to function in the femur of *Alligator mississippiensis*. Journal of Anatomy 204: 197-207.

Lee AH. 2006. Evolution of rapid limb growth and vascular canal organization in ceratopsian dinosaurs. Journal of Vertebrate Paleontology 26(3): 89A.

Lee AH, Werning S. 2008. Sexual maturity in growing dinosaurs does not fit reptilian growth models. Proceedings of the National Academy of Sciences 105: 582-587.

Lehman TM. 1990. The ceratopsian subfamily Chasmosaurinae: sexual dimorphism and systematics. In: Carpenter K, Currie JR, eds. Dinosaur systematics: Approaches and perspectives. Cambridge: Cambridge University Press, 211-229.

Lehman TM. 2007. Growth and population age structure in the horned dinosaur *Chasmosaurus*. In: Carpenter K, ed, Horns and beaks: ceratopsian and ornithopod dinosaurs. Bloomington: Indiana University Press, 259-317 pp.

Lehman TM, Woodward HN. 2008. Modeling growth rates for sauropod dinosaurs. Paleobiology 34(2): 264-281.

Long JA, McNamara KJ. 1997. Heterochrony. In: Currie PJ, Padian K, eds, Encyclopedia of dinosaurs. London: Academic Press, 311-317.

Lull RS, Wright NF. 1942. Hadrosaurian dinosaurs of North America. The Geological Society of America, Special Paper 40, 242 pp. (cited in Appendix 5)

Lyman RL. 1994. Vertebrate Taphonomy. Cambridge: Cambridge University Press, 524 pp.

Maier G. 2003. African Dinosaurs Unearthed. Bloomington: Indiana University Press.

Maisano JA. 2002. Terminal Fusions of Skeletal Elements as Indicators of Maturity in Squamates. Journal of Vertebrate Paleontology 22(2): 268-275.

Makovicky PJ, Kobayashi Y, Currie PJ. 2004. Ornithomimosauria. In: Weishampel DB, Dodson P, Osmólska H, eds. The Dinosauria. Second edition. Berkeley: University of California Press, 137-150.

Makovicky PJ, Li D, Gao K-Q, Lewin M, Erickson GM, Norell MA. 2009. A giant ornithomimosaur from the Early Cretaceous of China. Proceedings of the Royal Society of London B 277: 191-198.

de Margerie E, Cubo J, Castanet J. 2002. Bone typology and growth rate: Testing and quantifying ‘‘Amprino’s rule’’ in the mallard (*Anas platyrhynchos*). Compte rendu de l’Academie des Sciences Paris, Biologies 325: 221-230.

de Margerie E, Robin J-P, Verrier D, Cubo J, Groscolas R, Castanet J. 2004. Assessing the relationship between bone microstructure and growth rate: A fluorescent labelling study in the king penguin chick (*Aptenodytes patagonicus*). Journal of Experimental Biology 207: 869-879.

Martin AJ. 2009. Dinosaur burrows in the Otway Group (Albian) of Victoria, Australia, and their relation to Cretaceous polar environments. Cretaceous Research 30: 1223-1237.

Martin V. 1994. Baby sauropods from the Sao Khua Formation (Lower Cretaceous) in northeastern Thailand. Gaia 10: 147-153.

Martinez R. 1998. *Notohypsilophodon comodorensis* gen. et sp. nov. Un Hypsilophodontidae (Ornitischia [sic]: Ornithopoda) del Cretacico Superior de Chubut, Patagonia, Central Argentina. Acta Geologica Leopoldensia 21: 119-135.

Maryanska T, Osmolska H. 1984. Postcranial anatomy of *Saurolophus angustirostris* with comments on other hadrosaurs. Paleontologica Polonica 46: 119-141. (Cited in Appendix V)

Mihlbachler MC. 2003. Demography of late Miocene rhinoceroses (*Teleoceras proterum* and *Aphelops malacorhinus*) from Florida: linking mortality and sociality in fossil assemblages. Paleobiology 29: 412-428.

Milner, A. R. & Norman, D. B. 1984. The biogeography of advanced ornithopod dinosaurs (Archosauria: Ornithischia) – a cladistic-vicariance model. In Reif W-E & Westphal F, eds. Third Symposium on Mesozoic Terrestrial Ecosystems, short papers. Tübingen: Attempto Verlag, 145-150.

Moreno K, Carrano MT, Snyder R. 2007. Morphological changes in pedal phalanges through ornithopod dinosaur evolution: a biomechanical approach. Journal of Morphology 268(1): 50-63.

Mulhern DM, Ubelaker DH. 2003. Histologic examination of bone development in juvenile chimpanzees. American Journal of Physical Anthropology 122: 127-133.

Myers TS, Fiorillo AR. 2009. Evidence for gregarious behavior and age segregation in sauropod dinosaurs. Palaeogeography, Palaeoclimatology, Palaeoecology 274: 96-104.

Nopcsa F, Heidsieck E. 1933. On the histology of the ribs in immature and half-grown trachodont dinosaurs. Proceedings of the Zoological Society of London 1933: 221-223.

Norman DB. 1980. On the Ornithischian Dinosaur *Iguanodon bernissartensis* from the Lower Cretaceous of Bernissart (Belgium). Memoire, Institut Royal des Sciences Naturelles de Belqique 178: 1-104.

Norman DB. 1984. On the cranial morphology and evolution of ornithopod dinosaurs. Symposia of the Zoological Society of London 52: 521-547.

Norman DB. 1986. On the anatomy of *Iguanodon atherfieldiensis* (Ornithischia: Ornithopoda). Bulletin d'Institut Royal de la Sciences Naturelles de Belgique: Sciences de la Terre 56: 281-372.

Norman DB. 1991. Dinosaurier. Munich: C. Bertelsmann Verlag GmbH, 192 pp. (in german, original version Boxtree Limited, London)

Norman DB. 1998. On Asian ornithopods (Dinosauria: Ornithischia). 3. A new species of iguanodontid dinosaur. Zoological Journal of the Linnean Society 122: 291-348.

Norman DB. 2002. On Asian ornithopods (Dinosauria: Ornithischia). 4. *Probactrosaurus* Rozhdestvensky, 1966. Zoological Journal of the Linnean Society 136: 113-144.

Norman DB. 2004. Basal Iguanodontia. In: Weishampel DB, Dodson P, Osmólska H, eds. The Dinosauria. Second

edition. Berkeley: University of California Press, 413-437.

Norman DB, Weishampel DB. 1985. Ornithopod feeding mechanisms: Their bearing on the evolution of herbivory. American Naturalist 126: 151-164.

Norman DB, Sues H-D, Witmer LM, Coria RA. 2004. Basal Ornithopoda. In: Weishampel DB, Dodson P, Osmólska H, eds. The Dinosauria. Second edition. Berkeley: University of California Press, 393-412.

Novas FE, Cambiaso AV, Ambrosio A. 2004. A new basal iguanodontian (Dinosauria, Ornithischia) from the Upper Cretaceous of Patagonia: Ameghiniana 41(1): 75-85.

O'Connor PM. 2007. The postcranial axial skeleton of *Majungasaurus crenatissimus* (Theropoda: Abelisauridae) from the Late Cretaceous of Madagascar. In: Sampson SD, Krause DW, eds. *Majungasaurus crenatissimus* (Theropoda: Abelisauridae) from the Late Cretaceous of Madagascar. Society of Vertebrate Paleontology Memoir 8: 127-162.

Ohashi T. 2006. Structural analysis of derived ornithopod skull using 3D Finite Element Method: reconsideration of their feeding mechanisms. Journal of Vertebrate Paleontology 26(3): 107A.

Ostrom JH. 1961. Cranial morphology of the hadrosaurian dinosaurs of North America. Bulletin of the American Museum of Natural History 122: 37-186.

Ostrom JH. 1970. Stratigraphy and Paleontology of the Cloverly Formation (Lower Cretaceous) of the Bighorn Basin Area, Wyoming and Montana. Peabody Museum Bulletin 35: 1-234.

Owen-Smith N. 1993. Comparative mortality rates of male and female kudus: the costs of sexual size dimorphism. Journal of Animal Ecology 62: 428-440.

Padian K, Horner JR. 2004. Dinosaur physiology. In: Weishampel DB, Dodson P, Osmólska H, eds. The Dinosauria. Second edition. Berkeley: University of California Press, 660-671.

Padian K, Horner JR, de Ricqles A. 2004. Growth in small dinosaurs and pterosaurs: the evolution of archosaurian growth strategies. Journal of Vertebrate Paleontology 24(4): 555-571.

Parks WA. 1926. *Thescelosaurus warreni*, a new species of ornithopodous dinosaur from the Edmonton Formation of Alberta. University of Toronto Studies, Geological Series 21: 1-42.

Peabody FE. 1961. Annual growth zones in living and fossil vertebrates. Journal of Morphology 108: 11-62.

Pincemaille-Quillevere M, Buffetaut E, Quillevere F. 2006. Description ostéologique de l'arrière-crâne de *Rhabdodon* (Dinosauria: Euornithopoda) et implications phylogénétiques. Bulletin de la Société Géologique de France 177: 97-104.

Pompeckj JF. 1920. Das angebliche Vorkommen und Wandern des Parietalforamens bei Dinosauriern. Sitzungsberichte der Gesellschaft Naturforschender Freunde zu Berlin: 109-129.

Pompeckj JF. 1922. Bemerkungen über Formen und Gebrauch der Gebisse ornithopoder Dinosaurier. Paläontologische Zeitschrift 4: 87-90.

Ponton F, Elzanowski A, Castanet J, Chinsamy A, de Margerie E, de Ricqles A, Cubo J. 2004. Variation of the outer circumferential layer in the limb bones of birds. Acta Ornithologica 39(2): 21-24.

Prieto-Marquez A. 2007. Postcranial osteology of the hadrosaurid dinosaur *Brachylophosaurus canadensis* from the Late Cretaceous of Montana. In: Carpenter K, ed. Horns and beaks: ceratopsian and ornithopod dinosaurs. Bloomington: Indiana University Press, 91-116.

Prieto-Marquez A. 2008. Phylogeny and historical biogeography of hadrosaurid dinosaurs. PhD Thesis. Tallahassee: Florida State University, 860 pp.

Pritchard JJ, Scott JH, Girgis FG. 1956. The structure and development of cranial and facial sutures. Journal of Anatomy 90(1): 73-89.

Proaktor G, Coulson T, Milner-Gulland EJ. 2008. The demographic consequences of the cost of reproduction in ungulates. Ecology 89(9): 2604-2611.

Raath MA. 1990. Morphological variation in small theropods and its meaning in systematics: Evidence from *Syntarsus rhodesiensis*. In: Carpenter K, Currie JR, eds. Dinosaur systematics: Approaches and perspectives. Cambridge: Cambridge University Press, 91-106.

Rauhut OWM. 2001. Herbivorous dinosaurs from the Late Jurassic (Kimmeridgian) of Guimarota, Portugal. Proceedings of the Geologist's Association 112: 275-283.

Rauhut OWM, Fechner R. 2005. Early development of the facial region in a non-avian theropod dinosaur. Proceedings of the Royal Society London B 272: 1179-1183.

Ray S, Chinsamy A. 2004. *Diictodon feliceps* (Therapsida, Dicynodontia): Bone histology, growth, and biomechanics. Journal of Vertebrate Paleontology 24(1): 180-194.

Ray R, Botha J, Chinsamy A. 2004. Bone histology and growth patterns of some nonmammalian therapsids. Journal of Vertebrate Paleontology 24: 634-648.

Reck H. 1910. 3. Bericht über den weiteren Verlauf der Tendaguru-Expedition. Sitzungsberichte der Gesellschaft Naturforschender Freunde zu Berlin: 372-375.

Reck H. 1911. 4. Bericht über die Ausgrabungen und Ergebnisse der Tendaguru-Expedition (Grabungsperiode 1911). Sitzungsberichte der Gesellschaft Naturforschender Freunde zu Berlin: 385-397.

Reck H. 1925. Grabungen auf fossile Wirbeltiere in Deutsch-Ostafrika. Geologische Charakterbilder 31: 1-36.

Reck H. 1931. Die deutschostafrikanischen Flugsaurier. – Centralblatt für Mineralogie, Geologie und Paläontologie 1931: 321-336.

Redelstorff R, Sander PM. 2009. Long and girdle bone histology of *Stegosaurus*: implications for growth and life history. Journal of Vertebrate Paleontology 29(4): 1087-1099.

Redelstorff R, Csiki Z, Grigorescu D. 2009. The heritage of Nopcsa: Dwarf status of Hateg ornithopods supported by the histology of long bones. Journal of Vertebrate Paleontology 29(3): 170A.

Reid REH. 1984. The histology of dinosaurian bone, and its possible bearing on dinosaur physiology. Symposia of the Zoological Society of London 52: 629-662.

Reid REH. 1997. How dinosaurs grew. In: Farlow JO, Brett-Surman MK, eds. The complete dinosaur. Bloomington: Indiana University Press, 403-413.

Reisz RR, Scott D, Sues H-D, Evans DC, Raath MA. 2005. Embryos of an Early Jurassic prosauropod dinosaur and their evolutionary significance. Science 309: 761-764.

Reizner J, Horner JR. 2006. An ontogenetic series of the ceratopsid dinosaur *Einiosaurus procurvicornis* as determined by long bone histology. Journal of Vertebrate Paleontology 26(3): 114A.

Remes K. 2009. Taxonomy of Late Jurassic diplodocid sauropods from Tendaguru (Tanzania). Fossil Record 12(1): 23-46.

Rensberger JM, Watabe M. 2000. Fine structure of bone in dinosaurs, birds, and mammals. Nature 406: 619-621.

de Ricqles AJ. 1974. Evolution of endothermy: Histological evidence. Evolutionary Theory 1: 51-80.

de Ricqles AJ. 1976. On bone histology of fossil and living reptiles, with comments on its functional and evolutionary significance. In: Bellairs A d'A, Cox CB, eds. Morphology and Biology of Reptiles. Linnean Society Symposium Series 3: 123-150.

de Ricqles A. 1983. Cyclical growth in the long limb bones of a sauropod dinosaur. Acta Paleontologica Polonica 28: 225-232.

de Ricqles A, Meunier FJ, Castanet J, Francillon-Vieillot H. 1991. Comparative microstructure of bone. In: Hall BK, ed. Bone. Volume 3: Bone matrix and bone specific products. Boca Raton: CRC Press, 1-78.

de Ricqles AJ, Padian K, Horner JR, Francillon-Viellot H. 2000. Palaeohistology of the bones of pterosaurs (Reptilia: Archosauria): anatomy, ontogeny, and biomechanical implications. Zoological Journal of the Linnean Society 129(3): 349-385.

Rimblot-Baly F, de Ricqles A, Zylerberg L. 1995. Analyse paleohistologique d'une serie de croissance partielle chez *Lapparentosaurus madagascariensis* (Jurassique Moyen): Essai sur la dynamique de croissance d'un dinosaure sauropode. **Annales de Paleontologie** 81: 49-86.

Rinehart LF, Lucas SG, Heckert AB, Spielmann JA, Celeskey MD. 2009. The paleobiology of *Coelophysis bauri* (Cope) from the Upper Triassic (Apachean) Whitaker quarry, New Mexico, with detailed analysis of a single quarry block. New Mexiko Museum of Natural History and Science Bulletin 45, 260 pp.

Rogers RR. 1990. Taphonomy of three dinosaur bone beds in the Upper Cretaceous Two Medicine Formation of northwestern Montana – evidence for drought-related mortality. Palaios 5(5): 394-413.

Romer AS. 1927. The pelvic musculature of ornithischian dinosaurs. Acta Zoologica 8: 225-275.

Rosenbaum JN, Padian K. 2000. New material of the basal thyreophoran *Scutellosaurus lawleri* from the Kayenta Formation (Lower Jurassic) of Arizona. PaleoBios 20: 13-23.

Roth VL. 1984. How elephants grow: Heterochrony and the calibration of developmental stages in some living and fossil species. Journal of Vertebrate Paleontology 4(1): 126-145.

Rozhdestvensky AK. 1965. Growth changes and some problems of systematics of Asian dinosaurs. Paleontologischeskii Zhurnal 1965: 95-109. (Translated by Russell AD)

Ruiz-Omeñaca JI, Suberbiola XP, Galton PM. 2006. *Callovosaurus leedsi*, the earliest dryosaurid dinosaur (Ornithischia: Euornithopoda) from the Middle Jurassic of England. In: Carpenter K, ed. Horns and beaks: ceratopsian and ornithopod dinosaurs. Bloomington: Indiana University Press, 3-16.

Russell DA, Zhao Z-J. 1996. New psittacosaur occurrences in Inner Mongolia. Canadian Journal of Earth Sciences 33: 637-648. (Cited in Appendix V)

Russell D, Beland F, McIntosh JS. 1980. Paleoecology of the dinosaurs of Tendaguru (Tanzania). Memoires de Societe Geologique de France 59 (139): 169-175.

Ryan MJ. 1997. Dryosauridae. In: Currie J, Padian K, eds. Encyclopedia of Dinosaurs pp. San Diego/London:

Academic Press, 197-198.

Ryan MJ, Russell AP, Eberth DA, Currie PJ. 2001. The Taphonomy of a *Centrosaurus* (Ornithischia: Ceratopsidae) bonebed from the Dinosaur Park Formation (Upper Campanian), Alberta, Canada, with comments on cranial ontogeny. Palaios 16: 482-506

Rybczynski N, Tirabasso A, Bloskie P, Cuthbertson R, Holliday C. 2008. A three-dimensional animation model of *Edmontosaurus* (Hadrosauridae) for testing chewing hypotheses. Palaeontologia Electronica 11: 1-14.

Salgado L, Coria RA, Chiappe LM. 2005. Osteology of the sauropod embryos from the Upper Cretaceous of Patagonia. Acta Palaeontologica Polonica 50: 79-92.

Salgado L, Coria RA, Heredia SE. 1997. New materials of *Gasparinisaura cincosaltensis* (Ornithischia, Ornithopoda) from the Upper Cretaceous of Argentina. Journal of Paleontology 71: 933-940.

Sampson SD, Ryan MJ, Tanke DH. 1997. Craniofacial ontogeny in centrosaurine dinosaurs (Ornithischia: Ceratopsidae): taxonomic and behavioural implications. Zoological Journal of the Linnean Society 121: 293-337.

Sander PM. 1992. The Norian *Plateosaurus* bonebeds of central Europe and their taphonomy. Paleogeography, Paleoclimatology, Paleoecology 93:255-299.

Sander PM. 2000. Longbone histology of the Tendaguru sauropods: implications for growth and biology. Paleobiology 26(3): 466-488.

Sander PM, Andrassy P. 2006. Lines of arrested growth and long bone histology in Pleistocene large mammals from Germany: What do they tell us about dinosaur physiology? Palaeontographica A 277: 143-159.

Sander PM, Tückmantel C. 2003. Bone lamina thickness, bone apposition rates, and age estimates in sauropod humeri and femora. Paläontologische Zeitschrift 77(1): 161-172.

Sander PM, Mateus O, Laven T, Knötschke N. 2006. Bone histology indicates insular dwarfism in a new Late Jurassic sauropod dinosaur. Nature 441: 739-741.

Sander PM, Klein N, Buffetaut E, Cuny G, Suteethorn V, le Loeuff J. 2004. Adaptive radiation in sauropod dinosaurs: bone histology indicates rapid evolution of giant body size through acceleration. Organisms, Diversity & Evolution 4: 165-173.

Santa Luca AP. 1980. The postcranial skeleton of *Heterodontosaurus tucki* (Reptilia, Ornithischia) from the Stormberg of South Africa. Annals of the South African Museum 79: 159-211.

Scheetz RD. 1999. Osteology of *Orodromeus makelai* and the phylogeny of basal ornithopod dinosaurs. PhD Thesis. Bozeman: Montana State University, 186 pp.

Schrank E. 2005. Dinoflagellate cysts and associated aquatic palynomorphs from the Tendaguru Beds (Upper Jurassic – Lower Cretaceous of southeast Tanzania. Palynology 29: 49-85.

Schwartz HL, Gillette DD. 1994. Geology and taphonomy of the *Coelophysis* quarry, Upper Triassic Chinle Formation, Ghost Ranch, New Mexico. Journal of Paleontology 68: 1118-1130.

Schwarz D, Wings O, Myer CA. 2007. Super sizing the giants: first cartilage preservation at a sauropod dinosaur limb joint: Journal of the Geological Society, London 164: 61-65.

Schweitzer MH, Wittmeyer JL, Horner JR. 2005. Gender-specific reproductive tissue in ratites and *Tyrannosuarus rex*. Science 308: 1456-1460.

Seitz AL. 1907. Vergleichende Studien über den makroskopischen Knochenbau fossiler und rezenter Reptilien. Nova Acta Academiae Caesareae Leopoldino-Carolinae Germanicae Naturae Curiosorum 87: 230-370.

Sereno PC. 1986. Phylogeny of the bird-hipped dinosaurs (Order Ornithischia). National Geographic Research 2: 234-256.

Sereno PC. 1991. *Lesothosaurus*, "Fabrosaurids", and the early evolution of Ornithischia. Journal of Vertebrate Paleontology 11: 168-197.

Shepherd JD, Galton PM, Jensen JA. 1977. Additional specimens of the hypsilophodontid dinosaur *Dryosaurus altus* from the Upper Jurassic of Western North America. Brigham Young University, Geology Studies 24: 11-15.

Singh IJ, Tonna EA, Gandel CP. 1974. A comparative histological study of mammalian bone. Journal of Morphology 144: 421-431.

Silva da JKL, Garcia GJM, Barbosa LA. 2006. Allometric scaling laws of metabolism. Physics of Life Reviews 3(4): 229-269.

Starck JM, Chinsamy A. 2002. Bone microstructure and developmental plasticity in birds and other dinosaurs. Journal of Morphology 254: 232-246.

Stein M. Sander PM. 2009. Long bone histology and growth patterns in ankylosaurs. Journal of Vertebrate Paleontology 29(3): 185A.

Sternberg CH. 1940. *Thescelosaurus edmontonensis*, n. sp., and classification of the Hypsilophodontidae. Journal of Paleontology 14: 481-494.

Straight WH, Davis GL, Skinner CW, Haims A, McClennan BL, Tanke DH. 2009. Bone lesions in hadrosaurs: computed tomographic imaging as guide for paleohistologic and stable-isotopic analysis. Journal of Vertebrate Paleontology 29(2): 315-325.

Sues H-D. 1980. Anatomy and relationships of a new hypsilophodontid dinosaur from the Lower Cretaceous of North America. Palaeontographica *A* 169(1-3): 51-72.

Sues H-D, Norman DB. 1990. Hypsilophodontidae, *Tenontosaurus*, and Dryosauridae. In: Weishampel DB, Dodson P, Osmolska H, eds. The Dinosauria, First edition. Berkeley: University of California Press, 498-509.

Tanke DH, Brett-Surman MK. 2001. Evidence of hatchling- and nestling-size hadrosaurs (Reptilia: Ornithischia) from Dinosaur Provincial Park (Dinosaur Park Formation: Campanian), Alberta. In: Tanke DH, Carpenter K, eds. Mesozoic vertebrate life. Bloomington and Indianapolis: Indiana University Press, 206-218.

Tanke D, Currie PJ. 1998. Head-biting in theropod dinosaurs: paleopathological evidence. Gaia 15: 167-184.

Taquet P. 1976. Géologie et Paléontologie du Gisement de Gadoufaoua (Aptien du Niger). Cahiers de Paléontologie. Éditions du Centre National de la Recherche Scientifique: 1-191.

Thulborn RA. 1971. Origin and evolution of ornithischian dinosaurs. Nature 234: 75-78.

Tidwell V, Wilhite DR. 2005. Ontogenetic variation and isometric growth in the forelimb of the Early Cretaceous sauropod *Venenosaurus*. In: Tidwell V, Carpenter K, eds. Thunder Lizards. Bloomington, Indiana: Indiana University Press, 187-196.

Tidwell V, Stadtman K, Shaw A. 2005. Age-related characteristics found in a partial pelvis of *Camarasaurus*. In: Tidwell V, Carpenter K, eds. Thunder Lizards. Bloomington, Indiana: Indiana University Press, 180-186.

Tsuihiji T. 2007. Homologies of the iliocostalis, iliocostalis, and hypaxial muscles in the anterior presacral region of extant Diapsida. Journal of Morphology 268(11): 986-1020.

Turnbull WD, Martill DM. 1988. Taphonomy and preservation of a monospecific titanothere assemblage from the Washakie Formation (Late Eocene), southern Wyoming. An ecological accident in the fossil record: Palaeogeography, Palaeoclimatology, Palaeoecology 63: 91-108.

Tumarkin-Deratzian AR. 2003. Bone surface textures as ontogenetic indicators in extant and fossil archosaurs: Macroscopic and histological evaluations. PhD Thesis. Philadelphia: University of Pennsylvania, 333 pp.

Tumarkin-Deratzian AR, Vann DR, Dodson P. 2006. Bone surface texture as an ontogenetic indicator in long bones of the Canada goose *Branta canadensis* (Anseriformes: Anatidae). Zoological Journal of the Linnean Society 148: 133-168.

Tumarkin-Deratzian AR, Vann DR, Dodson P. 2007. Growth and textural ageing in long bones of the American alligator *Alligator mississippiensis* (Crocodylia: Alligatoridae). Zoological Journal of the Linnean Society 150: 1-39.

Tumarkin-Deratzian AR. 2009. Evaluation of long bone surface textures as ontogenetic indicators in centrosaurine ceratopsids. The Anatomical Record 292: 1485-1500.

Turvey ST, Holdaway RN. 2005. Postnatal ontogeny, population structure, and extinction of the giant moa *Dinornis*. Journal of Morphology 265: 70-86.

Turvey ST, Green OR, Holdaway RN. 2005. Cortical growth marks reveal extended juvenile development in New Zealand moa. Nature 435: 940-943.

Tykoski RS, Rowe T. 2004. Ceratosauria. In: Weishampel DB, Dodson P, Osmólska H, eds. The Dinosauria. Second edition. Berkeley: University of California Press, 47-70.

Unwin D., Heinrich W-D. 1999. On a pterosaur jaw remain from the Late Jurassic of Tendaguru, East Africa. Mitteilungen aus dem Museum für Naturkunde Berlin, Geowissenschaftliche Reihe 2: 121-134.

Upchurch P, Barrett PM, Dodson P. 2004. Sauropoda. In: Weishampel DB, Dodson P, Osmólska H, eds. The Dinosauria. Second edition. Berkeley: University of California Press, 259-322.

Varricchio DJ. 1993. Bone microstructures of the Upper Cretaceous theropod dinosaur *Troodon formosus*. Journal of Vertebrate Paleontology 13: 99-104.

Varricchio DJ, Horner JR. 1993. Hadrosaurid and lambeosaurid bone beds from the Upper Cretaceous Two Medicine Formation of Montana: taphonomic and biologic implications. Canadian Journal of Earth Science 30: 997-1006.

Varricchio DJ. 1995. Taphonomy of Jack's Birthday Site, a diverse dinosaur bonebed from the Upper Cretaceous Two Medicine Formation of Montana. Palaeogeography, Palaeoclimatology, Palaeoecology 114: 297-323.

Varricchio DJ, Martin AJ, Katsura Y. 2007. First trace and body fossil evidence of a burrowing, denning dinosaur. Proceedings of the Royal Society B 274(1616): 1361-1368.

Varricchio DJ, Sereno PC, Zhao X, Tan L, Wilson JA, Lyon GH. 2008. Mud-trapped herd captures evidence of distinctive dinosaur sociality. Acta Palaeontologica Polonica 53(4): 567-578.

Vickaryous MK, Maryanska T, Weishampel DB. 2004. Ankylosauria. In: Weishampel DB, Dodson P, Osmólska H, eds. The Dinosauria. Second edition. Berkeley: University of California Press, 363-392.

Virchow H. 1919. Atlas und Epistropheus bei den Schildkröten. Sitzungsberichte der Gesellschaft Naturforschender Freunde zu Berlin: 303-332.

Voorhies MR. 1969. Taphonomy and population dynamics of an early Pliocene vertebrate fauna, Knox County, Nebraska. University of Wyoming, Contributions to Geology Special Paper 1: 1-69.

Voorhies MR. *1985.* A Miocene rhinoceros herd buried in volcanic ash. National Geographic Society Research Reports 19: 671-688.

Wang Q, Strait DS, Dechow PC. 2006. Fusion patterns of craniofacial sutures in rhesus monkey skulls of known age and sex from Cayo Santiago. American Journal of Physical Anthropology 131: 469-485.

Webster M, Zelditch ML. 2005. Evolutionary modifications of ontogeny: heterochrony and beyond. Paleobiology 31(3): 354-372.

Weishampel DB. 1984. Evolution of jaw mechanisms in Ornithopod Dinosaurs. Advances in Anatomy, Embryology, and Cell Biology 87: 1-109.

Weishampel DB, Chapman RE. 1990. Morphometric study of *Plateosaurus* from Trossingen (Baden-Wurttemberg, Federal Republic of Germany). In: Carpenter K, Currie JR, eds. Dinosaur systematics: Approaches and perspectives. Cambridge: Cambridge University Press, 43-52.

Weishampel DB, Heinrich RE. 1992. Systematics of Hypsilophodontidae and basal Iguanodontia (Dinosauria: Ornithopoda). Historical Biology 6: 159-184.

Weishampel DB, Horner JR. 1994. Life history syndromes, heterochrony, and the evolution of Dinosauria. In: Carpenter K, Hirsch KF, Horner JR, eds. Dinosaur eggs and babies. Cambridge: Cambridge University Press, 229-243.

Weishampel DB, Jianu C-M, Csiki Z, Norman DB. 2003. Osteology and phylogeny of *Zalmoxes* (n.g.), an unusual euornithopod dinosaur from the latest Cretaceous of Romania. Journal of Systematic Palaeontology 1(2): 65-123.

Weishampel DB, Norman DB, Grigurescu D. 1993. *Telmatosaurus transsylvanicus* from the Late Cretaceous of Romania: the most basal hadrosaurid dinosaur. Palaeontology 36: 361-386.

Welles SP. 1984. *Dilophosaurus wetherilli* (Dinosauria, Theropoda). Osteology and comparisons. Palaeontographica A 185: 85-180.

Wells JW. 1963. Coral growth and geochronometry. Nature 197: 948-950.

Werning S. 2005. Long bone histology of *Tenontosaurus tilletti* Ostrom 1970 (Early Cretaceous, North America), with comments on ontogeny. Master's Thesis. Norman: University of Oklahoma, 150 pp.

White PD, Fastovski DE, Sheehan PM. 1998. Taphonomy and suggested structure of the dinosaurian assemblage of the Hell Creek Formation (Maastrichtian), Eastern Montana and Western North Dakota. Palaios 13: 41-51.

Wiffen J, Molnar RE. 1989. An Upper Cretaceous ornithopod from New Zealand. Geobios 22: 531-536.

Winkler DA. 1994. Aspects of growth in the Early Cretaceous Proctor Lake ornithopod. Journal of Vertebrate Paleontology 14 (3): 53A.

Winkler DA, Murry PA. 1989. Paleoecology and hypsilophodontid behavior at the Proctor Lake dinosaur locality (Early Cretaceous), Texas. In: Farlow JO, ed. Paleobiology of the Dinosaurs. Boulder: Colorado. Geological Society of America Special Paper 238: 55-61.

Winkler DA, Murry PA, Jacobs LL. 1997. A new species of *Tenontosaurus* (Dinosauria: Ornithopoda) from the Early Cretaceous of Texas. Journal of Vertebrate Paleontology 17: 330-348.

Witmer LM. 1995. The extant phylogenetic bracket and the importance of reconstructing soft tissues in fossils. In: Thomason JJ, ed. Functional morphology in vertebrate paleontology. Cambridge: Cambridge University Press, 19-33.

Xu X, Tan Q, Wang J, Zhao X, Tan L. 2007. A gigantic bird-like dinosaur from the Late Cretaceous of China. Nature 447: 844-847.

Zelditch ML, Swiderski DL, Sheets HD, Fink WL. 2004. Geometric morphometrics for biologists – a primer. San Diego: Elsevier, 443 pp.

Zils W, Werner C, Moritz A, Saanane C. 1995. Tendaguru, the most famous dinosaur locality of Africa. Review, survey and future prospects. Documenta naturae 97: 1-41.

Appendices

Appendix I

All preserved isolated and articulated skull elements were measured with a calliper in mm scale. These measurements were, among others, used for the described Multivariate Allometric Analysis. Every measured distance (variable in the MAA) has a special number which is explained in appendix II. The small letters r or l at the end of some element labels indicate if the element is a right or left one. Some measured distances of incomplete elements have a "+" for a minimum value or a "?" for an uncertain value. The abbreviations are as in chapter 4.2.

Basioccipital	1	2	3	4	5	6	7
MB.R.1373	16.9	9.8	14.1	22.3	6	6.8	6.8
MB.R.1367	17.3	—	14	23.1	—	—	5.8
MB.R.3536	4.9	2.2	5.1	7.6	1.9	2	—
BSPGASI834	8.8	5	8.5	15.2	3.1	3.7	—
GZG.V.6481	17	10.3	14.8	—	5.8	6.7	6

Exoccipital	8	9	10	11	12	13	14	15
MB.R.1370l	10.9	14.6	27	16,5	18,3	16,3	16	9,2
MB.R.1374r	9.9	16	31	17,9	19,1	16,7	15,8	9.3
BSPGASI834l	—	—	—	—	9.1	—	10.3	—
BSPGASI834r	—	—	—	—	8.8	9.2	10.3	4.9

Prootic	16	17	18	19
MB.R.1371r	19	11.2	21.4	10.7
MB.R.1348l	20	13.7	21	10.9
MB.R.1370l	19.3	11.9	21	12
MB.R.1367r	24	15.9	26.1	11
MB.R.1353r	10.7	5.9	13.3	—
GPIT/RE/5845l	16.2	13.6	18.1	5
GPIT/RE/9533l	14.2	11.3	16.9	5.1

Laterosphenoid	20	21	22	23
MB.R.1370l	9	19.8	20.8	6.1
MB.R.1371r	10.2	18.1	21	6.1
MB.R.1340l	—	20.2	25.2	6.9
MB.R.1346r	10.4	20.1	20.7	6.8
BSPGASI834r	—	11.5	12.8	3
GPIT/RE/9000l	12.8	21.9	21.9	8.1

Supraoccipital	24	25	26	27	28
MB.R.1372	25.4	8.9	7	24	7.5
BSPGASI834	17.2	—	—	13.5	2.3

Parietal	29	30	31	32	33
MB.R.1372	11	6	8.3	42.8	41.2
MB.R.1341	14	6.4	—	49	40.7+
MB.R.1317	10.2	5.5	8	38.1	36.1
BSPGASI834	7.1	—	—	26.2	23.2

Frontal	34	35	36	37	38	39
MB.R.1378l	19	5.2	5.9	14.7	23.6	54.8
MB.R.1377r	18.2	5.5	5.8	14.2	20.5	—

MB.R.1319r	22.9	—	—	—	23.3	62.7
MB.R.1349l	19.6	6.4	5.5	13.8	23.6	—
MB.R.1369r	17	4.1	4	11.3	18	—
BSPGASI834l	16	3.2	2.8	9.6	12.1	40
SoNl	—	5.2	6.3	14	24	58.1
GPIT/RE/1595/15r	16.8	2.7	2.3	9.9	12.3	—
GPIT/RE/1595/17l	16.6	2.9	2.3	10.3	14	40.7
GPIT/RE/1595/14r	19.8	4	5	12	21.4	—

Jugal	**40**	**41**	**42**	**43**	**44**	**45**	**46**	**47**	**48**	**49**	**50**	**51**
MB.R.1333l	62.8	36.8	19.5	7.1	10.9	8.2	10.9	26	—	33.2	32.9	36.8
BSPGASI834l	34	28	14	4.5	6.3	—	—	17	3	23	18	17.8

Quadrate	**52**	**53**	**54**	**55**	**56**	**57**	**58**	**59**	**60**	**61**
MB.R.1320l	16.2	18	71.3	30.8	8.1	9.8	12.3	8.5	32.8	8.8
MB.R.1345r	18.7	16.9	—	27.9	9	7.7	—	—	—	6
MB.R.1326l	9.8	10.3	40	17	5	5.4	6.3	5.6	19.8	4.7
BSPGASI834l	8.2	—	37	—	3	5.7	4.5	4.1	17	—
GPIT/RE/3608l	16.3	16.9	62.2	28.3	8.1	11	—	7.9	29.5	9

Maxilla	**62**	**63**	**64**	**65**	**66**	**67**	**68**
MB.R.1358r	13	77.8	17.4	25.9	15.7	10.8	16.4
MB.R.1365l	—	—	—	24.9	16.2	—	—
MB.R.1357r	—	—	—	—	13.8	—	—
MB.R.1316l	12	—	14.8	24.5	16.2	11.6	17
BSPGASI834	10	—	—	—	—	—	10
MB.R.3468r	13	70	14.3	—	15.7	—	16.5
S52349r	11	57+	—	—	14.8	11	16.2
GPIT/RE/9533l	11?	47.3+	12	16.3	10	7.9	13

Dentary	**69**	**70**	**71**	**72**	**73**	**74**	**75**	**76**
BSPGASI834r	31.4	10	5.8	—	3.9	7.8	—	10.2
MB.R.1350l	60.6	11	—	14.2	—	14.2	11.5	17.7
MB.R.1365r	59.1	11	10	14.5	6.9	15.2	9.8	17.9
MB.R.1351l	61.5	11	9.2	15	6.8	14.5	12.2	17.8
MB.R.1318l	62.5	12	—	—	—	—	—	—
GPIT/RE/1595/22r	30.8	10	6	8.6	3.9	7.2	4.5	—
GPIT/RE/3612r	44	10-11	6.9	11.2	5.2	9.1	6.3	11.2
GPIT/RE/1595/21l	45.8	12	8.2	11.6	—	11.7	8.2	—
S52359r	64.5	13	11.3	15.6	—	17.3	—	20.2
S52361l	—	13	—	15.7	—	17.1	—	18.8
S52358r	63	13	10.2	14.5	—	14.8	11.8	17.2

Surangular	**77**	**78**	**79**	**80**	**81**	**82**
MB.R.1335r	33.8	12	7	61	31.1	20.6?
MB.R.1339r	31.7	13	7	59	30.2	—
BSPGASI834r	16	5.5	3	27.9	16.1	5.6

Angular	**83**	**84**	**85**
MB.R.1335r	64.2	13	7
BSPGASI834r	32	7	3.5

Articular	**86**	**87**	**88**
BSPGASI834r	6.6	7.9	—
BSPGASI834l	6.9	—	7.2

Prearticular	**89**
MB.R.1321l	52.9
BSPGASI834l	27.5

Appendix II

Explanatory list of all measured distances presented in appendix I.

Basioccipital:

1 – Total width of occipital condyle

2 – Height of condyle at foramen magnum

3 – Minimum width of condyle neck

4 – Maximum width at tubera basioccipitalia

5 – Width of foramen magnum groove at posterior exit (not width of foramen itself)

6 – Average of maximum width of suture area for exoccipital

7 – Width between the tubera basioccipitalia

Exoccipital:

8 – Minimum height of paroccipital process neck

9 – Lateral height of paroccipital process

10 – Maximum width of paroccipital process

11 – Height of main body until ventral edge of paroccipital process

12 – Length of suture area for basioccipital

13 – Length of suture area for supraoccipital

14 – Part taken at foramen magnum

15 – Anteroposterior minimum length of main body short above foramina

Prootic:

16 – Ventral maximum length anteroposteriorly

17 – Minimum length at middle of its height

18 – Height between foramina (V and VII) along crista prootica

19 – Maximum width anteroventrally

Laterosphenoid:

20 – Maximum anterior width of suture area for parietal

21 – Maximum height of suture area for prootic

22 – Length of suture area for parietal

23 – Maximum thickness of suture area for prootic

Supraoccipital:

24 – Maximum width

25 – Middle height along and with central ridge

26 – Minimum distance of suture areas for exoccipitals

27 – Length along central ridge

28 – Width of edge bordering foramen magnum dorsally

Parietal:

29 – Median length anteroposteriorly without lateral wings

30 – Thickness of suture area for the frontals, median

31 – Ventral width of frontal process

32 – Maximum width anterior plus lateral wings

33 – Complete length plus the lateral wings

Frontal:

34 – Length of orbital rim

35 – Minimum distance between ventral orbital ridge and median suture

36 – Thickness of median suture area at central dome

37 – Measured perpendicular from the median suture area, maximum width of ventral groove for the cerebellum

38 – Width between median suture area and posterior end of orbital rim dorsally

39 – Total length

Jugal:

40 – Total length

41 – Maximum height at postorbital process

42 – Height of main body at lowest point of infratemporal fenestra

43 – Anteroposterior thickness of postorbital process at beginning of postorbital suture

44 – Height of anterior bar at anterior beginning of medial processes

45 – Lateromedial thickness of anterior bar at lower medial process

46 – Medially, maximum length of ectopterygoid process beginning at the maxilla facet

47 – Length between the posterior end of the lacrimal facet and the theoretical midline of the postorbital process

48 – Mediolateral thickness of postorbital process at the beginning of the postorbital facet

49 – Distance between posterior end of lacrimal facet and lowest point of infratemporal fenestra

50 – Height of postorbital facet alone

51 – Height of squamosal process

Quadrate:

52 – Width of distal condyle

53 – Maximum anteroposterior length below the quadrate notch

54 – Total height

55 – Height up to lowest point of quadrate notch

56 – Minimum anteroposterior length at the quadrate notch

57 – Anteroposterior thickness/length of distal condyle

58 – Maximum height of quadrate notch at its posterior edge

59 – Mediolateral width of upper neck of cotylar head

60 – Inclined maximum distance between posterodorsal edge of quadrate notch and end of cotylar head

61 – Anteroposterior thickness of distal condyles neck

Maxilla:

62 – Number of alveoli

63 – Total length

64 – Anteroposterior length between anterior notch (between the two anterior processes) and large foramen located inside the premaxilla facet

65 – Height between alveolar edge and top of the laterodorsal process

66 – Height between alveolar edge and posteromedial bulge

67 – Anterior minimum mediolateral thickness

68 – Maximum mediolateral thickness just before the posteromedial bulge

Dentary:

69 – Tooth row length

70 – Number of alveoli

71 – Mediolateral thickness of coronoid process at the last tooth position

72 – Maximum mediolateral thickness

73 – Anteroposterior thickness of coronoid process at the upper end

74 – Minimum lateral height without teeth

75 – Posterior width between the lateral wall and the medial (splenial) wall

76 – Maximum height of anterior toothless part

Surangular:

77 – Maximum height along the inclined anterior edge of the laterally visible part of the anterior plate

78 – Glenoid mediolateral width

79 – Anteroposterior length of medial glenoid process

80 – Total length without the anterior dentary-covered part

81 – Anteroposterior distance between posterior edge of dentary facet and lowest point in front of the glenoid

82 – Height of the retroarticular process

Angular:

83 – Length

84 – Height

85 – Posterior thickness

Articular:

86 – Lateral length

87 – Medial length

88 – Maximum height

Prearticular:

89 – Length

Appendix III

All elements complete enough were measured with a calliper in mm scale. These measurements were used for the described Multivariate Allometric Analysis. Every measured distance (variable in the MAA) has a special number which is explained in appendix IV. The small letters r or l at the end of some labels indicate the right or left side. Some measured distances of incomplete elements have a "+" for a minimum value. The abbreviations are as in chapter 4.2.

Measured values of the postcranium – Scapula.

Labels	1	2	3	4	5	6	7	8	9	10	11	12	13
MB.R.Aststl	160	65.7	24.3	45.2	55.7+	11.7	11	7.3	5.2	14	18.8	27.2	19
MB.R.Aststr	160	63.1	26.2	44.5	61	11.5	10.5	6.8	5.8	13.1	18.2	26.2	21
MB.R.1707l	180	—	26.4	—	60.4	12.5	9.3	—	5.2	13.4	16	26.8	19.3
GZG.V.6556l	—	—	17.1	34	42	10.1	10	4.5	—	10.2	12.9	27.5	9
GPIT/RE/5330l	125.3	44	17.8	38.4	46	13.3	7.3	5.6	2.8	10.5	12.9	16.7	9.8
GPIT/RE/5651l	78.2	24.9	11.7	23.8	28.9	8.3	6.3	2.9	2.7	5.6	9.8	13.3	9.5
GPIT/RE/6152l	—	—	23.3	43.6	51.4	—	11	—	—	10	15.5	18	12.6
GPIT/RE/4218r	—	—	14.5	23	29.2	7	6.1	2	—	5.2	10.7	13	9.5
GPIT/RE/4559l	—	—	26	48.2	61.8	14.8	10.2	5.5	—	12.9	17.9	26	19.2
GPIT/RE/4570r	—	—	—	48.1	63.7	17.5	11.5	—	—	—	23	26.2	21.5
GPIT/RE/4595l	—	—	14	22.2	31	8	6.3	3	—	5	12.5	13.1	9.3
GPIT/RE/5503r	—	—	10.8	19.8	25	6.4	4.1	—	—	4.2	7.3	9.8	8
GPIT/RE/5483r	—	—	25.8	52.3	64.9	16.3	13.1	5.7	—	13.8	22	25.6	22.3
GPIT/RE/5720l	—	—	12.3	23.9	28.7	9.1	6.2	3.6	—	5.9	11.2	13.2	11.2
GPIT/RE/6990r	—	—	10.6	22.3	26	8	6.1	2.7	—	5.7	9.8	10.2	9.8
GPIT/RE/6753l	—	—	17.3	28	34.2	11.1	6.2	4.9	—	7.9	12.9	17.8	13.1
GPIT/RE/6660l	—	—	15.9	29.6	33.4	11	6.8	3.7	—	7.3	12	19.8	12
GPIT/RE/6617r	—	—	28.8	49.4	59.4	18.5	12.9	5.9	—	14.5	22	26.1	21.9
GPIT/RE/6271r	—	—	11.1	23.1	28.2	9	5.2	2.4	—	5.9	10	15.6	8.2
GPIT/RE/6316l	—	—	—	43.8	56.2	16	11	4.3	—	—	20.2	24.5	19
SNMSoN1l	210	—	33.9	65.4	81	24.8	—	—	8.9	—	32.9	35.5	29.9
SNMSoN2r	185	—	26.6	59	68.6	20	16.7	—	—	15	29	—	22.7
SNMSoN3l	161	72.6	27.8	—	—	17	—	—	9	15	—	26	20.6
SNMSoN4l	—	—	26.4	57.2	66.9	20.2	12	7.9	—	—	27.2	31	27.9
SNMSoN5l	—	—	16.1	33.6	41.7	12.8	5.9		—	8.3	13.8	15.8	12.8

Appendix III continued

Measured values of the postcranium – Coracoid.

Labels	1	2	3	4	5	6	7	8	9	10	11	12	13	14	15	16	17	18
MB.R.1485r	74	51.2	28.2	49	41	34.5	32.8	32.8	10.5	5.9	22.4	2.1	11	7.7	24	2.8	22.3	38.8
MB.R.1476r	32.5	22.3	12.4	22.9	20.1	15.8	13	15	6.2	2.1	7.7	1.7	2.9	3	9.5	2.1	7.9	15.8
MB.R.Aststl	66.4	44.2	26	45.6	32.7	30.8	28.8	27.1	7.9	5.7	17.4	3.6	7.2	5.6	23	3.8	16.9	32.2
MB.R.Aststr	66.5	43.2	23.9	46.8	33	34	27.3	30.5	6.1	7.6	18.2	2.6	5.5	5.9	22.2	3.2	18.1	32.2
MB.R.3474r	84.2	57.6	31.1	57.4	45.9	41	35.3	38.8	11.4	9.5	—	4	—	6.1	22.3	3.6	17.8	42.9
GZG.V.6575l	—	18.5	—	18.9	16.1	—	—	12.1	4.5	2.6	7.9	1.1	1.9	2.2	—	—	7.1	—
GPIT/RE/3871r	39	26.9	13.7	25.9	23	19	16.9	19.1	5.1	3.2	10.7	—	—	3.8	11.3	1.3	9.2	17.8
GPIT/RE/5439l	78.9	53.7	44.4	54.5	42	36.8	39.2	34.5	13.9	6	23.3	4.4	11.5	4.8	23	3	21.2	45.7
GPIT/RE/5588r	34.7	23.2	13	20	20.8	15.8	14.2	17.4	4.2	3.2	8.9	1.8	5.5	3.9	9.9	1.3	7.1	16.7
GPIT/RE/6801r	66.8	46.1	23.3	42.7	39.2	32.2	28.1	30.7	11.2	2.9	19.8	—	—	7	—	—	17	31.4
GPIT/RE/4130l	77	56	32.2	51	45.3	38.4	38	36.9	11.5	5.7	26	5	10.2	9.7	22.4	2	22	42.2
SMNSoNr	70.1	49.1	26.2	47.9	44	35.9	31.7	34.3	11	6.1	22.7	3	10	7.5	28.8	2	17.1	36
SMNSoN1r	32.8	23.6	13.1	23.4	19.6	15.3	13.9	15.5	5.8	2.8	8.8	1.4	2.2	3.3	10.2	2	8.1	16
SMNSoN2l	34.3	23.8	12.8	23.2	19.8	16.9	14.3	16.6	4.2	3	9.9	1.4	—	2.8	10.2	1.8	8.8	17

Appendix III continued

Measured values of the postcranium – Humerus.

Labels	1	2	3	4	5	6	7	8	9	10	11	12	13	14
MB.R.1711r	96.6	—	15.3	9.2	19.1	30	65	10.8	10	8	11.5	10.1	7.9	7.9
MB.R.Aststl	157	38.6	22	16	30.7	50	100	14	20	12.8	19.5	15.5	—	17.2
MB.R.Aststr	—	37.2	23	—	30.4	—	—	13.5	20.7	—	19.4	16.1	—	—
GPIT/RE/3450r	68.7	16.1	10.5	6	12.4	20	46.9	6.5	7	4.9	7.3	5.8	3	7.8
GPIT/RE/3948l	70.8	17.4	10.9	7.2	13.3	22	48.2	7	8	5.8	8.6	6.2	4.3	—
GPIT/RE/4013r	82.1	19.3	12.3	8.5	—	25	—	—	9.1	6.1	—	—	—	11.2
GPIT/RE/4167l	66.7	—	9.6	—	12.2	19.8	46	7.5	7.8	5.8	7.8	5.6	4.1	9
GPIT/RE/5114l	77.9	18.1	11.6	7.8	14.8	24.4	53.9	—	—	6.3	8.2	7	5	10.3
GPIT/RE/5731r	104.7	28.3	16.5	11	19.9	34	66.4	9.3	12.8	9.1	11.4	9.8	7.2	14.1
GPIT/RE/6543l	83	21.1	13	8.8	16	28	52.7	9.4	10.9	6.5	9.2	8.1	6	11.2
GPIT/RE/3448r	143	39	23.5	14.5	28.6	44	99	14.2	20.1	14	17.1	15.9	11.8	23.2
SMNSoN1r	102.2	26.2	15.3	8.5	20.9	30.4	71.6	10.5	—	9.7	11.4	9.9	7.3	14.7
SMNSoN2r	113.8	29.5	15.7	10.2	21.6	41.4	70.6	11.7	13.7	9.8	12	10.7	8.7	13.9
SMNSoN3r	173	47.1	25.7	14.8	33.6	56	113	17	24.8	15.2	18	—	12.7	24.9
SMNSoN4l	170	—	26	16	36.7	—	109.7	21.4	—	15.7	20	19.5	15.2	—

Measured values of the postcranium – Radius.

Labels	1	2	3	4	5	6	7	8
MB.R.Aststl	105	21.9	8.5	12.8	13	9	18	10
GPIT/RE/6407r	52.8	9.1	4	7.7	5.4	3.8	6	5.3
GPIT/RE/3841l	105.8	22.1	8.9	12.6	13.4	8.9	15.6	11.4
SMNSoNl	72.3	14	6	11.5	8.7	5.7	8.1	6.8

Appendix III continued

Measured values of the postcranium – Ulna.

Labels	1	2	3	4	5	6	7	8	9	10	11
MB.R.Aststl	111	24	9.5	19.7	13.3	10.5	11.8	16	17.3	13.5	13.1
MB.R.1408r	111.7	—	9.8	24.4	13	10.6	10.2	—	—	—	13.8
MB.R.1414l	76.8	—	6.8	15.6	10.1	7.1	—	—	11.8	—	8.6
R12327l	—	30.7	14.9	—	—	—	18	21	23.3	11	—
GPIT/RE/3451r	83.2	16.3	6.8	13.8	8	6.2	6.8	11.6	12.9	7	9.1
GPIT/RE/3909r	121	—	11	23.4	14.7	8.5	12.5	—	21.1	11.3	14.5
GPIT/RE/4324r	148	29.3	—	26.9	16.7	10.4	17.8	21.7	24	9	14.9
GPIT/RE/5224l	135	31.2	13	27	17.2	10	16.9	18.2	25.7	9.3	14.8
GPIT/RE/5567l	110	21.3	—	22.1	12.3	10.1	12	16	17.3	—	11.1
GPIT/RE/5729r	—	—	10.8	24	15.3	10	14	—	22.1	7.4	12.7
GPIT/RE/3885l	121.8	29.8	11.1	22.5	13.9	8.8	14.9	16.4	22.9	7	14.2
SMNSoN1r	113.8	27.2	11.8	24	14.7	9.7	12.5	—	21.2	5.2	14.3
SMNSoN2r	62	—	5.2	10.9	6.2	4.5	5.6	—	8.7	3.3	5.9

Appendix III continued

Measured values of the postcranium – Ilium 1.

Labels	1	2	3	4	5	6	7	8	9	10	11	12	13	14	15	16	17	18
MB.R.1718l	177	79.1	97.9	47.1	27.6	17.8	13	9.5	16	17.1	28	13.8	25.2	29.9	56.5	20	7.1	33.3
MB.R.3471r	—	—	60.1	37.8	28.7	—	—	—	9.8	—	17.2	8	15.3	20	33.8	—	4.7	20.6
MB.R.WJ4318l	—	—	—	—	53	—	—	—	—	—	56.7	22.2	29.6	43.4	—	—	14.1	—
MB.R.Aststr	—	—	145	67.4	39.2	29.5	19	14.3	35.9	—	45	18.9	27.5	41.3	81.5	—	11.6	44.1
MB.R.Aststl	—	—	140	65	38.8	27.5	19.4	14	25.8	25.9	45.5	18.4	30.2	38.6	81	29.9	—	—
GZG.V.6539l	—	—	154	68.8	—	—	—	—	26.2	29.4	39.8	22.8	37.5	48.2	—	—	12.3	—
GPIT/RE/3750r	—	—	141	61.9	39.3	28.8	—	—	21.1	22.8	41.3	14.4	31	46	82.5	23.9	10.8	52
GPIT/RE/5639l	—	—	177	75.2	51.9	39.8	—	—	32.5		48.9	20	37.1	49.2	—	—	13.2	62.8
GPIT/RE/6544l	—	—	150	74.8	54	35.8	—	—	30.7	33	47.7	20.8	33.3	47.8	88	32.2	12.5	56.2
GPIT/RE/3453l	—	—	100	45.9	31	20.3	15.2	9.8	19.2	21.4	27	12.3	23.2	28.9	66.9	—	7.7	39.2
SMNSoN1r	—	—	160	75.8	—	34.8	—	—	33.3	35.7	48.4	20.7	38	55.5	86.2	38.7	11.6	53
SMNSoN2r	—	—	190	79.9	58.5	38	—	—	28.3	34	59.2	19.8	44.5	63.7	113.2	36.8	14.4	77
SMNSoN3l	—	—	150	69	46	30	—	—	26	28.2	38.1	16.7	22.8	46.5	88.7	31	12.3	58.7
SMNSoN4l	—	—	98	42.7	30.2	19.3	—	—	15.7	18.1	29.3	11.9	21.1	31.2	16.1	19	7.1	34

Appendix III continued

Measured values of the postcranium – Ilium 2.

Labels	19	20	21	22	23	24	25	26	27	28	29	30	31	32	33	34	35	36
MB.R.1718l	54.8	43.8	4.2	7.8	54.1	8	17.7	13.9	12.7	12	10.8	10.2	28.4	14	20	4.8	56	13.4
MB.R.3471r	35.8	24.4	3	—	33.7	—	7.6	7.2	7.3	—	—	—	17.8	—	10.4	—	33	—
MB.R.WJ4318l	—	—	19	—	—	—	29.4	—	—	—	—	—	40.6	—	—	—	—	—
MB.R.Aststr	80.8	67.1	6.4	9.2	78	—	26.7	18.8	18	14.9	14.3	—	40	25.6	24.8	8	72.5	15.4
MB.R.Aststl	—	67.5	6.2	10.5	84.7	—	23.3	21.6	19	16.4	14	—	36.4	—	22	6.9	73	14
GZG.V.6539l	—	65.8	—	—	95.9	—	17.2	—	16.8	14.5	—	—	40	—	—	9	69.4	16.6
GPIT/RE/3750r	71.4	—	6.8	—	—	13.9	22.2	23	18.3	16	—	—	—	22	28.4	8.3	—	13.7
GPIT/RE/5639l	88	—	8.9	—	—	—	29.6	28.7	24.4	20.4	—	—	43	—	—	11.9	—	15.7
GPIT/RE/6544l	82.7	70.4	9.1	—	76.9	15	29.7	19.5	23.3	18.4	—	—	44	31.2	36.7	10.7	82	19
GPIT/RE/3453l	55.3	43.3	5	—	—	10	13.6	14.7	15.2	14.4	11	—	27	12.5	21.6	5.8	—	7.2
SMNSoN1r	88.2	64.2	7	—	83.2	12.8	22.2	28.2	—	—	—	—	37.6	26	39.8	8.1	76	15.6
SMNSoN2r	109	73.8	10.9	—	108	13.1	—	31.2	—	20.3	—	—	50.7	29.4	38	10.2	—	23
SMNSoN3l	—	—	6.2	—	89	11.2	18.5	—	25	21.6	—	—	31.4		35.1	7.3	80	16
SMNSoN4l	—	—	4.9	—	—	8.8	12.8	14.6	—	11.4	—	—	23.1	18	20.7	5.3	—	10

Appendix III continued

Measured values of the postcranium – Ischium.

Labels	1	2	3	4	5	6	7	8	9	10	11	12	13	14	15	16	17	18	19
MB.R.1474r	—	12.2	6.2	4.8	6	33.9	9	34.1	30.2	20.8	11.8	10.8	11.7	8.5	11.2	5.9	—	—	2.4
MB.R.1478r	38.2	28.9	26.1	16.6	15.6	81.2	—	—	—	—	—	23.9	22.9	—	—	—	—	—	—
MB.R.Aststr	34.5	27.7	25.8	13.9	16.5	84	27.7	73.5	—	—	—	26	25.8	16	—	11.2	190	270	8
MB.R.Aststl	36.8	30.3	23.3	15	17	81	21.9	68.4	—	—	—	24	21.8	—	—	—	—	—	6.1
GZG.V.6456r	—	35.4	26.8	15.9	17	94	—	84.8	—	—	—	31.8	25.9	—	—	—	—	—	6
GZG.V.6334r	44.3	35	23.9	18	20	85	—	—	—	—	—	29.8	22.2	—	—	—	—	—	9.8
GZG.V.Aststl	—	29.3	—	12	—	83	21.4	56.1	54.3	38.8	20.7	24	21	20.7	—	15.9	—	—	6
GPIT/RE/4668r	41	—	31	—	—	—	26.8	68.8	—	40.8	—	30.6	26.9	—	—	—	—	—	6.6
GPIT/RE/3442r	32.8	30.3	24.7	13.8	19.9	76	22.6	68.2	—	—	—	23	21.3	14.3	—	—	—	—	—
GPIT/RE/3438r	21.2	18.9	17.1	5.5	9.1	55.8	15.9	52	—	—	—		12.2	13.7	—	—	—	—	—
GPIT/RE/3441r	22.2	21.6	17.2	9.4	10.1	55.7	—	—	—	—	—	14.7	12.9	—	—	—	—	—	4
GPIT/RE/3440l	35.9	—	24.1	—	14.8	—	21.5	72.4	—	40.3	—	25	21	19.8	21.1	—	—	—	4.8
SMNSoN1l	18	15	—	6	—	44	12.3	39.3	—	—	—	13	—	8.4	—	5.1	—	—	3
SMNSoN2r	—	—	—	—	—	—	23.2	68.9	—	50	—	26	25	16.8	25.8	—	—	—	5.5
SMNSoN3r	44	—	28	—	17.3	—	26	81.2	—	—	—	31.1	26.8	20.3	—	—	—	—	6
SMNSoN4l	40	—	25	19	—	—	25.7	73	—	—	—	26	25.5	—	—	—	—	—	—
SMNSoN5l	44.4	36.4	27	—	19.2	91.6	26	82	—	—	—	30.2	23	21.2	—	11.5	—	—	—
SMNSon6l	—	39	29	—	—	—	26	75	—	—	28.2	28.7	27.2	21	24	—	—	—	—

Appendix III continued

Measured values of the postcranium – Femur 1.

Labels	1	2	3	4	5	6	7	8	9	10	11	12
MB.R.2511r	330	75.3	55.6	26	87.7	68.4	160	165	73.1	44.7	35	45.5
MB.R.2517l	188	43.5	33.2	12.3	46	42.3	89	95.5	38	22.5	19.7	26.1
MB.R.2519l	119	26.9	20	9	30	29.1	57	58.5	27.1	15.7	10.6	18.6
MB.R.3299l	—	43	40.2	14	47	40.9	93	—	—	25.8	20.8	28.6
MB.R.3302l	300	70	50.8	24	76	68	150	150	57	37	—	44.5
MB.R.2144l	—		68.7	31	—	—	—	—	—	—	44.5	55
MB.R.2508r	—	73.1	54.9	25.6	74	67.9	153	—	65	40.2	—	47.1
MB.R.2507l	306	—	—	21	67	70	150	155	—	—	33.1	41.9
MB.R.2506l	298	—	49.5	—	—	68.5	140	155	—	40	—	49
MB.R.1502l	320	69.2	54.8	20.2	74	74	155	168	58.3	39.5	34.2	50
MB.R.2503r	310	68.9	53.8	23	73.7	—	—	—	62.6	40.2	28	—
MB.R.2500r	—	52.9	39	19.1	55	—	—	—	47.8	31.1	24.7	—
MB.R.2509r	185	—	30.8	—	—	39.7	85	95	36.3	23.9	19.1	—
MB.R.2501r	225	48.9	36.4	17.1	50	48.2	108	112	—	29.2	—	—
MB.R.Aststr	—	63.2	47.3	21.4	67	61	135	—	55	37	32	41.4
MB.R.Aststl	280	62.7	48.2	22.2	71	—	—	—	55	36.2	32	40
R12278r	—	—	—	25.6	—	—	—	—	—	43.5	38	—
R12277r	350	78.1	63.3	25	85	—	166	180	69.3	45.3	—	47.2
R6861r	198	—	33.5	—	—	44	94	101	—	25	21.8	28.4
GZG.V.6273l	295	69.5	52	26	—	67.5	112.5	115.5	55.2	37	33.3	43
GZG.V.6277l	—	76.1	57	26	75	—	—	—	63.4	40.8	—	—
GZG.V.6574r	160	35	26.9	11.8	—	—	75	82.1	—	20	17.8	—
GZG.V.6211r	195	38.9	30.2	—	—	—	—	—	—	25	—	—
GZG.V.6314l	290	65.1	48	22.8	75	—	—	—	54	36.3	—	42
GPIT/RE/4156r	85	18	14.1	5.2	20.1	21	40	40	14.8	10.3	—	10.6
GPIT/RE/3524l	—	—	—	—	—	—	—	67.7	27	17.7	15.5	—
GPIT/RE/3522r	128	27.1	21.2	8.9	33	—	59.6	65	20	13	13	—
GPIT/RE/3584l	208	43.9	33.8	12.4	51.8	47.1	97	108	42	26.5	23	28.1
GPIT/RE/3586r	210	44.4	33.6	13.6	52	47	100	110	39.1	26.1	—	27.4
GPIT/RE/3580r	150	30.7	24.4	7.6	34.1	31.6	69.9	80.9	28	17.1	16.6	22.2
GPIT/RE/3582r	206	46.8	36	15	54	43.6	98	108	41.5	27.3	23.2	30.8
SMNSoN1l	308	71.2	51.7	23.2	83	73	155	153	—	41.8	36.7	48
SMNSoN2r	162	36.9	28.8	11.2	38.2	—	—	—	—	18	17.8	22.1
SMNS7855l	211	46.3	34.2	16	48	44	92	111	40	25	21.9	27.9
SMNSoN3l	222	47.9	37.2	16	57.2	49	107	118	43.2	28.2	24	33.9
SMNSoN4l	279	64	49.3	22.8	70.2	60.8	—	138	—	34.6	32.6	41
SMNSoN5l	290	67.5	49	25.2	78	63.7	138	148	—	34	39.7	—
SMNSoN6l	275	—	—	21.6	71.6	60.8	133	140	56.9	34.1	30.3	39.9
SMNSoN7r	270	64	49	19.7	67.7	62.3	134	136	58	37.5	31.1	38.8
SMNSoN8l	144	35	26	11.2	34	36	69.4	75	24.7	14	15.4	21.5

Appendix III continued

Measured values of the postcranium – Femur 2.

Labels	13	14	15	16	17	18	19	20	21	22	23	24
MB.R.2511r	77.1	7	36.7	42	47.8	79	18.5	32	68.5	13.5	33.2	128
MB.R.2517l	43	4	19.5	23.7	28	42.2	8.2	18.3	39	6.7	20.2	72.5
MB.R.2519l	26.3	2.8	13.7	15.5	18	28	6.3	12.2	23.7	3.2	13.5	50.9
MB.R.3299l	44.3	4.6	20.4	22.2	26.3	44.1	9	19.5	39.7	7.2	20.9	75.8
MB.R.3302l	64	6	—	—	—	65.7	17	31.4	60.3	5.2	36.5	120
MB.R.2144l	89.6	7	—	51	59	90	21.2	45.2	83.3	11	44.2	—
MB.R.2508r	—	—	34	—	—	79	18	34.1	66.2	13.9	—	130
MB.R.2507l	70	6	32.5	37.9	—	71.4	—	—	—	—	36	—
MB.R.2506l	—	—	33.5	38.6	46	72.8	13	32	63.6	15	—	110
MB.R.1502l	72	5.8	33.5	39.8	37.5	74.5	14.3	34	64.6	11.9	39.5	—
MB.R.2503r	65	6.9	—	—	—	69	15.9	32	64.9	10	36.7	—
MB.R.2500r	—	—	—	—	—	53.5	11.4	24.8	47.1	8.8	—	—
MB.R.2509r	41.1	3.4	20	—	23.9	40	9.2	17	36.2	7	18.7	70.2
MB.R.2501r	—	—	—	—	31.5	49.2	—	23.9	44	—	—	—
MB.R.Aststr	64.9	6.8	30.7	37.5	34.8	65.2	13.9	25.5	56.9	10.8	28.2	—
MB.R.Aststl	63.2	7	30.2	37	—	64.3	13.5	29.6	57.3	12	32	—
R12278r	—	—	—	40.6	—	77.8	—	35.7	75.1	13.6	—	—
R12277r	78.1	10	37.8	47.5	51	84	19.2	38.8	73.5	12.6	41.8	—
R6861r	45	4	20	—	26.2	44	—	19.6	40	—	24	78
GZG.V.6273l	71.2	4.6	33.6	38.9	47.3	71.9	14	35.9	61.9	13.2	40	117
GZG.V.6277l	84.2	7.1	—	—	—	78.1	—	36	65.4	—	45.9	—
GZG.V.6574r	35.8	3.8	16.7	19.7	22.3	34.4	—	16.2	31.2	—	18	61.9
GZG.V.6211r	43	3.8	19	23.7	27.3	43.2	9.8	19	37.2	18.1	21.2	76.9
GZG.V.6314l	69.2	—	31.5	—	—	68.9	13.1	31.6	59.1	—	35.5	—
GPIT/RE/4156r	18.3	1.7	8.6	—	—	18.7	3.5	7	16	5	8.3	33
GPIT/RE/3524l	—	3.2	—	17.8	—	31.6	6.9	12.9	27.8	6.2	—	—
GPIT/RE/3522r	—	2.1	12.5	15.3	20.5	29.1	7.9	12.5	23.7	4.2	—	45.6
GPIT/RE/3584l	46.1	4.2	21.7	25	31.2	46.1	10.1	18.7	43.5	6.7	22.3	74.7
GPIT/RE/3586r	46.8	4.8	22.9	—	—	45	9.3	—	—	5.8	22.2	85
GPIT/RE/3580r	33	3.4	17	19.1	28	33.2	7.5	14.8	29.8	6.9	16	59.2
GPIT/RE/3582r	50.4	5.2	21.8	26.8	30.2	50	12.8	21.2	42.3	7.9	23.8	87
SMNSoN1l	—	6	33.1	39.8	53	70.8	—	33.9	65.6	—	36.2	125
SMNSoN2r	35.6	3.2	17.8	19.6	—	36	—	17.2	30.8	—	18.4	60
SMNS7855l	44.5	4.2	21.1	26	—	46.9	11.2	20.3	40.2	—	23.6	80
SMNSoN3l	53.2	5	23.8	28.8	32.3	52	11.8	22.2	46.9	9.3	24.9	88
SMNSoN4l	68.9	—	31.2	37.9	—	63.3	—	—	—	—	36.4	118
SMNSoN5l	—	—	33	43	54.8	70	—	—	66.2	—	—	119
SMNSoN6l	—	6	28.5	32.9	—	61.8	13	28.1	57.2	9.2	32.6	—
SMNSoN7r	58.2	6.9	29.8	33.1	43.5	61.2	13.3	26.2	57	13	32	108
SMNSoN8l	29.6	3	15.6	17.9	18.5	29.2	5.8	12.9	27.3	—	16	57.2

Appendix III continued

Measured values of the postcranium – Femur 3.

Labels	25	26	27	28	29	30	31	32	33	34	35	36	C midshaft
MB.R.2511r	190	24	15	73.2	32.9	21.5	9.5	4.9	30.6	45	26	185	122
MB.R.2517l	115.6	13	9.2	38.2	16.7	10.5	5	6	14	24.7	13.9	111	67
MB.R.2519l	67	8	5.3	27.2	11.2	5	2.8	2	13	15.5	10.2	68.2	45
MB.R.3299l	—	12	8.6	—	18.5	11	5	3.7	—	28.6	14.2	—	—
MB.R.3302l	173	19	12	56	26.2	14.4	9	3.9	21.8	—	26.3	173	—
MB.R.2144l	—	—	—	—	37	22	11	—	—	—	—	—	—
MB.R.2508r	—	22	13	65.3	31.3	27.9	7	3.1	26.6	47.3	23.9	—	121
MB.R.2507l	—	—	—	—	28.6	—	8.3	—	—	42	22	175	110
MB.R.2506l	185	17	—	—	27.5	16.1	10.4	7	—	49.2	24.7	180	113
MB.R.1502l	—	—	—	61	27.2	16	10	—	25	46.3	28.2	190	111
MB.R.2503r	—	—	—	63	28.7	15.7	10	—	28.5	42.7	18.9	180	—
MB.R.2500r	—	—	—	47.8	21.4	12.9	7.1	—	23.6	—	—	—	—
MB.R.2509r	111.7	8.8	7.2	36.6	16	10.9	4.2	4.3	18.3	27.8	18	110	65
MB.R.2501r	—	—	—	—	20.5	—	6.6	—	—	—	18	135	—
MB.R.Aststr	—	—	—	55.6	26	15.8	8	—	—	—	—	—	117
MB.R.Aststl	—	—	—	56.6	27	16.1	7.3	—	—	—	—	—	—
R12278r	—	—	—	63.5	—	22	—	—	—	52.6	31	190	—
R12277r	—	—	—	69.4	—	—	10.7	—	21.2	47.2	28.8	200	—
R6861r	118	15.1	11.2	—	16.6	9.8	5.5	2.2	—	30.4	15.9	115	—
GZG.V.6273l	177	21.1	15.1	55.2	28.5	14.8	6.8	4.4	—	43.3	26.8	173	—
GZG.V.6277l	—	—	—	63.4	34.5	—	9	—	21	40.7	26.2	—	—
GZG.V.6574r	96	9.6	7.1	—	15	7.8	3	2.7	—	25	14	91.5	—
GZG.V.6211r	112	12	8.5	—	18.2	11.9	4.9	3.9	—	—	17.3	—	—
GZG.V.6314l	—	21	12.3	—	—	—	7.2	—	—	40.5	26	170	—
GPIT/RE/4156r	46	5	3.9	15	6.8	4.3	2	2	4.3	12.8	6.1	50	35
GPIT/RE/3524l	82	8.9	6.2	27	13	7.9	2.9	2.9	11	17	8.2	78	53
GPIT/RE/3522r	79.1	8.8	5.9	20.5	10.7	6.9	3.1	1.6	7.5	18.2	10.1	71.4	45
GPIT/RE/3584l	130	11.2	9.3	41.2	17.5	11	6.9	2.9	14.8	30	17	120	75
GPIT/RE/3586r	125	—	—	39.8	17.8	8.8	5.9	3.5	15	—	—	—	—
GPIT/RE/3580r	90	9.8	6.9	28.2	12.8	8	4	2.1	10	23.8	11.8	87.2	54
GPIT/RE/3582r	116	16.1	8.6	42	18.6	10.3	6.3	1.8	17	36	18.7	117	81
SMNSoN1l	182	15.2	12.3	—	25.2	—	8.8	4.6	—	47	26	179	116
SMNSoN2r	103	—	—	—	15.1	—	4.2	—	—	28	11.4	97.3	57.5
SMNS7855l	128		—	—	—	8.2	5.1	—	—	32.3	17.9	117	—
SMNSoN3l	136	—	—	43.9	22	—	7	—	—	34.6	20.1	130	82
SMNSoN4l	157	—	—		27.2	—	7.8	3.3	—	—	—	—	108
SMNSoN5l	170	—	—	63.2	—	—	7.2	4.6	—	43.9	23	175	118
SMNSoN6l	—	—	—	55.8	—	—	—	—	—	42.9	21.8	156	97
SMNSoN7r	160	—	—	57.9	24.2	16	9.2	4.2	23.8	41.9	21.8	157	97
SMNSoN8l	87.2	—	—	25.3	—	—	—	2.2	11.5	—	—	—	52

Appendix III continued

Measured values of the postcranium – Tibia.

Labels	1	2	3	4	5	6	7	8	9	10	11	12	13	14	15	16	17	18	19	20
MB.R.2510l	174	168	16.1	—	—	—	—	—	15	13.2	12.3	—	39.3	12.2	24	15.5	7.6	14.6	10	—
MB.R.2512r	340	326	31	—	58.8	41	24	27	—	32.4	35	13	89	31	51	38	12.5	26	20.3	54
MB.R.2513r	325	307	26.7	—	—	—	—	—	—	30.8	33.4	—	79.6	25	44	30.5	—	26	20.8	—
MB.R.2514r	300	286	23.6	—	—	—	—	—	—	28.7	—	—	76.4	25	45	29	15.5	22.6	—	—
MB.R.2515r	265	250	—	—	—	—	—	—	—	—	30	—	61.5	20.5	41	20	—	23	16.8	—
MB.R.2516r	200	190	—	48.8	28.3	22.2	11	11.7	16.3	15.3	18.9	6	49	13	30	19.3	7.9	15.5	11	25
MB.R.2523l	165	160	13.5	39.6	27	16.3	11.2	10.8	—	13	15.3	6	38.2	11.3	22.3	15.9	6.8	15.2	9.2	21.9
MB.R.2522r	—	—	10.8	—	18.2	13.8	9	8.8	—	—	11.5	5	—	—	—	—	—	—	—	12.8
MB.R.2520r	—	—	10.7	—	—	—	—	—	—	—	—	—	28.9	9.9	17	11.8	4.9	12.3	8.2	—
MB.R.1709l	116	111	9.9	30.7	17	12.5	7.3	7.3	9	8.5	10.4	4.8	25.3	8.8	16	9.5	—	10.5	7.6	14
MB.R.Aststr	325	310	25.4	89.6	53.6	37.7	22	23	32.7	31.8	37.7	11	75.8	25	43.5	31.4	—	—	—	49.6
MB.R.Aststl	—	—	27	77	53	31	22	22	30	31	30.6	12.8	77.8	28	47.3	31	10	—	20.8	50
R12279r	370	360	29.6	97.2	65.3	44.7	27	30.1	37.8	—	—	—	89.5	30.9	51.9	38.5	—	28.8	23.9	59
R8351r	—	—	16.5	54.2	—	23.8	15.8	—	—	18.6	20.2	7.9	—	—	—	—	—	—	—	30
GZG.V.6613r	—	—	14.9	51.8	32	23.5	13.3	—	15.7	11	20.5	—	—	—	—	—	—	19.7	—	—
SMNSoN1r	—	—	13.7	46.8	28.7	—	10.7	—	14.8	12.9	—	—	36.7	11.3	21	14.8	6	15.9	10.8	—
SMNSoN2l	173	163	15.4	42.8	26.9	—	9.2	—	13.5	—	14.3	—	38.1	12	24.1	14.3	—	14.9	9.8	—
SMNSoN3r	166	160	12.5	40.1	24.1	15.3	8.7	10.2	13.5	11	12.1	—	35.9	11.9	21.8	13.6	—	14.3	9.1	17
SMNSoN4r	296	280	22.4	77.1	43.7	33.4	18.2	19.4	24.2	23.5	31.3	10	69.2	23.9	42.1	26	10	27	18	45.6
SMNSoN5l	—	—	—	79.8	47.2	34.8	14.7	21	25.4	25	30.9	9.8	70.4	24	40.1	28.3	10.9	26.1	18.1	41.3

Appendix III continued

Measured values of the postcranium – Fibula.

Labels	1	2	3	4	5	6	7	8	9	10
MB.R.1532l	—	18.9	5.4	3.2	2.5	9.2	8.3	3.5	5	5.2
GZG.V.6535r	—	44.7	13.7	14.9	2.5	29.8	18.7	—	11.2	—
GPIT/RE/6841r	—	23.9	5.2	5	1.8	8.2	—	—	—	—
GPIT/RE/6306l	—	47.1	14.5	17	2.6	15	18.9	—	11.8	—
GPIT/RE/6069r	—	33.6	9.4	12.6	2.4	10	—	—	—	—
GPIT/RE/4754l	—	30.8	9	8.5	2.1	8.4	—	—	—	—
GPIT/RE/4922r	—	44.5	13	16.3	1.5	12.3	—	—	—	—
GPIT/RE/5036r	—	49.7	15.3	17.6	2.1	15	—	—	—	—
GPIT/RE/5109r	—	49.2	15	16	4.9	16.2	—	—	—	—
GPIT/RE/5166l	—	55.1	16.4	20.4	3.7	21	—	—	—	—
GPIT/RE/5323r	—	40.4	12.6	14	2.9	12.8	—	—	10.1	—
GPIT/RE/5513l	—	40.3	12.3	14	2.2	14.5	—	—	—	—
GPIT/RE/3751r	—	33.3	10.2	10.2	2.8	12.3	—	—	—	—
SMNSoN1l	—	48.8	13	14.7	2.9	12	19.1	—	10.3	—

Appendix III continued

Measured values of the postcranium – Astragalus.

Labels	1	2	3	4	5	6	7	8	9	10	11	12	13	14
MB.R.1396l	52	28.5	15.5	13.5	6.2	7.5	13	7.2	34.5	38.5	16	8.2	4.8	2
MB.R.1391r	44.8	20.4	11.9	9.8	—	6.7	—	—	—	33.7	8.8	5.6	3.2	—
MB.R.1392r	25.6	—	8.7	—	—	5	—	—	—	—	5.8	2.7	1.1	—
MB.R.1394l	43.8	21.4	11.9	10.7	4.8	—	13.7	7.8	29.7	30.4	—	5	—	1.3
MB.R.1383r	20.9	10.2	6	4.5	2.4	2.5	—	—	15.8	15.5	4.1	2.4	1	1
MB.R.Aststl	50	26.2	16.2	—	—	—	—	—	—	40	12	6.3	—	—
MB.R.3472r	51.2	24.7	15.3	11.7	5.6	7.8	13.8	5	31.2	37	12.5	7.3	—	1.8
GZG.V.6426r	55	27.7	17.5	28.3	7	—	—	7.9	—	41.3	—	—	—	—
GPIT/RE/3634l	54	27	14.3	14	—	7.9	15	7	—	40	14.6	7.3	4.2	—
GPIT/RE/3990r	56.7	27	16	12	7.3	8.4	—	—	30	42	12.5	7.2	4.8	—
GPIT/RE/4155l	54.8	27.8	15.1	13.1	5	7	15.1	7	35.3	40.8	16	7.2	4.4	4
GPIT/RE/5861r	51.4	26.8	12.3	11.3	5.3	—	—	—	28.8	40.1	—	—	—	3.1
GPIT/RE/5707l	52.2	26	16.9	9.8	6.1	6.9	14	6	24.3	40	14.2	6.3	3.2	4.7
GPIT/RE/5463l	—	17	10.6	6.7	3.3	4.2	8.2	4.2	21	30.8	6.9	3.8	—	2.3
GPIT/RE/5456r	20.3	10.1	5.1	4	1.8	2.8	5	2.9	14	15.3	5	3.2	1.5	1.1
GPIT/RE/5006r	55.3	31	16.4	13.7	6.3	7.7	14.5	8.9	36.3	45.7	14.9	7.8	5	3.1
GPIT/RE/4929l	47.6	24.9	14	11.2	5.2	7	12.2	6.1	32	36.4	12.3	7.3	4.6	3
GPIT/RE/4685l	—	23.9	12.9	14.4	5.9	7.8	—	6	28.8	37.4	9.2	5.3	—	3.7
GPIT/RE/6848r	51.3	24.8	14.1	10.5	5.5	6.9	—	6.1	30.9	38	13.1	6.6	3.2	3.6
SMNSoN1l	33.4	15.9	8.2	7.3	3.4	4.9	—	—	21	24	7	3.2	—	2.8
SMNSoN2l	—	23.4	12.9	10	5.2	—	—	—	31	31.8	—	—	—	3.1
SMNSoN3r	51.8	25.9	13.2	12.7	5.4	6.2	—	—	33.2	35.8	13.2	7.9	3.1	4.2
SMNSoN4r	50.2	28.3	15.1	13.1	6.7	7.8	—	—	34.5	38.9	13.4	—	3.7	5.3
SMNSoN5l	59.8	31	15.3	14.3	7.2	8	—	—	39.2	45	14.3	7.2	4.6	4.8
SMNSoN6l	—	31.7	18.7	14.9	7.2	10.8	—	—	40	46	—	—	—	4.2

Appendix III continued

Measured values of the postcranium – Calcaneum.

Labels	1	2	3	4	5	6	7
MB.R.1379r	41	30.6	25	19.5	64	18	19
MB.R.1548r	51	41	30	—	85	23.6	27
MB.R.1384r	42.1	—	—	—	68	16.2	—
MB.R.1385r	20.6	15.8	12.4	10.5	30	7.8	7.7
MB.R.Aststl	45.3	34.7	28	22.7	70	18.8	23.6
MB.R.Aststr	43.8	29	—	21.5	65	17.4	20.5
MB.R.1390r	25.1	16.1	15.2	12.5	39	9.5	—
GZG.V.6665l	40	—	—	—	65	18.1	—
GZG.V.oNrl	26.9	—	—	—	35	12.7	—
GPIT/RE/WJ8400l	18.8	12.2	9	8	29	6.3	5.9
GPIT/RE/3893r	18.2	11.8	9	—	27	5.3	—
GPIT/RE/5931r	42.2	30.1	22.7	21.4	67	18.5	19
GPIT/RE/5932r	44	31	23.5	21.1	72	22.6	29
GPIT/RE/5808r	40.5	27.2	21.4	19.4	64	18.2	18.2
GPIT/RE/5457r	16.4	10.2	9.8	7.8	24	6.8	—
GPIT/RE/5304r	39.2	27.6	21.6	19.2	63	17.8	—
GPIT/RE/5245l	42.8	27	27.6	18.9	63	17.9	20.9
GPIT/RE/6102l	18.7	13.6	11.1	8.9	30	8	9.9
GPIT/RE/6486r	43.1	26.9	22.9	19.2	70	18.9	—
SMNSoN1r	41.8	32.7	25.3	21.2	69	19	22.9
SMNSoN2r	47.1	34.3	25.3	23.7	74	—	—
SMNSoN3r	—	15.8	11.9	—	—	7.7	10.9

Appendix III continued

Measured values of the postcranium – Metatarsal II.

Labels	1	2	3	4	5	6	7	8	9	10	11	12
MB.R.1540.1r	63	60.5	18	5	4.7	4.5	10.6	9	7	9.5	6.3	3.5
MB.R.1410l	110.5	103.8	39.6	12.2	12.1	8.6	21.9	17.9	14	18.8	13.8	8.6
MB.R.1413l	99.2	94.6	34.1	11.3	11.2	8.8	20.1	19	—	16.5	—	8.3
MB.R.1398l	123.5	116.4	45	15.9	15	11.7	26	22.1	19.1	21	17.8	11
MB.R.1710r	91.1	86	27.1	8.9	—	7.2	17.9	16	12.8	15.7	12.2	6.8
MB.R.2526l	138	130	47.3	18.6	13.5	12	27	24.8	19.7	22.8	18.6	12.8
MB.R.1415l	—	—	—	—	—	4.8	11	9.5	—	8.9	7.3	—
MB.R.Aststl	137	130	54	16	14	13.4	27.5	24.9	19.6	22.8	19.7	12.9
GPIT/RE/6448l	90	85	30.3	10	9	—	16.3	15.4	12	13.9	12	10.5
GPIT/RE/5273l	94	88	30.9	10.2	9	6.1	16.9	15.1	11.9	14	11.3	8
GPIT/RE/5566l	75	71	23.1	8.2	7.9	5.8	13.7	13.2	8.6	10.9	8.2	6.1
GPIT/RE/5685l	122	112	47.2	13.9	14.9	—	26.8	22.2	19.5	21.9	17.3	10
GPIT/RE/3892r	84	79.2	28.9	8.8	8.9	6.9	16.5	14	11.2	14.2	10.9	7.9
SMNSoNl	116.2	111.7	35.9	11.2	12	8.2	19.9	18.3	14.2	14.3	13	13

Appendix III continued

Measured values of the postcranium – Metatarsal III.

Labels	1	2	3	4	5	6	7	8	9	10	11	12
MB.R.1541.1r	70	16.2	5.3	9	4.9	12.5	9	8.5	11	14.1	7.6	12.1
MB.R.1539l	69	14.8	5.5	10.5	6	10.7	9	8.6	10.9	14.5	7.6	13
MB.R.1397l	155	41.3	11.7	27	18.9	25.2	22	21.8	27	35.8	22.4	32.8
MB.R.1412r	163	42	13.9	32.4	17.5	31.1	29.8	23.4	—	—	22.8	—
MB.R.1411r	140	36.7	11.8	24.6	15.1	25.7	—	—	—	—	18.2	—
MB.R.1407l	105.8	—	8.2	18.1	12.2	—	13.8	13.1	19	22.9	12.3	21.3
MB.R.Aststl	158	39.8	13	30	16	24	23	22.4	28.8	36.4	20.8	34.5
MB.R.Aststr	155	37.8	13.7	29	26.8	—	21.9	21.1	26.1	36.3	21	31.2
R12282r	157	39	14	27.7	16.8	29	—	—	—	—	21.4	—
GPIT/RE/6664r	93	26.3	7.3	15.2	9.8	16.4	13.1	12.7	16	20.8	—	19.3
GPIT/RE/6655r	68	15.2	5.3	11.2	7.2	10.3	8.8	8.1	10.1	13.9	7.3	13.1
GPIT/RE/6538l	—	38.9	11.6	25.7	17.7	28	19.9	20.4	24.9	32.1	19.2	30
GPIT/RE/6009r	88	21.4	6.4	13.8	8.7	14.8	—	9.4	13.8	16.9	9.8	15.2
GPIT/RE/3641l	76.7	18.7	5.3	12.4	6.8	13.1	9.2	8.6	12.1	15.1	8.9	14.1
GPIT/RE/3630l	73	17.2	5.7	11	6.3	11.9	9	8.2	11	14	—	13.6
GPIT/RE/3455r	144	37.4	11	23.9	11.3	28	19.2	18.5	24.2	31.9	16.2	28.7
SMNSoN1r	70	17.2	5.9	11.1	5.9	12.7	9	8.8	—	14	7.8	—
SMNSoN2l	81.9	19.9	7.4	13.7	9.2	14.2	—	11	13.2	—	9.9	—
SMNSoN3r	138	37	12.2	23.9	16	25	20	19.6	24.9	33.3	18.4	29.4
SMNSoN4l	149	38.4	12.3	29.2	15.9	25.6	—	—	26.1	34.2	19.7	—
SMNSoN5l	152	42.9	12.8	28.4	17.4	29	21.9	—	29.4	35.7	19.3	31.9

Appendix III continued

Measured values of the postcranium – Metatarsal IV.

Labels	1	2	3	4	5	6	7	8	9	10	11	12	13	14	15	16	17	18
MB.R.1409l	140	144	24.6	16.4	18	14.4	12.3	33.2	8.2	21.2	12	14.8	3.2	34.6	25.7	—	21.3	16.8
MB.R.1542.1r	60	62	8.1	5.9	12	5	5	12	3.2	7.9	4.1	3.7	1.1	13.2	9.1	8.5	8.1	6.5
MB.R.1399r	135	140	—	—	—	14.2	—	33	7.8	20.9	11.3	13.4	3.2	33.1	23.5	20.7	19.8	16
MB.R.1472r	77	79	8.8	7.5	19	7.2	7.1	—	—	8.5	5.8	—	1.7	16.6	12.4	10.2	9.3	8.8
MB.R.Aststr	140	143	21.4	15.8	26	14.1	12.9	33.8	6	23	12	—	2.9	34.7	23.2	21.4	20.8	18
MB.R.Aststl	—	—	21.3	15.8	—	13.8	12.1	—	—	—	—	—	—	—	—	—	—	—
GPIT/RE/5646l	94	96	11	8.6	12	9.2	—	19.9	4.3	12.6	7	8.2	2.8	21.4	14.1	13.1	12.7	11.2
GPIT/RE/5778r	—	70	—	—	—	—	—	16.7	3.9	10.3	3.7	6.1	1.2	16	10.8	9.4	10.2	8.2
GPIT/RE/3910l	115	—	17.3	14	—	11.8	11.6	—	5.3	18.4	12	10	2	27.7	20	18.4	17.8	15.8
GPIT/RE/6554l	107	111	16.5	12.2	15	10.9	10.5	27.3	7	17.2	8.5	8.5	3.1	29.3	20.6	17.3	17.9	14.8
SMNSoN1r	82	85	11.2	9.2	16	7.6	—	18.2	3.7	11.8	7.9	6.9	—	21.8	15.2	12.6	14.4	11.3
SMNSoN2l	132	135	19.7	15	26	13	11.5	30.8	7.2	21	11	13.1	3.3	30.7	22.8	19	19.7	16.2
SMNSoN3l	136	140	22	16.9	25	12.4	11.2	—	—	21.8	12.8	12.2	—	31	23.8	—	19.2	16.6

Appendix III continued

Measured values of the postcranium – Phalanx II1 (top) & II2.

Labels	1	2	3	4	5	6	7	8	9	10	11	12	13	14	15
MB.R.1540.2r	23.7	24.2	25	9.9	6.1	6.3	9.1	11.7	6.2	6.2	8.7	8	6.5	20.2	20.1
MB.R.1445r	52.5	53.6	55.6	24.9	14.4	15.8	22.7	29.8	14	13.7	20.2	19	16	43	44
MB.R.1545l	26.7	26.4	28.1	12	7	7.7	10	13	7.2	7.3	10.2	—	8	22.8	21.5
MB.R.1544l	—	23.3	24.8	10.3	6.2	6.1	8.9	—	6.5	6.6	8.5	8	6.8	—	19.7
MB.R.Aststl	45.9	45.2	48.1	25	14.1	13.3	19.9	28	13.2	13.2	19.3	17.9	15	34.6	33.8
MB.R.Aststr	48.2	48.1	50.4	22.5	13.8	14	20.2	28	13.6	13.3	18.8	17.8	14.1	40.1	38.6
R12315l	42	41	44.6	28.2	11.3	11	16.6	20.7	13.2	13	15.8	14.2	12	35.7	32.6
GZG.V.6580r	56.7	57.9	59.4	29.7	16.4	17.5	23.4	30.9	16.6	15.2	22.8	20.7	17.3	45.1	44.9
GPIT/RE/3840r	27.6	27.8	30.2	13.5	8.1	7.8	10.8	15.2	7.8	7.9	9.8	9	7.9	23.6	22.2
GPIT/RE/5953r	27	28	29.7	13	8.1	8	11.3	14.1	7.3	7.3	9.9	8.8	7.3	24.4	24
GPIT/RE/5939r	47	47.8	51.2	25	14	13.7	19.8	27.9	13.8	13.9	18.8	17.4	14	37.9	37.2
GPIT/RE/5697l	54.3	55.2	58.9	—	15.3	15.1	20.9	31.1	15.2	15.1	22.3	17.8	16.3	45	44.6
GPIT/RE/4498r	46.1	45.8	48.3	25	13.1	14.7	19.2	30	13.6	13.6	18.1	17	14.3	37	37.2
SMNSoN1l	56.8	56.7	60.9	28.7	17.2	18.4	—	34.2	16.2	15.9	22.8	19.2	17	46.2	42.6

Labels	1	2	3	4	5	6	7	8	9	10	11	12	13	14	15
MB.R.1540.3r	14.1	12.1	12.7	9.4	7	5.4	8.1	8.7	4.7	5.1	6	5.9	4.9	12	10.1
MB.R.1459r	19.8	16.8	17.3	13.7	10.7	8.4	12	12.8	7	7.2	9.5	9	7.2	16.2	14.3
MB.R.1446r	36.3	32.3	32.3	28.8	21.3	14.2	25	25.6	15	14.1	16.6	16.6	14.8	27.4	25.7
MB.R.1453r	21	18.1	19.1	14	10.7	8.3	12.8	12.9	7.6	7.8	9	8.9	7.1	17.8	16.2
MB.R.1462l	20	17.1	17.2	14.7	10.9	9.1	12.8	13.3	7	7.1	9.2	8.7	7.2	16.1	14.7
MB.R.1463r	18.1	15.3	16.6	12.8	10.2	8	11.8	11.3	6.2	6.2	8	7.8	6.1	15.1	13.5
MB.R.1464l	14.8	13	13.1	10.2	8	5.7	8.9	9.7	5.7	5.8	6.7	6.8	5.4	12.1	11.6

Appendix III continued

Measured values of the postcranium – Phalanx III1.

Labels	1	2	3	4	5	6	7	8	9	10	11	12	13	14	15
MB.R.1541.2r	20.6	20.4	20.8	—	9.1	8.7	11.8	11.1	5.8	5	8.4	8.1	6.9	17.5	15.9
MB.R.1419l	41.2	40	41.5	33.6	19.6	18.9	25	24.8	12	11	18.2	16.6	14.2	32.9	31.2
MB.R.1421l	30	28.5	29.8	22.9	13.8	—	18	16.3	8.3	7.7	12.7	—	10.2	—	23.2
MB.R.1420l	36	34.9	35.8	28.3	16.2	15.3	21.2	21	10.4	—	15.7	14.2	12.3	30.2	28.2
MB.R.1418l	42.9	41.4	42	38.4	21	19.7	28.4	27.5	13.2	12.2	20.3	17.3	15.1	35.2	31.1
MB.R.1426r	42	40	41.1	34.8	20.8	18.6	24.9	24.8	12.8	11.9	16.9	17.3	14	33.6	32.4
MB.R.1425r	43.2	42.5	43.9	37	21.2	19.1	26.2	27	12.4	11.2	19.9	18.1	14.6	33	32.2
MB.R.Aststl	45	42.3	43.2	—	20	20	26.8	27.8	13	12.1	20.2	18.5	15.4	34	34.1
GZG.V.6511r	41	40.2	40.8	33.2	19	18.9	26.7	24.3	12.1	10.8	17.5	15.7	13.6	32.3	31.2
GPIT/RE/3946l	30.8	29.2	31.1	23	13.7	11.7	17.1	16.9	8.6	7.8	12.8	11.7	10	22.9	23.7
GPIT/RE/3952l	31.4	31	31.3	25	15.1	13.8	18.4	18.2	9.4	9.2	12.9	12.2	10	23.2	24.9
GPIT/RE/4114l	29	28.2	29.2	23.2	13.5	12.8	17	16.8	8.7	7.6	12.4	11.1	9.7	23.3	22.9
GPIT/RE/6064l	51.3	50	53.4	45.3	26.7	24.2	33.3	32.8	16.9	15.2	25.9	24.1	19.9	45.1	38
GPIT/RE/6636l	47.1	46.8	47	40.2	22.6	20.2	29.8	29.6	13.8	11.4	20.8	20.2	16.3	36.3	36
SMNSoN1l	41.3	39.3	41.7	34.2	21.1	19.2	27.3	26.3	13.7	12	19.7	18.9	15.7	32.2	29.9
SMNSoN2l	40.2	40	38.8	33.8	18.4	17.2	25	24.2	11.3	10	17.7	16.2	13.2	33	29.7
SMNSoN3l	29	29.2	28.8	21.7	13	12.2	16.6	16.4	8.9	7	12.9	11	9.8	23	23.5
SMNSoN4r	24.2	24.8	24.8	18	11.1	10.3	14	13.6	7.2	5.8	10.2	9.2	7.9	19.2	20

Appendix III continued

Measured values of the postcranium – Phalanx III2.

Labels	1	2	3	4	5	6	7	8	9	10	11	12	13	14	15
MB.R.1541.3r	15.8	14.1	14	12	8.7	7.7	10.3	9.1	5.1	5	—	7.4	5.8	12.6	12.8
MB.R.1460r	14.3	13	13	11.1	8.6	6.9	9.9	8.8	5	4.8	7	6.9	5.2	11	11.7
MB.R.1435l	29.1	24.3	23.7	26.7	20	15.3	23	18.7	10.8	10	15	13	12	22.9	19.2
MB.R.1436l	28.3	25.1	24.8	24.1	16.9	14.9	20.6	17.1	10.1	10.1	14.2	14.4	11.3	21.7	20.8
MB.R.1437r	25.3	21.3	20.8	22.1	18	14.6	20.2	16.6	9.6	8.7	12.4	11.8	10	20	17.3
MB.R.1432l	—	28.8	28.5	28.9	20.5	16.8	24.7	20.2	11	11	16.3	16.8	13.1	—	24.8
MB.R.1461l	26	21.8	22	24.2	20	15.9	22	17	10.2	9	13.4	12.3	11	18.9	18
GZG.V.6208r	28.1	23.9	22.5	24.8	19.2	14.8	20.8	19.8	8.5	9.5	12.9	13.5	11.3	22	18.4

Appendix III continued

Measured values of the postcranium – Phalanx IV1 (top) & IV2.

Labels	1	2	3	4	5	6	7	8	9	10	11	12	13	14	15
MB.R.1542.2r	15.4	15.4	16.4	8.8	6.3	6.2	8.9	10	5.3	5.3	7.5	6.8	5.6	12	12.8
MB.R.1448l	29.1	28	31.9	20.7	14.2	13.4	19	22.1	11.7	9.7	17.2	13.8	11.3	22.1	23.3
MB.R.1450l	20.9	21.4	22.2	—	9.3	8.7	12.2	—	7.5	6.9	11	9.9	7.9	—	16.7
MB.R.1452r	17	17	18.7	10.6	7.8	6.7	—	11.8	6.9	5.7	—	7.9	6.8	13.1	14
MB.R.1451l	19.3	19.2	21.2	12.3	8.8	8.4	11.3	13.9	7.2	6.5	10.7	9.1	7.4	15	16.3
MB.R.1429r	19.1	19	20.7	12	8.2	7.6	11.1	13.5	7.2	6.2	10.5	8.8	7.3	14	16.3
MB.R.Aststl	34.9	35.7	38	22.7	16	17	21.2	24.8	11.6	10.9	—	16.2	12.1	26.7	26.8
GPIT/RE/4161l	34.9	36	39.2	22.9	16.8	16.1	22.3	30	12.8	12	20.2	16.9	13.8	24.1	27.5
GPIT/RE/6240l	19.2	19.9	20.2	12.2	8.6	7	10.1	10.2	6	4.6	8.4	7.2	6.1	14.8	16.1
GPIT/RE/6226l	28.1	29.2	30.6	18.8	13.8	13	18	21.4	10.3	9.3	15.2	12.8	10.7	19.8	22.3
SMNSoN1r	31	32.1	35	22	15.1	15.5	20.5	26.1	14.3	13.8	18.3	16.3	14.3	24.3	23.8
SMNSoN2l	29.9	30	32.3	19.7	14.3	14	17.9	22	11.1	10	16.1	13.7	11	21.9	23.8
SMNSoN3l	32.2	32.3	35.2	21.9	15	—	20.2	23.7	12.5	11.2	17.1	15.2	12.2	25.3	25.9

Labels	1	2	3	4	5	6	7	8	9	10	11	12	13	14	15
MB.R.1542.3r	11.6	10	10	—	7	5.6	8.1	8.1	5.3	4.8	7	—	4.9	8.4	9.3
MB.R.1434r	27.5	23	22.9	24	19	14.7	22.1	21.1	12.8	11.1	17	14.1	11.3	19.3	21.2
MB.R.1457l	—	17.8	—	16.8	13.4	9.9	14.2	14.3	9.5	8.2	12.5	—	8.2	—	14.9
MB.R.1455l	25.7	22.1	22.5	21.9	17	—	20.2	19.7	12.3	11.8	16	13.3	10.6	—	19.9
MB.R.Aststr	22.8	19.6	20.1	20.7	16.4	13.1	17.8	16.9	10.9	9.3	14	12.8	10.4	15.3	17.8
GZG.V.6682l	18	15.2	15.8	13.8	11.9	9	12.6	12.2	8.3	6.4	11	9	7.3	11.9	13
GZG.V.oNr	25.8	22.4	—	22	17	14.5	19.2	17.9	13.4	10.9	—	—	10.6	18	19.6

Appendix IV

Explanatory list of all measured distances presented in appendix III.

Scapula:

1 – Maximum length

2 – Maximum width of distal blade

3 – Shaft minimum

4 – Maximum distance of lateral depression

5 – Maximum width distally between acromion process and glenoid

6 – Length of glenoid

7 – Width of ridge adjacent to the glenoid

8 – Depth of the glenoid

9 – Thickness of the proximal end of the blade

10 – Maximum thickness of the shaft

11 – Thickness of humerus joint face including depth of glenoid

12 – Length of humerus joint face

13 – Maximum thickness of articular surface for the coracoid dorsal to the Fo. supracoracoideum

Coracoid:

1 – Maximum anteroposterior length

2 – Distance between the lateroventral corner and the anterior end of the humeral joint face

3 – Length of humeral joint face

4 – Length between sternal process and lateroventral corner

5 – Minimum distance between the dorsal concavity and the lateroventral corner

6 – Length between the anterior corner and the centre of the Fo. supracoracoideum

7 – Length between the posterior end of the humeral joint face and the centre of the Fo. supracoracoideum

8 – Distance between the lateroventral corner and the centre of the Fo. supracoracoideum

9 – Distance between the centre of the Fo. supracoracoideum and the dorsal concavity

10 – Maximum diameter of the Fo. supracoracoideum

11 – Maximum thickness of the scapular articular surface

12 – Thickness of the open canal within the scapular articular surface

13 – Length of this canal, which leads to the Fo. supracoracoideum

14 – Thickness of the lateroventral corner

15 – Distance between the sternal process and the posterior end of the humeral joint face

16 – Maximum depth between the corners of measured distance “15”

17 – Maximum thickness of the humeral joint face

18 – Distance between the dorsal concavity and the posterior end of the humeral joint face

Humerus:

1 – Length

2 – Proximal width

3 – Width at the deltopectoral crest

4 – Minimum shaft width

5 – Maximum width distally

6 – Length proximal from the deltopectoral crest to the lateral corner of the proximal end

7 – Length distal from the deltopectoral crest to the condyles

8 – Width between the distal condyles

9 – Maximum thickness proximally

10 – Maximum thickness at the deltopectoral crest

11 – Maximum thickness of the lateral (radial) condyle

12 – Maximum thickness of the medial (ulnar) condyle

13 – Thickness at the fossa olecranii

14 – Depth of the whole bone medially

Radius:

1 – Length

2 – Maximum width proximally in anterior view

3 – Minimum shaft thickness mediolaterally

4 – Maximum width distally in anterior view

5 - Maximum width proximally in lateral view

6 - Minimum shaft thickness anteroposteriorly

7 - Maximum width distally in anterior view

8 – Width of the ulnar joint face distally

Ulna:

1 – Length

2 – Maximum width proximally in medial view

3 – Minimum shaft thickness in medial view

4 – Maximum width distally in medial view

5 – Width distally of medial face

6 – Width distally of the anteromedial face articulating with the radius

7 – Medial width of the base of the olecranon process

8 – Distance between the top of the olecranon process and the anterior most tip proximally

9 – Maximum thickness of the olecranon process mediolaterally

10 – Height of olecranon process measured from the level of the distance “2”

11 – Maximum thickness distally in posterior view

Ilium:

1 – Total length

2 – Length of the preacetabular process

3 – Length without the preacetabular process

4 – Maximum height at the ischiadic peduncle

5 – Height above the acetabulum

6 – Height of the base of the preacetabular process

7 – Height at the midshaft of the preacetabular process

8 – Fractional height up to the dorsolateral muscle attachment site

9 – Height of the neck of the postacetabular process

10 – Distance between the ventral and dorsal end of postacetabular muscle attachment sites

11 – Maximum width of the ischiadic peduncle

12 – Height of the formerly cartilaginous area lateral at the ischiadic peduncle

13 – Height from the anterior edge of the ischiadic peduncle to the top of the triangular muscle attachment site laterally on this peduncle

14 – Distance from the posterior edge of the ischiadic peduncle to the top of the triangular muscle attachment site laterally on this peduncle

15 – Distance from the posterior edge of the ischiadic peduncle laterally up to the posterior most corner of the postacetabular process

16 – Height of the muscle attachment site located at the posterior end of the ilium

17 – Anteroposterior thickness of the pubic peduncle

18 – Length of the acetabulum medially

19 – Length of the acetabulum laterally

20 – Maximum width of the ilium at the brevis shelf

21 – Minimum thickness of the dorsal ridge

22 – Maximum thickness of the preacetabular process

23 – Length of the brevis shelf up to the level of distance “26” anteriorly

24 – Width of the muscle attachment site at the posterior end of the ilium

25 – Width at the level of the posterior edge of the ischiadic peduncle

26 – Height of the medial concavity above the centre of the ischiadic peduncle and at the distinct ventral step of the anterior end of the brevis shelf

27 – Height of the medial concavity above the acetabulum

28 – Height of the medial concavity at the base of the preacetabular process

29 – Height of the medial concavity at mid length of the preacetabular process

30 – Height of the medial concavity at the anterior end of the dorsomedial muscle attachment site

31 – Height between the anterior edge of the ischiadic peduncle and the ventral rim of the medial concavity

32 – Width of the pubic peduncle

33 – Width of the ischiadic peduncle along its posterior edge

34 – Ventral thickness of the base of the preacetabular process

35 – Distance between the posteromedial edge of the ischiadic peduncle and the posteromedial end of the brevis shelf

36 – Height of the posterior end up to the brevis shelf

Ischium:

1 – Length of the iliac peduncle

2 – Length of pubic peduncle

3 – Thickness of iliac peduncle

4 – Thickness of pubic peduncle

5 – Depth of acetabulum

6 – Maximum anteroposterior length proximally

7 – Minimum Distance of the ischiadic blade

8 – Distance between the acetabulum and the neck of the obturator process

9 – Distance between the tip of the obturator process and the pubic peduncle

10 – Anteroposterior length at the obturator process

11 – Depth of the concavity between the obturator process and the pubic peduncle

12 – Minimum width of the neck of the pubic peduncle

13 – Minimum width of the neck of the iliac peduncle

14 – Minimum width of the neck of the obturator process

15 – Maximum height of the obturator process

16 – Minimum thickness of the ischiadic shaft

17 – Length of the ischiadic shaft

18 – Total length

19 – Thickness of the acetabular edge at the position of the distance “5”

Femur:

1 – Total length between the greater trochanter and the distal end laterally

2 –Anteroposterior maximum width proximally

3 – Anteroposterior width of the greater trochanter

4 – Anteroposterior maximum width of the lesser trochanter

5 – Height of the lesser trochanter

6 – Height of the base of the 4^{th} trochanter

7 – Fractional length from the greater trochanter to the neck of the 4^{th} trochanter

8 – Fractional length from the neck of the 4^{th} trochanter to the distal end laterally

9 – Anteroposterior width distally at the lateral condyle

10 – Fractional anteroposterior width distally without the lateral condyle

11 – Minimum anteroposterior thickness of the shaft distal to the 4^{th} trochanter

12 – Minimum anteroposterior thickness of the shaft proximal to the 4^{th} trochanter

13 – Maximum lateromedial width proximally

14 – Depth between the femoral head and the greater trochanter

15 – Shaft thickness at the dorsal end of the base of the 4^{th} trochanter

16 – Maximum thickness of the distal shaft at the lateral shelf

17 – Depth between the greater trochanter and the medial condyle

18 – Maximum lateromedial width distally

19 – Thickness of the lateral condyle

20 – Thickness of the medial condyle

21 – Anteroposterior width distally at the medial condyle

22 – Minimum distance between both distal condyles

23 – Maximum thickness of the femoral head slightly inclined to the dorsoventral axis

24 – Fractional length from the greater trochanter to the posterior nutrient foramen

25 – Fractional length from the posterior nutrient foramen to the distal end laterally

26 – Fractional shaft width laterally at the posterior nutrient foramen

27 – Fractional shaft width medially at the posterior nutrient foramen

28 – Anteroposterior width distally at the lateral condyle

29 – Minimum anteroposterior thickness of the distal end

30 – Maximum distance between both distal condyles

31 – Depth of the intercondylar extensor groove

32 – Height of the posterior nutrient foramen

33 – Anteroposterior length of the lateral condyle

34 – Height of the medial depression

35 – Maximum width of the medial depression

36 – Fractional length from the ventral end of the medial depression to the distal end laterally

37 – Width of the posterior nutrient foramen

Tibia:

1 – Total length laterally

2 – Total length medially

3 – Minimum lateromedial thickness of the shaft

4 – Maximum length of the proximal end anteroposteriorly

5 – Maximum width of the proximal end including the medial condyle

6 – Length of the medial condyle

7 – Fractional width of the medial condyle alone

8 – Distance between the posterior and anterior tips of the medial condyle

9 – Posterior fractional width of the proximal end without the medial condyle

10 – Anterior fractional width of the cnemial crest

11 – Anteroposterior length of the base of the medial condyle

12 – Depth between the anterior tip of the medial condyle and the cnemial crest

13 – Maximum width of the distal end

14 – Fractional width of the lateral part of the distal end articulating with the calcaneum

15 – Fractional lateral width

16 – Fractional medial width

17 – Diameter of the circular depression at the top of the articular surface for the astragalus

18 – Maximum thickness distally

19 – Maximum thickness at the border between articular surface for the astragalus and calcaneum

Fibula:

1 – Total length

2 – Maximum width proximally

3 – Posterior thickness proximally

4 – Thickness at the bend proximally

5 – Depth of this bend

6 – Distance between the proximal end and the medial visibility of the posteromedial muscle attachment site

7 – Anteroposterior width of the shaft at the distal end of the posteromedial muscle attachment site

8 – Minimum shaft thickness at the end of the shaft rotation distally

9 – Lateromedial thickness of the shaft at the level of the distance “7”

10 – Lateromedial thickness of the shaft at the level of the distance “8”

Astragalus:

1 – Maximum lateromedial width

2 – Height posteriorly by holding the anterior and posterior ascending processes in equal heights

3 – Maximum thickness posteromedially

4 – Maximum depth between the anterior and posterior ascending processes

5 – Thickness of the posterolateral process

6 – Thickness of the anterolateral process

7 – Length of the dorsolateral depression

8 – Width of the dorsolateral depression

9 – Distance between the top of the posterior ascending process and the posterolateral end

10 – Distance between the top of the posterior ascending process and the medial extremity

11 – Width of the anterior depression

12 – Height of the anterior depression

13 – Anterior depth between the anterolateral corner and the main body

14 – Posterior depth between the posterolateral corner and the main body

Calcaneum:

1 – Total length anteroposteriorly

2 – Maximum height

3 – Distance between the dorsal process and the posterior edge

4 – Distance between the dorsal process and the anterior edge

5 – Fractional circumference ventrally

6 – Maximum lateromedial width

7 – Width along the dorsal process

Metatarsal II:

1 – Total length posteriorly

2 – Total length anteriorly

3 – Maximum anteroposterior length proximally

4 – Maximum lateromedial thickness proximally

5 – Minimum shaft thickness anteroposteriorly

6 – Minimum shaft thickness lateromedially

7 – Length of distal end medially

8 – Lateromedial width of distal end posteriorly

9 – Lateromedial width of distal end anteriorly

10 – Median anteroposterior length of distal end

11 – Minimum lateromedial width distally

12 – Minimum thickness of proximal end

Metatarsal III:

1 – Total length

2 – Anteroposterior total width proximally

3 – Minimum anteroposterior shaft thickness

4 – Maximum lateromedial width proximally

5 – Thickness of the posterior process of the proximal end

6 – Fractional anteroposterior width proximally without the posterior process

7 – Width of the medial condyle distally

8 – Median anteroposterior thickness distally

9 – Width of the lateral condyle distally

10 – Maximum lateromedial width distally

11 – Minimum lateromedial shaft thickness

12 – Minimum lateromedial width distally

Metatarsal IV:

1 – Total length

2 – Total length along the curvature of the shaft

3 – Lateromedial thickness at midshaft

4 – Minimum lateromedial shaft thickness

5 – Length of the deviation of the distal end from the long axis of the bone

6 – Anteroposterior thickness at midshaft

7 – Minimum anteroposterior shaft thickness

8 – Maximum anteroposterior width proximally

9 – Depth between the anteromedial and posteromedial proximal processes

10 – Median lateromedial thickness proximally

11 – Basal thickness of the anteromedial proximal process

12 – Basal thickness of the posteromedial proximal process

13 – Depth of the depression on the proximal end

14 – Maximum distance of the distal end

15 – Distance of the distal end almost perpendicular to distance “14”

16 – Distance between the anteromedial and anterolateral corner of the distal end

17 – Posterior lateromedial width of the distal end

18 – Median lateromedial width of the distal end

Phalanges:

1 – Median total length

2 – Total length between the medial condyle and the medial edge of the proximal end

3 – Total length between the lateral condyle and the lateral edge of the proximal end

4 – Maximum width of the proximal end

5 – Minimum lateromedial shaft width

6 – Dorsal condyle width

7 – Ventral condyle width

8 – Height of the proximal end

9 – Medial midshaft height

10 – Lateral midshaft height

11 – Height of the medial condyle measured along its side

12 – Height of the lateral condyle measured along its side

13 – Minimum height between both condyles

14 – Dorsal length between the condyle facets and the proximal end

15 – Ventral length between the condyle facets and the proximal end

Appendix V

Lengths of all long bones in mm. Note that many specimens used here are incomplete, so that the missing values were calculated by the extrapolation from other specimens of the respective taxon. In the case of known pairs of elements, the values were averaged. The length of the mt III of MNAPl.175 was derived by using the specimen UCMP130580. The tibia length of R196 was derived from the relation of distal width to length in other specimens. The values from MOR979 are gained out of a figure in Boyd et al., 2009. The length of the mt III of YPM5459 was calculated by using the relation of femur length and tibia length to mt III in the specimens OMNH10132 and YPM-PU16338. The missing lengths for Dy I were derived from the missing individual Dy VI (Janensch, 1955: fig. 40) and the allometric effect is minimized by integrating YPM1876 and CM1949 into the calculation as well. The missing value of the mc III of Dy I is calculated by using the average ratio of all known humerus to radius ratios in both dryosaurids. The length of the mt III of YPM1876 is derived from the ratio of proximal and distal femur width to the known mt III length in CM21768. The femur and tibia lengths of USNM4282 („*C. browni*“) is derived from USNM2210 (“*C. nanus*”) and its mt III length by using relations in USNM4277.

Taxa	Label	Sources	Humerus	Radius	Metacarpal III	Femur	Tibia	Metatarsal III
Heterodontosaurus tucki	SAM-K-1332	Santa Luca, 1980	83.5	58.5	21.9	112	145	67.9
Scutellosaurus lawleri	MNAPl.175	Colbert, 1981	68.5	57	16.5	93.2	95.7	53.2
Psittacosaurus neimongoliensis	IVPP12-0888-2	Russel & Zhao, 1996	105	82.5	24	150	194.7	84
Hypsilophodon foxii	R196	Galton, 1974	284.3	191.2	44.1	451	387.3	142.2
Thescelosaurus neglectus	MOR979	Boyd et al., 2009	344.4	210	72	415	500	180
Tenontosaurus tilletti	YPM5459	Ostrom, 1970	157	105	22.2	280	318.2	168.4
Dysalotosaurus lettowvorbecki	Dy I	Janensch, 1955; Galton, 1981; this study	190	146	30	360	395	238.5
Dryosaurus altus	YPM1876	Galton, 1981	360	232	75	657.3	598.7	230.9
Camptosaurus dispar	USNM4282	Gilmore, 1909	243.5	160.5	49.7	437.5	401.5	143.6
Camptosaurus aphanoecetes	CM11337	Carpenter & Wilson, 2008	430	345	153	760	710	280
Mantellisaurus atherfieldensis	IRSNB1551	Norman, 1986	805	515	190	1025	905	340
Iguanodon bernissartensis	IRSNB1534	Norman, 1986	555	416	128	850	785	290
Ouranosaurus nigeriensis	GDF300	Taquet, 1976	632.7	720.3	290.9	1142.9	1020.5	368.2
Brachylophosaurus canadensis	MOR794	Prieto-Marquez, 2007	650	600	310	1240	1000	410
Edmontosaurus regalis	ROM5167	Lull & Wright, 1942	610	620	330	1150	1020	420
Saurolophus osborni	AMNH5220	Lull & Wright, 1942	600	530	280	1200	1000	330
Saurolophus angustirostris	PIN551-8	Maryanska & Osmolska, 1984	546	577	241.5	987	924	378
Corythosaurus casuarius	AMNH5338	Lull & Wright, 1942	292	277	124	420	550	193
Tethyshadros insularis	SC57021	Dalla-Vecchia, 2009	105	69	25	130	141.5	66

Appendix V continued

Length ratios of long bones. These values are derived from the values presented above and are used for the PCA shown in Fig. 5.20. **Abbr.: F** – Femur; **FoLi** – Fore limb; **H** – Humerus; **HiLi** – Hind limb; **McIII** – Metacarpal III; **MtIII** – Metatarsal III; **R** – Radius; **Ti** – Tibia.

Labels	H/R	H/McIII	H/F	H/Ti	H/MtIII	R/McIII	R/F	R/Ti	R/MtIII	McIII/F	McIII/Ti	McIII/MtIII	F/Ti	F/MtIII	Ti/MtIII	FoLi/HiLi
SAM-K-1332	1.43	3.81	0.75	0.58	1.23	2.67	0.52	0.4	0.86	0.2	0.15	0.32	0.77	1.65	2.14	0.5
MNAPl.175	1.2	4.15	0.73	0.72	1.29	3.45	0.61	0.6	1.07	0.18	0.17	0.31	0.97	1.75	1.8	0.59
IVPP12-0888-2	1.52	4.2	0.81	0.74	1.59	2.76	0.53	0.49	1.05	0.19	0.18	0.38	0.92	1.97	2.14	0.59
R196	1.27	4.38	0.7	0.54	1.25	3.44	0.55	0.42	0.98	0.16	0.12	0.29	0.77	1.79	2.32	0.49
MOR979	1.49	6.45	0.63	0.73	2	4.34	0.42	0.49	1.34	0.1	0.11	0.31	1.16	3.17	2.72	0.53
YPM5459	1.64	4.78	0.83	0.69	1.91	2.92	0.51	0.42	1.17	0.17	0.14	0.4	0.83	2.31	2.78	0.57
Dy I	1.5	7.07	0.56	0.49	0.93	4.73	0.38	0.33	0.62	0.08	0.07	0.13	0.88	1.66	1.89	0.37
YPM1876	1.3	6.33	0.53	0.48	0.8	4.87	0.41	0.37	0.61	0.08	0.08	0.13	0.91	1.51	1.66	0.37
USNM4282	1.55	4.8	0.55	0.6	1.56	3.09	0.35	0.39	1	0.11	0.13	0.32	1.1	2.85	2.59	0.45
CM11337	1.52	4.9	0.56	0.61	1.7	3.23	0.37	0.4	1.12	0.11	0.12	0.35	1.09	3.05	2.8	0.46
IRSNB1551	1.25	2.81	0.57	0.61	1.54	2.25	0.45	0.49	1.23	0.2	0.22	0.55	1.07	2.71	2.54	0.53
IRSNB1534	1.56	4.24	0.79	0.89	2.37	2.71	0.5	0.57	1.51	0.19	0.21	0.56	1.13	3.01	2.66	0.67
GDF300	1.33	4.34	0.65	0.71	1.91	3.25	0.49	0.53	1.43	0.15	0.16	0.44	1.08	2.93	2.71	0.57
MOR794	0.88	2.17	0.55	0.62	1.72	2.48	0.63	0.71	1.96	0.25	0.29	0.79	1.12	3.1	2.77	0.65
ROM5167	1.08	2.1	0.52	0.65	1.59	1.94	0.48	0.6	1.46	0.25	0.31	0.76	1.24	3.02	2.44	0.59
AMNH5220	0.98	1.85	0.53	0.6	1.45	1.88	0.54	0.61	1.48	0.29	0.32	0.79	1.13	2.74	2.43	0.6
PIN551-8	1.13	2.14	0.5	0.6	1.82	1.89	0.44	0.53	1.61	0.23	0.28	0.85	1.2	3.64	3.03	0.56
AMNH5338	0.95	2.26	0.55	0.59	1.44	2.39	0.58	0.62	1.53	0.24	0.26	0.64	1.07	2.61	2.44	0.6
SC57021	1.05	2.35	0.7	0.53	1.51	2.23	0.66	0.5	1.44	0.3	0.23	0.64	0.76	2.18	2.85	0.6

Erklärung

Ich versichere, dass ich die vorliegende Arbeit selbstständig verfasst habe, in gleicher oder ähnlicher Fassung noch nicht in einer anderen Institution als Prüfungsleistung vorgelegt und keine anderen als die angegebenen Hilfsmittel und Quellen benutzt habe.

Hannover, den 18.01.2011

Tom Hübner